Mémoire présenté en vue de l'obtention du diplôme de
Master en Sciences Physiques

Constraints from L∞p Quantum Gravity and the Memory Burden Effect in Primordial Black Hole Cosmologies

Antoine Dierckx

Promoteur·rices

Sébastien Clesse (Université Libre de Bruxelles)
Francesca Vidotto (University of Western Ontario)

Université Libre de Bruxelles
Faculté des Sciences
Service de Physique Théorique
Année académique 2024–2025

ULB FACULTÉ DES SCIENCES

PHYS

> “In order for me to write poetry that isn’t political
> I must listen to the birds
> and in order to hear the birds
> the warplanes must be silent.”
> *Marwan Makhoul*

PREFACE

Acknowledgments

I would like to express my deepest gratitude to my supervisors, Prof. Sébastien Clesse and Prof. Francesca Vidotto, for their guidance and for agreeing to co-supervise this transatlantic thesis and this somewhat unconventional project.

It all started three years ago in a QFT class, when Sébastien overheard me talking about Loop Quantum Gravity. Years later, at a workshop on Primordial Black Holes, he shared with Francesca the idea of this joint master's project — which they then proposed to me — an opportunity I could only dream of.

Sébastien and Francesca arranged for me to spend a semester at the University of Western Ontario, where I met Francesca's interdisciplinary team. I'm especially grateful to her PhD student Mateo Pascual and postdoctoral researcher Emmanuel Frion for countless stimulating discussions (and for pulling me up when Mathematica was luring me into the abyss), and to the broader group, including physicists Fabio Mele, Carlo Rovelli, and the researchers at the Perimeter Institute who made my stay so enriching.

Back at ULB, I would like to thank my friends from the seventh floor of the NO building and beyond for their support and the (dangerously long) coffee breaks.

To my parents and to my best friends Gallian and Sinouhé: thank you for always believing in me and for patiently listening to my physics rants, no matter how long they went on. Your unwavering encouragement made this work possible.

Résumé

Déterminer la nature de la matière noire est l'un des plus grands défis de la cosmologie moderne. La récente détection d'ondes gravitationnelles a relancé l'intérêt pour les trous noirs primordiaux comme candidats potentiels à la matière noire.

Dans ce mémoire, nous étudions la possibilité que les trous noirs primordiaux constituent une fraction significative de la matière noire de l'univers, en tenant compte des effets de gravitations quantiques. Deux cadres théoriques proposant une suppression de l'évaporation de Hawking sont envisagés : la gravitation quantique à boucles et l'effet de fardeau mémoriel.
Nous proposons un modèle cosmologique simplifié dans lequel les trous noirs primordiaux sont formés après la fin de l'inflation et dont l'évaporation est modifiée dans les deux scénarios. Les trous noirs primordiaux, après avoir converti une partie de leur masse en émission de Hawking, se stabilisent pour former des reliques. Nous nous concentrons sur les trous noirs de faible masse (i.e. qui ne pourraient subsister aujourd'hui que sous forme de reliques), et nous étudions les contraintes sur l'abondance initiale des trous noirs primordiaux et les paramètres du modèle afin de déterminer la fraction de matière noire qui peut être expliquée par les reliques.

Nous avons développé un code en `Mathematica` pour simuler l'évolution de l'univers qui permet d'obtenir une variété d'histoires cosmologiques qualitativement différentes, en fonction de la masse initiale des trous noirs primordiaux et du cadre théorique considéré. Nous montrons que les fenêtres de masse viables pour que les reliques constituent une fraction significative de la matière noire ($f \gtrsim 10^{-5}$) sont $m^i_{\text{PBH}} \in [10^{-3}, 10^5]$ kg dans le scénario de la gravitation quantique à boucles, et $m^i_{\text{PBH}} \in [10^{-3}, 10^9]$ kg dans le scénario du fardeau mémoriel.

Mots-clés : Cosmologie, Trous noirs Primordiaux, Gravitation Quantique à Boucles, Effet de Fardeau Mémoriel.

Abstract

Discovering the nature of dark matter is one of the greatest challenges facing modern cosmology. The recent detection of gravitational waves has renewed interest in primordial black holes as potential candidates for dark matter.

In this master's thesis, we investigate the possibility that primordial black holes constitute a significant fraction of the dark matter in the universe, taking into account quantum gravitational effects. Two theoretical frameworks proposing a suppression of Hawking evaporation are considered: loop quantum gravity and the memory burden effect. We propose a simplified cosmological model in which primordial black holes are formed after the end of inflation, and in which their evaporation is affected in both scenarios. After converting part of their mass into Hawking emission, primordial black holes stabilize to form remnants. We focus on low-mass black holes (i.e., those that could survive today only as remnants), and study constraints on the initial abundance of primordial black holes and model parameters to determine the fraction of dark matter that can be explained by remnants.

We have developed a code in `Mathematica` to simulate the evolution of the universe which yields a variety of qualitatively different cosmological histories, depending on the initial mass of primordial black holes and the theoretical framework considered. We show that the viable mass windows for remnants to constitute a significant fraction of dark matter ($f \gtrsim 10^{-5}$) are $m^i_{\rm PBH} \in [10^{-3}, 10^5]$ kg in the loop quantum gravity scenario, and $m^i_{\rm PBH} \in [10^{-3}, 10^9]$ kg in the memory burden scenario.

Keywords: Cosmology, Primordial Black Holes, Loop Quantum Gravity, Memory Burden Effect.

Units and conventions

Throughout this master's thesis, we will use the mostly positive signature for the metric $(-,+,+,+)$. Greek indices $\alpha, \beta, \ldots, \mu, \nu, \ldots$ are *world indices* (moved by an arbitrary metric $g_{\mu\nu}$) and run from 0 to 3. The spatial part of world indices is denoted by $i, j, \ldots$ running from 1 to 3. Internal lorentzian indices are denoted by $I, J, \cdots = 0, \ldots, 3$ and their spatial part is $a, b, \cdots = 1, \ldots, 3$.
A dotted symbol $\dot{f}$ denotes the derivative with respect to cosmic time t or proper time τ (e.g. $\dot{f} = \frac{df}{dt}$ or $\dot{f} = \frac{df}{d\tau}$). A prime symbol f' denotes the derivative with respect to the conformal time η (e.g. $f' = \frac{df}{d\eta}$).

Unless otherwise specified, we will use Planck units $c = \hbar = G = k_B = 1$. From this set of universal constants, we can build fundamental (and derived) *Planck* quantities which are summarized in table 1.

Quantity	Expression		Approximation in SI units
Length	$l_P = \sqrt{\frac{\hbar G}{c^3}}$	(0.1)	$1.6 \cdot 10^{-35}$ m
Mass	$m_P = \sqrt{\frac{\hbar c}{G}}$	(0.2)	$2.2 \cdot 10^{-8}$ kg
Time	$t_P = \sqrt{\frac{\hbar G}{c^5}}$	(0.3)	$5.4 \cdot 10^{-44}$ s
Temperature	$T_P = \sqrt{\frac{\hbar c^5}{G k_B^2}}$	(0.4)	$1.4 \cdot 10^{32}$ K
Area	$A_P = l_P^2$	(0.5)	$2.6 \cdot 10^{-70}$ m^2
Volume	$V_P = l_P^3$	(0.6)	$4.2 \cdot 10^{-105}$ m^3
Density	$\rho_P = \frac{m_P}{V_P}$	(0.7)	$5.2 \cdot 10^{96}$ kg·m^{-3}
Curvature	$R_P = \frac{1}{l_P^2}$	(0.8)	$3.8 \cdot 10^{69}$ m^{-2}

Table 1: Planckian quantities

Nomenclature and acronyms

The following are lists of symbols and acronyms used in this report.

Symbol	Meaning
	Chapter 2
z	redshift
a	scale factor
η	conformal time
ω	equation of state parameter
ρ	energy density
H	Hubble rate
$\mathcal{H}$	conformal Hubble rate
Ω_A	density parameter of species A
ϵ_1, ϵ_2	Slow-Roll parameters
N	number of e-folds
ϕ	scalar field / inflaton
Φ	random scalar field
$\mathtt{P}$	probability distribution function
$\mathtt{P}_{\mathrm{G}}$	Gaussian probability distribution function
δ_D	Dirac delta function
δ	perturbation or density contrast
$\mathcal{P}_\delta$	power spectrum
Δ_δ	dimensionless power spectrum
n_s	scalar spectral index
A_s	amplitude of the scalar fluctuations
$\mathcal{R}$	comoving curvature perturbation
	Chapter 3
K	Kretschmann scalar
u, v	Eddington-Finkelstein coordinates
$\hat{u}, \hat{v}$	Kruskal-Szekeres or inertial lightcone coordinates
T, X	Kruskal-Szekeres coordinates
$\bar{u}, \bar{v}$	Carter-Penrose coordinates
i^+	future timelike infinity
i^0	spatial infinity
i^-	past timelike infinity
$\mathscr{I}^+$	future null infinity
$\mathscr{I}^-$	past null infinity
τ	proper time
η, ξ	Rindler coordinates
$\tilde{u}, \tilde{v}$	comoving lightcone coordinates
T_{U}	Unruh temperature
T_{H}	Hawking temperature
Γ	gray body factor
	Chapter 4
δ_c	density threshold
β	initial PBH density fraction
	Chapter 5
$S_{\text{E-H}}[g]$	Einstein-Hilbert action
$e^I{}_\mu$	vierbein / tetrad
$\omega^{IJ}{}_\mu$	Lorentz connection
$F^{IJ}{}_\mu$	curvature 2-form of the Lorentz connection

Continued on next page

Table 2: List of commonly used symbols (continued)

Symbol	Meaning
$S_{\mathrm{T}}[e]$	Tetrad action
$S_{\mathrm{P}}[e,\omega]$	Palatini action
$S_{\mathrm{H}}[e,\omega]$	Holst action
$E_i{}^a$	densitized triad
A_a^i	Ashtekar-Barbero connection
$S_{\tilde{\mathrm{H}}}[A,E,N^\mu]$	Holst hamiltonian action
G_i	Gauss constraint
H	Hamiltonian constraint
H_a	space-diffeomorphism constraint
F^i_{ab}	curvature 2-form of the Ashtekar-Barbero connection
K_a^i	extrinsic curvature
$E_i(S)$	flux of the densitized triad
$h_\gamma(A)$	holonomy of the Ashtekar-Barbero connection
τ_i	generator of $\mathfrak{su}(2)$
$\triangle$	triangulation
$\triangle^\star$	dual triangulation
v	vertex of the dual triangulation
n	node of the dual triangulation (vertex on the boundary)
s	segment of the triangulation
e	edge of the dual triangulation
l	link of the dual triangulation (edge on the boundary)
t	triangle of the triangulation
f	face of the dual triangulation
$S_\triangle$	discrete action of GR
$\mathcal{H}_{\mathrm{kin}}$	kinematical Hilbert space
$\mathcal{H}_{\mathrm{phys}}$	physical Hilbert space
Γ	graph
	Chapter 6
K	number of quantum fields
$\bar{m}$	mass gap of a memory mode
$\lvert\bar{m}\rangle$	memory state/ pattern
$E_{\bar{m}}$	energy cost of a memory state
$\mathcal{H}_{\mathrm{mem}}$	memory space
N_K	total occupation number of the memory modes
$\bar{m}_0$	mass gap of the master mode
N_c	critical occupation number of the master mode
p	critical exponent
$\lvert n_0,\bar{m}\rangle$	pattern with assisted gaplessness
$\bar{m}^{\mathrm{eff}}$	effective mass gap
q	mass fraction of the remnant
	Chapter 7
m^i_{PBH}	initial mass of the PBHs
k_{LQG}	LQG lifetime parameter
k_{MB}	MBE lifetime parameter
q_{MB}	MBE remnant mass parameter
P0	phase before the formation of PBHs
$A \in \{b,\, c,\, \gamma,\, \nu,\, \Lambda\}$	species $A \in$ {baryons, cold dark matter, photons, neutrinos, cosmological constant}
ρ_A^{obs}	observed energy density of species A
$\widetilde{\rho}_A$	initial energy density of species A
$\alpha_A{}^{\mathrm{P}i}$	initial abundance of species A parameter, in phase Pi

Continued on next page

Table 2: List of commonly used symbols (continued)

Symbol	Meaning
P1	phase after the formation of PBHs, before their evaporation
N_i	number of e-folds at which PBHs form
N_i^-	number of e-folds just before PBH formation
$\rho_{\rm PBH}$	energy density of PBHs
ρ_A^i	energy density of species A right after PBHs formation
P2	phase after the evaporation of PBHs, before the decay of the remnants
N_b	number of e-folds at which PBHs decay
N_b^-	number of e-folds just before PBH decay
$\rho_{\rm REM}$	energy density of the remnants
δN	number of e-folds between the formation of PBHs and their evaporation
ρ_A^H	energy density of species A from Hawking radiation
ϵ	mass fraction of the remnants w.r.t PBHs
ϵ_A	fraction of energy density of species A from Hawking radiation
P3	phase after the decay of the remnants
N_r	number of e-folds at which remnants decay
N_r^-	number of e-folds just before remnant decay
$\beta_{\rm max}$	initial abundance of the PBHs obtained by maximizing β

Table 2: List of commonly used symbols

abbreviations	Meaning
DM	Dark Matter
BH	Black Hole
PBH	Primordial Black Hole
HR	Hawking Radiation
LQG	Loop Quantum Gravity
MB	Memory Burden effect
QG	Quantum Gravity
FLRW	Friedmann-Lemaître-Robertson-Walker
EFE	Einstein Field Equations
F1,F2	Friedmann equations
RD	Radiation Dominated
MD	Matter Dominated
ΛD	Cosmological constant Dominated
EOM	Equation of Motion
SVT	Scalar-vector-tensor
BD	Bunch-Davies
PDF	Probability Density Function
GW	Gravitational Waves
WH	White Hole
CDM	Cold Dark Matter
MBPBH	Memory Burdened Primordial Black Hole

Table 3: List of abbreviations

Contents

CHAPTER

1

INTRODUCTION

1.1 Motivation

The nature of Dark Matter (**DM**) is one of the most important open questions in modern cosmology. We will not review the abundant evidence for DM, or the various candidates, mostly in the "DM particle" category, already proposed to explain DM, since extensive literature exists on this topic [Bertone and Hooper, 2018; Arbey and Mahmoudi, 2021]. Instead, we focus on Primordial Black Holes (**PBHs**), which are a compelling candidate for DM, as they do not require new physics[1] . The recent detection of gravitational waves from merging Black Holes (**BHs**) has renewed interest in PBHs as a possible DM candidate [Bird et al., 2016; Sasaki et al., 2016; Clesse and García-Bellido, 2017].

Until recently, light PBHs were commonly considered excluded as DM candidates due to their rapid evaporation via Hawking Radiation (**HR**). However, HR is a semiclassical effect that has not yet been observed, and its extrapolation may break down when quantum-gravity effects become important. Any constraints on PBHs based on HR must therefore be taken with caution. The Memory Burden effect (**MBe**) and Loop Quantum Gravity (**LQG**) are two approaches that motivate scenarios in which HR is suppressed at late times, allowing for the existence of PBH remnants. We investigate whether PBH remnants could account for a significant fraction of DM in the universe.

1.2 State of the Art

The idea that BHs do not evaporate completely is not new [MacGibbon, 1987]. However, a coherent theory in which planckian remnants are formed, inside the LQG framework, has only recently been proposed [Rovelli and Vidotto, 2014a, 2024]. The LQG approach suggests that the evaporation of BHs can be suppressed by a minimal-area gap and information-storage considerations, potentially preventing complete evaporation.

Some of the phenomenological consequences of this theory have already been studied, such as the production of daily gamma-ray bursts of $\sim$ 10 MeV [Barrau and Rovelli, 2014], the existence of a diffuse radiation bath [Kazemian et al., 2023], and estimates of the abundance needed for planckian remnants to account for the DM energy density in bouncing cosmologies [Trivedi and Loeb, 2025].

[1] PBHs do not require new physics in the sense that their formation is based on the gravitational collapse of inhomogeneities. However, the mechanism at the origin of the inhomogeneities would likely involve new physics, such as a specific inflation model. One can nevertheless point out an example model of PBHs formation in the standard model from the dynamics of the Brout-Englert-Higgs field [Espinosa et al., 2018].

However, an exhaustive study of (non-bouncing) possible cosmologies with light PBHs in LQG is, to our knowledge, still lacking and motivates this work.

Another approach, the memory burden effect, suggests an analogous idea, where the evaporation of systems with large storage capacity is also suppressed by a universal effect of memory burden [Dvali et al., 2020]. Since its recent proposal, the MBe has been studied in various contexts, including its implications for PBHs. This effect opens a new window for small PBHs as DM and re-evaluates evaporation-based bounds on the initial abundance of PBHs [Dvali et al., 2024; Montefalcone et al., 2025]. Currently transitioning PBHs could produce high-energy neutrinos [Dvali et al., 2025].

HR being highly suppressed for large BHs, it is completely negligible for astrophysical ones. A class of BHs where the HR becomes important is PBHs, which are formed in the early universe, and span a wide mass range. PBHs are formed early enough and (possibly) light enough such that their expected lifetime (assuming standard HR) is shorter than the age of the universe, and the implication from a modified evaporating rate becomes relevant. A pictorial representation of the evolution of a BH and its remnant is shown in fig. 1.1.

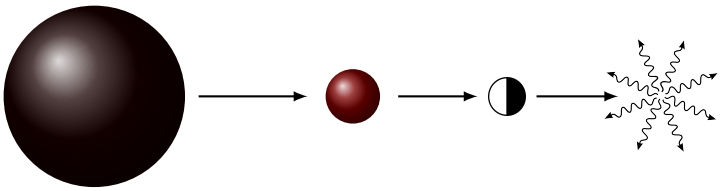

Figure 1.1: Pictorial representation of the evolution of a BH and its remnant. Once formed and in the vacuum, the BH starts evaporating, emitting particles with a (quasi-)thermal spectrum, here represented by the red ball. Once the BH reaches a minimal mass, it stops evaporating and becomes a remnant, here represented by the black-and-white ball. Eventually, the remnant too evaporates.

1.3 Approach and objectives

Cosmologies with remnants are nontrivial to study, as several effects must be taken into account. Additional injection of radiation and Standard Model species from PBH evaporation can significantly modify the cosmic energy budget: in particular, if today's radiation were sourced predominantly by Hawking radiation, then PBHs (or their remnants) would necessarily have induced an early matter-dominated era.

We develop a modular, general framework to track PBH formation and evaporation under LQG and MB prescriptions, exploring multiple viable cosmological histories. The framework is semi-analytical and implemented in `Mathematica`.
Given the initial mass of the PBHs (and theory parameters), we evolve the energy densities of species present in the model and allow the PBHs to evaporate. By requiring that the energy density of the PBH remnants at the present time accounts for the total DM energy density while also recovering the contemporary energy density of photons and baryonic matter, we obtain constraints on the initial mass of the PBHs and the parameters of the theory. We find that these requirements cannot always be satisfied simultaneously, so that some initial masses and parameters are excluded and new constraints on the initial PBH abundance as a function of mass and model parameters are derived.
In addition to the initial objective of this master's thesis, we use the `BlackHawk` code [Arbey and Auffinger, 2019, 2021] to obtain a quantitative picture of Hawking radiation and more precise cosmological histories.

1.4 Summary of methodology and results

We build a modular semi-analytical model in `Mathematica` that evolves the energy densities of the components of the universe, including PBHs, their remnants, and decay products. We start after inflation ends and assume a monochromatic distribution of PBHs with a given initial mass m^i_{PBH}. We then evolve their mass and number densities through the radiation, matter and dark-energy dominated eras. Both the evaporation of the PBHs and the transition from semiclassical regime to the Quantum Gravity (**QG**) regime are assumed to be instantaneous. The model is run for different values of initial PBH masses and theory parameters. From this, we extract the fraction of DM accounted for by PBH remnants.
In addition to the numerical results, we also derive analytical expressions for the initial conditions of the energy densities of the species present in the model.

We find that the fraction of DM that can be accounted for by PBH remnants increases as the initial PBH mass decreases (i.e., it is a decreasing function of initial mass). For large initial masses, the energy injected in the universe by their evaporation is also large, constraining the number density of PBHs. For small initial masses, less energy is injected and the lifetime is shorter (evaporation occurs earlier), which facilitates thermalization of the decay products.

1.5 Thesis outline

This master's thesis is structured as follows: chapter 2 provides an overview of standard cosmology, establishing the framework for the rest of the thesis. The standard cosmological model is reviewed, as well as the physics of the early universe and how quantum perturbations evolve throughout the history of the universe.

Chapter 3 reviews BH physics, starting with the Schwarzschild solution and going through the various extensions and coordinate transformations, allowing to introduce the conformal diagram of a Schwarzschild BH. We then review the semiclassical treatment of BHs, including a quantitative and qualitative description of Hawking radiation, and its implications for the lifetime of BHs.
Chapter 4 discusses PBH formation and the existing constraints on their abundance, focusing on the one from evaporating PBHs.
In chapter 5, a brief introduction to loop quantum gravity and how it modifies BH evaporation is given. We do not cover the full theory, but rather give some of the main results that are relevant for our work, such as the existence of a minimal area and the formation of planckian remnants.
Chapter 6 introduces the memory burden effect through a qualitative toy model, its connection to BHs, and how it modifies BH evaporation. We also review some of the phenomenological consequences of the MBe for PBHs.

Chapters 2 to 6 review existing results rather than present new ones. Because the theories are technically involved and in places still developing, we adopt a *"simplest but nontrivial"* policy: we present minimal models that already display the essential mechanisms and omit inessential technicalities. When helpful, ideas are illustrated in simplified or analogous settings before indicating how they extend to the full theory. A significant part of the work consisted of synthesizing material scattered across different topics, frameworks, and notational conventions, and harmonizing them into a coherent narrative with consistent assumptions.

The original content of this thesis starts in chapter 7, where we present our semi-analytical model for PBH evolution, including the LQG and MBe effects. We go through the several steps of the model, from the initial conditions to the final results. We also discuss the limitations of our model and the assumptions.
The results are presented in chapter 8, where we first present pedagogical case studies before turning to the general results.
We conclude in chapter 9 with a discussion of the findings and possible future work.

CHAPTER

2

OVERVIEW OF COSMOLOGY

Chapter 2 assembles some basic concepts of cosmology that the rest of this thesis will rely on. All results are standard: when a derivation serves a purpose, we provide it, otherwise we cite the result from the literature. This chapter is based on [Baumann, 2022; Peter and Uzan, 2013] for the general introduction, and the inflation part is inspired by [Baumann, 2011; Byrnes and Cole, 2021].

Starting from Friedmann-Lemaître-Robertson-Walker metric and Einstein's field equations, the Friedmann and continuity equations (sec. 2.1) are derived. We then restate the main issues with the Hot Big Bang cosmology and motivate a single field slow-roll inflationary model (sec. 2.2). Linear perturbation theory is introduced, and the power spectrum of the perturbations is computed (sec. 2.3).

This chapter provides useful relations for the chapter 4 and chapter 7.

2.1 Standard Cosmological Model

This section reviews the *background* (homogeneous and isotropic) cosmological model. We start from the metric formulation of General Relativity (see sec. 5.1 for more modern formulations) and re-derive the Friedmann equations (eq. (F1) and eq. (F2)). The conservation of the stress-energy tensor leads to the continuity equation (eq. (2.6)), which is used to derive the evolution of the energy density of different components (eq. (2.9)). Finally, we solve the Friedmann equations for a flat universe with a single component (eq. (2.17)).

2.1.1 The expanding universe

Supposing a spatially homogeneous and isotropic universe, the metric $g_{\mu\nu}$ takes a simpler form.

Definition 2.1. The Friedmann-Lemaître-Robertson-Walker metric (**FLRW**) can be defined in polar coordinates as:

$$\mathrm{d}s^2 = -\mathrm{d}t^2 + a^2(t)\left(\frac{\mathrm{d}r^2}{1-kr^2} + r^2\mathrm{d}\Omega^2\right) \tag{FLRW}$$

Where $\mathrm{d}\Omega^2 = \mathrm{d}\theta^2 + \sin^2\theta\mathrm{d}\phi^2$ is the metric on S^2 the 2-sphere and $k \in \{-1, 0, 1\}$.

Property 2.1. *The **redshift** z defined by $1+z = \lambda_{today}/\lambda_{emission}$ is related to the scale factor $a(t)$ by:*

$$1+z = \frac{a(t_{today})}{a(t_{emission})} \tag{2.1}$$

One can reformulate eq. (FLRW) by introducing a change of variable.

Definition 2.2. The **conformal time** η is defined as:

$$\mathrm{d}\eta = \frac{\mathrm{d}t}{a(t)} \tag{2.2}$$

The **particle horizon** is the maximum distance from which we can be influenced by past events:

$$d_h = \Delta\eta = \int_0^t \frac{\mathrm{d}t'}{a(t')} \tag{2.3}$$

Setting $\mathrm{d}\chi = \frac{\mathrm{d}r}{\sqrt{1-kr^2}}$, eq. (FLRW) becomes:

$$\mathrm{d}s^2 = a^2(\eta)\left(-\mathrm{d}\eta^2 + \mathrm{d}\chi^2 + S_k^2(\chi)\mathrm{d}\Omega^2\right) \tag{2.4a}$$

Where:

$$S_k(\chi) = \begin{cases} \sinh(\chi) & \text{for } k=-1 \quad (2.4b) \\ \chi & \text{for } k=0 \quad (2.4c) \\ \sin(\chi) & \text{for } k=1 \quad (2.4d) \end{cases}$$

Equipped with this metric, one can compute the dynamics of a homogeneous and isotropic universe thanks to the theory of General Relativity (**GR**) whose dynamics are given by the Einstein Field Equations, relating the geometry of spacetime (encoded in $R_{\mu\nu}$, the Ricci curvature tensor) to the distribution of matter and energy within it (encoded in $T_{\mu\nu}$, the stress-energy tensor)[1].

Definition 2.3. The Einstein Field Equations (**EFE**) are:

$$R_{\mu\nu} - \frac{1}{2}Rg_{\mu\nu} = 8\pi T_{\mu\nu} \tag{EFE}$$

The stress-energy tensor $T^{\mu\nu}$ is conserved in GR:

$$\nabla_\alpha T^\alpha{}_\mu = 0 \tag{2.5}$$

This gives 4 equations. The evolution of the energy density corresponds to $\mu = 0$, and the non-vanishing Christoffel symbols are $\{\Gamma_j{}^j{}_0\}$. Given that $T^i{}_0 = 0$ by isotropy, one finds the following relation eq. (2.6).

Property 2.2. *The **continuity equation** of the FLRW metric is given by:*

$$\dot{\rho} + 3\frac{\dot{a}}{a}(\rho + P) = 0 \tag{2.6}$$

[1] The stress energy tensor $T_{\mu\nu}$ can be defined for any action, as done in subsec. 2.2.3.

Definition 2.4. The **equation of state parameter** ω is defined as:

$$\omega = \frac{P}{\rho} \tag{2.7}$$

Writing eq. (2.6) using eq. (2.7), and assuming a constant equation of state, one gets $\dot{\rho}/\rho = -3(1+\omega)\dot{a}/a$, so that

$$\rho \propto a^{-3(1+\omega)} \tag{2.8}$$

From eq. (2.8), one finds the evolution of the energy density as a function of the scale factor for the different types of fluids:

$$\begin{cases} \rho_{\mathrm{r}} \propto a^{-4} & \text{for radiation} \quad (2.9a) \\ \rho_{\mathrm{m}} \propto a^{-3} & \text{for matter} \quad (2.9b) \\ \rho_{\mathrm{k}} \propto a^{-2} & \text{for curvature} \quad (2.9c) \\ \rho_{\Lambda} \propto a^{0} & \text{for the cosmological constant} \quad (2.9d) \end{cases}$$

From eq. (2.9), assuming $\rho_k = 0$, one can see that the standard cosmological evolution of the universe will first undergo a Radiation Dominated (**RD**) era, followed by a Matter Dominated (**MD**) era, and finally a cosmological constant (Λ) Dominated (Λ**D**) era.
Skipping the algebra, we get two equations corresponding to the purely temporal and purely spatial part of the EFE:

Definition 2.5. The First and Second **Friedmann equations** are:

$$H^2 = \left(\frac{\dot{a}}{a}\right)^2 = \frac{8\pi}{3}\rho - \frac{k}{a^2} \tag{F1}$$

$$\frac{\ddot{a}}{a} = -\frac{4\pi}{3}(\rho + 3P) \tag{F2}$$

Where we used the **Hubble rate** H defined as:

$$H \equiv \frac{\dot{a}}{a} \tag{2.10}$$

We also define the **Conformal Hubble rate** $\mathcal{H}$ as:

$$\mathcal{H} \equiv \frac{a'}{a} = aH \tag{2.11}$$

Where the prime denotes the derivative with respect to the conformal time η (see eq. (2.2))

It is convenient to measure all densities relative to the one such that the universe is flat ($k = 0$).

Definition 2.6. The **critical density** ρ_{crit} is defined as:

$$\rho_{\mathrm{crit}} = \frac{3H^2}{8\pi G} \tag{2.12}$$

The **density parameter** Ω_A of a certain species A of energy density ρ_A is defined as:

$$\Omega_A = \left.\frac{\rho_A}{\rho_{\mathrm{crit}}}\right|_{\mathrm{today}} \tag{2.13}$$

Noticing that the universe is composed of radiation, matter, curvature and a cosmological constant (namely that $\rho = \rho_r + \rho_m + \rho_k + \rho_\Lambda$), eq. (F1) can be rewritten in the following form:

$$\frac{H^2}{H_0^2} = \Omega_r a^{-4} + \Omega_m a^{-3} + \Omega_k a^{-2} + \Omega_\Lambda \tag{2.14}$$

where we introduced the Hubble rate today H_0 and the curvature density parameter $\Omega_k = -k/H_0^2$.

Property 2.3. *Evaluating eq. (2.14) today where $a_0 = 1$ gives the constraint:*

$$1 = \Omega_r + \Omega_m + \Omega_\Lambda + \Omega_k \equiv \Omega_0 + \Omega_k \tag{2.15}$$

Let us compute some special cases of eq. (2.14) that will be useful later on. We consider a flat universe ($k = 0$) with a single type of fluid of energy density ρ_A. Since $H = \dot{a}/a = \mathrm{d}\ln(a)/\mathrm{d}t$, eq. (2.14) reduces to:

$$\frac{\mathrm{d}\ln(a)}{\mathrm{d}t} = H_0 \sqrt{\Omega_A} a^{-\frac{3}{2}(1+\omega_A)} \tag{2.16}$$

Solving eq. (2.16), one finds:

$$a(t) \propto \begin{cases} t^{2/3} & \text{for matter} \quad (2.17a) \\ t^{1/2} & \text{for radiation} \quad (2.17b) \\ e^{H_0\sqrt{\Omega_\Lambda}\cdot t} & \text{for the cosmological constant} \quad (2.17c) \end{cases}$$

2.1.2 The hot Big Bang

An important consideration for the rest of this work is the (chemical) equilibrium of species in the early universe. At early times, the neutrinos were in chemical equilibrium with the electrons through the weak nuclear interaction. The rate of weak interaction Γ_{weak} per neutrino can be approximated by:

$$\Gamma_{\text{weak}} \sim n \langle \sigma_{\text{weak}} v \rangle \sim T^3 G_{\text{F}}^2 T^2 \sim G_{\text{F}}^2 T^5 \tag{2.18}$$

Where G_{F} is Fermi's constant. Thermodynamics relates the energy density of radiation ρ_r to the temperature T by:

$$\rho_r = \frac{\pi^2}{30} g_*(T) T^4 \tag{2.19}$$

Where $g_*(T)$ is the effective number of relativistic degrees of freedom at temperature T. During RD era, $H \sim \sqrt{\rho_r} \sim T^2$, so that the condition for the neutrinos to be in equilibrium is [Baumann, 2022]:

$$\frac{\Gamma_{\text{weak}}}{H} \approx \left(\frac{T}{\text{MeV}}\right)^3 \tag{2.20}$$

The decoupling of neutrinos happens when $\Gamma_{\text{weak}}/H \lesssim 1$, which corresponds to a temperature of about $T_\nu \approx 1$ MeV or a cosmic time of $t \sim 1$ s.

The electron-positron pairs chemically equilibrate with the photons through $e^+ + e^- \leftrightarrow \gamma + \gamma$. Conservation of entropy imposes that:

$$T_\nu = \left(\frac{4}{11}\right)^{1/3} T_\gamma \tag{2.21}$$

Approximating the neutrinos as massless, the energy density of the neutrinos is related to the one of the photons by Baumann [2022]:

$$\rho_\nu \equiv C_{\nu\gamma} \rho_\gamma = \frac{7}{8} N_{\text{eff,SM}} \left(\frac{4}{11}\right)^{4/3} \rho_\gamma \tag{2.22}$$

Where $N_{\text{eff,SM}} \equiv 3.046$ is the effective number of relativistic degrees of freedom predicted by the Standard Model.
The electron-positron annihilation happens at a temperature of about $T_e \lesssim m_e \approx 0.5$ MeV, or a cosmic time of $t \approx 6$ s. Following the same type of reasoning as for the neutrinos, a whole thermal history of the universe can be constructed. We focus here on neutrinos and photons, as they are the most relevant for the rest of this work.

2.1.3 What do we observe?

Recent measurements found that the spatial curvature is compatible with a flat universe: $\Omega_k = 0.001 \pm 0.002$ [Planck, 2020]. In the following, we will assume a flat universe ($k = 0$). The other measurements of [Planck, 2020] give:

$$\begin{cases} H_0 = (67.4 \pm 0.5)\,\mathrm{km\,s^{-1}\,Mpc^{-1}} & \text{for the Hubble parameter today} \quad (2.23a) \\ \Omega_{\text{DM}} = 0.2643 \pm 0.0026 & \text{for dark matter} \quad (2.23b) \\ \Omega_b = 0.0493 \pm 0.0002 & \text{for baryonic matter} \quad (2.23c) \\ \Omega_m = 0.315 \pm 0.007 & \text{for matter} \quad (2.23d) \\ \Omega_\Lambda = 0.6847 \pm 0.0073 & \text{for Dark Energy} \quad (2.23e) \end{cases}$$

Notably, the DM is non-baryonic matter. [Planck, 2020] also gives the effective extra relativistic degrees of freedom to be $N_{\text{eff}} = 2.99 \pm 0.17$, in agreement with the Standard Model prediction. From the CMB blackbody spectrum temperature $T_0 = 2.728 \pm 0.004$ K [Fixsen, 2009], one can deduce the energy density of the photons eq. (2.19). The photons' density parameter Ω_γ today, the one of the neutrinos Ω_ν and of the total radiation Ω_r can then be estimated as [Baumann, 2022]:

$$\begin{cases} \Omega_\gamma = (5.38 \pm 0.15) \cdot 10^{-5} & \text{for photons} \quad (2.24a) \\ \Omega_r = (9.02 \pm 0.21) \cdot 10^{-5} & \text{for radiation} \quad (2.24b) \\ \Omega_\nu \approx 3.6 \cdot 10^{-5} & \text{for neutrinos} \quad (2.24c) \end{cases}$$

2.2 Early Universe Physics and the cosmological inflation

The universe's early history is reconstructed from the observations of the Cosmic Microwave Background (**CMB**) radiation ($z \sim 10^3$), and theoretical models that extrapolate the evolution of the universe back in time. The models of the Big Bang Nucleosynthesis (**BBN**) ($z \sim 10^8$) predict the formation (and the abundance) of light elements consistently with the observations [Navas et al., 2024]. By doing so, the BBN "*marks the boundary between the established and the speculative in Big Bang cosmology*" [C. Patrignani et al. (Particle Data Group), 2016]. Pushing the extrapolation earlier exposes three inconsistencies of the Hot Big-Bang model: the horizon, flatness and super-horizon correlation problems, which together motivate the introduction of a new dynamical era: *cosmic inflation*.

Inflation is kinematically defined as a period of accelerated expansion of the universe (def. 2.7), controlled by parameters (or Hubble flows) ϵ_1 and ϵ_2 (def. 2.8 and def. 2.10). This period causes the universe to grow (at least) by a factor $\sim e^{60}$. Focusing on a single scalar field, the *inflaton*, the equation of motion and the first Friedmann equation in the slow-roll approximation (equations (2.36) and (2.37)) are computed.

2.2.1 Motivations

There are three main problems caused by the Standard Cosmological Model:

1. The *Horizon Problem*:
   Why is the universe (so) homogeneous and isotropic? In particular, the variations of temperature in the CMB are very small: $\Delta T/T \sim 10^{-5}$, while points in the sky that are separated by more than 2 degrees seem (with standard cosmology) never to have been in causal contact (no thermal equilibrium possible).

2. The *Flatness Problem*:
   Why is the universe so close to being spatially flat? From eq.(2.9c), one can see that ρ_k must have been even smaller in the past.

3. *Superhorizon Correlations*:
   Even if we suppose perfect homogeneity and exact flatness for the initial conditions of the universe (thus solving both problems above), we still observe correlations in the CMB that extend to distances larger than the one that light could have traveled since the beginning of the hot Big Bang.

These three problems can be solved by a mechanism called *inflation*.

2.2.2 The inflation ...

Definition 2.7. Inflation refers to an early period in the universe's history when its expansion accelerated, namely when:

$$\ddot{a} > 0 \tag{2.25}$$

Equivalently, $\ddot{a} = \mathrm{d}/\mathrm{d}t\,(aH) > 0 \iff \mathrm{d}/\mathrm{d}t\,(aH)^{-1} < 0$: the comoving Hubble radius is shrinking during inflation. Note that:

$$\frac{\mathrm{d}}{\mathrm{d}t}\left(\frac{1}{aH}\right) = \frac{-1}{a}\left(1 + \frac{\dot{H}}{H^2}\right) < 0$$

This allows us to define a first Hubble flow, controlling that inflation actually happens. Even though the Hubble flow is not constant, it is often referred to as a *slow-roll parameter* in the literature. We will follow this convention, keeping in mind that it is not a constant parameter but rather a time-dependent function of the Hubble rate $H(t)$.

Definition 2.8. The **first Slow-Roll parameter** ϵ_1 is defined as:

$$\epsilon_1 = -\frac{\dot{H}}{H^2} \tag{2.26}$$

Property 2.4. *For inflation to happen, we need* $\epsilon_1 < 1$.

From eq. (F2), one can see that $\ddot{a} > 0$ implies that $\omega \equiv P/\rho < -1/3$. However, when working with inflation, the equation of state parameter is typically closer to $\omega \approx -1$. This corresponds to taking the limit $\epsilon_1 \to 0 \iff H \to$ constant. Doing so, the scale factor grows exponentially:

$$a(t) \propto e^{H_{\mathrm{inf}} t} \tag{2.27}$$

And we find a *de Sitter* spacetime $\mathrm{d}s^2 = -\mathrm{d}t^2 + e^{2Ht}\mathrm{d}\vec{x}^2$. Integrating $\mathrm{d}\eta$ with $a(t) = e^{Ht}$, $a(\eta)$ can be expressed as:

$$a(\eta) = -\frac{1}{H\eta} = \frac{1}{H|\eta|} \tag{2.28}$$

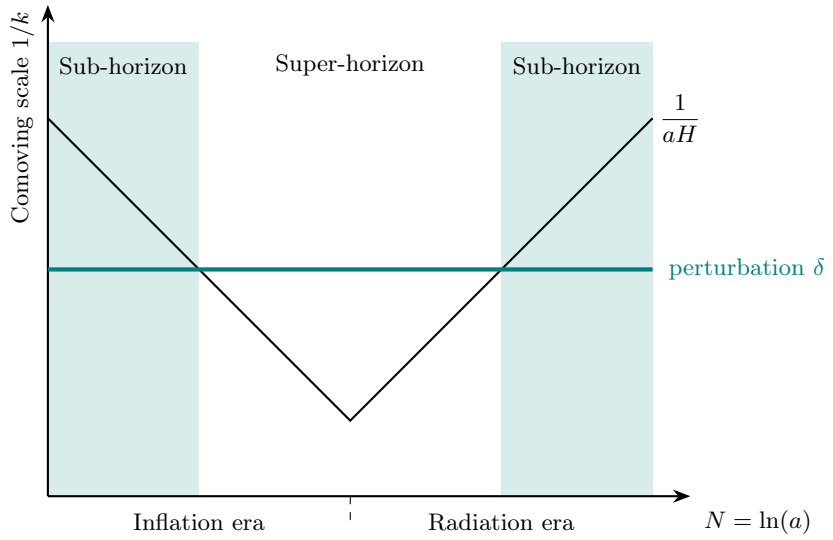

Figure 2.1: Illustration of the evolution of the comoving Hubble horizon $1/(aH)$ as a function of the number of e-folds N during the early universe. Perturbations with a constant comoving scale start inside the Hubble horizon (sub-horizon), exit it during inflation (super-horizon), and re-enter it during the radiation era.

The metric purely as a function of the conformal time reads $\mathrm{d}s^2 = (H\eta)^{-2}(-\mathrm{d}\eta^2 + \mathrm{d}\vec{x}^2)$.
A convenient measure of the growth of the universe during inflation is the number of times the universe has grown by a factor of e.

Definition 2.9. The **number of e-folds** is defined as:

$$N = \ln\left(\frac{a}{a_\star}\right) \tag{2.29}$$

Where $a_\star$ is a reference scale factor. When not specified, we take $a_\star = a_0$, the scale factor today.

During inflation, $N^{\mathrm{inf}} = \ln\left(a^{\mathrm{inf}}_{\mathrm{end}}/a^{\mathrm{inf}}_{\mathrm{initial}}\right) \sim H_{\mathrm{inf}}(t^{\mathrm{inf}}_{\mathrm{end}} - t^{\mathrm{inf}}_{\mathrm{initial}})$. For inflation to last long enough (or more practically, for the number of e-folds to be large enough), ϵ_1 must stay small long enough, so that the relative change $\mathrm{d}\epsilon_1/\epsilon_1 = \mathrm{d}\ln(\epsilon_1)$ per Hubble time H remains small. This leads to the definition of a second parameter (or Hubble flow) ϵ_2 which, when ϵ_1 is known and ϵ_2 is (almost) constant, controls the remaining length of inflation.

Definition 2.10. The **second Slow-Roll** parameter ϵ_2 is defined as:

$$\epsilon_2 = \frac{d\ln(\epsilon_1)}{dN} \tag{2.30}$$

Note that during inflation, $1/(aH) \sim 1/a$, while during the radiation domination, $a \sim t^{1/2}$ so $H \sim 1/t$ and $1/(aH) \sim t^{1/2} \sim a$. For a perturbation δ with fixed comoving scale k starting inside the Hubble horizon, inflation will stretch the perturbation outside the latter. It will then re-enter the Hubble horizon during the radiation era. Perturbations with bigger comoving wavenumber k (smaller comoving length) re-enter earlier. This is illustrated in fig. 2.1.

We need inflation to last long enough so that all the observed perturbations were once inside the particle horizon: $(a_i H_i)^{-1} > (a_0 H_0)^{-1}$. This depends on the temperature at which inflation ends (the *reheating temperature*) but a good estimate to keep in mind is that we need $N_{\mathrm{inf}} \gtrsim 60$.

2.2.3 . . . and the inflaton

Consider a scalar field ϕ (called the **inflaton**) with a potential energy $V(\phi)$ and no space dependence: $\phi = \phi(t)$. The associated action is:

$$S = \int \mathrm{d}^4x\sqrt{-g}\left(\frac{1}{2}R - \frac{1}{2}g^{\mu\nu}\partial_\mu\phi\partial_\nu\phi - V(\phi)\right) \tag{2.31}$$

One can compute the stress-energy tensor $T_{\mu\nu} = -\frac{2}{\sqrt{-g}}\frac{\delta S}{\delta g^{\mu\nu}}$ of the inflaton field:

$$T_{\mu\nu} = \partial_\mu\phi\,\partial_\nu\phi + g_{\mu\nu}\left[-\frac{1}{2}g^{\alpha\beta}\partial_\alpha\phi\,\partial_\beta\phi - V(\phi)\right] \tag{2.32}$$

and identify the terms with a perfect fluid $T_{\mu\nu} = \mathrm{diag}\,[-\rho, P, P, P]$. One finds:

$$\rho = \frac{1}{2}\dot{\phi}^2 + V(\phi) \tag{2.33}$$

$$P = \frac{1}{2}\dot{\phi}^2 - V(\phi) \tag{2.34}$$

Then, as long as $V(\phi) \gg \frac{1}{2}\dot{\phi}^2$, $\omega \approx -1$. Ignoring the spatial curvature for simplicity, the Equation Of Motion (**EOM**) is:

$$\ddot{\phi} + 3H\dot{\phi} + \partial_\phi V = 0 \tag{EOM inf}$$

Where $3H\dot{\phi}$ is called the *Hubble Friction*. The Friedmann equation is:

$$H^2 = \frac{8\pi}{3}\left(\frac{1}{2}\dot{\phi}^2 + V\right) \tag{F1 inf}$$

Eq. (EOM inf) and eq. (F1 inf) are coupled: the Friedmann equation tells the Hubble rate given the kinetic and potential energy of the field, and the EOM gives the evolution of the field where the Hubble rate acts as a friction.
The first slow-roll parameter becomes $\epsilon_1 = 4\pi\dot{\phi}^2/H^2 \sim$ (kinetic energy/potential energy).

Definition 2.11. The **Slow-Roll approximation** consists in taking the limit:

$$\begin{cases} \ddot{\phi} \ll H\dot{\phi} & \text{(2.35a)} \\ \dot{\phi}^2 \ll V & \text{(2.35b)} \end{cases}$$

Considering the slow-roll approximation simplifies eq. (EOM inf) and eq. (F1 inf):

$$\dot{\phi} \approx -\frac{\partial_\phi V}{3H} \tag{2.36}$$

$$H^2 \approx \frac{V}{3} \tag{2.37}$$

After considering the dynamics of inflation in the homogeneous universe, the next step is to look at dynamics of the linear perturbations and their generation mechanism at the quantum level. This is the subject of the next section.

2.3 Cosmological Perturbation Theory

This section, mainly following [Baumann, 2022; Scoccimarro, 2024], extends the homogeneous picture to the inhomogeneous universe by developing the *linear cosmological perturbation theory*. While the mean densities of baryons, photons, neutrinos, dark matter, ... fix the background expansion $a(t)$, *perturbations* in these densities (and in the metric itself) source the local gravitational potential and seed structures.
Since we observe only one realization of the Universe, we adopt a statistical description in which the fluctuations are modeled as a random field; invoking the ergodic hypothesis (def. 2.12) to relate spatial and ensemble averages, their basic statistics are introduced: the two-points correlation function, the power spectrum, and its dimensionless form (eq. (2.45)). The Scalar-Vector-Tensor decomposition of the metric and the energy-momentum tensor is introduced, and gauge-invariant variables are defined. The dynamics of the perturbations (derived from the linearized EFE and the conservation of the stress-energy tensor) are given (eq. (2.66) and eq. (2.68)) in the *Newtonian gauge* (eq. (2.56)).
We then focus on the inflaton perturbations governed by the *Mukhanov-Sasaki equation* (eq. (2.75)). Quantizing the theory, we find the *Bunch-Davies vacuum* (eq. (2.84)) and compute the *power spectrum* of the inflaton perturbations (eq. (2.87)) and relate it to the one of the curvature perturbations (eq. (2.88)).

2.3.1 Random fields

The observable universe is considered to be a particular realization out of a statistical ensemble of possibilities. Since we can only access one universe, we need to assume the *ergodic hypothesis*.

Definition 2.12. The **ergodic hypothesis** states that the average over the statistical ensemble is equal to the spatial average of one realization, when the volume becomes infinite.

To be concrete, let us consider a *random* scalar field $\Phi(\vec{x})$ (that is, a random variable at each point of space). The time evolution of the field can depend on the physics, so that the statistical properties of $\Phi(t_1, \vec{x})$ and $\Phi(t_2, \vec{x})$ can be related.
It is always possible to rewrite the field as a sum of its average value and a fluctuation around it:

$$\Phi(t,\vec{x}) = \int \Phi\, \mathtt{P}(\Phi)\mathcal{D}\Phi + \delta\Phi(t,\vec{x}) \tag{2.38a}$$
$$= \langle\Phi(t,\vec{x})\rangle + \delta\Phi(t,\vec{x}) \tag{2.38b}$$
$$= \langle\Phi(t,\vec{x})\rangle\,(1+\delta(t,\vec{x})) \tag{2.38c}$$

Where $\mathtt{P}(\Phi)$ is the Probability Distribution Function (**PDF**) of the field Φ, and $\mathcal{D}\Phi$ indicates that the integration is done over all possible configurations of Φ. Def. 2.12 implies that:

$$\langle\Phi(t,\vec{x})\rangle = \lim_{V\to\infty}\frac{1}{V}\int_V \Phi(t,\vec{x})\mathrm{d}^3x \equiv \bar{\Phi}(t) \tag{2.39}$$

For a statistically homogeneous and isotropic field, correlation functions must be invariant under translation and rotation: it can only depend on $r = \|\vec{r}\| = \|\vec{x}-\vec{x}'\|$. After defining $\delta(\vec{k})$ as the Fourier transform of $\delta(\vec{x})$, the equal time correlation function is defined as:

$$\left\langle\delta(\vec{k})\delta(\vec{k}')\right\rangle = \int \mathrm{d}^3x\,\mathrm{d}^3x' e^{-i(\vec{k}\cdot\vec{x}+\vec{k}'\cdot\vec{x}')}\,\langle\delta(\vec{x})\delta(\vec{x}')\rangle \tag{2.40a}$$
$$= (2\pi)^3\delta_D(\vec{k}+\vec{k}')\int \mathrm{d}^3r e^{-i\vec{k}\cdot\vec{r}}\,\langle\delta(\vec{x})\delta(\vec{x}+\vec{r})\rangle \tag{2.40b}$$

Definition 2.13. The **power spectrum** is the Fourier transform of the correlation function:

$$\mathcal{P}_\delta(k) = \int \mathrm{d}^3r\, e^{-i\vec{k}\cdot\vec{r}}\,\langle\delta(\vec{x})\delta(\vec{x}+\vec{r})\rangle \tag{2.41}$$

The dimension of $\mathcal{P}_\delta(k)$ is [length]^3, so a more physical measure of the amplitudes of the perturbations is to consider the dimensionless power spectrum.

Definition 2.14. The **dimensionless power spectrum** is defined as:

$$\Delta^2_\delta(k) = \frac{k^3}{2\pi^2}\mathcal{P}_\delta(k) \tag{2.42}$$

Let us parametrize the power spectrum in terms of a power law.

Definition 2.15. Writing the power spectrum as:

$$\mathcal{P}_\delta(k) \approx A_s \left(\frac{k}{k_0}\right)^{n_s} \tag{2.43}$$

We introduced the (scalar) **amplitude** A_s and the (scalar) **spectral index** n_s and the amplitude A of the power spectrum.

The spectral index n_s can be obtained by taking the logarithm of the power spectrum and differentiating with respect to $\ln(k)$:

$$n_s = \frac{\mathrm{d}\ln(\mathcal{P}_\delta(k))}{\mathrm{d}\ln(k)} \tag{2.44}$$

Definition 2.16. A random field Φ with a spectral index n_s such that $\Delta^2_\Phi(k) \propto$ constant is said to have a **scale-invariant spectrum**.

For a field Φ satisfying a Poisson equation ($k^2\Phi \sim \delta$), $\mathcal{P}_\Phi(k) \sim k^{-4}\mathcal{P}_\delta(k) \sim k^{n_s-4}$. The dimensionless power spectrum thus follows $\Delta^2_\Phi(k) \sim k^{n_s-1}$ and the scale invariance condition becomes $n_s = 1$. From def. 2.15, the parametrization for the dimensionless power spectrum reads:

$$\Delta^2_\Phi(k) = A_s \left(\frac{k}{k_0}\right)^{n_s-1} \tag{2.45}$$

Definition 2.17. A random gaussian field δ has the following PDF:

$$\mathtt{P}_G(\delta) = \frac{1}{\sqrt{2\pi\sigma^2}} \exp\left(-\frac{1}{2}\frac{\delta^2}{\sigma^2}\right) \tag{2.46}$$

Where $\sigma^2 = \langle\delta^2\rangle$ is the variance of the field.

Since the PDF of a gaussian field only depends on the second moment, all the information about the field is contained in the two-point correlation function (or the power spectrum).

2.3.2 Linear perturbations

The goal of this section is to compute the power spectrum of the perturbations.
In general, the perturbations of the metric and of the stress-energy tensor can be written as:

$$g^{(1)}{}_{\mu\nu} = \bar{g}_{\mu\nu} + \delta g_{\mu\nu}(t,\vec{x}) \tag{2.47}$$

$$T^{(1)}{}_{\mu\nu} = \bar{T}_{\mu\nu} + \delta T_{\mu\nu}(t,\vec{x}) \tag{2.48}$$

Where the superscript (1) indicates that we are working at linear order in the perturbations.

2.3.2.A Metric perturbation

The background metric $\bar{g}_{\mu\nu}$ is taken to be eq. (FLRW) metric written in coordinates $(\eta, \vec{x})$ where η is the conformal time defined in eq. (2.2) so that the metric is conformally flat (as done already in eq. (2.4)):

$$\mathrm{d}s^2 = a^2(\eta)\left[-\mathrm{d}\eta^2 + \delta_{ij}\,\mathrm{d}x^i\,\mathrm{d}x^j\right] \tag{2.49}$$

Following the convention of [Baumann, 2022], the perturbed metric reads:

$$\mathrm{d}s^2 = a^2(\eta)\left[-(1+2A)\,\mathrm{d}\eta^2 + 2B_i\,\mathrm{d}\eta\,\mathrm{d}x^i + (\delta_{ij}+2E_{ij})\,\mathrm{d}x^i\,\mathrm{d}x^j\right] \tag{2.50}$$

Using the Scalar-Vector-Tensor (**SVT**) decomposition on the metric, eq. (2.50) can be rewritten as

$$g^{(1)}{}_{\mu\nu} = a^2(\eta)\left\{\left(\begin{array}{c|c} -1 & 0 \\ \hline 0 & \mathbb{1}_3 \end{array}\right) + \left(\begin{array}{c|c} -2A & B_j \\ \hline B_i & 2E_{ij} \end{array}\right)\right\} \tag{2.51a}$$

$$= a^2(\eta)\left(\begin{array}{c|c} -(1+2A) & \overbrace{\partial_j B}^{\text{scalar}} + \overbrace{\hat{B}_j}^{\text{vector}} \\ \hline \underbrace{\partial_i B}_{\text{scalar}} + \underbrace{\hat{B}_i}_{\text{vector}} & \delta_{ij} + 2\left(\underbrace{C\delta_{ij} + \partial_{\langle i}\partial_{j\rangle}E}_{\text{scalar}} + \underbrace{\partial_{(i}\hat{E}_{j)}}_{\text{vector}} + \underbrace{\hat{E}_{ij}}_{\text{tensor}}\right) \end{array}\right) \tag{2.51b}$$

Where we used the following notations:

$$\partial_{\langle i}\partial_{j\rangle} \equiv \partial_i\partial_j - \frac{1}{3}\delta_{ij}\nabla^2 \tag{2.52}$$

$$\partial_{(i}\hat{E}_{j)} \equiv \frac{1}{2}\left(\partial_i\hat{E}_j + \partial_j\hat{E}_i\right) \tag{2.53}$$

And where the following constraints are respected:

$$\partial_i\hat{E}^i = 0 \text{ and } \partial_i\hat{B}^i = 0 \tag{2.54}$$

$$\partial_i\hat{E}^{ij} = 0 \text{ and } \hat{E}^i{}_i = 0 \tag{2.55}$$

Property 2.5. *At linear order, the EFE for scalars, vectors and tensors are independent.*

Since an arbitrary foliation of spacetime was picked, these perturbations transform under change of coordinates. To extract the physical perturbation from eq. (2.50), one can either construct gauge independent variables (sometimes referred to as *Bardeen variables*) or fix the gauge and keep track of all the perturbations. Two gauges will be useful for us later on.

Definition 2.18. The **Newtonian gauge** is defined by the conditions:

$$B = 0 \text{ and } E = 0 \tag{2.56}$$

The **Spatially Flat gauge** is defined by the conditions:

$$C = 0 \text{ and } E = 0 \tag{2.57}$$

2.3.2.B Stress-energy tensor perturbation

Using the same foliation, we write the SVT decomposition of the perturbed stress energy tensor as:

$$T^{(1)}{}_{\mu\nu} = \left(\begin{array}{c|c} -\bar{\rho} & 0 \\ \hline 0 & \bar{P}\,\mathbb{1}_3 \end{array}\right) + \left(\begin{array}{c|c} -\delta\rho & -q_j \\ \hline -q_i & \delta P \cdot \delta_{ij} + \Pi_{ij} \end{array}\right) \tag{2.58a}$$

$$= \left(\begin{array}{c|c} -(\bar{\rho}+\delta\rho) & -(\overbrace{\partial_j q}^{\text{scalar}} + \overbrace{\hat{q}_j}^{\text{vector}}) \\ \hline -(\underbrace{\partial_i q}_{\text{scalar}} + \underbrace{\hat{q}_i}_{\text{vector}}) & (\bar{P}+\underbrace{\delta P}_{\text{scalar}})\delta_{ij} + \underbrace{\partial_{<i}\partial_{j>}\Pi}_{\text{scalar}} + \underbrace{\partial_{(i}\hat{\Pi}_{j)}}_{\text{vector}} + \underbrace{\hat{\Pi}_{ij}}_{\text{tensor}} \end{array}\right) \tag{2.58b}$$

Where we used the following notation:

$$q_i \equiv (\bar{\rho}+\bar{P})v_i \tag{2.59}$$

And the SVT decomposition of v_i is naturally defined as $v_i = \partial_i v + \hat{v}_i$. The following constraints are respected:

$$\partial_i \hat{q}^i = 0 \tag{2.60}$$

$$\partial_i \hat{\Pi}^i = 0 \tag{2.61}$$

$$\partial_i \hat{\Pi}^{ij} = 0 \text{ and } \Pi^i{}_i = 0 \tag{2.62}$$

Definition 2.19. We call v^i the **bulk velocity**, q^i the **momentum density** and Π_{ij} the **anisotropic stress**.

As for the metric perturbation, one can either find the gauge invariant perturbations of the stress-energy tensor[2] (sometimes referred to as *comoving density contrast*, the *uniform density curvature perturbation* and the *comoving curvature perturbation*) or fix the gauge and keep track of all the perturbations. More details can be found in [Baumann, 2022]. Let us briefly introduce two important variables for what follows.

Definition 2.20. The **curvature perturbations** are defined as:

$$\zeta = -C + \frac{1}{3}\nabla^2 E + \mathcal{H}\frac{\delta\rho}{\bar{\rho}'} \tag{2.63}$$

$$\mathcal{R} = -C + \frac{1}{3}\nabla^2 E - \mathcal{H}(v+B) \tag{2.64}$$

In the newtonian gauge, they reduce to $\zeta = -C + \mathcal{H}\delta\rho/\bar{\rho}'$ and $\mathcal{R} = -C - \mathcal{H}v$. Outside the Hubble horizon, both curvature perturbations are the same for adiabatic modes.

2.3.2.C Dynamics of the perturbations

The dynamics of the perturbations are given by two sets of equations: the conservation of the stress-energy tensor eq. (2.5) and the Einstein equations (EFE). Although the linearized Einstein equations decouple into scalar, vector and tensor sectors, the conservation of the stress-energy tensor re-couples all perturbations, even though the Christoffel symbols themselves (used in the covariant derivative) can be computed within each sector.

The computation of the dynamics of the perturbations is quite lengthy (and can be found in chapter 6 of [Baumann, 2022]), so we will only give the final results for a fluid without anisotropic stress ($\Pi_{ij} = 0$). Let us first highlight an important quantity that will be crucial in chapter 4:

[2] These variables are actually built from both metric perturbations and stress-energy tensor perturbations.

Definition 2.21. The density contrast δ is defined as the ratio of the perturbation of the density ρ to the background density $\bar{\rho}$:

$$\delta = \frac{\delta\rho}{\bar{\rho}} \tag{2.65}$$

In the newtonian gauge eq. (2.56), the EFE reads:

$$\begin{cases} \nabla^2 C + 3\mathcal{H}(\mathcal{H}A - C') = -4\pi a^2 \delta\rho & [G_{00}] & \text{(2.66a)} \\ (C' - \mathcal{H}A) = 4\pi a^2(\bar{\rho} + \bar{P})v & [G_{0i}] & \text{(2.66b)} \\ C + A = 0 & [G_{ij},\ G^i{}_i = 0] & \text{(2.66c)} \\ C'' + 3\mathcal{H}C' - \left(2\mathcal{H} + \mathcal{H}^2\right) C = -4\pi a^2 \delta P & [G_{ij},\ G^i{}_i \neq 0] & \text{(2.66d)} \end{cases}$$

The first two equations can be combined to give the *Relativistic Poisson equation*:

$$\nabla^2 C = -4\pi a^2 \bar{\rho} \left(\delta + \frac{\bar{\rho}'}{\bar{\rho}}\right) \tag{2.67}$$

The conservation of the stress-energy tensor gives:

$$\begin{cases} \delta' = -(1+\omega)\left(\partial_i v^i + 3C'\right) - 3\mathcal{H}(c_s^2 - \omega)\delta & \text{(2.68a)} \\ v'^i = \mathcal{H}(3\omega - 1)v^i - \dfrac{c_s^2}{1+\omega}\partial^i\delta + \partial^i C & \text{(2.68b)} \end{cases}$$

Where $c_s^2 = \delta P/\delta\rho$ is the sound speed of the fluid and $\omega = \bar{P}/\bar{\rho}$ is the equation of state parameter taken on the background. From eq. (2.67), going in Fourier space and inserting eq. (F1), one gets at perturbation order:

$$\delta = \frac{2}{3}\left(\frac{k}{aH}\right)^2 C \tag{2.69}$$

Using the property that in a universe dominated by a fluid with constant equation of state ω, the superhorizon limit of the comoving curvature perturbation is related to C (in newtonian gauge eq. (2.56)) by [Baumann, 2022]:

$$\mathcal{R} = \frac{5 + 3\omega}{3 + 3\omega} C \tag{2.70}$$

That limit in a radiation dominated universe ($\omega = 1/3$) gives $\mathcal{R} = (3/2)C$. Inserting this result above, one finds that the comoving curvature perturbation is related to the density perturbation by:

$$\delta = \frac{4}{9}\left(\frac{k}{aH}\right)^2 \mathcal{R} \tag{2.71}$$

Eq. (2.71) is a crucial relation that will be used in chapter 4 to relate the power spectrum of the curvature perturbation to the one of the density perturbation.

2.3.3 Inflationary perturbations

To compute the perturbations generated during inflation, let us place ourselves in another gauge, the spatially flat gauge eq. (2.57). We consider the perturbed FLRW metric given by eq. (2.50) for the scalar perturbations:

$$g^{(1,SF)}{}_{\mu\nu} = a^2(\eta) \left(\begin{array}{c|c} -(1+2A) & \partial_j B \\ \hline \partial_i B & \delta_{ij} \end{array}\right) \tag{2.72}$$

So that the inverse metric is given by:

$$g^{(1,SF)\mu\nu} = \frac{1}{a^2(\eta)} \left(\begin{array}{c|c} (1-2A) & \partial^j B \\ \hline \partial^i B & \delta^{ij} \end{array}\right) \tag{2.73}$$

Equations of motion

Varying the action eq. (2.31) with respect to ϕ gives the Klein-Gordon equation for the inflaton field:

$$\frac{1}{\sqrt{-g}}\partial_\mu\left(\sqrt{-g}\,g^{\mu\nu}\partial_\nu\phi\right) - \partial_\phi V(\phi) = 0 \tag{2.74}$$

At first order in perturbation of ϕ and using EFE to express the metric perturbation in terms of $\delta\phi$, the following equation can be derived[3]:

Property 2.6. *The **Mukhanov-Sasaki equation** is given by*

$$f'' + \left(k^2 - \frac{z''}{z}\right) f = 0 \tag{2.75a}$$

$$\text{with } z \equiv \frac{a\bar{\phi}'}{\mathcal{H}} \tag{2.75b}$$

$$\text{and } f \equiv a\delta\phi \tag{2.75c}$$

Eq. (2.75) is the equation of a harmonic oscillator with a time dependent frequency $\omega(\eta, k)$:

$$\omega^2(\eta, k) = k^2 - \frac{z''}{z} \tag{2.76}$$

Clearly, eq. (2.75) simplifies to two regimes:

$$\begin{cases} f'' + k^2 f = 0 & \text{subhorizon } \left(k^2 \gg |z''/z|\right) \quad (2.77a) \\ f'' - \dfrac{z''}{z} f = 0 & \text{superhorizon } \left(k^2 \ll |z''/z|\right) \quad (2.77b) \end{cases}$$

In the subhorizon regime, the solutions are $f \sim e^{\pm ik\eta}$ while on the superhorizon regime, there are growing mode solutions $f \sim z$ and decaying solutions $f \sim 1/z^2$.
In the spatially flat gauge, the comoving curvature perturbation eq. (2.64) reduces to $\mathcal{R} = -\mathcal{H}(v + B)$. Now, v was defined in eq. (2.59) in the SVT decomposition of the stress-energy tensor. Starting from eq. (2.32), one can show that $v + B = -\delta\phi/\bar{\phi}'$ so that:

$$\mathcal{R} = \frac{\mathcal{H}}{\bar{\phi}'}\delta\phi = \frac{f}{z} \tag{2.78}$$

Property 2.7. *The growing mode solution $f \sim z$ correspond to a frozen curvature perturbation on superhorizon scale:*

$$\mathcal{R} \overset{k\ll\mathcal{H}}{\longrightarrow} \text{constant} \tag{2.79}$$

Property 2.7 shows that the curvature perturbation is frozen on superhorizon scales.

2.3.4 Quantum fluctuations

To quantize the theory, eq. (2.75) needs to be derived from an action. Fixing normalization to obtain the right asymptotic behavior, we consider:

$$S^{\text{MS}} = \frac{1}{2}\int \mathrm{d}\eta\, d^3x\, \left((f')^2 - (\nabla f)^2 + \frac{z''}{z} f^2\right) \tag{2.80}$$

To simplify the procedure, we work in the slow-roll approximation in which $z''/z \approx 2/\eta^2$. The field $f(\eta, \vec{x})$ is quantized by imposing equal-time commutation relations between the field and its conjugate momentum $\pi = \delta S^{\text{MS}}/\delta f' = f'$:

$$\left[\hat{f}(\eta, \vec{x}), \hat{\pi}(\eta, \vec{x})\right] = i\delta_D(\vec{x} - \vec{x}') \tag{2.81}$$

[3]Derivation can be found in the chapter 8 of [Baumann, 2022] and in [Kim, 2017].

The operator can be expanded as:

$$\hat{f}(\eta,\vec{x}) = \int \frac{\mathrm{d}^3k}{(2\pi)^3}\left(e^{i\vec{k}\cdot\vec{x}}f_k(\eta)\hat{a}_{\vec{k}} + e^{-i\vec{k}\cdot\vec{x}}f_k^*(\eta)\hat{a}_{\vec{k}}^\dagger\right) \tag{2.82}$$

With the creation and annihilation operators satisfying the commutation relations:

$$\left[\hat{a}_{\vec{k}}, \hat{a}_{\vec{k}'}^\dagger\right] = (2\pi)^3\delta_D(\vec{k}-\vec{k}') \tag{2.83}$$

We want to find the variance of the operator $\hat{f}(\eta,\vec{x})$ in the vacuum state $|0\rangle$. We choose the vacuum state to be the ground state *at the beginning of inflation* when $\eta \to -\infty$. With the right normalization of $f_k(\eta)$ to obtain eq. (2.83) and by minimizing the vacuum expectation value of the Hamiltonian $\langle\hat{H}\rangle$, we find an initial condition of $f(\eta,\vec{x})$ when $\eta\to-\infty$. Solving eq. (2.75) with this asymptotic boundary condition gives a unique mode function $f_k(\eta)$ called the *Bunch-Davies mode function*.

Definition 2.22. The **Bunch-Davies mode function** is given by:

$$f_k(\eta) = \frac{1}{\sqrt{2k}}\left(1-\frac{i}{k\eta}\right)e^{-ik\eta} \tag{2.84}$$

Remark. Finding the (physical) vacuum state in a theory with time-dependent Hamiltonian is related to the QFT in curved spacetime. A short introduction to this topic is covered in sec. 3.2, where the time dependence is put in the annihilation operator $\hat{a}_{\vec{k}}(\eta)$ instead.

When the operator $\hat{f}(\eta,\vec{x})$ is expanded using the Bunch-Davies mode function, the corresponding vacuum state $|0\rangle$ (such that $\hat{a}_{\vec{k}}|0\rangle_{\text{BD}} = 0$) is called the *Bunch-Davies vacuum*. Note that $\langle\hat{\delta\phi}\rangle = {}_{\text{BD}}\langle 0|\,\hat{\delta\phi}\,|0\rangle_{\text{BD}} = 0$ but:

$$\left\langle|\hat{f}|^2\right\rangle = \int \frac{\mathrm{d}^3k\mathrm{d}^3p}{(2\pi)^6}f_k(\eta)f_p^*(\eta)\,{}_{\text{BD}}\langle 0|\left[\hat{a}_{\vec{k}},\hat{a}_{-\vec{p}}\right]|0\rangle_{\text{BD}} \tag{2.85a}$$

$$= \int \frac{\mathrm{d}^3k}{(2\pi)^3}\left|f_k(\eta)\right|^2 \tag{2.85b}$$

$$= \int \mathrm{d}\ln(k)\frac{k^3}{2\pi^2}\left|f_k(\eta)\right|^2 \tag{2.85c}$$

$$= \int \mathrm{d}\ln(k)\Delta_f^2(k,\eta) \tag{2.85d}$$

$$= \int \mathrm{d}\ln(k)a^2\Delta_{\delta\phi}^2(k,\eta) \tag{2.85e}$$

Now, using eq. (2.84) and eq. (2.28), the dimensionless power spectrum becomes

$$\Delta_{\delta\phi}^2(k,\eta) = (H\eta)^2\frac{1}{2k}\frac{k^3}{2\pi^2}\left(1+\frac{1}{k^2\eta^2}\right) \tag{2.86a}$$

$$= \left(\frac{H}{2\pi}\right)^2\left((k\eta)^2+1\right) \tag{2.86b}$$

Taking the superhorizon limit $\lambda_{\text{phys}}/H^{-1} \sim k\eta \to 0$, we find that the power spectrum is scale invariant. To implement the time dependence of the Hubble parameter, the power spectrum is evaluated at horizon crossing $k = aH(t)$:

$$\Delta_{\delta\phi}^2(k) \approx \left(\frac{H}{2\pi}\right)^2\Bigg|_{k=aH(t)} \tag{2.87}$$

2.3.5 Primordial curvature power spectrum and relevance for PBH formation

From eq. (2.78) and using the expression of the first slow-roll parameter in terms of ϕ derived in subsec. 2.2.3, the power spectrum of the curvature perturbation can be written as:

$$\Delta^2_{\mathcal{R}}(k) = \left(\frac{H}{\dot{\phi}}\right)^2 \Delta^2_{\delta\phi}(k) \tag{2.88a}$$

$$= \frac{1}{\pi}\frac{H^2}{\epsilon_1}\bigg|_{k=aH(t)} \tag{2.88b}$$

Parametrizing the power spectrum as in def. 2.15, recent results find [Planck, 2020]:

$$A_s = \left(2.101^{+0.031}_{-0.034}\right)\cdot 10^{-9} \text{ and } n_s = 0.9649 \pm 0.0042 \tag{2.89}$$

These quantities are related to the slow-roll parameters evaluated when the reference scale k_0 is crossing the horizon. In [Planck, 2020], the reference scale is taken to be $k_0 = 0.05$ Mpc^{-1}.

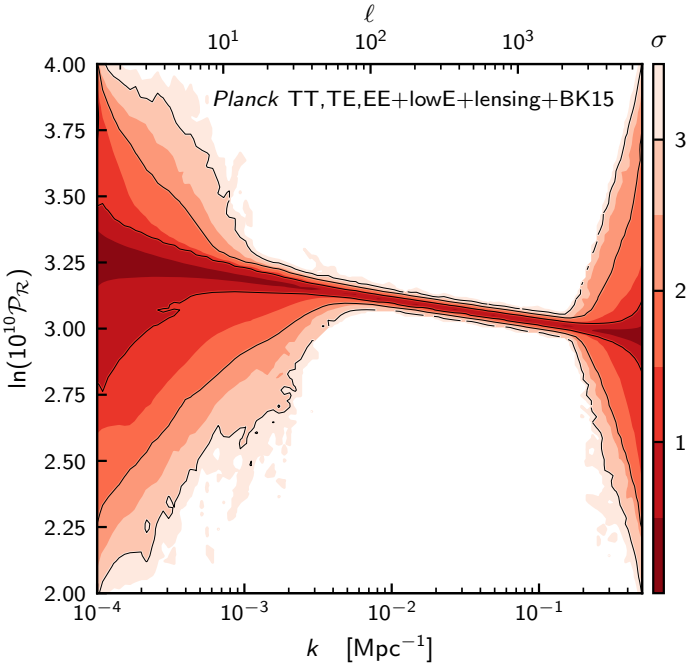

Figure 2.2: Reconstruction of the primordial scalar power spectrum from [Akrami et al., 2020]. The slope of the power spectrum comes from the spectral index n_s not being exactly 1: the power spectrum is slightly red-tilted ($n_s < 1$). Pay attention to the notation: their $\mathcal{P}_{\mathcal{R}}$ is our $\Delta^2_{\mathcal{R}}$.

As illustrated in fig. 2.2, the primordial power spectrum is nearly scale invariant, with a slight red tilt. Planck data tightly constrain both A_s and n_s on cosmological scales ($k \sim 10^{-2}$-10^{-1} Mpc^{-1}), but leave much smaller scales ($k \gg 1$ Mpc^{-1}) unconstrained.
On those scales, huge enhancements of the primordial power spectrum are possible, and could even lead to order one fluctuations, large enough to seed PBHs formation.

From eq. (2.88), one also sees that a transient suppression of Hubble flow $\epsilon_1 \to 0$ leads to a peak in the power spectrum $\Delta^2_{\mathcal{R}}$. Such conditions are realized, for instance, with potentials having a *near inflection point* leading to a so-called ultra-slow-roll phase, where the inflaton field slows down. Several formation mechanisms of PBHs include such a phase, such as the critical Higgs inflation, or the two-stage models [Bagui et al., 2023].

CHAPTER

3

BLACK HOLES

This chapter 3, based on [Misner, 1957; Chrusciel, 2023; Mukhanov and Winitzki, 2007], introduces the geometry of black holes and their quantum-mechanical instabilities. The first part (sec. 3.1) is devoted to the classical description of BHs, while the second part (sec. 3.2) explores their dissipative aspects.

Sec. 3.1 reviews the main extensions of the Schwarzschild geometry and introduces the useful *conformal* diagrams. The second part (sec. 3.2) derives the Hawking and Unruh temperatures, discusses the implications of BH evaporation and provides a quantitative picture of Hawking radiation using `BlackHawk`.

3.1 Schwarzschild geometry

This section presents the simplest nontrivial solution of the EFE in vacuum: the *Schwarzschild geometry*. We first state the line element in Schwarzschild coordinates (eq. (3.1)), then discuss its uniqueness (theorem 3.1) and singularities (subsec. 3.1.2). The Kretschmann scalar is used to differentiate between coordinate and physical singularities, and several extensions of the geometry (subsec. 3.1.3) are introduced, all the way to the maximal extension of the Schwarzschild geometry (eq. 3.12) and the associated compact conformal diagram (eq. (3.16)). Finally, the case of an astrophysical BH (subsec. 3.1.5) and the geometry inside the matter distribution are briefly mentioned.

3.1.1 Schwarzschild line element

A well-known solution of the eq. (EFE) in vacuum and with $\Lambda = 0$ is the Schwarzschild metric. This metric describes the exterior spacetime of a 3-dimensional spherically symmetric, non-rotating, electrically neutral body of mass m.

Definition 3.1. The **Schwarzschild metric** in Schwarzschild coordinates (t, r, θ, ϕ) is given by:

$$\mathrm{d}s^2 \equiv -F(r)\mathrm{d}t^2 + \frac{1}{F(r)}\mathrm{d}r^2 + r^2\left(\mathrm{d}\theta^2 + \sin^2(\theta)\mathrm{d}\phi^2\right) \tag{3.1a}$$

Where:

$$F(r) = \left(1 - \frac{2m}{r}\right) \tag{3.1b}$$

One can write the metric of the unit 2-sphere more compactly as $\mathrm{d}\Omega^2 = \mathrm{d}\theta^2 + \sin^2(\theta)\mathrm{d}\phi^2$. The radius of a Schwarzschild BH of mass m is:

$$r = 2m = \frac{2G}{c^2}m \tag{3.2}$$

The importance of the Schwarzschild geometry is highlighted by the *Birkhoff theorem*[1]. This theorem will reappear when we discuss the evolution of BHs within the framework of LQG in subsec. 5.3.2.

Theorem 3.1. ***Birkhoff theorem***
Let the geometry of a given region of spacetime be spherically symmetric and a solution to the Einstein field equations in vacuum. Then that geometry is necessarily a piece of the Schwarzschild geometry.

3.1.2 The singularity

The metric eq. (3.1) diverges in two sets: $\{r = 0\}$ and $\{r = 2m\}$. To differentiate between a physical singularity and a mere coordinate singularity, one can use scalar invariants to compute invariant (physical) quantities.

Definition 3.2. The **Kretschmann scalar** is defined as:

$$K \equiv R_{\alpha\beta\gamma\delta}R^{\alpha\beta\gamma\delta} \tag{3.3}$$

In the case of eq. (3.1), the Kretschmann reduces to:

$$K = \frac{48m^2}{r^6} \tag{3.4}$$

At $r \to 0$, $K \to \infty$; the curvature becomes infinite. We will address the issue later by the introduction of physics beyond General Relativity, such as loop quantum gravity (chapter 5) and the memory burden effect (chapter 6).

Note that in the metric formulation, the connection is (pictorially) $\Gamma \sim g^{-1}\partial g$ and has dimension $[\text{length}]^{-1}$. Hence, the curvature $R \sim \partial\Gamma + \Gamma^2$ has dimension $[\text{length}]^{-2}$ and the Kretschmann scalar $K \sim R^2$ has dimension $[\text{length}]^{-4}$. The energy associated to the curvature is $E \sim K^{1/4}$ and reaches Planckian values when $K \sim 1$. This is when one can expect quantum gravitational effects to become non-negligible, namely when $r \sim m^{1/3}$, which is much larger than the Planck length $r = 1$ if $m \gg 1$ in Planck units.

Regarding the behavior at $r \to 2m$, the Kretschmann scalar is not singular :$K \to \frac{3}{4}m^{-4}$. This seems to indicate a pathology related to the choice of coordinates.

3.1.3 Alternative coordinates and extensions

3.1.3.A Eddington-Finkelstein extension

Note that the line element eq. (3.1) is defined on the manifold $\{t \in \mathbb{R}, r > 2m\} \times S^2$. It can be extended to $\{t \in \mathbb{R}, r > 0\} \times S^2$ by introducing new coordinates. By letting $v = t + f(r)$ with $f(r)$ such that the singularity in g_{rr} cancels, we are left with $(f')^2 = \left(1 - \frac{2m}{r}\right)^{-2}$. Choosing the sign + gives:

$$v = t + r + 2m\log\left(\frac{r - 2m}{2m}\right) \tag{3.5}$$

[1] The formulation of theorem 3.1 is taken from [Misner et al., 1973].

$f(r)$ is sometimes referred to as the *tortoise coordinate*. The *advanced* Eddington-Finkelstein coordinate is thus defined as $v = t + f(r)$, and similarly one defines a *retarded* time coordinate $u = t - f(r)$ that reads:

$$u = t - r - 2m \log\left(\frac{r - 2m}{2m}\right) \tag{3.6}$$

One gets the following extension:

Definition 3.3. The advanced **Eddington-Finkelstein extension** is the manifold $\{v \in \mathbb{R}, r > 0\} \times S^2$ equipped with the metric:

$$\mathrm{d}s^2 = -\left(1 - \frac{2m}{r}\right)\mathrm{d}v^2 + 2\mathrm{d}v\mathrm{d}r + r^2\mathrm{d}\Omega^2 \tag{3.7a}$$

Similarly, the retarded Eddington-Finkelstein extension is the manifold $\{u \in \mathbb{R}, r > 0\} \times S^2$ equipped with the metric:

$$\mathrm{d}s^2 = -\left(1 - \frac{2m}{r}\right)\mathrm{d}u^2 - 2\mathrm{d}u\mathrm{d}r + r^2\mathrm{d}\Omega^2 \tag{3.7b}$$

Now that the geometry is extended *beyond* the Schwarzschild radius $r = 2m$, the main object of this section can be defined: the black hole.

Definition 3.4. A Black Hole (**BH**) is a region of spacetime in which observers (or signals) can enter, but can never leave it.

Property 3.2. *The region $\{0 < r < 2m\}$ of the metric 3.7a is a BH region [Chrusciel, 2023].*

Therefore, the region $\{r = 2m, v \in R\} \times S^2$ is called the *BH event horizon*. Note that the region $\{0 < r < 2m\}$ in the metric 3.7b is a *white-hole region*: the surface surrounding it $\{r = 2m, u \in R\} \times S^2$ can only be crossed by the future-directed causal curves which originate from the inside of the white hole.

3.1.3.B Kruskal-Szekeres extension

The metric 3.7a is not yet the maximal extension. A further one can be made by using both coordinates 3.5 and 3.6; namely performing $(u, r) \mapsto (u, v)$. One gets:

$$\mathrm{d}s^2 = -\left(1 - \frac{2m}{r(u,v)}\right)\mathrm{d}u\mathrm{d}v + r^2(u,v)\mathrm{d}\Omega^2 \tag{3.8}$$

Now, we introduce:

$$\begin{cases} \hat{u} = -e^{-u/4m} & \text{(3.9a)} \\ \hat{v} = e^{v/4m} & \text{(3.9b)} \end{cases}$$

The metric is now of the form:

$$\mathrm{d}s^2 = -\frac{32m^3}{r(\hat{u},\hat{v})}e^{-r(\hat{u},\hat{v})/2m}\mathrm{d}\hat{u}\,\mathrm{d}\hat{v} + r^2(\hat{u},\hat{v})\mathrm{d}\Omega^2 \tag{3.10}$$

Where $(\hat{u}, \hat{v}) \in \{\mathbb{R} | \hat{u}\hat{v} < 1\}$. For convenience, one can diagonalize the metric by introducing:

$$\begin{cases} T = \dfrac{\hat{v} - \hat{u}}{2} & \text{(3.11a)} \\ X = \dfrac{\hat{v} + \hat{u}}{2} & \text{(3.11b)} \end{cases}$$

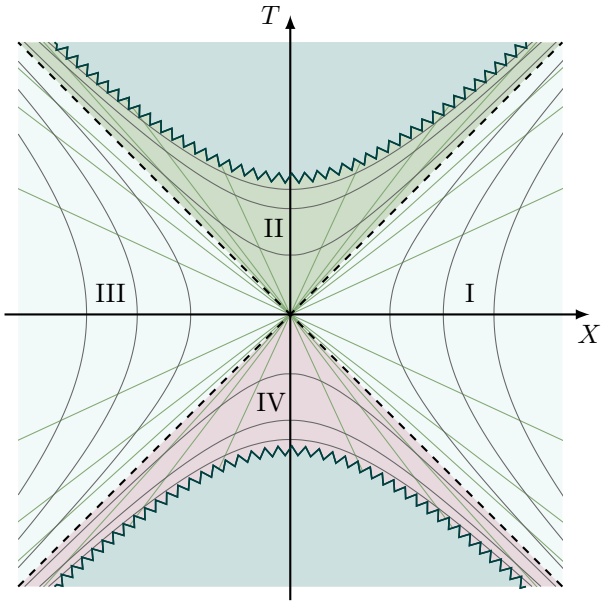

Figure 3.1: Kruskal-Szekeres diagram of a Schwarzschild BH. Adapted from [Neutelings, 2021].

Definition 3.5. The **Kruskal-Szekeres extension** is the manifold $\{(T,X) \in \mathbb{R}^2 | T^2 - X^2 < 1\} \times S^2$ equipped with the metric:

$$\mathrm{d}s^2 = \frac{32m^3 e^{-r(T,X)/2m}}{r(T,X)}(-\mathrm{d}T^2 + \mathrm{d}X^2) + r^2(T,X)\mathrm{d}\Omega^2 \tag{3.12}$$

This is the maximally extended Schwarzschild solution. It can be divided into four regions:

Property 3.3.

- *Region I:* $\{r > 2m\,,\ -X < T < X\}$*, the exterior region.*
- *Region II:* $\{r < 2m\,,\ |X| < T < \sqrt{1+X^2}\}$*, the black hole region.*
- *Region III:* $\{r > 2m\,,\ X < T < -X\}$*, the mirror exterior region.*
- *Region IV:* $\{r < 2m\,,\ -\sqrt{1+X^2} < T < -|X|\}$*, the white hole region.*

Region I corresponds to the spacetime (3.1), region I and II to (3.7a) and region I and III to (3.7b). The Kruskal-Szekeres extension of the Schwarzschild geometry is illustrated in fig. 3.1. The singularity is represented by a teal jagged line (∿∿) in the diagram. The $r =$ constant world lines are represented by a green curve (⌣) and the $t =$ constant world lines by a gray curve (⌒) . The lightcone $T = \pm X$ is represented by a dashed line (- -) .

3.1.4 Conformal Carter-Penrose Diagram

In order to make the metric easier to apprehend, one might want to be able to draw a representation of it on a finite subset of the plane, while preserving conformal properties (angles and causal structure). A way to build such a diagram is to introduce:

$$\begin{cases} \tan(\bar{u}) = \hat{u} & \text{(3.13a)} \\ \tan(\bar{v}) = \hat{v} & \text{(3.13b)} \end{cases}$$

The range of the new coordinates is $(\bar{u},\bar{v}) \in [-\pi/2, \pi/2]^2$. The metric 3.10 reads:

$$\mathrm{d}s^2 = \frac{32m}{r\cos(\bar{u})^2\cos(\bar{v})^2} e^{-r/2m}\mathrm{d}\bar{u}\mathrm{d}\bar{v} + r^2\mathrm{d}\Omega^2 \tag{3.14}$$

For convenience, one can diagonalize the metric by introducing:

$$\begin{cases} \bar{t} = \dfrac{\bar{v} + \bar{u}}{2} & \text{(3.15a)} \\ \bar{x} = \dfrac{\bar{v} - \bar{u}}{2} & \text{(3.15b)} \end{cases}$$

With range $(\bar{t}, \bar{x}) \in \{\mathbb{R}^2 | |\bar{t}| + |\bar{x}| < \pi/2\}$. The metric now reads:

$$\mathrm{d}s^2 = \frac{32m}{r\cos(\bar{u})^2\cos(\bar{v})^2} e^{-r/2m}\left(-\mathrm{d}\bar{t}^2 + \mathrm{d}\bar{x}^2\right) + r^2\mathrm{d}\Omega^2 \tag{3.16}$$

Eq. (3.16) is regular everywhere except at $r = 0$, $\cos(\bar{u}) = 0$ and $\cos(\bar{v}) = 0$.

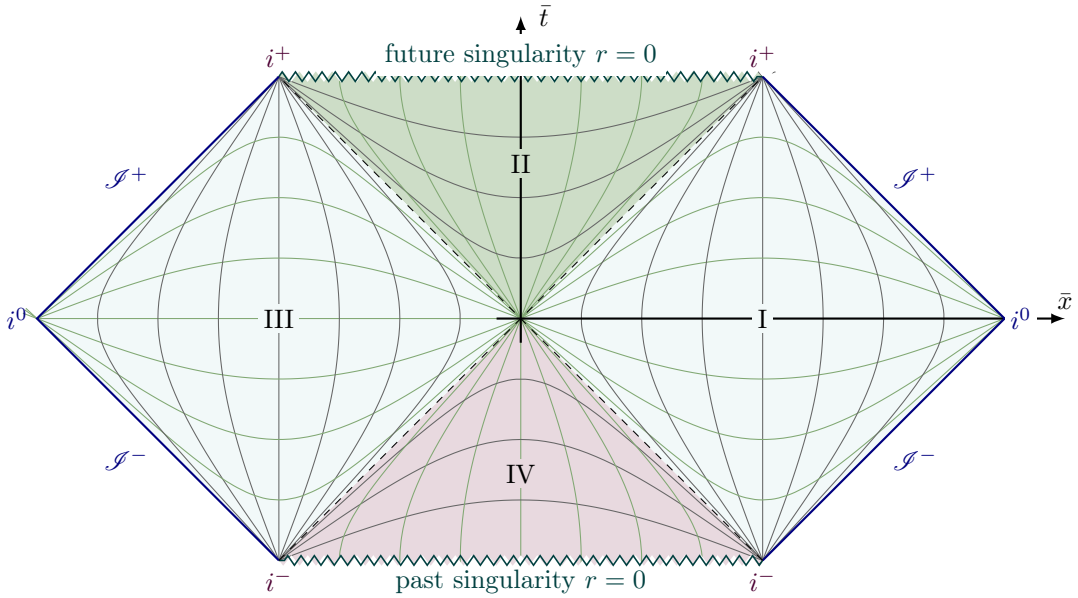

Figure 3.2: Conformal diagram of the maximal extension of the Schwarzschild geometry. Adapted from [Neutelings, 2021].

The (extended) geometry is only the *interior* of the diagram (as well as the singular $r = 0$ region). The boundaries are referred to as *conformal infinity*.

Definition 3.6. The conformal infinity is subdivided into different regions:

- i^+: the future timelike infinity, where $t \to +\infty$ at finite r.
  Intuitively, this is where the timelike curves end.
- i^0: the spatial infinity, where $r \to +\infty$ at finite t. Intuitively, this is where the spacelike curves end.
- i^-: the past timelike infinity, where $t \to -\infty$ at finite r. Intuitively, this is where the timelike curves come from.
- $\mathscr{I}^+$: the future null infinity, where $t + r \to \infty$ at finite $t - r$. Intuitively, this is where the lightlike curves end.
- $\mathscr{I}^-$: the past null infinity, where $t - r \to -\infty$ at finite $t + r$. Intuitively, this is where the lightlike curves come from.

The conformal diagram of the Schwarzschild geometry is shown in fig. 3.2. The regions are equivalent to the ones in property 3.3. The singularities ( ), the $r =$ constant world lines ( ), the $t =$ constant world lines ( ) and the lightcone $T = \pm X$ (- -) are represented as in fig. 3.2.

3.1.5 Astrophysical black hole

Let us briefly mention the case of a BH formed by a collapsing star. The geometry inside the star is not Schwarzschild ($T^{\mu\nu} \neq 0$), but the exterior geometry still is. Pictorially, an astrophysical BH can be illustrated as in fig. 3.3.

The simplest model for a collapsing star is to consider a spherically symmetric pressure-less and homogeneous matter distribution, free-falling under its own weight.

Definition 3.7. The **Oppenheimer-Snyder metric** inside such a matter distribution, written in proper time and co-moving coordinates $(\tau, R) \in \mathbb{R} \times [0; R_{\text{boundary}} = 1]$ is given by [Blau, 2025]:

$$\mathrm{d}s^2 = -\mathrm{d}\tau^2 + a^2(\tau)\left(\mathrm{d}R^2 + R^2\mathrm{d}\Omega^2\right) \tag{3.17}$$

The distribution of matter being homogeneous, the density ρ is simply the mass m divided by the volume of the star $V = \frac{4\pi}{3}a^3(\tau)R_\star$. The metric 3.17 being completely analogous to the FLRW metric 2.49 with $k = 0$, the first Friedmann equation F1 is recovered, which one can solve to obtain (taking the time of the collapse to be $\tau = 0$):

$$a(\tau) = \left(\frac{9m\tau^2}{2R_\star^3}\right)^{1/3} \tag{3.18}$$

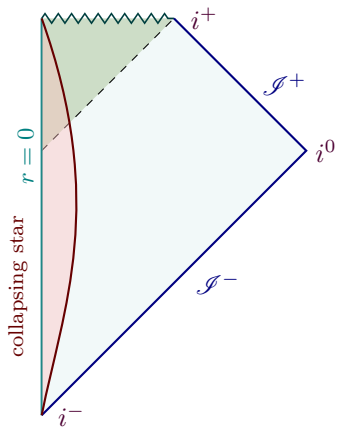

Figure 3.3: Conformal diagram of a black hole formed by gravitational collapse. Adapted from [Rovelli and Vidotto, 2024; Neutelings, 2021].

Fig. 3.3 is only a sketch: the metric in the red region is not Schwarzschild but eq. (3.17). This conformal diagram will be modified twice in the course of this work:

1. In the following sec. 3.2, modifications of the geometry due to quantum effects in the perturbative regime will be reviewed.
2. In chapter 5, non-perturbative effects of QG will be studied. This will address the singularity $a(\tau) \to 0$ as $\tau \to 0$ (see subsec. 5.3.1).

3.2 Dissipative aspects of black holes

The previous section was devoted to the study of the Schwarzschild (and the Oppenheimer-Snyder) geometry neglecting quantum effects. In this section, the dissipative aspects of BHs are reviewed. We will see that quantum corrections to the Schwarzschild geometry can be interpreted as a thermal flux of outgoing particles, leading to the evaporation of the BH.

We begin by introducing the *Unruh effect* (subsec. 3.2.1) as a toy model. The Unruh temperature is derived, as a consequence of the multiplicity of the vacuum quantum states for different observers, and the conversion between the local bases. Secondly, the *Hawking effect* in $(1+1)$ dimensions (subsec. 3.2.2) and in $(3+1)$ dimensions (subsec. 3.2.3) are reviewed, and the Hawking temperature is derived. In subsec. 3.2.5, we estimate the finite lifetime of a BH and sketch the modified geometry associated, before discussing a more quantitative picture of Hawking radiation in subsec. 3.2.4 using the `BlackHawk` code. This section concludes by giving a succinct derivation of the BH entropy.

3.2.1 Unruh effect: the toy model

3.2.1.A Rindler observer

Let us start with a much simpler case: an observer with constant acceleration $\vec{a}$ in $(1+1)$ Minkowski spacetime. The metric is $g_{\mu\nu} = \mathrm{diag}(-1,1)$. In *inertial lightcone coordinates* $(u,v) = (t-x, t+x)$, the metric reads $\mathrm{d}s^2 = -\mathrm{d}u\mathrm{d}v$. Writing the norm of the four-acceleration $a^\mu = \mathrm{d}^2x^\mu/\mathrm{d}\tau^2$ as $a^\mu a_\mu = a^2$ and taking initial conditions $x^\mu(0) = (0,0)$, the trajectory of the observer follows a hyperbola:

$$\begin{cases} t(\tau) = a^{-1}\sinh(a\tau) & (3.19) \\ x(\tau) = a^{-1}\cosh(a\tau) & (3.20) \end{cases}$$

Let us perform a change of coordinates to the *Rindler coordinates* (η,ξ) defined by:

$$\begin{cases} t(\eta,\xi) = a^{-1}e^{a\xi}\sinh(a\eta) & (3.21) \\ x(\eta,\xi) = a^{-1}e^{a\xi}\cosh(a\eta) & (3.22) \end{cases}$$

The line element in Rindler coordinates reads:

$$\mathrm{d}s^2 = \exp(2a\xi)(-\mathrm{d}\eta^2 + \mathrm{d}\xi^2) \tag{3.23}$$

That is the *Rindler metric*, from the comoving frame of the accelerated observer. Notice that the Rindler coordinates span the whole real axis $(\eta,\xi) \in \mathbb{R}^2$, but cover only the region $x > |t|$. Indeed, consider a spacelike hypersurface $\eta = \eta_0$. The induced metric on the hypersurface is $\mathrm{d}l^2 = \exp(2a\xi)\mathrm{d}\xi^2$. The acceleration horizon (or the *Rindler horizon*) is given by:

$$d = \int_{-\infty}^{0}\mathrm{d}l = \int_{-\infty}^{0}\exp(a\xi)\mathrm{d}\xi = \frac{1}{a} \tag{3.24}$$

The trajectories, for different values of a, are represented in fig. 3.4 by purple curves (—) and the $\eta =$ constant world lines by a green curve (—). The lightcone $t = \pm x$ is represented by a dashed line (- -).

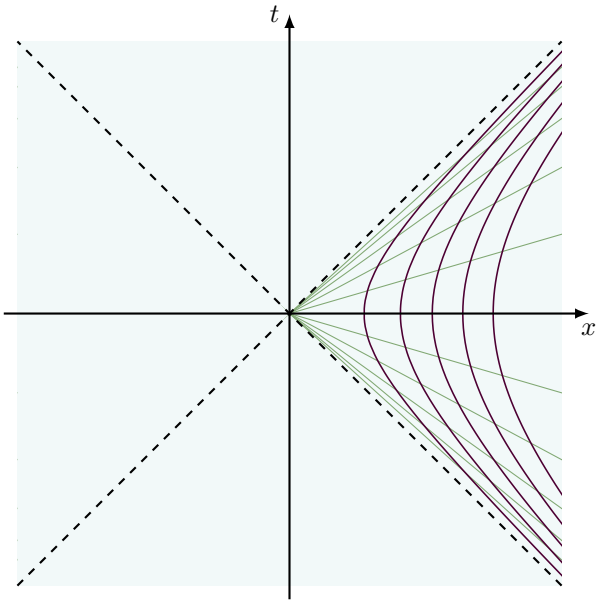

Figure 3.4: Trajectories of an accelerated observer in Minkowski spacetime. Inspired from [Semay, 2007; Neutelings, 2021].

Given a minimally coupled massless real scalar field ϕ in the Rindler metric, its action reads:

$$S = \frac{1}{2}\int \sqrt{-g}\mathrm{d}^2x\; g^{\mu\nu}\,\partial_\mu\phi\,\partial_\nu\phi \tag{3.25a}$$

$$= \frac{1}{2}\int \mathrm{d}\eta\mathrm{d}\xi\left(-\left(\partial_\eta\phi\right)^2 + \left(\partial_\xi\phi\right)^2\right) \tag{3.25b}$$

So that the EOM is simply the Klein-Gordon equation in Rindler coordinates: $\left(-\partial_\eta^2+\partial_\xi^2\right)\phi = 0$. Going to *comoving lightcone coordinates* $(\tilde{u},\tilde{v}) = (\eta+\xi, \eta-\xi)$, the metric reads $\mathrm{d}s^2 = -\exp(a(\tilde{u}-\tilde{v}))\mathrm{d}\tilde{u}\mathrm{d}\tilde{v}$ and the action becomes:

$$S = 2\int \mathrm{d}\tilde{u}\mathrm{d}\tilde{v}\;\partial_{\tilde{u}}\phi\partial_{\tilde{v}}\phi \tag{3.25c}$$

In the inertial frame in inertial lightcone coordinates, the action reads:

$$S = 2\int \mathrm{d}u\mathrm{d}v\;\partial_u\phi\partial_v\phi \tag{3.25d}$$

In the domain of spacetime where both coordinate systems are defined ($x > |t|$), one can expand the field operator $\hat{\phi}$ as follows:

$$\hat{\phi} = \begin{cases} \displaystyle\int_0^\infty \frac{\mathrm{d}k}{\sqrt{2\pi}}\frac{1}{\sqrt{2\omega_k}}\Big(\overbrace{e^{-i\omega_k u}\hat{a}_k^{R-} + e^{i\omega_k u}\hat{a}_k^{R+}}^{\text{right-moving modes}} + \overbrace{e^{-i\omega_k v}\hat{a}_k^{L-} + e^{i\omega_k v}\hat{a}_k^{L+}}^{\text{left-moving modes}}\Big) & \text{(inertial frame)} \quad (3.26a) \\ \displaystyle\int_0^\infty \frac{\mathrm{d}p}{\sqrt{2\pi}}\frac{1}{\sqrt{2\omega_p}}\Big(e^{-i\omega_p\tilde{u}}\hat{b}_p^{R-} + e^{i\omega_p\tilde{u}}\hat{b}_p^{R+} + e^{-i\omega_p\tilde{v}}\hat{b}_p^{L-} + e^{i\omega_p\tilde{v}}\hat{b}_p^{L+}\Big) & \text{(comoving frame)} \quad (3.26b) \end{cases}$$

Where $\omega_k = k$ and $\omega_p = p$. Below, we will drop the R and L indices and focus on the left moving modes.

The *Minkowski vacuum* $|0\rangle_M$ is defined as $\hat{a}_k^-|0\rangle_M = 0$ for all k and the *Rindler vacuum* $|0\rangle_R$ is defined as $\hat{b}_p^-|0\rangle_R = 0$ for all p [2]. A particle detector attached to the accelerated observer could detect particles from the Minkowski vacuum $|0\rangle_M$. Such a detector would remain unexcited only if the field

[2]The Rindler vacuum $|0\rangle_R$ is an *unphysical* state because it is not defined on the whole Minkowski spacetime. In particular, it is singular on $t = \pm x$. Discussion on the physicality of vacua can be found in [Mukhanov and Winitzki, 2007].

operator $\hat{\phi}$ is in the state $|0\rangle_R$. Now, we know that $\hat{\phi}$ is actually in the Minkowski vacuum $|0\rangle_M$. Our goal is to compute the expectation value of the *Rindler number operator* $\hat{N}_R = \hat{b}_p^+ \hat{b}_p^-$ in the Minkowski vacuum $|0\rangle_M$:

$$ {}_M\langle 0| \hat{N}_R |0\rangle_M \tag{3.27}$$

3.2.1.B Bogolyubov transformation

The two sets of creation and annihilation operators are related by a *Bogolyubov transformation* [Mukhanov and Winitzki, 2007]:

$$\begin{cases} \hat{b}_p^- = \displaystyle\int_0^\infty \mathrm{d}k_1 \left(\alpha_{pk_1} \hat{a}_{k_1}^- - \beta_{pk_1} \hat{a}_{k_1}^+\right) & \text{(3.28a)} \\ \hat{b}_p^+ = \displaystyle\int_0^\infty \mathrm{d}k_2 \left(\alpha_{pk_2}^* \hat{a}_{k_2}^+ - \beta_{pk_2}^* \hat{a}_{k_2}^-\right) & \text{(3.28b)} \end{cases}$$

The inverse transformation is not defined since the $(\tilde{u}, \tilde{v})$ coordinates only cover the region $x > |t|$. It is easy to see that $\delta(p_1 - p_2) = \left[\hat{b}_{p_1}^-, \hat{b}_{p_2}^+\right] = \int_{k>0} \mathrm{d}k \left(\alpha_{kp_1} \alpha_{kp_2}^* - \beta_{kp_1} \beta_{kp_2}^*\right)$.

3.2.1.C Unruh temperature

Let us now compute the expectation value of the Rindler number operator:

$$\begin{aligned} {}_M\langle 0| \hat{N}_R |0\rangle_M &= {}_M\langle 0| \int_{k_1>0} \int_{k_2>0} \mathrm{d}k_1 \mathrm{d}k_2 \left(\alpha_{pk_2}^* \hat{a}_{k_2}^+ - \beta_{pk_2}^* \hat{a}_{k_2}^-\right) \left(\alpha_{pk_1} \hat{a}_{k_1}^- - \beta_{pk_1} \hat{a}_{k_1}^+\right) |0\rangle_M & \text{(3.29a)} \\ &= {}_M\langle 0| \int_{k_1>0} \int_{k_2>0} \mathrm{d}k_1 \mathrm{d}k_2 \; \beta_{pk_2}^* \beta_{pk_1} \delta(k_2 - k_1) |0\rangle_M & \text{(3.29b)} \\ &= \int_{k>0} \mathrm{d}k \; |\beta_{pk}|^2 & \text{(3.29c)} \end{aligned}$$

Inserting eq. (3.28) into eq. (3.26) and identifying the coefficients of $\hat{a}_k^\pm$ gives the following relations:

$$\begin{cases} \dfrac{1}{\sqrt{\omega_k}} e^{-i\omega_k u} = \displaystyle\int_{p>0} \mathrm{d}p \; \frac{1}{\sqrt{\omega_p}} \left(\alpha_{pk} e^{-i\omega_p \tilde{u}} - \beta_{pk}^* e^{i\omega_p \tilde{u}}\right) & \text{(3.30a)} \\ \dfrac{1}{\sqrt{\omega_k}} e^{i\omega_k u} = \displaystyle\int_{p>0} \mathrm{d}p \; \frac{1}{\sqrt{\omega_p}} \left(\alpha_{pk}^* e^{i\omega_p \tilde{u}} - \beta_{pk} e^{-i\omega_p \tilde{u}}\right) & \text{(3.30b)} \end{cases}$$

By multiplying by $e^{\pm i\omega_{p_1} \tilde{u}}$, integrating over $\tilde{u}$, making delta functions appear and using that $\delta\left(\omega_p + \omega_{p_1}\right) = 0 \; \forall p, p_1 > 0$, one can express the Bogolyubov coefficients as:

$$\begin{cases} \alpha_{pk} = \displaystyle\int e^{-i\omega_k u + i\omega_p \tilde{u}} \mathrm{d}\tilde{u} & \text{(3.31a)} \\ \beta_{pk} = \displaystyle\int e^{i\omega_k u + i\omega_p \tilde{u}} \mathrm{d}\tilde{u} & \text{(3.31b)} \end{cases}$$

Now, comparing the line element in terms of the inertial lightcone coordinates and the comoving one, it is immediate to see that they are related by:

$$\begin{cases} u = -a^{-1} e^{-a\tilde{u}} & \text{(3.32a)} \\ v = \; a^{-1} e^{a\tilde{v}} & \text{(3.32b)} \end{cases}$$

Expressing $u = u(\tilde{u})$ and $v = v(\tilde{v})$, one can perform the integrals and find the following relation[3] :

$$|\alpha_{pk}|^2 = \exp\left(\frac{2\pi p}{a}\right) |\beta_{pk}|^2 \tag{3.33}$$

[3]The computation of the integrals is not trivial. Two different ways of finding eq. (3.33) can be found in [Mukhanov and Winitzki, 2007].

From the commutation relations, we have $\delta(0) = \int_{k>0} \left(|\alpha_{pk}|^2 - |\beta_{pk}|^2\right) = \int_{k>0} |\beta_{pk}|^2 \left(e^{2\pi p/a} - 1\right)$. The expectation value of the Rindler number operator eq. (3.29) is then given by:

$$ {}_M\langle 0|\, \hat{N}_R\, |0\rangle_M = \frac{1}{\exp\left(\frac{2\pi p}{a}\right) - 1}\delta(0) \tag{3.34} $$

The diverging part $\delta(0)$ simply comes from the infinite volume considered. If the field were to be quantized in a box of volume V, the $\delta(0)$ would be replaced by V.

The result of the computation is the following: an observer uniformly accelerated in a Minkowski vacuum of a massless scalar field will see a thermal bath of particles (Bose-Einstein distribution) at a temperature:

$$ T_U = \frac{a}{2\pi} = \frac{\hbar}{2\pi k_{\mathrm{B}} c} a \tag{3.35} $$

3.2.2 Hawking radiation in $1+1$ dimensions: the baby problem

In $(1+1)$ dimensions, the Schwarzschild metric can be written as:

$$ \mathrm{d}s^2 \equiv -F(r)\mathrm{d}t^2 + \frac{1}{F(r)}\mathrm{d}r^2 \tag{3.36} $$

Where $F(r)$ is defined in 3.1b. This metric is then conformally flat. Indeed, the $(1+1)$ dimensional version of the lightcone form (3.8) gives:

$$ \mathrm{d}s_B^2 = -\left(1 - \frac{2m}{r(u,v)}\right)\mathrm{d}u\mathrm{d}v \tag{3.37} $$

And the $(1+1)$ dimensional version of the Kruskal-Szekeres extension (3.10) gives:

$$ \mathrm{d}s_K^2 = -\frac{32m^3}{r(\hat{u},\hat{v})} e^{-r(\hat{u},\hat{v})/2m} \mathrm{d}\hat{u}\,\mathrm{d}\hat{v} \tag{3.38} $$

Notice that (eq. 3.37) only covers the exterior of the black hole region $\{r > 2m\}$, while (eq. 3.38) covers the whole Schwarzschild spacetime.

Since these two metrics are conformally flat, one can use the same techniques as in the previous section. The field operator $\hat{\phi}$ can be expanded in the same way as in eq. 3.26, where we trade the inertial frame for the Kruskal-Szekeres metric, and the comoving frame for the Schwarzschild metric. Two vacua are then defined:

1. the *Kruskal vacuum* $|0\rangle_K$ (analogous to the Minkowski vacuum):
$$ \hat{a}_k^-\, |0\rangle_K = 0 \tag{3.39} $$
2. the *Boulware vacuum* $|0\rangle_B$ (analogous to the Rindler vacuum):
$$ \hat{b}_p^-\, |0\rangle_B = 0 \tag{3.40} $$

To derive the expected value of the Boulware number operator $\hat{N}_\Omega = \hat{b}_p^+ \hat{b}_p^-$, we only need to compute the relation between coordinates (u,v) and $(\hat{u},\hat{v})$. To complete the analogy, we redefine $(\hat{u},\hat{v})$ as:

$$ \begin{cases} \hat{u} = -\kappa^{-1} e^{-\kappa u} & \text{(3.41a)} \\ \hat{v} = \quad \kappa^{-1} e^{\kappa v} & \text{(3.41b)} \end{cases} $$

Where $\kappa = 1/4m$ is the surface gravity of the black hole. [4] Now κ plays the role of the acceleration of the Rindler observer. The expected value reads:

$$ {}_K\langle 0|\, \hat{N}_\Omega\, |0\rangle_K = \frac{1}{\exp\left(\frac{2\pi p}{\kappa}\right) - 1}\delta(0) \tag{3.42} $$

[4] This change impacts the conformal factor of 3.38, from $-32m^3 \exp(-r/2m)/r$ to $2m \exp(-r/2m)/r$.

The corresponding temperature (the *Hawking temperature*) is then given by:

$$T_H = \frac{\kappa}{2\pi} = \frac{1}{8\pi}\frac{1}{m} = \frac{\hbar c^3}{8\pi G k_{\mathrm{B}}}\frac{1}{m} \tag{3.43}$$

A common *heuristic* for Hawking radiation is this: near the event horizon, vacuum fluctuations are pictured as producing a particle-antiparticle pair. One mode falls through the horizon carrying "negative energy", while its partner escapes to future null infinity and can be detected by distant static observers as part of a thermal flux. Energy conservation then implies the BH's mass decreases.

3.2.3 Hawking radiation in $3+1$ dimensions: the real problem

For completeness, we talk briefly about HR in $3+1$ dimensions. Let us consider the same minimally coupled massless scalar field ϕ, and expand it in spherical harmonics:

$$\phi(t,r,\theta,\varphi) = \sum_{\ell,m} \phi_{\ell m}(t,r) Y_{\ell m}(\theta,\varphi) \tag{3.44}$$

The wave equation $\Box^{(4)}\phi = 0$ in the metric 3.1 becomes [Mukhanov and Winitzki, 2007]:

$$\left(\Box^{(2)} + \overbrace{\left(1-\frac{2m}{r}\right)\left(\frac{2m}{r^3}+\frac{\ell(\ell+1)}{r^2}\right)}^{V_\ell(r)}\right)\phi_{\ell m}(t,r) = 0 \tag{3.45}$$

An outgoing wave must propagate through the potential $V_\ell(r)$, which decreases the intensity of the Hawking effect. This results in a modification of the black body spectrum, introducing a *gray body factor* $0 < \Gamma_\ell(\Omega) < 1$:

$${}_K\langle 0|\,\hat{N}_\Omega\,|0\rangle_K = \frac{\Gamma_\ell(\Omega)}{\exp(\Omega/T_H)-1}\delta(0) \tag{3.46}$$

This result can be generalized to rotating, charged black hole, and for a (massive) scalar field, spinor and vector field [Hawking, 1975; Auffinger, 2023]. One should also take into account the *secondary emission* of particles: how the primary emitted particles interact and decay.

Today, the standard theory of secondary radiation is the so-called *MacGibbon& Webber* (or MG&W) model [Auffinger, 2023]. The fundamental equation for the primary emission of particles of spin s with angular momentum numbers (ℓ, m), rest mass μ, electric charge q and energy E, from a general Kerr-Neumann black hole of mass M and described by the set of parameters $\{x_j\}$[5] is given by [Auffinger, 2023]:

$$\frac{\mathrm{d}^2 N^{(1)}}{\mathrm{d}t\mathrm{d}E} = \frac{1}{2\pi}\frac{\Gamma_{Esq\ell m}(M,\{x_j\})}{\exp\left(\frac{E-m\Omega-q\Phi}{T\{x_j\}}\right)-(-1)^{2s}}\Theta(E-\mu) \tag{3.47}$$

Where Θ is the Heaviside step function, $T\{x_j\}$ is the Hawking temperature of the black hole, Ω and Φ are the angular frequency and the electric potential of the BH and $\Gamma_{Esq\ell m}(M,\{x_j\})$ is the gray body factor. For a particle with internal multiplicity g_i (color, helicity, antiparticles), the rate of emission is:

$$\frac{\mathrm{d}^2 N_i^{(1)}}{\mathrm{d}t\mathrm{d}E} = g_i \sum_{\ell,m}\frac{\mathrm{d}^2 N}{\mathrm{d}t\mathrm{d}E} \tag{3.48}$$

The secondary emission, say of particle j, is obtained by multiplying the primary emission rate eq. (3.48) with the branching ratio of the primary particle i going to j at some energy $\mathcal{B}_{i\to j}(E,E')$, and integrating over the energy E' of the primary particle:

$$\frac{\mathrm{d}^2 N_j^{(2)}}{\mathrm{d}t\mathrm{d}E} = \int_0^\infty \mathrm{d}E'\ \mathcal{B}_{i\to j}(E,E')\frac{\mathrm{d}^2 N_i^{(1)}}{\mathrm{d}t\mathrm{d}E'} \tag{3.49}$$

These emission rates (primary and secondary) can be computed analytically in some limits, or numerically in the general case. Below, in subsec. 3.2.5, we compute the lifetime of a black hole using major simplifications, in order to get an order-of-magnitude estimate and the mass dependence.

[5] The parameters $\{x_j\}$ are obtained from the black hole mass spin, charge and angular momentum.

3.2.4 `BlackHawk`: a quantitative approach to Hawking radiation

We use `BLACKHAWK v2.3` [Arbey and Auffinger, 2019, 2021] to compute a realistic and quantitative estimate of HR. The primary emission rates are computed using Standard Model (SM) particles, listed in table 4.

Particle	Symbol	Spin	g_i	Stable?
Higgs boson	h^0	0	1	no
photon	γ	1	2	yes
gluons	G	1	16	yes
W bosons	$W^\pm$	1	6	no
Z boson	Z^0	1	3	no
neutrinos	$\nu_{e,\mu,\tau}$, $\bar{\nu}_{e,\mu,\tau}$	1/2	6	yes
electron	$e^\pm$	1/2	4	yes
muon	$\mu^\pm$	1/2	4	no
tau	$\tau^\pm$	1/2	4	no
up quark	u, $\bar{u}$	1/2	12	no
down quark	d, $\bar{d}$	1/2	12	no
charm quark	c, $\bar{c}$	1/2	12	no
strange quark	s, $\bar{s}$	1/2	12	no
top quark	t, $\bar{t}$	1/2	12	no
bottom quark	b, $\bar{b}$	1/2	12	no
graviton	g	2	2	yes
proton	p, $\bar{p}$	1/2	4	yes

Table 4: Particle species considered in this work (Standard Model plus graviton), with their spin, internal degrees of freedom g_i, and assumed stability. All quarks hadronize and are listed as unstable; the proton is included as a stable composite. Adapted from [Arbey and Auffinger, 2019; Zyla et al., 2020].

The primary emission rates are enough to compute the mass loss of the BH, but most of the SM particles are unstable (or only exist in bound states). Several particle-physics codes can evolve primary spectra into secondary ones. Each has its domain of validity; for our purposes (low-redshift cosmology), we consider only particles with infinite lifetime (marked as "stable" in table 4). For hadronization at the present epoch we use the Pythia code [Sjöstrand et al., 2015]. A schematic representation of the Hawking evaporation of a BH is shown in fig. 3.5.

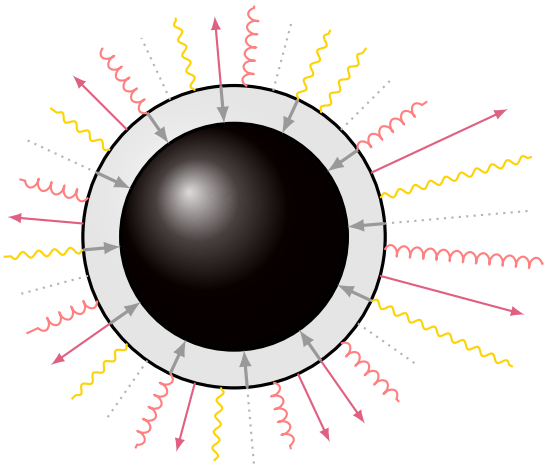

Figure 3.5: Pictorial representation of the Hawking evaporation of a BH.

As an example, let us look at a Schwarzschild BH of mass $m_0 = 10^7$ kg, evaporating until it reaches

a mass $m_{\text{REM}} \sim 10^{-8}$ kg[6]. Its primary emission rates at fixed time (respectively energy) are shown in fig. 3.6a (respectively fig. 3.6b). The secondary emission rates at fixed time (respectively energy) are shown in fig. 3.6c (respectively fig. 3.6d). We can integrate the emission rates over the energy to obtain the power $\dot{E}_j^{(2)}(t)$, as displayed in fig. 3.6e (respectively fig. 3.6f). The units on the vertical axes are arbitrary since we assume an arbitrary BH density.

Since this analysis extends beyond the original objectives of the master's thesis, we do not provide a detailed interpretation of the spectral features in these figures. We include them to document the spectra computed with `BlackHawk` and to extract effective coefficients that will be used later in our semi-analytical model (see chapter 7).

Starting from eq. (3.49), the power at some given time t is given by:

$$\dot{E}_j^{(2)}(t) = \int_0^\infty \mathrm{d}E' \, E' \frac{\mathrm{d}^2 N_j^{(2)}}{\mathrm{d}t \mathrm{d}E'} \tag{3.50}$$

Integrating over the lifetime of the BH gives E_j^{tot} the total energy emitted in the form of particles of species j. Computing E_j^{tot} for each species j, we can constitute a table of the proportion of the different species emitted by a monochromatic distribution of Schwarzschild BH of mass m_0. In the case of the example discussed here, the fractional energy budget in the secondary Hawking emission is given in table 5. In general, the evaporation stops when the mass of the BH reaches a certain value m_{REM}, that depends on the theory considered. The explicit choices of parameters and tables can be found in the chapter A.

Mass	ν (%)	γ (%)	$e^\pm$ (%)	$p^\pm$ (%)	g (%)	ν_e (%)	ν_μ (%)	ν_τ (%)
$m = 10^7$ kg	45.39	23.92	22.45	8.15	0.09	14.76	26.53	4.11

Table 5: Fractional energy budget in the secondary Hawking emission (plus gravitons) for a Schwarzschild BH of mass $m_0 = 10^7$ kg.

3.2.5 Lifetime and conformal structure of an evaporating black hole

Consider a Schwarzschild BH of mass m_0, isolated. The emission of Hawking radiation will lead to a decrease of the mass of the BH. The area emitting Hawking radiation is $A = 4\pi (2m_0)^2$. Using the Stefan-Boltzmann law, one can compute the luminosity of the black hole:

$$\frac{\mathrm{d}^2 E}{\mathrm{d}t \mathrm{d}A} = \Gamma\gamma \frac{\pi^2}{60} T^4 \tag{3.51}$$

Where Γ is the gray body factor and γ is the number of degrees of freedom of the emission flux. As the temperature rises and exceeds the rest mass of particles, the number of possibly emitted particles rises and the emission becomes explosive. We neglect this effect below and assume constant $\Gamma\gamma$.

$$\frac{\mathrm{d}E}{\mathrm{d}t} = \Gamma\gamma \frac{\pi^2}{60} \int \left(\frac{1}{16\pi m}\right)^4 \mathrm{d}A \tag{3.52a}$$

$$= \frac{\Gamma\gamma}{15360\pi} \frac{1}{m^2} \tag{3.52b}$$

$$\tag{3.52c}$$

The decrease of the mass with time is given by:

$$-\frac{\mathrm{d}m}{\mathrm{d}t} = \frac{\Gamma\gamma}{15360\pi} \frac{1}{m^2} \tag{3.53}$$

[6]This is typically the case in the LQG scenario, presented in chapter 5.

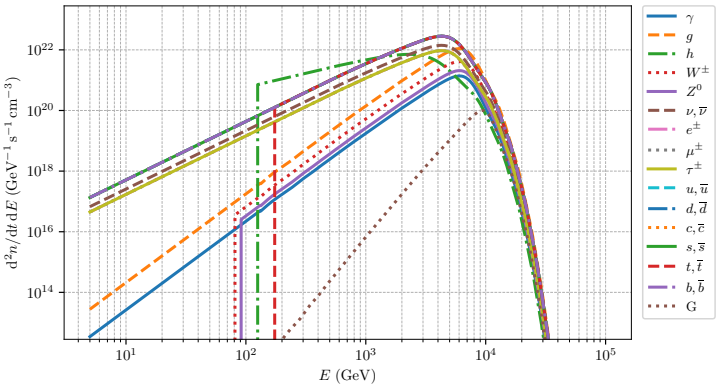

(a) Primary emission rates at fixed time $t = 2.5 \times 10^{-28}\,\mathrm{s}$.

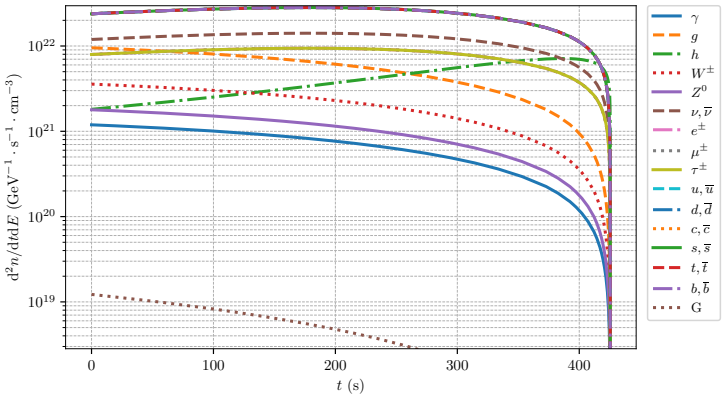

(b) Primary emission rates at fixed energy $E = 5.2 \times 10^3\,\mathrm{GeV}$.

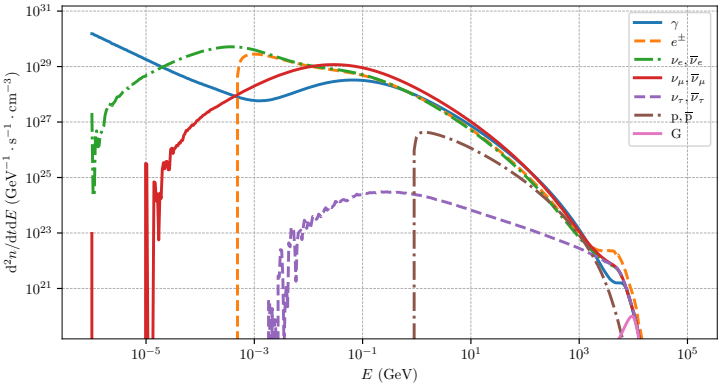

(c) Secondary emission rates at the same fixed time.

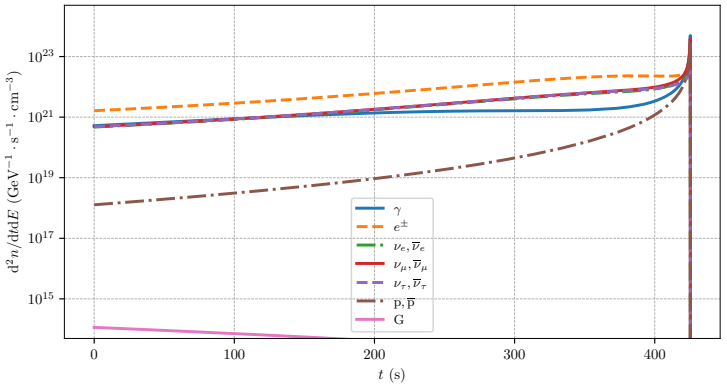

(d) Secondary emission rates at $E = 4.3 \times 10^2\,\mathrm{GeV}$.

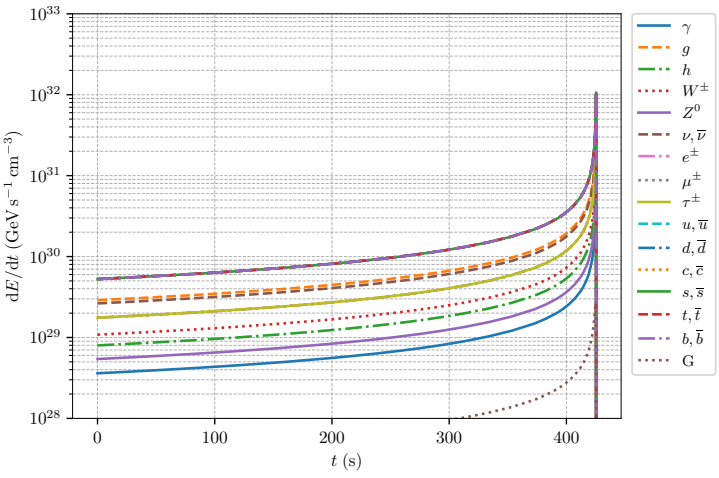

(e) Total primary emission power as a function of time.

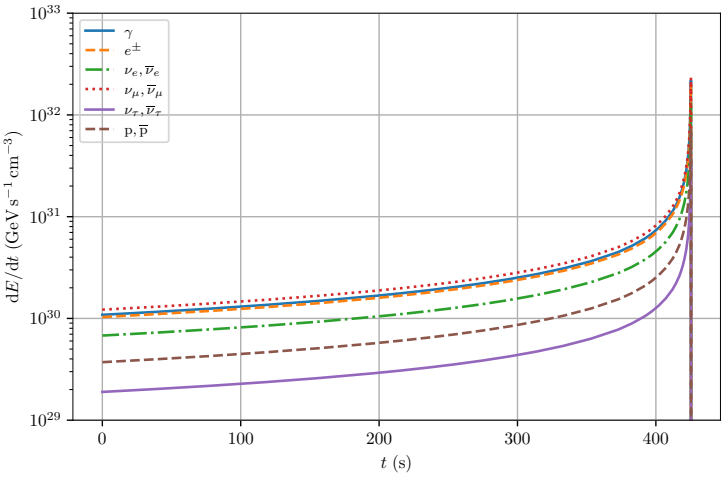

(f) Total secondary emission power as a function of time.

Figure 3.6: Primary and secondary Hawking-emission for a Schwarzschild BH of initial mass $m_0 = 10^7\,\mathrm{kg}$.

This gives a finite lifetime for the black hole:

$$\tau_{\text{BH}} = \frac{5120\pi}{\Gamma\gamma} m_0^3 \tag{3.54}$$

Taking $5120\pi/\Gamma\gamma \sim 10^4$ [Mukhanov and Winitzki, 2007], we can estimate the lifetime of BHs of different masses. The results are summarized in table 6.

	Mass	Lifetime	Temperature
$m \sim M_\odot$	$m = 10^{30}$kg	$\tau = 10^{74}$s	10^{-11} eV
$m \sim m_{\text{asteroid}}$	$m = 10^{12}$kg	$\tau = 10^{19}$s	10 MeV
$m \sim m_{\text{bluewhale}}$	$m = 10^{5}$kg	$\tau = 10^{-1}$s	10^{2} TeV
$m \sim \min m_{\text{PBH}}$	$m = 10^{-4}$kg	$\tau = 10^{-29}$s	10^{11} TeV

Table 6: Example of the lifetime and Hawking temperature of BHs of different masses.

Note that in the literature [Carr et al., 2010], the lifetime of a black hole is approximated as $\tau \approx 407(m/10^{10}\text{kg})^3$ s, which is equivalent to taking $5120\pi/\Gamma\gamma \sim 78$:

$$\tau_{\text{BH}} \approx 78\, m_0^3 \tag{3.55}$$

For BHs with a sufficiently large mass $m_0 \gg 10^{14}$ kg, numerical results from the 1970s predict that most of the emitted power is in the form of neutrinos (around 80%) and photons (around 20%) [Page, 1976]. Lighter (hotter) BHs can emit massive particles, since the temperature becomes larger than the rest mass of the particles. For example, a BH with a mass of $m_0 \sim 10^{11} - 10^{14}$ kg emits its power in the form of electrons and positrons (around 45%) and neutrinos (around 45%), and 9% in photons [Page, 1976]. Our results in tables 10 and 11 find different proportions, but are consistent with more recent results [MacGibbon, 1991].

If one trusts the above computation, the horizon radius $r = 2m(\tau)$ will reach $r = 0$ in a finite proper time τ. Consequently, the event horizon (which in the Schwarzschild metric extends all the way to i^+ as illustrated in fig. 3.3) is now only a finite lightlike surface. Fig. 3.7 shows a sketch of this scenario, in which all the radiation is emitted at once at the end of the evaporation process [Schindler et al., 2020].

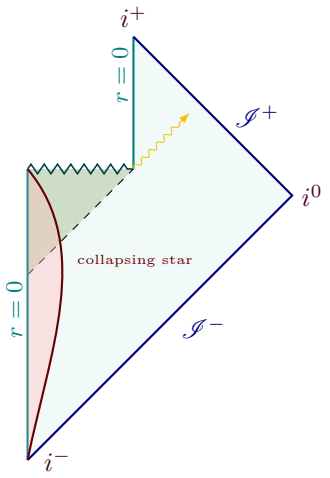

Figure 3.7: Conformal diagram of a black hole with a finite lifetime. Adapted from [Hawking, 1975; Schindler et al., 2020; Neutelings, 2021].

3.2.6 Thermodynamics of black holes

Let us differentiate the equation giving the area of the BH $A = 16\pi m^2$:

$$\mathrm{d}m = \frac{1}{8\pi m}\mathrm{d}\left(\frac{A}{4}\right) = T_H \mathrm{d}\left(\frac{A}{4}\right) \tag{3.56}$$

By analogy with the first law of thermodynamics $\mathrm{d}E = T\mathrm{d}S$, we can identify the entropy of the BH.

Definition 3.8. The **entropy of a black hole**, or Bekenstein-Hawking entropy, S_{BH} is defined as:

$$S_{\text{BH}} = \frac{A}{4} = 4\pi\, m^2 \tag{3.57}$$

Where A is the area of the event horizon and m is the mass of the black hole.

The *first law of* (non-rotating, electrically neutral) *BH thermodynamics* thus reads:

$$\mathrm{d}m = T_H \mathrm{d}S_{\text{BH}} \tag{3.58}$$

This intrinsic entropy of the BH allows us to formulate a *generalized second* law of thermodynamics:

$$\mathrm{d}S_{\text{total}} = \mathrm{d}S_{\text{matter}} + \mathrm{d}S_{\text{BH}} \geq 0 \tag{3.59}$$

The notion of BH entropy will be crucial when discussing the memory burden effect in chapter 6.

CHAPTER

4

PRIMORDIAL BLACK HOLES

This chapter begins with a review of PBH formation in sec. 4.1, covering the collapse of primordial overdensities and the derivation of the initial abundance. In sec. 4.2, we briefly discuss the main observational and theoretical limits on PBH abundance, ranging from evaporation and microlensing constraints to dynamical, accretion, and gravitational-wave bounds. Moreover, since PBHs would form in the early universe and interact only gravitationally, they behave as cold, non-baryonic matter and remain an attractive candidate for (all or part of) the DM.

4.1 PBH formation

Understanding PBH formation through the collapse of cosmological perturbations requires results from both the previous chapters. First, in subsec. 4.1.1, the causal re-entry condition $k = aH$ and the collapse criterion $\delta > \delta_c$ (eq. (4.1)) are introduced. The link between the mass fraction of PBHs (eq. (4.2)) and the power spectrum of the curvature perturbation (eq. (2.88)) is then established. In subsec. 4.1.2, we briefly discuss how the mass of the PBH is related to the horizon mass M_H and define the range of masses that we are interested in. We mostly follow [Byrnes and Cole, 2021; Carr and Kühnel, 2022; Bagui et al., 2023].

4.1.1 Collapse of the overdensities

From the discussion in subsec. 2.2.2, it is clear that an inhomogeneity of scale $1/k$ can only collapse when the perturbation is inside the comoving Hubble radius $1/(aH)$. Physically, the re-entrance of the perturbation into the Hubble radius means that the perturbation becomes causally connected again. The perturbation can then collapse under its own gravity, and if the density is high enough, it can form a black hole. Therefore, all quantities in this chapter are evaluated at $k = aH$.

We focus here on PBHs formed by the collapse of overdensities due to cosmological perturbations. However, there exist many other formation mechanisms (see for example [Bagui et al., 2023] for a review), which can, among other things, significantly alter the lower mass bound at formation.

For a PBH to form, the density perturbation must be large enough to overcome the pressure: the *attracting* gravitational force has to be greater than the *repulsive* pressure. One needs:

$$\delta > \delta_c \tag{4.1}$$

where δ is the density contrast defined in def. 2.21 and δ_c is the density threshold. Focusing on the radiation-dominated (RD) era and neglecting the *reheating* epoch, the equation of state during the PBH formation is given by $\omega = 1/3$. Using this assumption (among others), a first estimate of δ_c was given by [Carr, 1975] with $\delta_c \approx 1/3$. More recent estimates give $\delta_c \approx 0.4$ using numerical relativity simulations [Harada et al., 2013]. Taking Loop Quantum Cosmology into account could divide the value of δ_c by a factor of 2 for low-mass PBHs (close enough to the Cosmic Bounce) [Papanikolaou, 2023].

Another important quantity is the *mass fraction* of PBH at their time of formation.

Definition 4.1. The fraction between PBHs at given mass M and the total energy density at the time of their formation t_i is denoted:

$$\beta \equiv \beta_i(m_{\text{PBH}}) = \frac{\rho_{\text{PBH}}(t_i)}{\rho_{\text{tot}}(t_i)} \tag{4.2}$$

Eq. (4.2) depends on the Probability Density Function (**PDF**) of primordial density fluctuations $\mathtt{P}(m_{\text{PBH}}, \delta)$ and the threshold over-density required for PBH formation δ_c:

$$\beta_i(m_{\text{PBH}}) = \int_{\delta_c}^{\infty} \mathtt{P}(m_{\text{PBH}}, \delta, t_i)\mathrm{d}\delta \tag{4.3}$$

Note that $\mathtt{P}$ can indeed only depend on m_{PBH} and δ since non-rotating neutral BH are completely described by their mass.

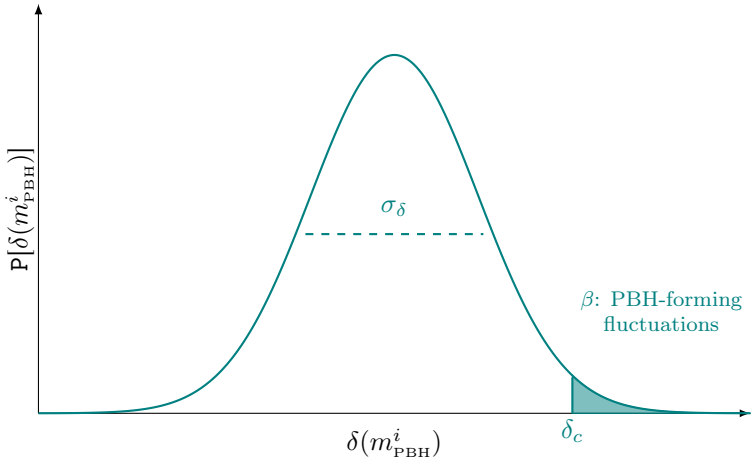

Figure 4.1: Sketch of the density threshold δ_c and the variance σ_δ of the density perturbation.

Let us consider the PDF to be Gaussian: $\mathtt{P} = \mathtt{P}_G$ (recall def. 2.17), as illustrated in fig. 4.1. The mass fraction now reads [Bagui et al., 2023]:

$$\beta = 2\int_{\delta_c}^{\infty} \frac{1}{\sqrt{2\pi}\sigma_\delta} \exp\left(-\frac{\delta^2}{2\sigma_\delta^2}\right)\mathrm{d}\delta \tag{4.4a}$$

$$= \operatorname{erfc}\left(\frac{\delta_c}{\sqrt{2}\sigma_\delta}\right) \tag{4.4b}$$

$$\sim \frac{2\sigma_\delta}{\delta_c\sqrt{2\pi}} \exp\left(-\frac{\delta_c^2}{2\sigma_\delta^2}\right) \tag{4.4c}$$

Where $\operatorname{erfc}(x) = 1 - \operatorname{erf}(x) = (2/\sqrt{\pi})\int_x \exp(-t^2)\mathrm{d}t \xrightarrow{\delta_c/\sigma \gg 1} (x\sqrt{\pi})^{-1}\exp(-x^2)$ is the complementary error function and where σ_δ is the variance of the density perturbation (up to a window function

$W(kR_s)$, used to smooth the perturbations within a smoothing scale R_s [Byrnes et al., 2025]), given by:

$$\sigma_\delta^2 = \langle \delta^2 \rangle = \int_0^\infty \frac{\mathrm{d}k}{k} W(kR_s)\Delta_\delta(k,r) \tag{4.5}$$

The factor of 2 in eq. (4.4a), borrowed from the Press-Schechter formalism, is the *fudge factor*. It ensures that when $\sigma_\delta \to \infty$, the mass fraction $\beta \to 1$.
Refinements can be considered, see e.g. [Byrnes et al., 2025], nevertheless for the purposes of this explanatory work in which β is treated as a model parameter, the above equations are sufficient to emphasize the connection with the primordial fluctuations from inflation.

The power spectrum of the density perturbation Δ_δ can be related to the power spectrum of the curvature perturbation $\Delta_\mathcal{R}$ through eq. (2.71). As illustrated in fig. 2.2, the primordial scalar power spectrum is well constrained when $k \sim [10^{-3}, 10^{0}]$ Mpc^{-1}. Now, the wave number associated with light PBHs is $\gtrsim 10^5$-10^{15} Mpc^{-1}, depending on the mass of the PBH [Özsoy and Tasinato, 2023]. To form PBHs, the primordial power spectrum must be large enough at these scales [Carr et al., 2021], which is not the case for the standard inflationary model. Many alternatives have been proposed to enhance the power spectrum at small scales, which will not be discussed here but can be found in the literature (see for example [Özsoy and Tasinato, 2023]).

4.1.2 PBH mass

The mass of a PBH is closely related to the mass of the horizon at the time of formation, called the *horizon mass*.

Definition 4.2. The **horizon mass** M_H is the energy within the Hubble radius $R_H = 1/H$. It reads:

$$M_H = \rho V = \frac{3H^2}{8\pi}\frac{4\pi}{3}\left(\frac{1}{H}\right)^3 = \frac{1}{2H} \tag{4.6}$$

During RD (resp. MD), $H \sim a^{-2}$ (resp. $H \sim a^{-3/2}$), so the horizon mass is given (in both cases) by:

$$M_H \sim t \tag{4.7}$$

The heavier PBHs are formed at later times. From the discussion in subsec. 3.2.5, we see that PBHs with $\tau_{\mathrm{PBH}} \sim 10^4 \left(m^i_{\mathrm{PBH}}\right)^3 < \tau_{\mathrm{universe}}$ will have evaporated by now. Since $\tau_{\mathrm{universe}} \sim 8 \cdot 10^{60} \sim 4 \cdot 10^{17}$ s, the constraint on the initial mass of the PBHs is $m^i_{\mathrm{PBH}} \lesssim 10^{19} \sim 10^{11}$ kg . In the literature, one often takes τ_{PBH} to be proportional to m^3 with a smaller prefactor (for example, $\tau_{\mathrm{PBH}} \sim 10^2 \left(m^i_{\mathrm{PBH}}\right)^3$ in [Carr et al., 2010]), leading to $m^i_{\mathrm{PBH}} \lesssim 10^{20} \sim 10^{12}$ kg instead.

There is a lower mass limit for PBH formation in the conventional inflationary scenario from the CMB observation constraints on the Hubble rate during inflation $H_{\mathrm{inf}} \lesssim 10^{-5}\, m_P$, which is: [Auffinger, 2023]:

$$m^i_{\mathrm{PBH}} \gtrsim 0.1 \text{ g } \sim 10^{-4} \text{ kg} \tag{4.8}$$

Thus, the range of masses that we are interested in is:

$$m^i_{\mathrm{PBH}} \in [10^{-4}, 10^{12}] \text{ kg} \tag{4.9}$$

In chapter 5 and chapter 6, we will see that modifications in the dissipative process of the PBHs can lead to different lifetimes and therefore different mass limits. The new constraints on the lifetime are illustrated in fig. 8.1.

4.2 Constraints on PBHs

PBHs are candidates for dark matter: they interact mostly through gravity and behave like Cold Dark Matter (**CDM**). Since the content of DM in the universe is well constrained (recall eq. (2.23b)), a convenient way to quantify the amount of PBHs in the universe as a DM candidate is to express it as a fraction of the DM density Ω_{PBH} evaluated today:

$$f_{\text{PBH}} \equiv \frac{\Omega_{\text{PBH}}}{\Omega_{\text{DM}}} = \left.\frac{\rho_{\text{PBH}}}{\rho_{\text{DM}}}\right|_0 \tag{4.10}$$

Since the radiation density redshifts faster than the matter density, the initial mass fraction of PBHs β can be small and still lead to $f_{\text{PBH}} \sim 1$. Roughly,

$$f_{\text{PBH}} \sim \left.\frac{\rho_{\text{PBH}}}{\rho_{\text{DM}}}\right|_{\text{eq}} \sim \frac{a_{\text{eq}}}{a_f}\beta \tag{4.11}$$

Where a_{eq} is the scale factor at matter-radiation equality and a_f is the scale factor at the time of formation of the PBHs. To express the constraints, one can either use the mass fraction β or the fraction of DM f_{PBH}.

The topic of constraints on f_{PBH} is well-developed and covered in many reviews. We will just give an overview of the different types of constraints here, and refer to the literature for more details [Carr et al., 2021; Bagui et al., 2023; Auffinger, 2023]. In the context of this work, our focus is on PBHs that have evaporated to form remnants, so these particular constraints do not apply.

4.2.1 PBH evaporation

For PBHs already evaporated, the products of their evaporation can influence the Big Bang Nucleosynthesis, the Cosmic Microwave Background and other astrophysical observations. In this section, we restrict ourselves to the constraints from the BBN, gamma-rays and the CMB. Extensive reviews on the constraints from PBH evaporation can be found in [Bagui et al., 2023; Auffinger, 2023]. In the following, we use the BH lifetime given in eq. (3.55).

4.2.1.A Big Bang Nucleosynthesis

The BBN starts when the chemical equilibrium between neutrons and protons is broken (when the reactions $n + \nu_e \leftrightarrow p^+ + e^-$ and $n + e^+ \leftrightarrow p^+ + \bar{\nu}_e$ become inefficient), which happens at $T \sim 1$ MeV. The neutrons start decaying until they combine with protons to form deuterium D around $T \sim 0.1$ MeV. Then, the deuterium can combine with protons to form helium 3 ^{3}He , then helium 4 ^{4}He. A chain of reactions follows, forming more light elements such as ^{6}Li and ^{7}Li [Baumann, 2022].

If PBHs evaporate during the BBN, they can inject particles into the plasma that can change the abundance of light elements produced then. For instance, PBHs with $m_{\text{PBH}} \sim 10^6 - 10^7$ kg have a lifetime of $\tau_{\text{PBH}} \sim 10^0 - 10^2$ s, which is comparable to the BBN duration. Their HR would increase the neutron-to-proton ratio, leading to a higher abundance of ^{4}He [Bagui et al., 2023; Carr et al., 2010, 2021]. PBHs with a slightly larger mass, $m_{\text{PBH}} \sim 10^7 - 10^9$ kg, can inject high-energy hadrons which would dissociate the light elements produced during the BBN.

4.2.1.B Gamma-rays and neutrinos from exploding PBHs

For PBHs with $m^i_{\text{PBH}} \sim 10^{12}$ kg, their lifetime is similar to the age of the universe, and they may have just exploded. The explosion can produce gamma-rays bursts and high-energy extra-galactic neutrinos, even though no gamma-ray that could be attributed to PBH explosions have been detected so far [Bagui et al., 2023]. PBHs could also produce high-energy neutrinos. Notably, the recent detection of a high-energy neutrino by the KM3Net collaboration [Aiello et al., 2025] as been interpreted as possibly originating from a PBH explosion[1] [Boccia and Iocco, 2025].

[1] The authors specify that such a PBH should be "memory burdened" in this scenario. The memory burden effect is discussed in chapter 6.

4.2.1.C Positron annihilation

Positrons are among the products of PBH evaporation. If they annihilate with electrons, they produce two photons of energy $E_\gamma = m_e \approx 0.511$ MeV. The signature of the annihilation is a peak in the gamma-ray spectrum at $E_\gamma = 0.511$ MeV, and can be used to constrain the fraction of PBHs in the universe. The center of the Milky Way can be screened for the Galactic 511 keV line thanks to the INTEGRAL satellite. Note that INTEGRAL orbits Earth (inside the heliosphere), whereas Voyager 1 is outside the heliopause and thus can measure sub-GeV flux of $e^\pm$ unaffected by solar modulation. Both Voyager 1 and the INTEGRAL satellite have been used to set limits on the fraction of PBHs as illustrated in fig. 4.3b.

4.2.1.D Cosmic Microwave Background

For PBHs with $m^i_{\text{PBH}} \gtrsim 10^{10}$ kg, $\tau_{\text{PBH}} \gtrsim 10^{11}$ s: they evaporate after recombination and can inject high-energy photons and electron-positron pairs into the plasma. The photon distribution of the CMB is then modified, leading to a distortion away from the blackbody spectrum. The e^+-e^- pairs can also maintain the ionization of the plasma, leading to a change in the CMB anisotropies: the scattering of the extra free electrons with the CMB photons tends to wash out the small-scale anisotropies.

4.2.2 Microlensing, BH dynamics and Gravitational Waves

It is possible to classify the numerous constraints on PBHs into several categories: microlensing, dynamical limits, accretion limits, ... We refer to [Bagui et al., 2023; Auffinger, 2023] for exhaustive lists of the constraints. Let us just mention some of the most important ones here:

- Microlensing:
  Any PBH acts like a lens due to its compactness. When passing between a light source and an observer, the light rays are bent by the gravitational field of the PBH. This produces a transient variation of the brightness of the source (typically, a distant star or quasar). For small PBHs, the effect is really short, hence the name *microlensing*.

- Dynamical limits:
  PBHs being massive objects, they can influence the dynamics of their surroundings through their gravitational interaction. Gravitational friction can trap them in the vicinity of compact objects, such as stars, that they can then accrete. In bound systems, PBHs can disturb the orbits and in the presence of stars, they can heat them through their gravitational effect.

- Accretion limits:
  If PBHs accrete matter, they could form an accretion disk, which would emit radiation. This radiation could then heat and ionize the surrounding matter, leading to a detectable signal. If this accretion happens sufficiently early in the universe, it could affect the CMB.

- Gravitational waves:
  Gravitational waves (**GW**) can be produced by PBHs when they form, evaporate and merge, creating a background of *stochastic* gravitational waves. It might be the only way to set constraints on the lighter PBHs, with $m^i_{\text{PBH}} \lesssim 10^6$ kg and $\tau_{\text{PBH}} \lesssim 100$ s, that evaporated before the BBN. The stochastic background of GWs is expected to be detected by future experiments, such as LISA.

4.2.3 Summary

The constraints on the fraction of PBHs in the universe are summarized and illustrated in fig. 4.2. We can see that it remains mainly one region where the DM fraction of PBHs f is not constrained and could reach unity: the mass range $m^i_{\text{PBH}} \in [10^{14}, 10^{20}]$ kg. Another region of interest is the mass range around a solar mass $m^i_{\text{PBH}} \sim 10^{30}$ kg, where it has been proposed that some constraints could instead be taken as support for the existence of PBHs [Carr et al., 2024]. Finally, light PBHs with $m^i_{\text{PBH}} \lesssim 10^{12}$ kg are also of interest, as the current constraints on their abundance are based on their semiclassical evaporation. In sec. 6.5, we will discuss how these constraints can be modified in the context of the memory burden effect.

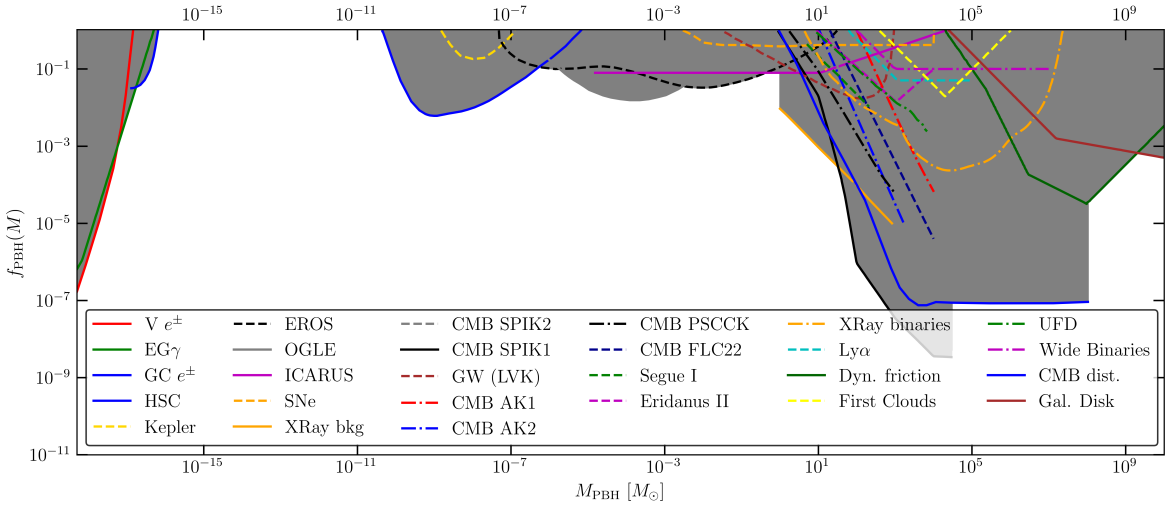

Figure 4.2: Limits on $f_{\rm PBH}$ as a function of the mass for a monochromatic mass function. $Ve^\pm$ comes from the observation of $e^\pm$ by Voyager 1, EG γ comes from extragalactic gamma-ray and CG $e^\pm$ comes from positron annihilation in the Galactic Center. For the rest of the constraints, see [Bagui et al., 2023].

In this work, we will focus on the limits affecting light PBHs, we thus zoom in on the low-mass region in figures 4.3a and 4.3b. Even though f is not properly defined in the case of the evaporating constraints, we can relate f to β through eq. (4.11).

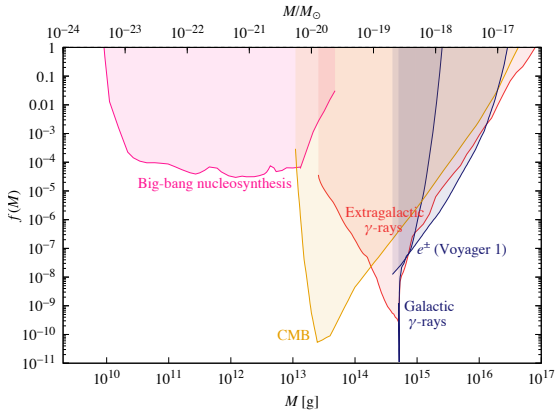

(a) Limit on the DM fraction of PBHs as a function of the mass for a monochromatic mass function. PBHs with a lifetime $\tau \lesssim 10^{-2}$ s are not constraint by the BBN. From [Carr et al., 2021].

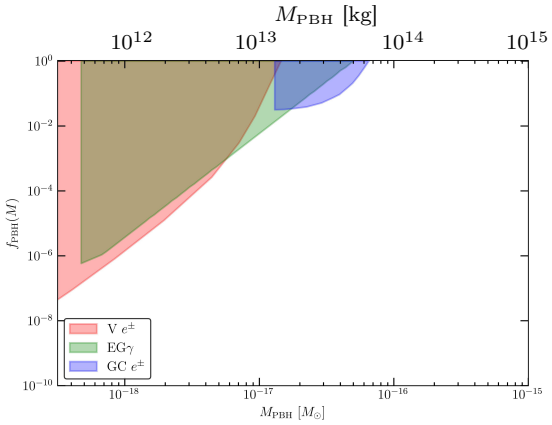

(b) Limits on $f_{\rm PBH}$ as a function of the mass for a monochromatic mass function zoomed in on evaporation-based limits. $Ve^\pm$ comes from the observation of $e^\pm$ by Voyager 1, EG γ comes from extragalactic gamma-ray and CG $e^\pm$ comes from positron annihilation in the Galactic Center. From [Bagui et al., 2023].

CHAPTER

5

LOOP QUANTUM GRAVITY

This chapter is a concise and practical overview of Loop Quantum Gravity (LQG), collecting only the definitions, equations and ideas that are relevant for the rest of the master's thesis. We do not aim to give a complete review of the theory, but rather to provide the necessary background to motivate the model presented in chapter 7.

The classical theory of gravity is reviewed in sec. 5.1 and recast into the language best suited for quantization. The metric and tetrad formulations are introduced, along with the Palatini-Holst action, and the Ashtekar variables to obtain the flux-holonomy algebra. This section concludes with a brief introduction to the discretization of the theory on a two-complex.

In sec. 5.2, we sketch the canonical quantization programme: how one constructs the kinematical Hilbert space out of spin-network states, imposes Gauss and diffeomorphism constraints, and constructs geometric operators such as the area operator $\hat{A}$. Throughout, we quote only the most relevant equations and results, and refer to the literature for more details.

Finally, the LQG picture of BH evolution is presented: how collapse leads to a nonsingular Planck star, the matching to a quantum-corrected exterior metric, the tunneling to a White Hole (**WH**), and the properties and lifetimes of the resulting Planck-scale remnants (the *rovellino*). Key formulae and conformal diagrams are presented, but full details can be found in [Rovelli and Vidotto, 2024].

5.1 Classical Gravity

This section reformulates classical General Relativity (**GR**) in a form ready for quantization. It is a compact review, most derivations are standard and can be found in the literature [Misner et al., 1973; Doná and Speziale, 2010; Rovelli and Vidotto, 2014b; Mele, 2017].

We start by recalling the best-known formulation of GR (subsec. 5.1.1) and its famous Einstein-Hilbert action ($S_{\text{E-H}}$). The tetrad formulation (subsec. 5.1.2) is introduced, motivated by the existence of fermionic matter. The action (S_{T}) is then naturally extended to the first-order formalism (S_{P}) and to the Holst action (S_{H}). In subsec. 5.1.3, the theory is reformulated in the Hamiltonian formalism, then using the Ashtekar variables (eq. (5.13)) and their smeared version (def. 5.7), leading to the flux-holonomy algebra (eq. (5.18)). Finally, a "baby version" of the discretization of GR is presented (the euclidean three-dimensional GR) on a two-complex in subsec. 5.1.4.

5.1.1 Metric formulation

Before diving into the basics of LQG, it is useful to reformulate GR in a way that is more suitable for quantization. The Einstein field equations (EFE) can be derived from a variational principle, by varying the Einstein-Hilbert action with respect to the metric $g_{\mu\nu}$.

Definition 5.1. The Einstein-Hilbert action $S_{\text{E-H}}[g]$ is given by:

$$S_{\text{E-H}}[g] = \frac{1}{16\pi}\int d^4x\sqrt{-g}\,(R - 2\Lambda) \tag{$S_{\text{E-H}}$}$$

Where $g = \det(g_{\mu\nu})$, $R = R^{\mu}{}_{\mu} = g^{\mu\nu}R_{\mu\nu} = g^{\mu\nu}R^{\rho}{}_{\mu\rho\nu}$ is the Ricci scalar and Λ is the cosmological constant.

For simplicity, we will set $\Lambda = 0$ in the following.

5.1.2 Tetrad formulation

We know that fermionic matter exists in the universe, governed *in flat spacetime* by the Dirac equation:

$$\left(i\gamma^I\partial_I - m\right)\psi = 0 \tag{5.1}$$

In order to couple geometry and matter, one needs to map world indices μ to internal flat indices I using a tetrad field $e^I{}_\mu(x)$ (and co-tetrad $e_I{}^\mu(x)$). The tetrad field is a map between the tangent space of the manifold $\mathcal{M}$ and the Minkowski space $\mathbb{R}^{(1,3)}$, as illustrated in fig. 5.1. Pictorially, it can be seen as a realization of the equivalence principle: at each point of the manifold, one can choose a local inertial frame where the metric is Minkowskian.

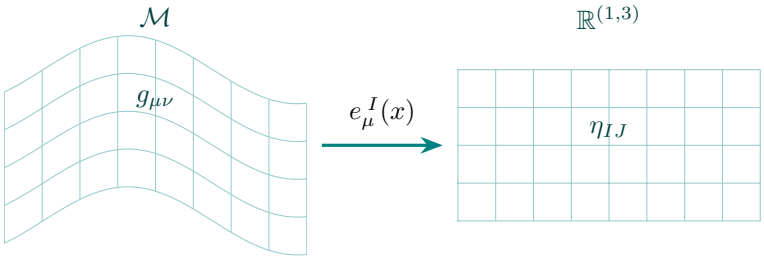

Figure 5.1: Illustration of the tetrad field $e^I{}_\mu(x)$. The tetrad maps the tangent space of the manifold $\mathcal{M}$ to the Minkowski space $\mathbb{R}^{(1,3)}$

The relation between the metric and the tetrad is given by:

$$g_{\mu\nu}(x) = e^I{}_\mu(x)e^J{}_\nu(x)\eta_{IJ} \tag{5.2}$$

Let us use the form notation $e^I = e^I_\mu(x)\mathrm{d}x^\mu$. From the invariance of η_{IJ} under Lorentz transformation, we have:

$$e^I(x)e^J(x)\eta_{IJ} \mapsto e^I(x)e^J(x)\Lambda^K{}_I(x)\Lambda^L{}_J(x)\eta_{KL} = e^K(x)e^L(x)\eta_{KL}$$

Thus, the tetrad field satisfies a local Lorentz $SO(3,1)$ gauge invariance $e^I \mapsto \Lambda^I_J(x)e^J$.

Definition 5.2. We introduce the 1-form, antisymmetric, *Lorentz connection* ω^{IJ}, defined by:

$$0 = De^I = \mathrm{d}e^I + \omega^I{}_J \wedge e^J \tag{5.3}$$

The antisymmetry of the connection is implied by the metricity:

$$0 = D\,\eta_{IJ} = \partial\,\eta_{IJ} - \omega^{K}{}_{I}\eta_{KJ} - \omega^{K}{}_{J}\eta_{IK} = -2\omega_{(IJ)}$$

The Lorentz connection then lies in the Lie algebra $\mathfrak{so}(1,3)$. The Dirac equation eq. (5.1) is extended to its covariant form [1]:

$$\left(i\gamma^{I}e_{I}{}^{\mu}D_{\mu} - m\right)\psi = 0 \qquad \text{with } D_{\mu}\psi = \partial_{\mu}\psi + \frac{1}{4}\omega^{IJ}{}_{\mu}\gamma_{I}\gamma_{J}\psi \tag{5.5}$$

Definition 5.3. It is useful to introduce the *curvature 2-form* F^{IJ}, defined by:

$$F^{I}{}_{J} = D\omega^{I}{}_{J} = \mathrm{d}\omega^{I}{}_{J} + \omega^{I}{}_{K}\wedge\omega^{K}{}_{J} \tag{5.6}$$

Property 5.1. *The curvature 2-form, when built from the Lorentz connection, is related to the Ricci scalar by [Doná and Speziale, 2010]:*

$$F^{IJ}{}_{\mu\nu}\,e_{I}{}^{\mu}e_{J}{}^{\nu} = R \tag{5.7}$$

The Einstein-Hilbert action $S_{\text{E-H}}$ can be rewritten in terms of the (co-)tetrad as[2]:

$$S_{\text{T}}[e] = \frac{1}{32\pi}\int e^{I}\wedge e^{J}\wedge F^{KL}\epsilon_{IJKL} = \frac{1}{16\pi}\int e\wedge e\wedge\star F[e] \tag{S_{T}}$$

Where we wrote $\star F_{IJ} = \frac{1}{2}\epsilon_{IJKL}F^{KL}$.

Definition 5.4. Promoting the connection ω^{IJ} as an independent field defines the *Palatini action*:

$$S_{\text{P}}[e,\omega] = \frac{1}{16\pi}\int e\wedge e\wedge\star F[\omega] \tag{S_{P}}$$

Note that the independent connection ω^{IJ} is not the spin connection anymore. We do recover it on shell. Indeed, varying the action S_{P} with respect to the connection ω^{IJ} constraints it to be torsion-free:

$$\delta_{\omega}S_{\text{P}} = \epsilon e\wedge De \implies De^{I} = 0 \tag{5.8}$$

The action S_{P} is polynomial in the tetrad and the connection (there is no square root like in $S_{\text{E-H}}$, only algebraic terms, ...), and can be written purely in terms of differential forms. If one asks what other terms could be added to the action with the same properties and symmetries, one finds that the only other possibility (up to boundary terms) is the *Holst term*.

Definition 5.5. The *Holst action* is defined as:

$$S_{\text{H}}[e,\omega] = \frac{1}{16\pi}\left(\int e\wedge e\wedge\star F[\omega] + \frac{1}{\gamma}\int e\wedge e\wedge F[\omega]\right) \tag{S_{H}}$$

Where γ is the Barbero-Immirzi parameter.

[1] In general, the covariant derivative acts on an object v in some representation ρ of the Lorentz group generated by M_{KL} as:

$$D_{\mu}v = \partial_{\mu}v + \frac{1}{2}\omega^{IJ}{}_{\mu}\rho\left(M\right)_{IJ}v \tag{5.4}$$

[2] Note that the actions $S_{\text{E-H}}$ and S_{T} are not completely equivalent since $S_{\text{E-H}}$ contains the absolute value of the determinant of the metric, while S_{T} does not. Since fermions can be coupled to the tetrad, the dynamics can be affected by this difference [Rovelli and Vidotto, 2024].

The Holst term does not affect the classical equation of motion (the field equations are given by $De = 0$ and $G_{\mu\nu} = 0$), but it does change the canonical variables.

Notice that the action can be rewritten as:

$$S_{\mathrm{H}}[e,\omega] = \frac{1}{16\pi}\int B[e]\wedge F[\omega] \quad \text{with } B[e] \equiv \star e\wedge e + \frac{1}{\gamma}e\wedge e \tag{5.9}$$

5.1.3 Ashtekar variables

Let us reformulate the theory in the Hamiltonian formalism. We assume a $3+1$ splitting of the spacetime $\mathcal{M} \cong \mathbb{R}\times\Sigma$ (with coordinates (t, x^a)). The metric can be decomposed as:

$$g_{\mu\nu} = \left(\begin{array}{c|c} N^2 - N_aN^a & N_b \\ \hline N_a & q_{ab} \end{array}\right) \tag{5.10}$$

Where we introduced $q_{ab} = g_{ab}$ the 3-metric, $N_a = g_{a0}$ the *Shift function* and $N = \sqrt{g^{00}}$ the *Lapse function*. The 3-metric g_{ab} is the metric induced on the surface Σ by the full metric $g_{\mu\nu}$. The lapse function N is the proper time elapsed between two slices Σ_t and $\Sigma_{t+\delta t}$, along the normal to the surface n^μ. The shift function N_a encodes how coordinates shift tangentially between slices. This decomposition is easier to understand with a sketch of the situation, given in fig. 5.2.

We introduce a field of *triads* $e^i{}_a(x)$ on each Σ_t:

$$g_{ab} = e^i{}_a e^j{}_b \delta_{ij} \tag{5.11}$$

The tetrad field can be decomposed as $e^I{}_0 = e^I{}_\mu \tau^\mu = Nn^I + N^a e^I{}_a$. In the time gauge, $n^I = \delta^I_0$ so that $e^I{}_0 = (N, N^a e^i{}_a)$.

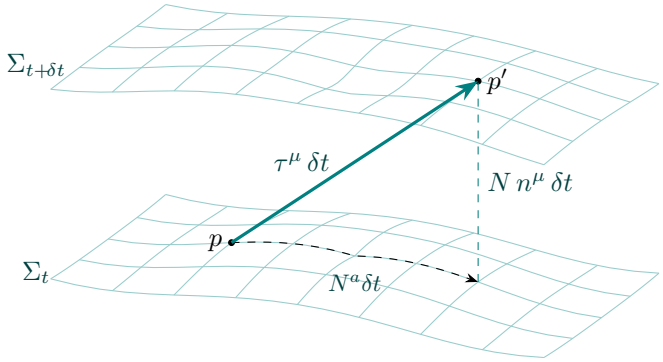

Figure 5.2: Illustration of the $3+1$ splitting of $\mathcal{M}$.

One could work out the canonically conjugate variables to both the tetrad $e^I{}_a$ and the connection $\omega^{IJ}{}_a$, but it turns out that the added local Lorentz symmetry $e \mapsto \Lambda e$ and the promotion of the connection ω to an independent variable leads to *second class* constraint algebra [Doná and Speziale, 2010] (constraints are said to be first class if their Poisson bracket vanishes on-shell, and second class otherwise).

However, a particular choice of variables allows one to implement part of the constraints and bring the constraint algebra back to *first class*.

Definition 5.6. The **densitized triad** is defined as:

$$E_i^{\ a} = e\, e_i^{\ a} = \frac{1}{2}\epsilon_{ijk}\epsilon^{abc}e^j_{\ b}e^k_{\ c} \tag{5.12}$$

The **Ashtekar-Barbero connection** is defined as:

$$A^i_{\ a} = \gamma\omega^{0i}_{\ \ a} + \frac{1}{2}\epsilon^{ijk}\omega_{jka} \tag{5.13}$$

These new variables satisfy:

$$\{A^i_{\ a}(x), E_j^{\ b}(y)\} = 8\pi\gamma\delta^b_a\delta^i_j\delta^3(x,y) \tag{5.14a}$$
$$\{A^i_{\ a}(x), A^j_{\ b}(y)\} = 0 \tag{5.14b}$$
$$\{E_i^{\ a}(x), E_j^{\ b}(y)\} = 0 \tag{5.14c}$$

The Holst action S_{H} can be rewritten in terms of the new variables as [Doná and Speziale, 2010]:

$$S_{\tilde{\mathrm{H}}}[A,E,N,N^a] = \frac{1}{16\pi\gamma}\int dt\int_\Sigma d^3x\left(\dot{A}^i_{\ a}E_i^{\ a} - A^i_{\ 0}G_i - NH - N^aH_a\right) \tag{5.15a}$$

With the constraints:

$$\begin{cases} G_i = D_aE_i^{\ a} = \partial_aE_i^{\ a} + \epsilon_{ijk}A^j_{\ a}E^{ka} & \text{Gauss constraints} \quad (5.15b)\\ H = \left(F^i_{ab} - \left(\gamma^2+1\right)\epsilon^i_{\ jk}K^j_{\ a}K^k_{\ b}\right)\dfrac{\epsilon_{ijk}E_j^{\ a}E_k^{\ b}}{\det(E)} + \sim G & \text{Hamiltonian constraint} \quad (5.15c)\\ H_a = \dfrac{1}{\gamma}F^j_{ab}E_j^{\ b} + \epsilon_{ijk}A^j_{\ a}E^{ka} & \text{Space-diffeomorphism constraints} \quad (5.15d)\end{cases}$$

Where we omit the term proportional to the Gauss constraints in the hamiltonian one, and with:

$$F^i_{ab} = \partial_aA^i_{\ b} - \partial_bA^i_{\ a} + \epsilon^i_{\ jk}A^j_{\ a}A^k_{\ b} \tag{5.15e}$$
$$K^i_{\ a} = K_{ab}e^i_{\ b} = \frac{1}{2N}\left(\dot{q}_{ab} - \nabla_{(a}N_{b)}\right)e^i_{\ b} \tag{5.15f}$$

Let us now integrate the Ashtekar variables in order to smear the algebra 5.14.[3]

Definition 5.7. The **flux** of $E_i^{\ a}$ across a surface S is defined as:

$$E_i(S) = \int_S n_aE_i^{\ a}\mathrm{d}^2\sigma = \int_S \star E_i \tag{5.16}$$

Where $n_a = \epsilon_{abc}\partial_{\sigma_+}x^b\partial_{\sigma_-}x^c$ is the unit normal to the surface S and $\mathrm{d}^2\sigma$ is the area element on the surface.
The **holonomy** of $A^i_{\ a}$ along a path γ is defined as:

$$h_\gamma(A) = \mathcal{P}\exp\left(\int_\gamma A^i_{\ a}\tau_i\mathrm{d}x^a\right) \tag{5.17}$$

Where $\mathcal{P}$ is the path ordering operator and $\tau_i = \frac{i}{2}\sigma_i$ are the generators of the $SU(2)$ algebra.

The flux $E_i(S)$ thus lives in $\mathfrak{su}(2)$, while the holonomy $h_\gamma(A)$ lives in $SU(2)$. The Poisson algebra eq. (5.14) can be rewritten in terms of the flux and holonomy as [Mele, 2017]:

$$\{h_\gamma(A)\,,\, h_{\gamma'}(A)\} = 0 \tag{5.18a}$$
$$\{E_i(S)\,,\, E_j(S')\} = -\delta_{S,S'}\epsilon_{ijk}E_k(S) \tag{5.18b}$$
$$\{E_i(S)\,,\, h_\gamma(A)\} = \tau_ih_\gamma(A) \tag{5.18c}$$

[3] The def. 5.7 has been simplified for clarity. For more rigorous mathematical treatments, see for example section 2.3 of [Doná and Speziale, 2010].

5.1.4 Discretization of GR on a two-complex

For simplicity, we consider the euclidean theory in 3 dimensions. The discretization of full $1+3$ lorentzian theory is a generalization of the latter (it can be found in chapter 7 of [Rovelli and Vidotto, 2014b]), and is not required to achieve the results needed for this thesis.
Let us first introduce the notion of triangulation before defining the discretization of the theory.

Definition 5.8. A **simplex** is a generalization of a triangle in d-dimensions. A k-simplex is a k-dimensional polytope that is the convex hull of its $k+1$ vertices

A 0-simplex is a point, a 1-simplex is a line, a 2-simplex is a triangle and a 3-simplex is a tetrahedron.

In 3 dimensions, one can discretize the manifold $\mathcal{M}$ thanks to a *triangulation* $\triangle$. The space is "chopped" into tetrahedra, bounded by triangles that are themselves bounded by segments, which meet at points. In LQG, we need an extra structure associated to the triangulation: its dual.

Definition 5.9. Let $\triangle$ be a triangulation of the manifold $\mathcal{M}$. The **dual triangulation** $\triangle^\star$ is obtained by putting a *vertex* at the center of each tetrahedron, and joining adjacent vertices with *edges*.

Each *vertex* $v \in \triangle^\star$ is then dual to a *tetrahedron* $\vartheta \in \triangle$, each *edge* $e \in \triangle^\star$ is dual to a *triangle* $t \in \triangle$, and each *face* $f \in \triangle^\star$ is dual to a *segment* $s \in \triangle$. When on the boundary $\partial\triangle$, the vertices are referred to as *nodes* $n \in \partial\triangle^\star$ and the edges as *links* $l \in \partial\triangle^\star$. Together, the nodes and the links form a graph $\Gamma = \partial(\triangle^\star)$. This duality is illustrated in fig. 5.3.

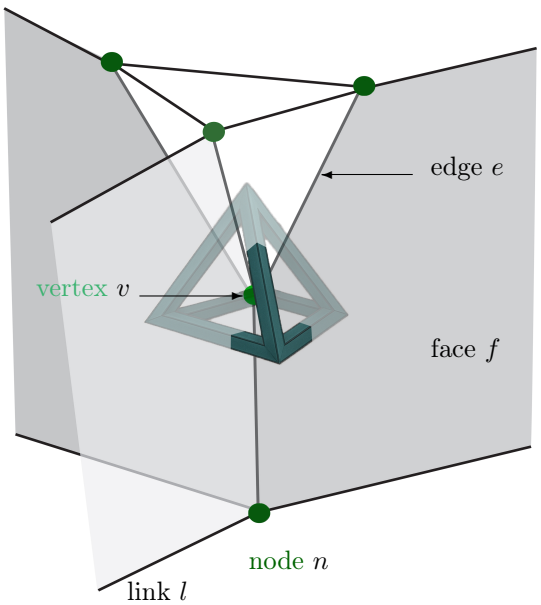

Figure 5.3: Illustration of a triangulation and its dual. Adapted from [Rovelli and Vidotto, 2024].

The dual triangulation $\triangle^\star$ is a *2-complex*: a set of vertices, edges and faces, with faces meeting at edges and edges meeting at vertices. Now that we have a triangulation, we can assign discrete variables to it, or, equivalently, to its dual:

$$\forall e \in \triangle^\star, \quad e \mapsto h_e \in SU(2) \tag{5.19a}$$
$$\forall f \in \triangle^\star, \quad f \mapsto E_i(f) \in \mathfrak{su}(2) \tag{5.19b}$$

Group elements h_e around a face f can be multiplied together to form a *holonomy* around the face f.

Definition 5.10. Denoting by $e \in f$ the edges around the face f, we define the holonomy around the face f as:

$$h_f \equiv \prod_{e \in f} h_e \tag{5.20}$$

The discrete action can be written as:

$$S_\triangle = \frac{1}{8\pi} \sum_f \mathrm{Tr}\left(E^i(f)\tau_i h_f\right) \tag{5.21}$$

If $h_f \neq \mathbb{1}_{SU(2)}$, there is curvature associated to the face $f \in \triangle^\star$ (thus to the corresponding segment $s \in \triangle$). To show it, let us place ourselves in the fundamental representation. The trace is on the internal representation indices of the $(\tau_i) = (\tau_i)^\alpha{}_\beta$ with $\alpha, \beta = 1, 2$. The action eq. (5.21) can be rewritten as $S \sim \sum_f E^i(f)\mathrm{Tr}(\tau_i h_f)$ (since $h_f \sim \exp\left(A^i \tau_i\right)$ also carries $su(2)$ representation indices). Thus, the variation of the action with respect to $E^i(f)$ gives:

$$\delta_{E_i(f')} S_\triangle = \frac{1}{8\pi} \sum_f \delta E^i(f) \mathrm{Tr}\left(\tau_i h_f\right) \tag{5.22}$$

$$\implies \mathrm{Tr}\left(\tau_i h_f\right) = 0 \quad \forall f \in \triangle^\star, \forall i \in \{1, 2, 3\} \tag{5.23}$$

Since $h_f \in SU(2)$, we can always write it as $h_f = \cos(\theta_f) + i(n^i \sigma_i)\sin(\theta_f)$ with $n^i n_i = 1$. The trace becomes:

$$\mathrm{Tr}\left(\tau_i h_f\right) = \mathrm{Tr}\left(\frac{i}{2}\sigma_i \left(\cos(\theta_f) + i(n^j \sigma_j)\sin(\theta_f)\right)\right) \tag{5.24}$$

$$= \frac{i}{2}\mathrm{Tr}(\sigma_i)\cos(\theta_f) - \frac{1}{2} n^j \mathrm{Tr}(\sigma_i \sigma_j)\sin(\theta_f) \tag{5.25}$$

$$= -n^j \delta_{ij} \sin(\theta_f) \tag{5.26}$$

$$= -n^i \sin(\theta_f) \tag{5.27}$$

Since $n^i \neq 0$, we have $\sin(\theta_f) = 0 \implies \theta_f = 0$ or π. Thus, the variation of the action eq. (5.21) with respect to the flux $E^i(f)$, up to a sign, imposes flatness (as expected for a solution of the EFE in 3D):

$$h_f = \pm \mathbb{1}_{SU(2)} \tag{5.28}$$

Notice that the (smeared) Gauss constraint 5.15b is equivalent to the *closure constraint* that the sum of the fluxes bounding a node must vanish:

$$C_n^i = \sum_{l \text{ connected to } n} E_i = 0 \tag{5.29}$$

The Gauss constraint is also smeared, but over the whole Σ:

$$G(\Lambda) = \int_\Sigma \mathrm{d}^3x\, G_i(x)\Lambda^i(x) \tag{5.30}$$

Now, consider a region $R \in \Sigma$ surrounding a node n, and a test function $\tilde{\Lambda}^i(x)$ constant on R. Then:

$$G(\tilde{\Lambda}) = \int_R \mathrm{d}^3x\, \tilde{\Lambda}^i(x) D_a E_i{}^a \tag{5.31a}$$

$$= -\int_{\partial R} \mathrm{d}^2\sigma\, n_a \tilde{\Lambda}^i(x) E_i{}^a \tag{5.31b}$$

$$\implies \sum_{l \text{ connected to } n} E_i(S_\alpha) = 0 \tag{5.31c}$$

Where we denote by l the links dual to the surface S_α such that $\cup_\alpha S_\alpha = \partial R$.

We now have a discretization of the theory, where the lengths and areas can be taken as small as desired. It is important to note the difference between the discretization and the quantization of the theory. The discretization is a truncation of the degrees of freedom, while the quantization is a procedure to promote the variables to operators acting on a Hilbert space.

5.2 Canonical Quantization and LQG

Until now, we simply defined a *discretization* of the classical theory, a truncation of the degrees of freedom. The next step is the *quantization* of the theory. The quantization procedure is not an easy task and the goal of this section is not to provide the complete quantization of the theory, but rather to extract from it a few important results for the rest of this thesis. Detailed treatments of the quantization of LQG can be found in [Rovelli, 2004; Doná and Speziale, 2010; Rovelli and Vidotto, 2014b].

Subsec. 5.2.1 briefly presents the canonical quantization procedure of gauge theories. The construction of the Hilbert space is recalled in subsec. 5.2.2 by introducing the *spin network*. Subsec. 5.2.3 presents one of the main results of LQG: the spectrum of the area operator (eq. (5.50)).

5.2.1 Canonical quantization of gauge theories

A procedure to quantize gauge theories is the following:

1. Promote the phase space variables (h, E) to operators acting on a *kinematical* Hilbert space $\mathcal{H}_{\text{kin}}$ satisfying:
$$\{h, E\} \mapsto [\hat{h}, \hat{E}] = i\hbar\{h, E\} \tag{5.32}$$
2. Promote the constraints $C = (H^\mu, G^i)$ to operators acting on $\mathcal{H}_{\text{kin}}$
3. Select the physical Hilbert space $\mathcal{H}_{\text{phys}}$ as the kernel of the constraint operators:
$$\mathcal{H}_{\text{phys}} = \left\{\psi \in \mathcal{H}_{\text{kin}} \mid \hat{C}\psi = 0\right\} \tag{5.33}$$

In our case, we first need to find a kinematical Hilbert space $\mathcal{H}_{\text{kin}}$ on which the operators $\hat{h}$ and $\hat{E}$ act. Then, impose the constraints $\hat{G}_i$ and $\hat{H}^\mu$ to obtain the physical Hilbert space $\mathcal{H}_{\text{phys}}$:

$$\mathcal{H}_{\text{kin}} \overset{\hat{G}_i=0}{\longrightarrow} \mathcal{H}^0_{\text{kin}} \overset{\hat{H}^\mu=0}{\longrightarrow} \mathcal{H}_{\text{phys}} \tag{5.34}$$

5.2.2 Construction of the kinematical Hilbert space

The kinematical Hilbert space $\mathcal{H}_{\text{kin}}$ of LQG is a space of functionals equipped with a scalar product.

Definition 5.11. A graph $\Gamma \subset \Sigma$ is a finite and ordered collection of smooth oriented paths $\gamma_l \in \Sigma$ with $l = 1, \dots, L$ meeting at most at their endpoints.
Such paths are called *links* or *edges*, and their intersection points are called *nodes* or *vertices*. The total number of links is L and the total number of nodes is N.

We start from a graph $\Gamma \subset \Sigma$ and define on it the set of smooth functions depending on the Ashtekar connection ${A^i}_a$ only through the holonomies $h_\gamma(A)$:

$$f : \begin{pmatrix} SU(2)^L & \to & \mathbb{C} \\ (h_1(A), \dots, h_L(A)) & \mapsto & \psi_\Gamma = f\left[h_1(A), \dots, h_L(A)\right] \end{pmatrix} \tag{5.35}$$

Now, we need a scalar product on the space of functionals $\{\psi_\Gamma\}$. Let ψ_{Γ_1} and χ_{Γ_2} be two functionals. We define $\Gamma = \Gamma_1 \cup \Gamma_2$, and ψ_Γ and χ_Γ as the previous functionals trivially extended to Γ. The scalar product is then defined as:

$$\langle \psi_{\Gamma_1} | \chi_{\Gamma_2} \rangle = \int_{SU(2)^L} \mathrm{d}h_1 \dots \mathrm{d}h_L \, \overline{\psi_\Gamma} \chi_\Gamma \tag{5.36}$$

Where $\mathrm{d}h$ is the Haar measure on $SU(2)$. The kinematical Hilbert space of a given graph Γ $\mathcal{H}_{\text{kin}}|_\Gamma$ is then:

$$\mathcal{H}_{\text{kin}}|_\Gamma = L_2\left[SU(2)^L\right] \tag{5.37}$$

The states are wavefunctions $\psi_\Gamma[h_l]$ of L group elements $h_l \in SU(2)$, one for each link $l \in \Gamma$. The holonomies and the fluxes act on states as:

$$\hat{h}_\gamma(A)\,|\psi\rangle = h_\gamma(A)\,|\psi\rangle \tag{5.38}$$

$$\hat{E}_i(S)\,|\psi\rangle = -i8\pi\gamma \int_S \mathrm{d}\sigma_a\, n^i \frac{\delta}{\delta A^i{}_a}\,|\psi\rangle \tag{5.39}$$

Now, one needs to select the $SU(2)$-invariant states in $\mathcal{H}_{\text{kin}}$, namely implement the Gauss constraint $\hat{G}_i$. To do so, let us notice that under a local gauge transformation $g(x) \in SU(2)$, the holonomy transforms as:

$$h_\gamma(A) \mapsto g(\gamma(0))h_\gamma(A)g^{-1}(\gamma(1)) \tag{5.40}$$

The gauge transformation only acts on the endpoints (the nodes) of the edge (the *source* and *target*). The gauge-invariant states are then the states ψ_Γ for which the transformations at the end points of the holonomies cancel each other. The kinematical Hilbert space is then reduced to:

$$\mathcal{H}^0_{\text{kin}}\big|_\Gamma = \text{Inv}_{\text{SU(2)}}(\mathcal{H}_{\text{kin}}|_\Gamma) = L_2\left[SU(2)^L \diagup SU(2)^N\right] \tag{5.41}$$

Eq. 5.41 is "guessed" here, but can be derived rigorously with the concept of *intertwiner*. In the 3D case, each node is trivalent, and the space of gauge-invariant states is at most one-dimensional. In the 4D case, the nodes are generically 4-valent, and the space of gauge-invariant states can have dimension greater than one. This introduces a second quantum number.

Definition 5.12. In 3D euclidean LQG, a **spin network** $(\Gamma, \{j_l\}_{l=1,\dots,L})$ is a graph Γ with a spin j_l assigned to each link $l \in \Gamma$.

In the full Lorentzian $1+3$ case, the spin network is labelled by $|j_l, k_n\rangle$, where j_l is *coloring* the link l and k_n is the *intertwiner* quantum number, labeling the volume eigenvalue at each node n.

Property 5.2. *In LQG, a state ψ_Γ is a superposition of spin network states*

$$\psi_\Gamma = \sum_{j_l} \hat{\psi}_{j_1,\dots,j_L}\,|\Gamma, \{j_l\}\rangle \tag{5.42}$$

5.2.3 Quantum geometry

At the classical level, the area of a surface S is given by:

$$A(S) = \int_S \mathrm{d}^2\sigma\,\sqrt{g|_S} \tag{5.43a}$$

In terms of the triad field, we have:

$$A(S) = \int_S \mathrm{d}\sigma_+\mathrm{d}\sigma_-\,\sqrt{\det\left(q_{ab}\frac{\partial x^a}{\partial\sigma^+}\frac{\partial x^b}{\partial\sigma^-}\right)} \tag{5.43b}$$

Let us rewrite the determinant as:

$$\begin{aligned}\det\left(q_{ab}\frac{\partial x^a}{\partial\sigma^+}\frac{\partial x^b}{\partial\sigma^-}\right) &= q_{ab}q_{cd}2\frac{\partial x^a}{\partial\sigma^+}\frac{\partial x^{[b}}{\partial\sigma^-}\frac{\partial x^{c]}}{\partial\sigma^+}\frac{\partial x^d}{\partial\sigma^-}\\ &= \det(q_{ab})\,q^{cd}n_cn_d\\ &= \det\left(e^i{}_a\right)^2 e_i{}^c e^{id}n_cn_d\end{aligned}$$

The area as a function of the densitized triad is then given by:

$$A(S) = \int_S \mathrm{d}^2\sigma \sqrt{E_i{}^a E^{ib} n_a n_b} \tag{5.43c}$$

Now, for small enough surfaces, the flux reads $E_i(\delta S) \approx E_i{}^a n_a \delta S$, so that:

$$A(\delta S) \approx \int_{\delta S} \mathrm{d}^2\sigma \sqrt{E_i(\delta S) E^i(\delta S)} \tag{5.44}$$

It is then possible to define the *area operator* $\hat{A}(S)$.

Definition 5.13. The **area operator** $\hat{A}(S)$ is defined as:

$$\hat{A}(S) = \lim_{N\to\infty} \sum_{j=1}^{N} \sqrt{E_i(\delta S_j) E^i(\delta S_j)} \tag{5.45}$$

To compute the spectrum of the area operator, let us decompose our states in terms of Wigner matrices $D^j_{mn}(h)$. As a warmup, let us consider the case of a graph Γ_0 with a single link γ_0. A state $\psi_{\Gamma_0}[A]$ will then depend on a single holonomy $h_0 \in SU(2)$ (thus living in $L_2[SU(2)]$). The state can be written as:

$$\psi_{\Gamma_0}[A] = \sum_{jmn} \hat{\psi}_{jmn} D^j_{mn}[h_0(A)] \tag{5.46}$$

For a general graph Γ with L links, the state can be written as:

$$\psi_\Gamma[A] = \sum_{\substack{j_1,\dots,j_L \\ m_1,\dots,m_L \\ n_1,\dots,n_L}} \hat{\psi}_{j_1\dots j_L\, m_1\dots m_L\, n_1\dots n_L} D^{j_1}_{m_1 n_1}[h_1(A)] \dots D^{j_L}_{m_L n_L}[h_L(A)] \tag{5.47}$$

Recall the action of the flux operator on the states eq. (5.39). It can be shown that the action of the flux operator on h_γ is [Rovelli, 2004]:

$$E_i(S) h_\gamma(A) = \pm i\, 8\pi\gamma h_{\gamma_1}(A) \tau_i h_{\gamma_2}(A) \tag{5.48}$$

Where γ_1 and γ_2 are the two segments of the link γ, separated by the surface S. The sign depends on the orientation of the segments with respect to the normal n_a of the surface. The action of the flux operator on the holonomy is represented in fig. 5.4.

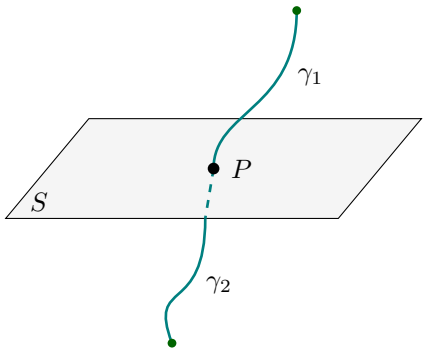

Figure 5.4: Pictorial representation of the action of the flux operator $E_i(S)$ on $h_{\gamma_1 \cup \gamma_2}$

The action of two fluxes acting inside the link is therefore given by:

$$E^2(S)h_\gamma(A) = -(8\pi)^2\gamma^2 h_{\gamma_1}(A)\tau_i\tau^i h_{\gamma_2}(A) \tag{5.49a}$$
$$= (8\pi)^2\gamma^2 j(j+1)h_\gamma(A) \tag{5.49b}$$

The spectrum of the area operator for one holonomy is then given by:

$$A(S) = 8\pi\gamma\sqrt{j(j+1)} = \frac{8\pi G}{c^3}\hbar\gamma\sqrt{j(j+1)} \tag{5.50}$$

The smallest non-vanishing eigenvalue (taking the Immirzi parameter $\gamma = 1$) is given by ($j = 1/2$):

$$\boxed{A(S)_{\min} = \frac{4\sqrt{3}\pi G}{c^3}\hbar \approx 10^{-69}\ \mathrm{m}^2} \tag{5.51}$$

In Loop Quantum Gravity, the space geometry becomes discrete when approaching the Planck scale. Each surface pierced by a holonomy is given an area related to the spin j of the representation of the holonomy. In the full theory, each region around a vertex is given a volume determined by the intertwiner ι_n as well as by the spin of the link starting (or ending) at the vertex [Rovelli, 2004; Doná and Speziale, 2010; Rovelli and Vidotto, 2014b].

5.3 From Planck Stars to Remnants

This section, mostly based on [Rovelli and Vidotto, 2024][4], reviews the full LQG scenario for a BH's lifecycle: from collapse through bounce to final remnant.

Instead of a singularity, the collapsing matter distribution reaches a maximal density $\rho_{\max} \sim \rho_{\mathrm{P}}$ becoming a *Planck star* (subsec. 5.3.1). Using the Oppenheimer-Snyder geometry as a guide, a new exterior geometry is proposed (subsec. 5.3.2). In subsec. 5.3.3, we discuss the transition amplitude between the past and the future boundary of the interior geometry as a result of the covariant LQG (subsec. 5.3.3.A), as well as the interior volume to get an idea of the interior geometry (subsec. 5.3.3.B). The Hawking evaporation breaks the time-reversal symmetry of the bounce, and we adopt the term *remnant* or, in the case of LQG, *rovellino*, to refer to bounced objects. Its lifetime is estimated in subsec. 5.3.4, and its quantum aspects are discussed in subsec. 5.3.5. We conclude with a summary of the scenario in subsec. 5.3.6.

5.3.1 Planck stars

As noticed in subsec. 3.1.2, one can expect quantum gravitational effects to be important when $K \sim 1$, which can span a much larger region than the vicinity of the singularity. In particular, *the quantum region extends outside the horizon* [Rovelli and Vidotto, 2024].
The distance L between the region where the matter distribution reaches Planckian density (region c in fig. 5.5) and the one outside the horizon (region b in fig. 5.5), where the curvature is also Planckian because of Hawking radiation is of order [D'Ambrosio et al., 2021]:

$$L \sim m^{10/3} \tag{5.52}$$

Indeed, the line element, taken from eq. 3.1, is $dl^2 = -(1-2m/r)dt^2$ for constant (r, θ, ϕ). Since Planckian curvature is reached when $r \sim m^{1/3}$ and the time for the black hole to evaporate is $\Delta t \sim m^3$, the distance is $L \sim \sqrt{2m/m^{1/3}}m^3 \sim m^{10/3}$.

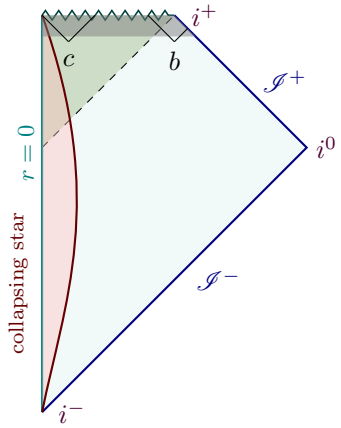

Figure 5.5: Conformal diagram of a black hole formed by gravitational collapse, with the region where quantum gravity effect becomes important in gray. Region c is where the matter distribution reaches Planck density, and region b is where Planck curvature is reached. Adapted from [Rovelli and Vidotto, 2024; Neutelings, 2021].

This spacelike separation between these two events implies that their evolution must be independent; they are causally disconnected.

[4] [Rovelli and Vidotto, 2024] presents, on top of a review of the LQG motivated scenario of a BH, heuristic arguments for the existence of a stable remnant. Recent works derive similar results from first-principle calculations [Belfaqih et al., 2025].

Recall subsec. 3.1.5 and its simplest model of a collapsing star: the *Oppenheimer-Snyder model*. This led to a singularity of the scale factor $a(\tau)$ when the proper time vanishes.

A major result from Loop Quantum Cosmology (**LQC**) is the existence of a maximal density $\rho_{\max} \sim \rho_{\text{Planck}}$ [Ashtekar and Singh, 2011]. This must modify the Friedmann equation. In LQC, at the moment of the bounce, the Hubble rate vanishes while the density is maximal. The simplest modification of the Friedmann equation, requiring the classical limit F1 and $H^2(\rho_{\max}) = 0$ is [Ashtekar and Singh, 2011]:

$$\frac{\dot{a}^2}{a^2} = \frac{8\pi G}{3}\rho\left(1 - \frac{\rho}{\rho_{\max}}\right) \tag{5.53}$$

This modifies the solution to:

$$a(\tau) = \left(\frac{9m\tau^2 + \frac{3}{2\pi}m/\rho_{\max}}{2R_\star^3}\right)^{1/3} \tag{5.54}$$

Where $R_\star$ is the radial comoving coordinate of the boundary of the matter distribution. The scale factor a as a function of the proper time τ is represented in fig. 5.6.

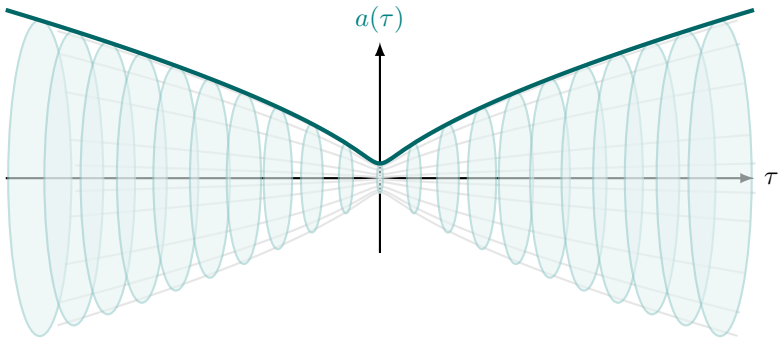

Figure 5.6: Sketch of the bouncing dynamics in LQC. The scale factor $a(\tau)$ is represented as a function of the proper time τ. The bounce occurs at $\tau = 0$, where the density reaches its maximal value $\rho_{\max}$.

Definition 5.14. A **Planck star** is a star reaching its maximal density.

$$\rho_\star = \rho_{\max} \equiv \rho_{\text{Planck star}} \tag{5.55}$$

5.3.2 The exterior geometry

One could wonder which metric could be compatible with the modified geometry of the star. Since eq. 3.17 is formulated in proper time and co-moving coordinates, the Friedmann equation gives the physical radius of the star (in proper time, along comoving worldlines): $r_\star(\tau) = \int \sqrt{g_{rr}}dr = a(\tau)R_\star$. Rewriting eq. F1 as:

$$\dot{a}^2 = \frac{2m}{a} - \frac{3m}{2\pi\,\rho_{\max}}\frac{1}{a^4} \tag{5.56a}$$

The same relation holds for the physical radius of the star:

$$\dot{r}_\star^2 = \frac{2m}{r_\star} - \frac{3m}{2\pi\,\rho_{\max}}\frac{1}{r_\star^4} \tag{5.56b}$$

Now, consider the interface between the Oppenheimer-Snyder metric and the Schwarzschild one. It is a free-falling spherical shell, following a timelike geodesic (satisfying $-1 = -F(r)\dot{t}^2 + \dot{r}^2/F(r)$). The independence of the metric 3.1 on the coordinate t gives an immediate Killing vector $\xi^\mu = \delta^\mu_t$. Since

$\xi^\mu u_\mu$ must be conserved along this geodesic, one can write $-E = \xi^\mu u_\mu = -F(r)\dot{t}$. For a shell released from infinity from rest, $E = 1$. Injecting this into the geodesic equation gives:

$$\dot{r}^2 = \frac{2m}{r} \tag{5.57}$$

This suggests an extension of the Schwarzschild metric as a candidate for the effective metric with quantum corrections [Hayward, 2006; Rovelli and Vidotto, 2014a, 2024].

Definition 5.15. The **Hayward-Rovelli-Vidotto metric** is given by:

$$\mathrm{d}s^2 = -\left(1 - \frac{2m}{r} - \frac{3m}{2\pi\rho_{\max} r^4}\right)\mathrm{d}t^2 + \frac{\mathrm{d}r^2}{\left(1 - \frac{2m}{r} - \frac{3m}{2\pi\rho_{\max} r^4}\right)} + r^2\mathrm{d}\Omega^2 \tag{5.58}$$

This new metric has two asymptotic regions and a time-like singularity, and it is not obvious that it respects Birkhoff's theorem. For an in-depth analysis of the metric and how to solve the previous issues, see [Han et al., 2023; Rovelli and Vidotto, 2024]. The details are beyond the scope of this thesis, but we can give a sketch of the process using conformal diagrams, scissors and tape.

The maximal extension of the new metric 5.58 can be represented using a conformal diagram as shown in fig. 5.7.

The two asymptotic regions **U** and **L** are bounded by the outer horizons r_+. Between the inner horizon r_- and r_+, there is a trapped region **T** and an anti-trapped region **A**. There are two interior regions, one next to the star's bounce where $r_\star < r < r_-$, indicated by **I**, and one next to the singularity where $0 < r < r_-$ indicated by **S**.
The outer horizon is similar to the classical event horizon with correction in

$$r_+ = 2m + \mathcal{O}\left((\rho_{\max} \cdot m)^{-1}\right)$$

while the inner horizon "deeply quantum":

$$r_- = (3m/4\pi\rho_{\max})^{1/3} + \mathcal{O}\left((\rho^2_{\max} \cdot m)^{-1/3}\right)$$

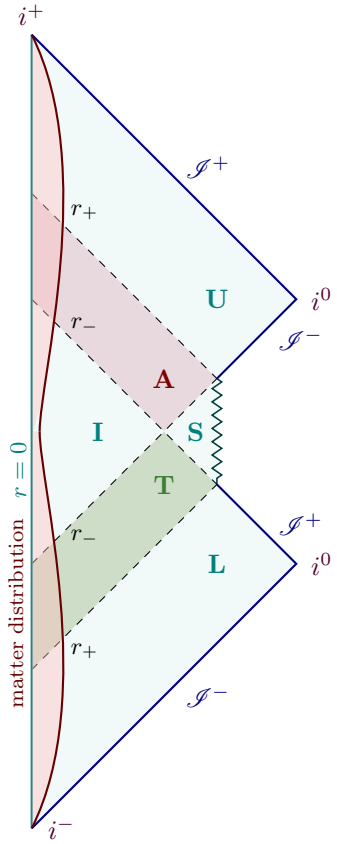

Figure 5.7: Conformal diagram of the maximal extension of the metric 5.58. Adapted from [Rovelli and Vidotto, 2024]

Let us now show a sketch of how these issues (the Birkhoff theorem, the two asymptotic regions and the singularity) can be solved.

1. Birkhoff theorem: it has been shown in [Haggard and Rovelli, 2015], for the metric eq. (5.58) in the case of a collapsing photon sphere, that there exists a (surjective) map between the new metric and the maximal extension of the Schwarzschild metric. In some sense, the new metric is a "portion of a double cover of the Kruskal extension" [Haggard and Rovelli, 2015].

2. Asymptotic regions and singularity: as illustrated in fig. 5.7, the corrected geometry has two copies of spatial infinity i^0 and two copies of future $\mathscr{I}^+$ and past null infinity $\mathscr{I}^-$. One can

construct a geometry with a single asymptotic region by cutting (see fig. 5.8) and gluing (see fig. 5.9) the maximal extension of the metric eq. (5.58).

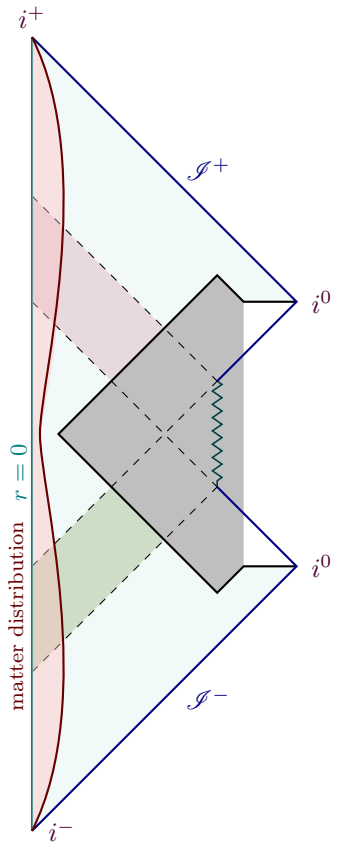

Figure 5.8: Cutting the maximal extension along the chosen surface. Adapted from [Han et al., 2023].

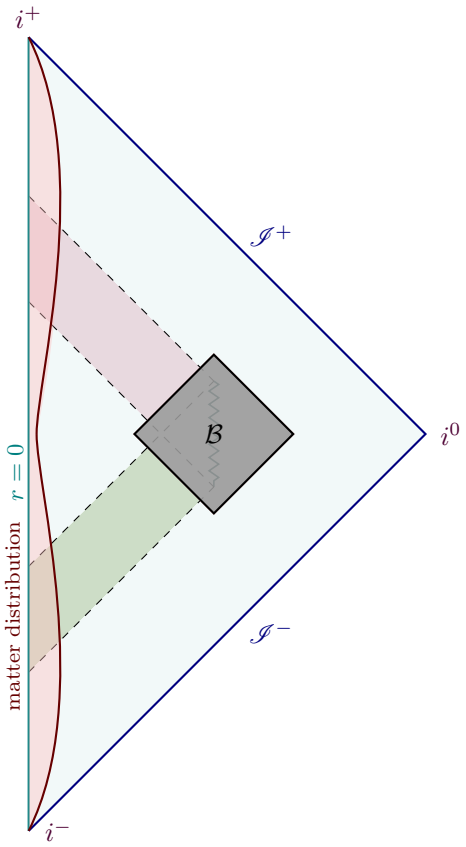

Figure 5.9: Gluing process to obtain a single asymptotic region. Adapted from [Han et al., 2023].

We are left with a single asymptotic region geometry, locally isomorphic to eq. (5.58), with a hole in the middle (the $\mathcal{B}$ region).

5.3.3 The interior geometry

5.3.3.A The transition

To compute what happens in the region where $K \sim 1$ (recall the grey region in fig. 5.5), one can construct a triangulation of the boundary of the latter and compute the transition amplitude between the two states. The transition amplitude is constructed in the covariant formulation of LQG, which is beyond the scope of this thesis. Details can be found in [Rovelli and Vidotto, 2014b].

As illustrated in fig. 5.11, the past and the future boundaries are taken outside the (iridescent) quantum region.
They are both 3-dimensional balls, and they meet at a point on the conformal diagram, which represents a 2-sphere. The boundary can simply be triangulated by two tetrahedra for the two balls, linked together by their nodes. The simplest bulk triangulation is an 8-valent vertex connecting the nodes of the two tetrahedra. Concretely, one replaces a unique 8-valent vertex by two 5-valent vertices linked by a single virtual segment for computational simplicity. The triangulation is illustrated in fig. 5.10.

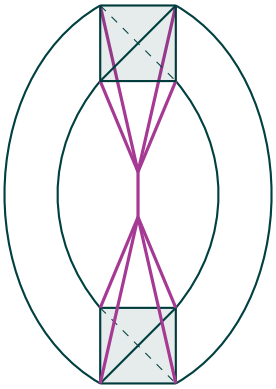

Figure 5.10: Triangulation of the boundary and the bulk of the quantum region.

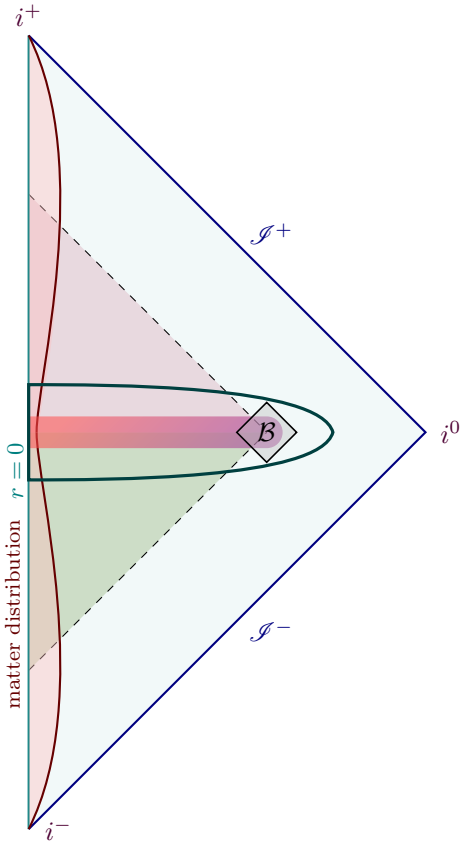

Figure 5.11: Conformal diagram of the transition from a black hole to a white hole, starting from a Schwarzschild metric. Adapted from [Rovelli and Vidotto, 2024].

Several methods show that the transition amplitude is exponentially suppressed by the square of the mass [Rovelli and Vidotto, 2024]:

$$P \sim e^{-m^2} \tag{5.59}$$

Along with the discussion of the section 3.2, this suggests that at the end of the evaporation, a BH could *tunnel* into a WH. The tunneling process takes a time of the order of the current mass [Christodoulou and D'Ambrosio, 2024]:

$$\tau_{\text{tunnel}} \sim m_P \tag{5.60}$$

5.3.3.B The interior volume

To get a geometric intuition of the situation in the interior of the BH, let us focus of the volume *inside* the horizon. First, one needs to specify which three-dimensional surface one is interested in since V depends on it:

$$V(\Sigma) = \int_\Sigma \mathrm{d}^3x \, \sqrt{g|_\Sigma} \tag{5.61}$$

Furthermore, since the interior of the BH is a dynamical region, the final result should be time-dependent. The horizon is naturally foliated by two-spheres S_v (where $v = t + r$ is the advanced time), which suggests computing the interior volume associated with a given two-sphere. In [Christodoulou and Rovelli, 2015], it was proposed to use the maximal-volume spacelike ball as the volume $V(v)$, which is the largest volume that can be contained in the two-sphere S_v. Setting $v = 0$ at the moment of the collapse, the volume is given by [Christodoulou and Rovelli, 2015]:

$$V(v) \xrightarrow{v/m\to\infty} 3\sqrt{3}\pi m^2 v \tag{5.62}$$

Inside the horizon, most of the volume comes from a long, almost cylindrical region at roughly fixed radius that grows with v. For a BH of initial mass m_0 and lifetime $\tau(m_0) \sim m_0^3$, the volume inside it can be roughly estimated as:

$$V(m_0) \sim m^5 \tag{5.63}$$

While the length of the cylinder grows with v, the radius of the cylinder shrinks. The transition from a white hole to a black hole is a bounce that exchanges the roles of the two coordinates. The bounce is illustrated in fig. 5.12.

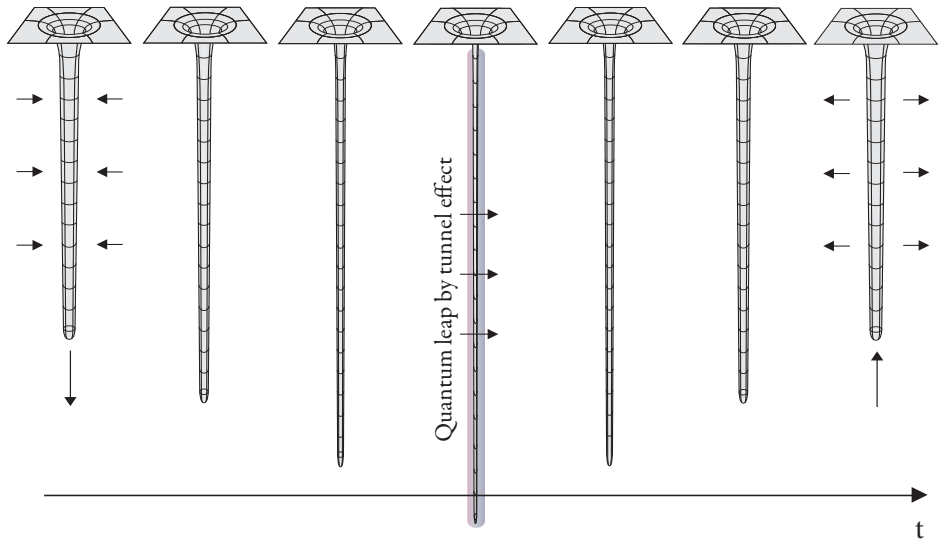

Figure 5.12: A sketch of the evolution of the internal geometry of the hole at the bounce (up to some quantum gravity phenomena). Adapted from Rovelli and Vidotto [2024].

5.3.4 The lifetime of the remnant

A lower bound on the lifetime of the remnant can be obtained by asking that all the information contained in the remnant is released. For a BH of initial mass m_0, its entropy is given by eq. (3.57):

$$S = 4\pi m_0 \tag{5.64}$$

By assuming that the remnant diffuses all its information through radiation, its radiation can be modelled as a gas of photons [Kazemian et al., 2023]. At the end of the diffusion (the end of the lifetime of the remnant), the radiation is spread over a length $L = \tau_{\text{REM}}$. Now, for a one-dimensional photon gas, the entropy and the energy are related to the temperature T and the length L of the gas by:

$$S = \frac{2\pi}{3} LT \tag{5.65a}$$

$$E = \frac{1}{6} LT^2 \tag{5.65b}$$

Since the energy of the remnant is $E \sim 1$, eq. (5.65) gives:

$$L = 6m_0^4 \tag{5.66a}$$

$$T = m_0^{-2} \tag{5.66b}$$

Therefore a *lower bound* on the lifetime of the remnant is given by [Kazemian et al., 2023]:

$$\tau_{\text{REM}}^{\text{LQG}} \gtrsim 6m_0^4 \tag{5.67}$$

A recent paper [Martin-Dussaud, 2025] uses the result from subsec. 5.3.3.B to suggest that the lower bound on the lifetime of the remnant is actually given by:

$$\tau_{\text{REM}}^{\text{LQG}} \gtrsim m_0^5 \tag{5.68}$$

A rough estimate of the maximum wavelength of the radiation that could be emitted by the remnant is then given by $\lambda \sim m^5$. Examples of the typical wavelength of the radiation emitted by the remnant are given in table 7.

	Mass	Wavelength	Range
$m \sim M_\odot$	$m = 10^{30}$kg	$\lambda \sim 10^{153}$ m	radio
$m \sim m_{\text{asteroid}}$	$m = 10^{12}$kg	$\lambda \sim 10^{63}$ m	radio
$m \sim m_{\text{bluewhale}}$	$m = 10^{5}$kg	$\lambda \sim 10^{28}$ m	radio
$m \sim m_{\text{ant}}$	$m = 10^{-2}$kg	$\lambda \sim 10^{-6}$ m	visible
$m \sim \min m_{\text{PBH}}$	$m = 10^{-4}$kg	$\lambda \sim 10^{-17}$ m	gamma-ray

Table 7: Examples of the typical wavelengths diffusing from the remnant of BHs of different initial masses.

In sec. 8.2, we show the lifetime of the remnant τ_{REM} as a function of the initial mass m_0 for different dependence of τ_{REM} on m_0.

5.3.5 Quantum remnant

By the discussions in subsections 5.3.3 and 5.3.4, we can infer that a Schwarzschild BH must be described by at least two numbers: the current mass m and the initial mass of the BH m_0. Pictorially, the current mass m determines the size of the exterior, while the initial mass m_0 determines the size of the interior. The quantum state of a Schwarzschild BH can then be written as $|m_0, m\rangle_B$. As discussed in subsec. 5.3.3.A, when $m \to m_P$, the BH tunnels into a WH in about a Planck time t_P:

$$|m_0, m_P\rangle_B \xrightarrow{\text{tunneling}} |m_0, m_P\rangle_W \tag{5.69}$$

Consider now an evaporated BH that already tunneled into a WH. Classically, BHs are stable (small perturbations of a BH are believed to decay). Time reversing the geometry, WHs must be unstable objects (small perturbations of a WH are believed to grow). This instability is triggered when the perturbation has an associated wavelength smaller than the size of the WH. In the case of planckian remnants, this would require a trans-planckian wavelength. Let us assume anyway that a planckian WH could be unstable towards a planckian BH:

$$|m_0, m_P\rangle_W \xrightarrow{\text{instability}} |m_0, m_P\rangle_B \tag{5.70}$$

Since these objects are quantum, the system will settle in its lowest energy state: the superposition of the two states $|m_0, m_P\rangle_B$ and $|m_0, m_P\rangle_W$.

Definition 5.16. A **rovellino** is a quantum superposition of a planckian BH and a planckian WH:

$$|\text{rov}\rangle = \alpha\,|m_0, m_{\text{REM}}\rangle_B + \beta\,|m_0, m_{\text{REM}}\rangle_W \tag{5.71}$$

Remark. The term *rovellino* can be traced back to a presentation from 2024 given by Laura Baudis [Baudis, 2024].

The rovellino being on the minimal energy state, it should also have minimal *non-vanishing* area, that is, the minimal eigenstate of the area operator eq. (5.51). The mass of the rovellino is obtained by inverting $A_{\text{min}} = 4\pi r^2 = 16\pi m_{\text{rov}}^2$:

$$m_{\text{rov}} = \sqrt{\frac{A_{\text{min}}}{16\pi}} \sim \frac{\sqrt[4]{3}}{2} \approx 0.65 m_P \tag{5.72}$$

5.3.6 Summary

Let us summarize the full LQG picture of the history of a BH:

1. A matter distribution collapses into a BH of mass m_0 and quantum state $|m_0, m_0\rangle_B$.[5]
2. Due to HR, the BH evaporates in a time $\tau(m_0) \sim m_0^3$ until it reaches a planckian mass $m_{\text{REM}} \sim m_P$. Its quantum state now reads $|m_0, m_{\text{REM}}\rangle_B$.
3. The planckian BH has now a high probability to tunnel into a planckian WH. Both states (black and white) being accessible, the system settles in its lowest energy state, the rovellino $|\text{rov}\rangle = \alpha\,|m_0, m_{\text{REM}}\rangle_B + \beta\,|m_0, m_{\text{REM}}\rangle_W$.
4. Finally, the rovellino diffuses its information through radiation in a time $\tau_{\text{rov}} \gtrsim m_0^4$.

[5] Actually, in chapter 7, we consider PBHs that are not formed by the collapse of a matter distribution.

CHAPTER

6

MEMORY BURDEN EFFECT

The Memory Burden effect concerns objects with maximal entropy (*saturon* [Dvali, 2021]) found not only in gravity (BHs) but also in renormalizable field theories. Saturons share properties with BHs, among which are the entropy (eq. (3.57)) proportional to the radius of the object $S \sim A \sim mr_g$, where r_g is the Schwarzschild radius, and a (quasi) thermal spectrum of emission. Assuming that BHs are indeed a type of saturon, this formalism allows one to derive microscopic properties of BHs without the need for a full quantum gravity theory. In addition to recovering some of the properties of BHs, saturons display a new property: the *Memory Burden* effect.

This new framework is quite recent and mathematically involved, so we will only give a brief overview of it. In sec. 6.1, the main ideas of the MBe are summarized. In the next sec. 6.2, a toy model hamiltonian is introduced, that shows how a memory burden effect can arise from the assisted gaplessness of the memory modes. The link from the toy model to the BHs is made in sec. 6.3, and the implications on HR are discussed in sec. 6.4. Finally, the modified constraints on memory burdened PBHs are discussed in sec. 6.5.

6.1 Main ideas of the Memory Burden effect

The MBe is a phenomenon that occurs in systems with a large capacity to store information. In these systems, the information is stored in the form of *memory pattern*: the excitation of the *memory modes* is nearly-gapless. Along with the high number of memory modes, this leads to an enhanced capacity to store information. In the case of BHs, Hawking radiation makes the size of the BHs shrink, say to half of its initial mass. The corresponding entropy is divided by a factor of 4 while the information remains in the BH leading to a large decrease of the storage capacity. The information patterns can no longer be encoded in gapless modes, it becomes energetically costly to excite the memory modes: this is the memory burden effect. In [Dvali et al., 2020], toy models show that stabilization of the system occurs after a time $t_{1/2}$ corresponding to the evaporation of half of the initial mass of the BH. After $t_{1/2}$, there are two possibilities:

1. The system starts to evaporate due to a new classical mechanism, not studied in the current literature. This could lead to decay of the BH.

2. The system is stabilized, and the HR is suppressed.

In the second case, a remnant would form after $t_{1/2}$, with an increased lifetime compared to a BH of the same mass. We will focus on this second case in the following section.

6.2 The toy model

Let us consider K quantum fields ϕ_j ($j = 1, \dots, K$), each with corresponding creation and annihilation operators $\hat{a}_j^\dagger$, $\hat{a}_j$ satisfying the usual bosonic commutation relations:

$$[\hat{a}_j, \hat{a}_k^\dagger] = \delta_{jk}, \quad [\hat{a}_j, \hat{a}_k] = 0 \tag{6.1}$$

A *memory state* (or pattern) $|\bar{m}\rangle$ is the record of the occupation numbers $n_j \equiv \langle \bar{m}| \hat{n}_j |\bar{m}\rangle$ of each quantum field ϕ_j, where $\hat{n}_j = \hat{a}_j^\dagger \hat{a}_j$ are the so-called *memory modes*, storing the information of the system.

$$|\bar{m}\rangle = |n_1, n_2, \dots, n_K\rangle \tag{6.2}$$

The space of memory states forms the *memory space* $\mathcal{H}_{\text{mem}}$ [Dvali, 2021]. For simplicity, the occupation numbers are constrained to be *q-bits*: $n_j = 0$ or $n_j = 1$. The total occupation number of q-bits is denoted as $N_K \equiv \sum_j n_j$.

In the vacuum, the Hamiltonian of the system can be written as [Dvali, 2021]:

$$\hat{H}_{\text{free}} = \sum_{j=1}^{K} m_j \hat{n}_j \tag{6.3}$$

Where $\{m_j\}$ are the energy gaps of the memory modes $\hat{n}_j$. The energy cost of a given pattern is therefore $E_{\bar{m}} = \sum m_j n_j$, which is arbitrarily large if the m_j-s are large. To change pattern, say go from $|\bar{m}\rangle$ to $|\bar{m}'\rangle$, the gap is $\Delta E = E_{\bar{m}'} - E_{\bar{m}}$.

Let us simplify the system further by assuming that all the memory modes have the same energy gap $m_j = \bar{m}$ for all j [Dondarini et al., 2025]: the energy cost becomes $E_{\bar{m}} = \bar{m} N_K$.
The system is effective at storing information if n_{states}, the number of patterns that can fit within an energy gap ΔE, is large [Dvali, 2021]. If the energy gap is small enough, different patterns are degenerate and provide a large entropy $S = \ln n_{\text{states}}$ ($k_B = 1$). Dvali introduced the term *saturon* to refer to objects with maximal microscopic entropy, saturating upper bounds imposed by QFT [Dvali, 2021].

A way to make the energy gap smaller was proposed in [Dvali, 2018] with the introduction of *master modes* whose goal is precisely to assist the gaplessness of the memory modes. The corresponding Hamiltonian reads:

$$\hat{H} = \bar{m}_0 \hat{n}_0 + \left(1 - \frac{\hat{n}_0}{N_c}\right)^p \bar{m} \sum_{j=1}^{K} \hat{n}_j \tag{6.4}$$

Where m_0 is the mass gap of the master mode, and $p > 1$ is a critical exponent. A memory state is now labeled by both the master mode occupation number n_0 and the energy cost of the memory modes $\bar{m}$: $|n_0; \bar{m}\rangle$ [Dondarini et al., 2025]. The effective gap of the memory modes reads:

$$\bar{m}^{\text{eff}} = \left(1 - \frac{n_0}{N_c}\right)^p \bar{m} \tag{6.5}$$

Note that when $n_0 \to 0$, $\hat{H} \to \hat{H}_{\text{free}}$. Since $m^{\text{eff}} \to 0$ when $n_0 \to N_c$, the system becomes gapless when the master mode is in the critical state $n_0 = N_c$: the pattern becomes favored.

$$E_{0,\bar{m}} \equiv \langle 0; \bar{m}| \hat{H} |0; \bar{m}\rangle = \bar{m} N_K \qquad E_{N_c,\bar{m}} \equiv \langle N_c; \bar{m}| \hat{H} |N_c; \bar{m}\rangle = \bar{m}_0 N_c \tag{6.6}$$

The region near the critical point is therefore a minimum of the Hamiltonian, up to the mass gap of the master mode. Minimizing the hamiltonian eq. (6.4) with respect to the master mode occupation number n_0 gives:

$$n_0^{\text{opt}} = N_c \left(1 - \left(\frac{\bar{m}_0 N_c}{\bar{m} p N_K}\right)^{\frac{1}{p-1}}\right) \tag{6.7}$$

When the memory modes are gapless, the microstate degeneracy is $n_{\text{states}} = 2^K$ (equivalently, $\dim(\mathcal{H}_{\text{mem}}) = 2^K$) and the entropy is of the same order as the number of quantum fields: $S = K \ln 2$. It is clear

that the emission of the master mode will increase the value of the effective gap eq. (6.5) and thus the energy cost of the memory modes: this is the heart of the *memory burden effect*. The dissipation of the master mode is performed through extra interaction terms in the Hamiltonian eq. (6.4) that we do not discuss here [Dondarini et al., 2025].

6.3 What about black holes?

A classical BH being fully determined by its mass, charge and angular momentum, the information stored in it must have zero energy: it must be gapless. This is achieved by requiring the master mode to be in the critical state $n_0 = N_c$. From eq. (6.6), one reads:

$$E_{\text{young}} = E_{N_c,\bar{m}} = \bar{m}_0 N_c = m_0 \tag{6.8}$$

Where m_0 is the initial mass of the BH. A typical quantum of energy emitted by the BH is of the order of $1/r_g$ (c.f. eq. (3.43)), in a purely thermal way: the memory modes are not affected by HR. The mass gap of the master mode can then be mapped to the inverse of the Schwarzschild radius of the BH:

$$N_c = \frac{m_0}{\bar{m}_0} \sim r_g^2 \sim S \tag{6.9}$$

It can be shown that if one views the BH geometry as a coherent state of gravitons, one can identify the gapless memory modes with spherical harmonics of gravitons $Y_{\ell m}$. The dominant part of which has angular momentum $\ell_{\max} \sim m_P r_g$ [Dvali and Gomez, 2011], where m_P act as a cutoff of the theory. The multiplicity of memory flavors is then:

$$K = \sum_{\ell=0}^{\ell_{\max}} (2\ell + 1) \sim \ell_{\max}^2 \sim (m_P r_g)^2 \tag{6.10}$$

Where we used that $\sum^L \ell = L(L+1)/2$. Since $K \sim S$, eq. (6.10) recovers an entropy of the form eq. (3.57). In order to derive the typical momentum of a free graviton in terms of its harmonics, the relation eq. (3.45) for a massless scalar field in the asymptotic flat region ($r \gg 2m$) can be used:

$$\left(\Box^{(2)} + \frac{\ell(\ell+1)}{r^2} \right) \phi_{\ell m}(t, r) = 0 \tag{6.11}$$

From eq. (6.11), one can read the transverse momentum of the graviton as $k_\perp^2 = \ell(\ell+1)/r^2 \sim (\ell/r)^2 \sim m_P^2$. The energy gap of the memory modes is then taken to be $\bar{m} = k_\perp \sim m_P$.

The last ingredient to translate the hamiltonian eq. (6.4) to the BH case is the total occupation number of the q-bits N_K. Taking a binomial distribution for N_K, the average is $\bar{N}_K = K/2 \sim S/2$ [Dvali, 2021]. The dictionary of the parameters of the assisted gaplessness and the BHs is summarized in table 8.

	Mass gap of the master mode	Critical occupation number	mass gap of the memory modes	Total occupation number of q-bits
Assisted gaplessness	$\bar{m}_0$	N_c	$\bar{m}$	N_K
Black holes	$1/r_g$	$K = S$	m_P	$S/2$

Table 8: Dictionary of the parameters of the assisted gaplessness and the black holes [Dvali, 2021].

6.4 Suppression of Hawking radiation

With the hamiltonian eq. (6.4) and the identification of the parameters with the BH parameters table 8, one can now study the memory burden effect on Hawking radiation. As stated in sec. 6.2, the HR tends to decrease the master mode, until it stabilizes at $n_0 = n_0^{\text{opt}}$ (given by eq. (6.7)) due to the MBe. The difference between the initial master occupation number $n_0 = S$ and the optimal one is [Dondarini et al., 2025]:

$$\Delta n_0 \equiv S - n_0^{\text{opt}} = S\left(\frac{2}{p\sqrt{S}}\right)^{\frac{1}{p-1}} \tag{6.12}$$

Where we set $m_P = 1$. Each emission from the center of the BH to its horizon takes a time $\delta t \sim r_g$, so a rough estimate of the period of time before the master mode stabilizes is:

$$t_{\text{memory}} \sim r_g \Delta n_0 \sim \begin{cases} r_g\sqrt{S} & \text{for } p = 2 \quad (6.13a) \\ r_g S & \text{for } p \gg 1 \quad (6.13b) \end{cases}$$

When the critical exponent p is large, t_{memory} is of the order of the BH lifetime eq. (3.54). Over t_{memory}, a part of the mass of the BH is emitted, leading to a remnant. Let us parametrize the mass at which the MB effect becomes important for a BH of initial mass m_0 as:

$$m_{\text{REM}} = q\, m_0 \tag{6.14}$$

The fractional mass emitted before stabilization is then:

$$q \equiv \frac{\Delta m}{m_0} \sim \frac{\Delta n_0}{S} \sim \left(\frac{2}{p\sqrt{S}}\right)^{\frac{1}{p-1}} = \begin{cases} \dfrac{1}{\sqrt{S}} & \text{for } p = 2 \quad (6.15a) \\ \mathcal{O}(1) & \text{for } p \gg 1 \quad (6.15b) \end{cases}$$

In the literature, the critical exponent p is usually taken to be very large, $p \gg 1$, and $q = 1/2$. Once the BH enters the memory burden phase, two possibilities arise [Dvali et al., 2020]:

1. A new classical instability occurs, which could lead to the decay of the BH. To our knowledge, this scenario has not yet been studied in the literature.
2. The BH continues to decay, starting to release the memory modes, but at a suppressed rate.

Once the MB effect becomes important, HR emission rate is modified. The memory burdened emission rates can be parametrized as [Thoss et al., 2024; Chaudhuri et al., 2025]:

$$\frac{\mathrm{d}^2 N_{i,\text{MB}}}{\mathrm{d}E\mathrm{d}t} = \frac{1}{\left(S(q\, m_0)\right)^k} \frac{\mathrm{d}^2 N_{i,SC}}{\mathrm{d}E\mathrm{d}t} \tag{6.16}$$

where k is a parameter that quantifies the suppression of Hawking radiation, and $d^2N_{i,SC}/\mathrm{d}E\mathrm{d}t$ is the primary emission rate defined in eq. (3.48). This leads to a lifetime of the memory burdened BH of [Dvali et al., 2024; Chaudhuri et al., 2025]:

$$\tau_{\text{tot}}^{\text{MB}k} \equiv \tau_{\text{BH}} + \tau_{\text{REM}} \approx r\, S_0^{1+k} \sim (m_{\text{REM}})^3 S_0^k \sim m_0^{3+2k} \tag{6.17}$$

where $S_0 \equiv S_{\text{BH}}(m_0)$ is the BH entropy evaluated at the initial mass m_0 and $r = 2m_0$. When $k = 0$, we recover the standard Hawking radiation lifetime eq. (3.54).

For completeness, let us just mention the peculiar case of merging BHs. In [Zantedeschi and Visinelli, 2025], it is shown that two "old" BHs merging would result in a "young" BH, hence with a semiclassical HR.

6.5 Modified constraints on PBHs

The modification of HR discussed in sec. 6.4 modifies the constraints on Memory Burdened Primordial Black Holes (**MBPBH**s). In general, the constraints on evaporating PBHs discussed in subsec. 4.2.1 are relaxed due to reduced injection in the environment.

In [Alexandre et al., 2024], it is argued that MBPBHs with a mass 10^3 kg $\lesssim m^i_{\rm PBH} \lesssim 10^6$ kg stabilize before BBN and could constitute the totality of DM today, even in the most conservative case of $k = 1$.
A subsequent work [Thoss et al., 2024] confirms and explores this new mass window in more detail. They focus on constraints from γ-rays (both galactic and extragalactic), CMB anisotropies and BBN. Main changes compared to the standard constraints are obtained when the MBPBHs have stabilized before recombination. The updated constraints are shown in fig. 6.1a.

[Dvali et al., 2025] explores the possibility of a smooth transition from the semiclassical regime to the MB one and studies the implications for the constraints on MBPBHs. MBPBHs currently transitioning between these regimes could be a source of high-energy neutrinos, such as the one detected by [Aiello et al., 2025]. In [Chaudhuri et al., 2025], the effects of ultra-light MBPBHs on the BBN are studied. They show that increasing values of k lead to a shift of the BBN constraints to lower masses. The case $k = 2$ is shown in fig. 6.1b.

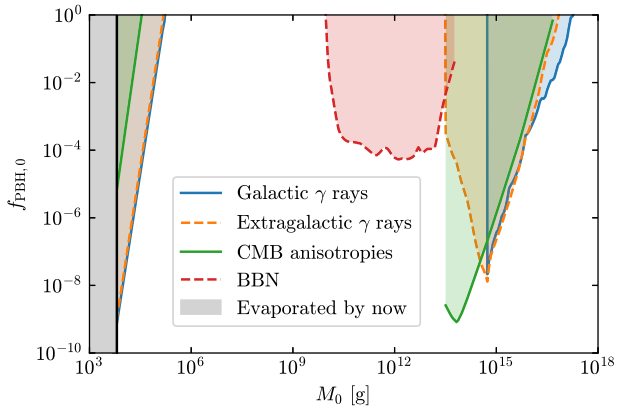

(a) Constraints on $f_{\rm PBH}$ as a function of the initial mass of the PBHs $m^i_{\rm PBH}$, with $q = 1/2$ and $k = 2$. From [Thoss et al., 2024].

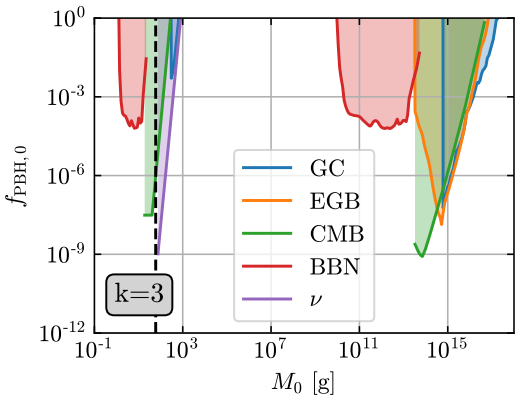

(b) Constraints on $f_{\rm PBH}$ as a function of the initial mass of the PBHs $m^i_{\rm PBH}$, with $q = 1/2$ and $k = 3$. From [Chaudhuri et al., 2025].

Figure 6.1: Updated constraints on the fraction $f_{\rm PBH}$ of DM in the form of MBPBHs as a function of their initial mass $m^i_{\rm PBH}$.

CHAPTER

7

DESCRIPTION OF THE MODEL

7.1 Introduction

This section develops an effective and simplified set of cosmic histories with PBHs and LQG or MB effects. The common idea between these two beyond semiclassical theories is the stabilizing role of the information giving rise to remnants, namely suppressing Hawking radiation.

The novelty of this work is the introduction of PBHs as a new component of the universe, combined with the study of their evolution including stabilizing effects. The model is based on the assumption that PBHs are formed after the end of inflation, and that they "decay" into radiation, matter and remnants. The remnants are assumed to be (quasi-)stable and to contribute to the energy density of the DM.

The full evolution of PBHs is illustrated in fig. 7.1. After formation, the BH undergoes HR until it reaches a critical mass, which is theory-dependent. At this point, the BH transitions into a remnant. Eventually, the remnant converts into photons, contributing to the radiation density of the Universe.

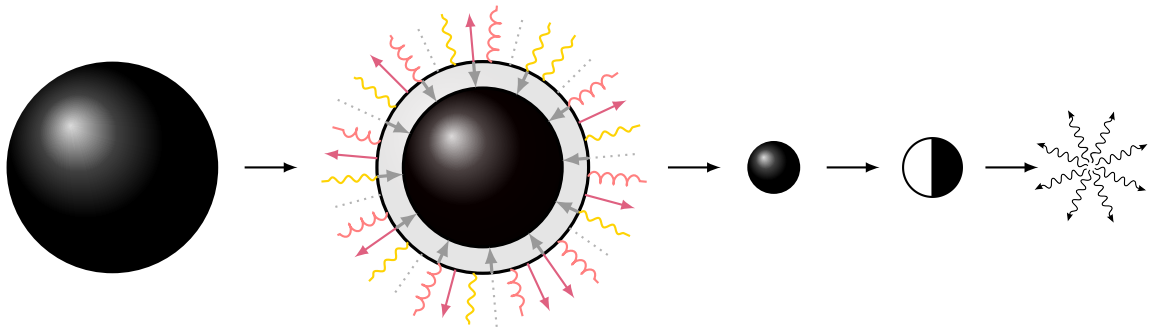

Figure 7.1: Pictorial representation of the evolution of a BH and its remnants.

The goal of this study is to develop and implement a semi-analytical model for the evolution of the population of PBHs formed at the end of inflation. Given an initial mass $m^i_{\rm PBH}$, the initial PBH mass fraction β and the theory (parametrized by $k_{\rm LQG}$ or $k_{\rm MB}, q_{\rm MB}$), the model gives back a cosmic history: the density of each species as a function of the number of e-folds N, the Hubble rate, the cosmic time, etc. Once this model is built, it can be iterated to maximize some quantity (such as the fraction of

DM made of PBHs) in order to explore several cosmological scenarios.
The initial mass of PBHs determines which phase of the model we are in (discussed in sec. 7.2), and how the initial conditions must be set to match today's observations (see sec. 7.3). The modelling allows exploring generically all the possible regimes in a unified way.

7.2 The Phases of the model

The model assumes a simplified cosmological background, neglecting interactions between different species, except for the interactions explicitly modeled between PBHs and their evaporation products. Specifically, we set all non-gravitational couplings among standard cosmological species to zero, isolating PBH dynamics and remnant production as the sole interacting processes.

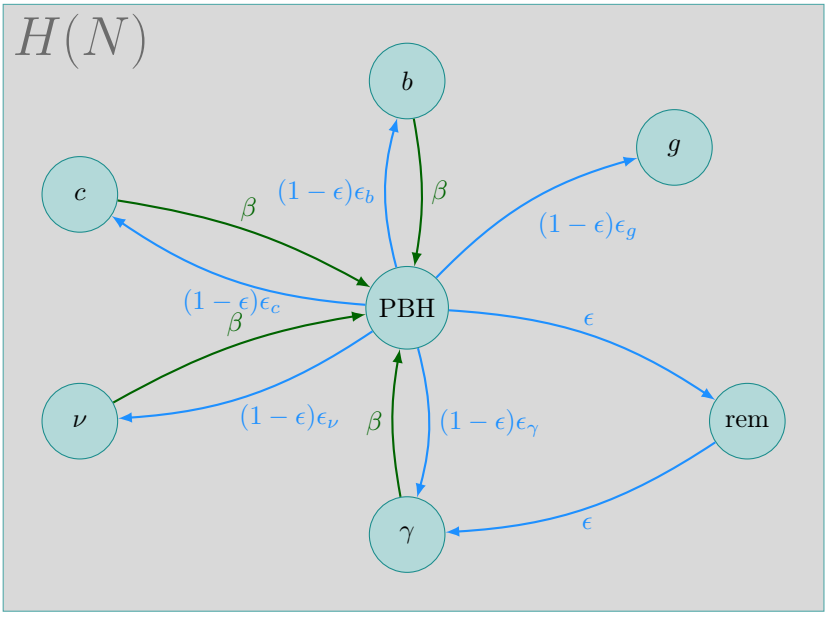

Figure 7.2: Pictorial representation of the model. A fraction β of each species (baryons b, initial cold DM c, photons γ, neutrinos ν) collapses into PBHs {in green}. At the end of the lifetime of PBHs, they evaporate "back" into the initial species, gravitons g and remnants {in blue}. After the lifetime of the remnants, the energy density is transferred to the photons {in blue}.

Fig. 7.2 illustrates the interactions between PBHs and the different species in the model. In green, the fraction β of the energy density of each species $A \in \{\gamma, \nu, b, c\}$ that collapses into PBHs after inflation. In blue, HR "giving back" some of the energy density to the remaining species, as well as the remnant. Eventually, the energy density of the remnant is transferred to the photons.

7.2.1 The phase `P0`

Let us begin with the initial conditions. We place ourselves at the end of inflation, after reheating happened. Following standard background cosmology, we assume that the Universe is filled with the following species:

- γ: photons
- b: baryonic matter
- Λ: cosmological constant
- ν: neutrinos
- c: *pre-existing* CDM

At some number of e-folds N_i, PBHs form. This ends the phase `P0` and starts the phase `P1`. Just before the formation of PBHs, we parametrize the energy density of each species $A \in \{b, c, \gamma, \nu\}$ in the following way:

$$\widetilde{\rho}_A \equiv \rho_A(N_i^-) = \alpha_A e^{-3(1+\omega_A)N_i} \rho_A^{\rm obs} \tag{7.1}$$

The neutrino energy density is related to the photon energy density by the relation given in eq. (2.22) that we denote for convenience $\rho_\nu = C_{\nu\gamma}\rho_\gamma$. We thus have:

$$\widetilde{\rho}_\gamma = \alpha_\gamma e^{-4N_i}\rho_\gamma^{\rm obs} \tag{7.2a}$$
$$\widetilde{\rho}_\nu = C_{\nu\gamma}\widetilde{\rho}_\gamma \tag{7.2b}$$
$$\widetilde{\rho}_b = \alpha_b e^{-3N_i}\rho_b^{\rm obs} \tag{7.3a}$$
$$\widetilde{\rho}_c = \alpha_c e^{-3N_i}\rho_{\rm DM}^{\rm obs} \tag{7.3b}$$

7.2.2 The phase P1

The beginning of the phase P1 is defined by the formation of PBHs. A mass fraction β of the energy density of the universe collapses into PBHs. The energy density of PBHs at the beginning of the phase P1 is given by:

$$\rho_{\rm PBH}(N_i^+) = \beta\left(\widetilde{\rho}_\gamma + \widetilde{\rho}_\nu + \widetilde{\rho}_b + \widetilde{\rho}_c\right) \equiv \rho_{\rm PBH}^i \tag{7.4a}$$

The energy densities of the remaining species are:

$$\rho_\gamma(N_i^+) = (1-\beta)\widetilde{\rho}_\gamma \equiv \rho_\gamma^i \tag{7.4b}$$
$$\rho_\nu(N_i^+) = (1-\beta)\widetilde{\rho}_\nu \equiv \rho_\nu^i \tag{7.4c}$$
$$\rho_b(N_i^+) = (1-\beta)\widetilde{\rho}_b \equiv \rho_b^i \tag{7.4d}$$
$$\rho_c(N_i^+) = (1-\beta)\widetilde{\rho}_c \equiv \rho_c^i \tag{7.4e}$$

During the phase P1, the species are assumed to simply redshift, and PBHs to be stable:

$$\rho_\gamma^{\texttt{P1}}(N) = \rho_\gamma^i e^{-4(N-N_i)} \tag{7.5a}$$
$$\rho_\nu^{\texttt{P1}}(N) = \rho_\nu^i e^{-4(N-N_i)} \tag{7.5b}$$
$$\rho_b^{\texttt{P1}}(N) = \rho_b^i e^{-3(N-N_i)} \tag{7.5c}$$
$$\rho_c^{\texttt{P1}}(N) = \rho_c^i e^{-3(N-N_i)} \tag{7.5d}$$
$$\rho_{\rm PBH}^{\texttt{P1}}(N) = \rho_{\rm PBH}^i e^{-3(N-N_i)} \tag{7.5e}$$

The phase P1 ends when HR becomes non-negligible. This also corresponds to the moment when PBHs lose a significant fraction of their mass and decay into remnants. For PBHs with $m \gtrsim 10^{12}$ kg, the phase P1 is still ongoing today, as illustrated in fig. 7.3.

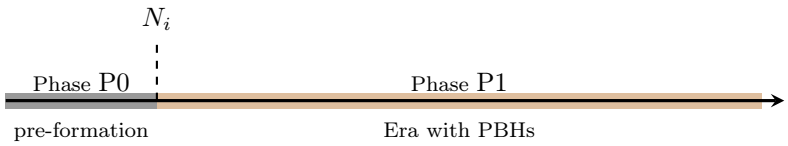

Figure 7.3: Timeline in e-folds N for a large-mass PBH scenario. PBHs form at N_i. Their lifetime exceeds the age of the universe, so evaporation has not completed by today, and PBHs survive to the present.

7.2.3 The phase P2

The beginning of phase P2 corresponds to the epoch where PBHs decay into Hawking products and remnants. The lifetime of the PBH is derived from its semiclassical Hawking radiation and given in eq. (3.54). We denote the number of e-folds corresponding to the decay of PBHs by N_b. At the end of the previous phase, the total energy density reads:

$$\rho(N_b^-) = \left(\rho_\gamma^i + \rho_\nu^i\right)e^{-4\delta N} + \left(\rho_b^i + \rho_c^i + \rho_{\rm PBH}^i\right)e^{-3\delta N} + \rho_\Lambda \tag{7.6}$$

Where $\delta N = N_b - N_i$. At $N = N_b$, HR becomes important and PBHs decay into massless particles (photons γ, neutrinos ν and gravitons g), as well as massive ones (baryons b). When the backreaction becomes important, HR stops and leaves a remnant. This whole process being very explosive, we model it as instantaneous:

$$\rho_{\rm PBH}(N_b) \mapsto \rho_{\rm REM} + \rho_\gamma^H + \rho_\nu^H + \rho_b^H + \rho_g^H \tag{7.7}$$

Where $\rho_{\text{REM}} \equiv \epsilon e^{-3\delta N}\rho^i_{\text{PBH}}$ is the energy density of the remnant and $\rho^H_A \equiv (1-\epsilon)\epsilon_A e^{-3\delta N}\rho^i_{\text{PBH}}$ is the energy density of HR of species $A \in \{b,\, g,\, \gamma,\, \nu\}$. The sets of $\{\epsilon_A\}$ are computed with `BlackHawk` and are given in appendix A.

However, if PBHs are so light that they decay before the neutrino decoupling (or the electron-positron annihilation era), HR is (partly) thermalized and the $\{\epsilon_A\}$ are modified.
Equivalently, ϵ is defined as the mass fraction between the remnant and the PBH: ϵ is typically very small in the case of a rovellino, and can be as large as 0.5 in the case of the MB effect.

For intermediate PBH mass, the P2 phase is still occurring today, as illustrated in fig. 7.4.

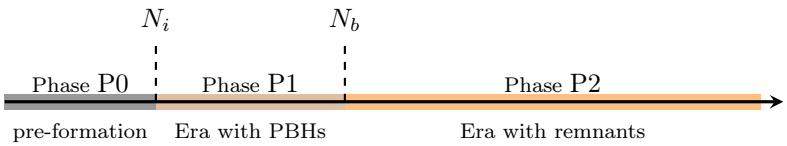

Figure 7.4: Timeline in e-folds N for an intermediate-mass PBH scenario. PBHs form at $N = N_i$, then evaporate via Hawking radiation; evaporation completes at $N = N_b$, at which point remnants remain. Because their lifetime is shorter than the age of the universe, PBHs have already evaporated, while their remnants can survive to the present.

7.2.4 The phase `P3`

The phase `P3` corresponds to the epoch where remnants of PBHs have decayed into radiation. We denote the number of e-folds corresponding to the decay of the remnants by N_r. At the end of the previous phase, the total energy density reads:

$$\rho(N_r^-) = \left(\rho^i_\gamma + \rho^i_\nu\right) e^{-4(\delta N+\Delta N)} + \left(\rho^i_b + \rho^i_c\right) e^{-3(\delta N+\Delta N)} + (\rho^H_\gamma + \rho^H_\nu + \rho^H_g) e^{-4\Delta N} + \left(\rho^H_b + \rho_{\text{REM}}\right) e^{-3\Delta N} + \rho_\Lambda \tag{7.8}$$

Where $\Delta N = N_r - N_b$. At $N = N_r$, the remnants decay into (diffuse) radiation:

$$\rho_{\text{REM}}(N_r) \mapsto \rho_d \tag{7.9}$$

Where $\rho_d \equiv \epsilon e^{-3\Delta N}\rho_{\text{REM}}$ is the energy density of the diffuse radiation.

For the lightest PBHs, the P3 phase is already occurring today, as illustrated in fig. 7.5.

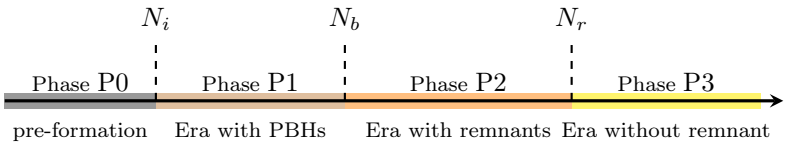

Figure 7.5: Timeline in e-folds N for a small-mass PBH scenario. PBHs form at N_i, then evaporate via Hawking radiation; evaporation completes at N_b, leaving remnants that decay at N_r (before today), so neither PBHs nor remnants survive to the present — only their decay products remain.

7.3 Controlling the initial conditions

To each phase corresponds a set of parameters $\{\alpha_A\}^{Pi}$ controlling the initial conditions of the energy density of each species A such that the model recovers the observed energy density today:

$$\rho_A^{\text{model}}\big|_{\text{today}} \stackrel{!}{=} \rho_A^{\text{obs}} \quad \forall A \in \{\gamma,\, b,\, \text{DM}\} \tag{7.10}$$

These parameters are analytical functions of the external parameters of the model $\{\beta,\, m^i_{\text{PBH}},\, k_{\text{LQG}}/k_{\text{MB}},\, q_{\text{MB}}\}$, as well as internal parameters $\{N_i,\, N_b,\, N_r,\, \epsilon,\, \epsilon_A\}$. Their analytical expression can be found in the appendix B.

The constraints expressed in eq. (7.10) tie initial parameters to final observational data, effectively creating a boundary value problem. This significantly increases the computational complexity of our model and necessitates iterative optimization of multiple internal parameters to ensure consistency between theory and observation. We describe the various steps involved in detail in sec. 7.5.

7.4 Assumptions and simplifications

As stated in the introduction, the model is a simplified version of the cosmological history of the universe. The objective is to determine qualitative behaviors and orders of magnitude, rather than to provide a precise description of the cosmic history. We start with background cosmology, and then add the interactions we are interested in.

The model developed in this work is lacking an important aspect of cosmology: the temperature. Even though the dynamics of the universe can be fully described by the energy density of each species, their relativistic classifications require a temperature. In our model, we neglect the relativistic behavior of baryons, electrons, protons and cold dark matter, and we assume that they behave as non-relativistic species. We note, however, that such an assumption does not affect most of our results, since as a matter component it does not significantly contribute to the early-universe density, especially if the universe's content is mostly produced by PBH evaporation with only negligible amounts of pre-existing baryonic matter.

The temperature is also needed to understand more precisely the fate of HR products. For simplicity, we assume that the initial temperature in our model is the same as given in subsec. 2.1.2. The evaporation of PBHs itself is assumed to be instantaneous, allowing us to avoid numerical errors in the evolution of the cosmic history.

The model is agnostic about the specific formation mechanism of PBHs, and we only assume that they are formed after the end of inflation. The mass fraction β is defined for a monochromatic distribution of PBHs, and is a free parameter of the model.

7.5 Building the model

The model is written in `Mathematica` and is available on the GitHub repository [Dierckx, 2025][1]. It is constructed in a modular way as illustrated in fig. 7.6.

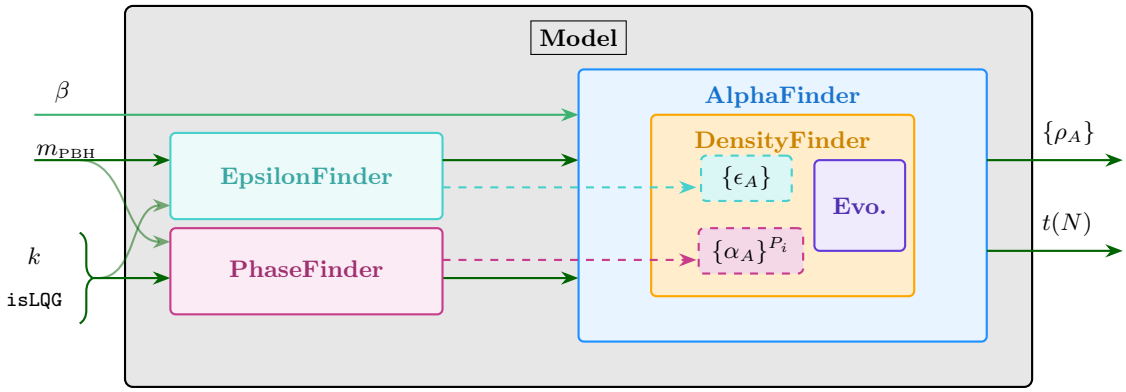

Figure 7.6: Pictorial representation of the model.

The model accepts as inputs the initial PBH mass m^i_{PBH}, the initial mass fraction β, and the theory parameters: a boolean flag `isLQG` $\in \mathbb{B}$ indicating which theory is considered, and associated parameters k_{LQG}, $k_{\text{MB}} \in \mathbb{N}^0$ and $q_{\text{MB}} \in [0, 1]$. It then produces the complete cosmic evolution history, including the densities of all species, the cosmic time, and the Hubble rate. In fig. 7.6 and in the following illustrations, we denote by k — by slight abuse of notation — either k_{LQG} or $(k_{\text{MB}}, q_{\text{MB}})$ to simplify the presentation.

The first step is to find the corresponding phase of PBHs — whether they are still evaporating, have decayed into remnants, or have fully turned into radiation — using the `PhaseFinder` module. In parallel, the `EpsilonFinder` module harvests the proportion of energy going into each of the products of Hawking radiation, depending on the mass of the PBH and the theory considered.
Once the phase and the Hawking coefficients are identified, the system can be evolved accordingly, using nested modules `AlphaFinder` $\subset$ `DensityFinder` $\subset$ `EvolutionP1/P2/P3`. Once the evolution is complete and in agreement with the observational data, the model is iterated to maximize the mass fraction of PBHs in the universe by the `BetaFinder` module.

The structure of the model and its iterative procedure are detailed in the following sections.

7.5.1 The `EpsilonFinder` module

The `EpsilonFinder` module is responsible for determining the proportion of energy going in each of the products of Hawking radiation. We use the previous subsec. 3.2.4 to build a table analogous to table 5. The tables used by the `EpsilonFinder` module depend on the mass of the remnant (and therefore on the flag `isLQG`), and are given in appendix A.

Alongside the initial PBH mass m^i_{PBH}, the `EpsilonFinder` module takes as input two flags: `isDec`$_\nu$ and `isEPAnnih`, which indicate whether the neutrino decoupling and the electron-positron annihilation era have occurred before the PBH decay. For clarity, these flags are not represented in fig. 7.7. If the PBH decays before the neutrino decoupling (`isDec`$_\nu$ = `False`), all HR products (but the gravitons) are thermalized and the set of $\{\epsilon_A\}$ is modified as:

$$\begin{cases} \epsilon_\gamma \to (1-\epsilon_g)\dfrac{1}{1+C_{\nu\gamma}} & \text{(7.11a)} \\ \epsilon_\nu \to (1-\epsilon_g)\dfrac{C_{\nu\gamma}}{1+C_{\nu\gamma}} & \text{(7.11b)} \\ \epsilon_e, \epsilon_p \to 0 & \text{(7.11c)} \end{cases}$$

[1] To request access to the code, please contact me on GitHub: @adierckx.

Where $C_{\nu\gamma}$ is defined in eq. (2.22). If the PBH decays after the neutrino decoupling but before the electron-positron annihilation epoch ($\texttt{isDec}_\nu = \texttt{True}$ and $\texttt{isEPAnnih} = \texttt{False}$), ϵ_ν is unchanged, while ϵ_e and ϵ_p are transferred to photons: $\epsilon_\gamma \to \epsilon_\gamma + \epsilon_e + \epsilon_p$ and $\epsilon_e, \epsilon_p \to 0$.

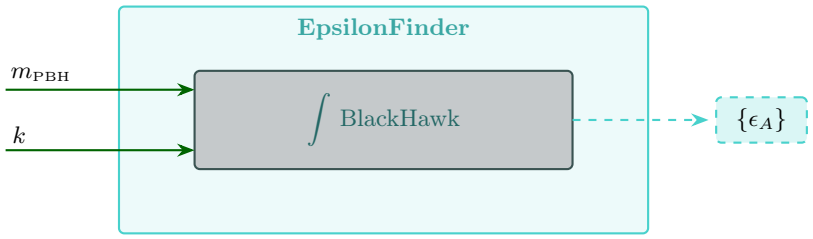

Figure 7.7: Pictorial representation of the `EpsilonFinder` module.

The output of the `EpsilonFinder` module is an array containing the following objects:

$$\{\texttt{output}\} = \{\epsilon_A\} = \left\{ \begin{array}{ll} \epsilon_{\rm g} & : \text{proportion of gravitons} \\ \epsilon_\gamma & : \text{proportion of photons} \\ \epsilon_\nu & : \text{proportion of neutrinos} \\ \epsilon_{\rm e} & : \text{proportion of electrons} \\ \epsilon_{\rm p} & : \text{proportion of protons} \end{array} \right\} \tag{7.12}$$

7.5.2 The `PhaseFinder` module

The `PhaseFinder` module, illustrated in fig. 7.8, simply compares the lifetime of PBHs and remnants (which depends on `isLQG` and k) with the age of the universe. It returns the phase of PBHs Pi as well as the analytical expressions of the parameters $\{\alpha_A\}^{P_i}$ for the corresponding phase.

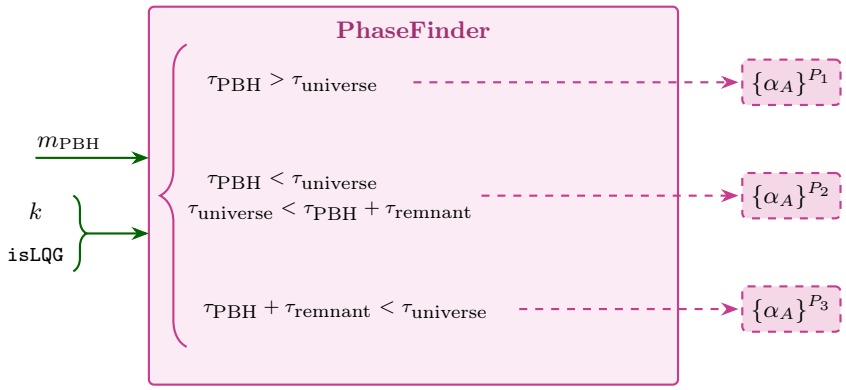

Figure 7.8: Pictorial representation of the `PhaseFinder` module.

The output of the `PhaseFinder` module is an array containing the following objects:

$$\{\texttt{output}\} = \left\{ \begin{array}{ll} \alpha_b(\beta, N_i, N_b, N_r, \epsilon, \epsilon_A) & : \text{baryon parametric coefficient} \\ \alpha_c(\beta, N_i, N_b, N_r, \epsilon, \epsilon_A) & : \text{CDM parametric coefficient} \\ \alpha_\gamma(\beta, N_i, N_b, N_r, \epsilon, \epsilon_A) & : \text{photon parametric coefficient} \\ \texttt{Current Phase} & : \text{current phase of PBHs} \end{array} \right\} \tag{7.13}$$

The sets of parametric coefficients $\{\alpha_A\}^{P_i}$ are derived in appendix B and are given by eq. (B.8) for the phase `P1`, eq. (B.14) for the phase `P2` and eq. (B.20) for the phase `P3`.

7.5.3 The `DensityFinder` module

Before diving into the `AlphaFinder` module, let us first understand the main module of this code: the `DensityFinder` module.
The `DensityFinder` module is schematically represented in fig. 7.9.

1. The first step is to take the analytical expressions $\{\alpha\}^{Pi}$ and evaluate them using the external parameter β and the internal parameters $\{N_i,\, N_b,\, N_r,\, \epsilon\}$. The internal parameters are provided by the `AlphaFinder` module.

2. Once the parameters $\{\alpha\}^{Pi}$ are evaluated, one can compute the Hubble parameter H (given by `AlphaFinder` too).

3. The initial number of e-folds N_i is obtained from solving def. 4.2:

$$\frac{1}{H(N_i)} = m^i_{\text{PBH}} \tag{7.14}$$

   Equipped with the $\{\alpha\}$ and N_i, one can finally compute all the initial densities $\{\widetilde{\rho}_A\}$ and $\{\rho^i_A\}$

4. The next step is to find the cosmic time as a function of the number of e-folds. This is done by performing a numerical integration:

$$\frac{\mathrm{d}t^{\mathtt{P1}}}{\mathrm{d}N} = \frac{1}{H^{\mathtt{P1}}(N)} \quad \text{s.t. } t^{\mathtt{P1}}(N_i) = 0 \tag{7.15}$$

   Where:

$$H^{\mathtt{P1}}(N) = \sqrt{\frac{8\pi}{3}}\sqrt{\left(\rho^i_b + \rho^i_c + \rho^i_{\text{PBH}}\right) e^{-3(N-N_i)} + \left(\rho^i_\gamma + \rho^i_\nu\right) e^{-4(N-N_i)} + \rho_\Lambda} \tag{7.16}$$

   To avoid steep behavior in the numerical integration, the actual integration variable is $a = e^N$, so we solve instead:

$$\frac{\mathrm{d}t^{\mathtt{P1}}}{\mathrm{d}a} = \frac{1}{a\, H^{\mathtt{P1}}(\ln(a))} \quad \text{s.t. } t^{\mathtt{P1}}(e^{N_i}) = 0 \tag{7.17}$$

   And then redefine the cosmic time $t^{\mathtt{P1}}(a) \mapsto t^{\mathtt{P1}}(N)$. This technical detail is later omitted. We thus have a cosmic time $t^{\mathtt{P1}}(N)$ valid until the end of the phase `P1`. Now, if the `PhaseFinder` module found `P1` as the current phase, the code uses `EvolutionP1` to return the {`output`} eq. (7.24).
   Else, eq. (7.15) can be used to compute N_b by solving:

$$t^{\mathtt{P1}}(N_b) = \tau_{\text{PBH}}(m^i_{\text{PBH}}) \tag{7.18}$$

5. Computing the cosmic time during the phase `P2` requires updating the Hubble parameter eq. (7.16):

$$H^{\mathtt{P2}}(N) = \sqrt{\frac{8\pi}{3}}\sqrt{\rho^{\mathtt{P2}}_{\text{tot}}(N)} \tag{7.19a}$$

   Where:

$$\begin{aligned}\rho^{\mathtt{P2}}_{\text{tot}}(N) = {} & \left(\rho^i_b + \rho^i_c\right) e^{-3(N-N_i)} \\ & + \rho^i_{\text{PBH}} e^{-3(N_b-N_i)} \left([1-\epsilon][\epsilon_\gamma + \epsilon_\nu + \epsilon_{\text{g}}]\right) e^{-4(N-N_b)} \quad \text{(rel. Hawking rad.)} \\ & + \rho^i_{\text{PBH}} e^{-3(N_b-N_i)} \left(\epsilon + [1-\epsilon][\epsilon_{\text{e}} + \epsilon_{\text{p}}]\right) e^{-3(N-N_b)} \quad \text{(remnant + non-rel. Hawking rad.)} \\ & + \left(\rho^i_\gamma + \rho^i_\nu\right) e^{-4(N-N_i)} + \rho_\Lambda\end{aligned} \tag{7.19b}$$

   Note that in the case of the BH explosion happening before the neutrino decoupling (or the electron-positron annihilation era), thermalization takes place and the set of ϵ_A is modified accordingly. The cosmic time is then computed by solving:

$$\frac{\mathrm{d}t^{\mathtt{P2}}}{\mathrm{d}N} = \frac{1}{H^{\mathtt{P2}}(N)} \quad \text{s.t. } t^{\mathtt{P2}}(N_b) = t^{\mathtt{P1}}(N_b) \tag{7.20}$$

   This gives a cosmic time $t^{\mathtt{P2}}(N)$ valid during the phase `P2`. Now, if the `PhaseFinder` module found $P2$ as the current phase, the code uses `EvolutionP2` to return the {`output`} eq. (7.24).
   Else, eq. (7.20) can be used to compute N_r by solving:

$$t^{\mathtt{P2}}(N_r) = \tau_{\text{PBH}}(m^i_{\text{PBH}}) + \tau_{\text{REM}}(m^i_{\text{PBH}},\, \mathtt{isLQG},\, k) \tag{7.21}$$

6. Computing the cosmic time during the phase `P3` requires updating the Hubble parameter eq. (7.19):

$$H^{\texttt{P3}}(N) = \sqrt{\frac{8\pi}{3}}\sqrt{\rho_{\rm tot}^{\texttt{P3}}(N)} \tag{7.22a}$$

Where:

$$\begin{aligned}\rho_{\rm tot}^{\texttt{P3}}(N) = &\left(\rho_b^i + \rho_c^i\right) e^{-3(N-N_i)} \\ &+ \rho_{\rm PBH}^i e^{-3(N_b-N_i)}\left([1-\epsilon][\epsilon_\gamma+\epsilon_\nu+\epsilon_{\rm g}]\right) e^{-4(N-N_b)} && \text{(rel. Hawking rad.)} \\ &+ \rho_{\rm PBH}^i e^{-3(N_b-N_i)}\left([1-\epsilon][\epsilon_{\rm e}+\epsilon_{\rm p}]\right) e^{-3(N-N_b)} && \text{(non-rel. Hawking rad.)} \\ &+ \rho_{\rm PBH}^i e^{-3(N_b-N_i)}\epsilon e^{-3(N_r-N_b)} e^{-4(N-N_r)} && \text{(diffuse radiation)} \\ &+ \left(\rho_\gamma^i + \rho_\nu^i\right) e^{-4(N-N_i)} + \rho_\Lambda\end{aligned} \tag{7.22b}$$

The cosmic time is then computed by solving:

$$\frac{{\rm d}t^{\texttt{P3}}}{{\rm d}N} = \frac{1}{H^{\texttt{P3}}(N)} \quad \text{s.t. } t^{\texttt{P3}}(N_r) = t^{\texttt{P2}}(N_r) \tag{7.23}$$

The total cosmic time is obtained by continuously matching the cosmic times of each phase at the transition points.
Now, if the `PhaseFinder` module found `P3` as the current phase, the code uses `EvolutionP3` to return the {`output`} eq. (7.24).

7. If this part is reached, no phase was detected and the code returns an error.

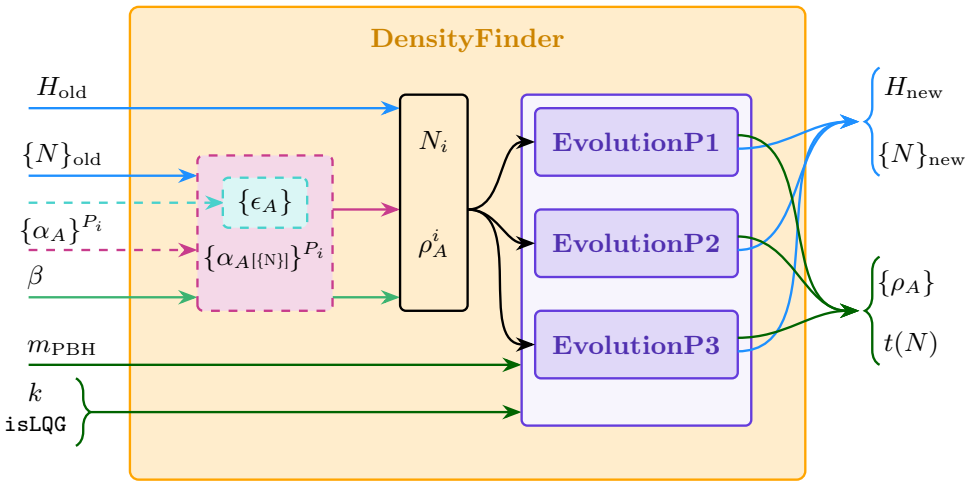

Figure 7.9: Pictorial representation of the `DensityFinder` module.

The output of the `DensityFinder` module is an array containing the following quantities:

$$\{\texttt{output}\} = \left\{ \begin{array}{ll} \rho_b^{\rm tot}(N) & : \text{total baryon density} \\ \rho_b(N) & : \text{initial baryon density} \\ \rho_p^H(N) & : \text{Hawking radiation proton density} \\ \rho_e^H(N) & : \text{Hawking radiation electron density} \\ \hline \rho_{\rm DM}^{\rm tot}(N) & : \text{total DM density} \\ \rho_c(N) & : \text{initial CDM density} \\ \rho_{\rm PBH}(N) & : \text{PBH density} \\ \rho_{\rm REM}(N) & : \text{remnant density} \\ \hline \rho_\gamma^{\rm tot}(N) & : \text{total photon density} \\ \rho_\gamma(N) & : \text{initial photon density} \\ \rho_\gamma^H(N) & : \text{Hawking radiation photon density} \\ \rho_d(N) & : \text{diffuse radiation density} \\ \hline \rho_\nu^{\rm tot}(N) & : \text{total neutrino density} \\ \rho_\nu(N) & : \text{neutrino density} \\ \rho_\nu^H(N) & : \text{Hawking radiation neutrino density} \\ \hline \rho_g^H(N) & : \text{Hawking radiation graviton density} \\ \rho^{\rm tot}(N) & : \text{total energy density} \\ t(N) & : \text{cosmic time} \\ H(N) & : \text{Hubble parameter} \\ \alpha|_b & : \text{baryon coefficient} \\ \alpha|_c & : \text{CDM coefficient} \\ \alpha|_\gamma & : \text{photon coefficient} \\ N_i & : \text{initial } e\text{-folds} \\ N_b & : \text{PBH decay } e\text{-folds} \\ N_r & : \text{remnant decay } e\text{-folds} \\ \texttt{isDec}_\nu & : \text{neutrino decoupling flag} \\ \texttt{isEPAnnih} & : \text{electron-positron annihilation era flag} \end{array} \right\} \tag{7.24}$$

7.5.4 The `AlphaFinder` module

The role of the `AlphaFinder` module is to iterate on the internal parameters $\{N\} = \{N_i,\, N_b,\, N_r,\, \epsilon,\, \epsilon_A{}^2\}$, as well as on the Hubble rate $H(\{\alpha_A\}, \{N\}; N)$ in order to reach the condition eq. (7.10). A pictorial representation of the module is shown in fig. 7.10.

1. To initialize the iteration, the code guesses some initial values $N_i^{\rm guess}$, $N_b^{\rm guess}$, $N_r^{\rm guess}$ and $\epsilon^{\rm guess}$ to evaluate the parametric coefficients $\{\alpha(\{N^{\rm guess}\})\} = \{\alpha|_{\rm guess}\}$. The code then computes a guessed Hubble rate $H^{\rm guess}$ of the form:

$$H^{\rm guess}(\{\alpha|_{\rm guess}\}; N) = H_0 \sqrt{(\alpha_b|_{\rm guess}\Omega_b^0 + \alpha_c|_{\rm guess}\Omega_{\rm DM}^0)\, e^{-3N} + \left(\alpha_\gamma|_{\rm guess}\Omega_\gamma^0 + \alpha_\nu|_{\rm guess}\Omega_\nu^0\right) e^{-4N} + \Omega_\Lambda^0} \tag{7.25}$$

   The eq. (7.14) is then solved using the guessed Hubble rate $H^{\rm guess}$ to obtain a new initial number of e-folds N_i. Following the previous steps, the `DensityFinder` module computes a set of new internal parameters $\{N^{\rm new}\}$ and a new Hubble rate $H^{\rm new}$.

2. The code then takes the average of $\{N^{\rm old}\}$ and $\{N^{\rm new}\}$[3], and $H^{\rm new}$ to compute the new iteration of `DensityFinder`.

[2]The set of $\{\epsilon_A\}$ is computed by the `EpsilonFinder` module and solely depends on the initial mass $m_{\rm PBH}^i$ and the flags $\texttt{isDec}_\nu$, `isEPAnnih`, k and q, so the actual parameters going through the iteration are the flags, but for illustration purposes we only write ϵ_A.

[3]Taking the average rather than using the new parameters directly avoids oscillatory behavior and facilitates convergence.

3. When the difference between the new and old parameters is smaller than a given threshold, the code stops iterating. The final values of $\{N\}$ and H are then used to compute the final parametric coefficients $\{\alpha\}$ and the final output eq. (7.24).

Notice that the iteration is neither directly done on the final densities nor the parametric coefficients but rather on the internal parameters $\{N\}$. This makes it possible to avoid the exponential dependencies of the densities and of $\{\alpha\}$ on the number of e-folds.

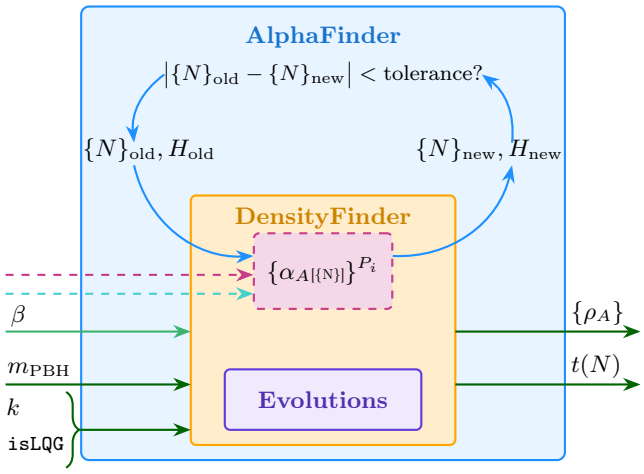

Figure 7.10: Pictorial representation of the `AlphaFinder` module.

7.5.5 The `BetaFinder` module

Given two *independent* inputs $(\beta, m^i_{\rm PBH})$ (and the theory), the `Model` module returns a cosmic history satisfying observational constraints when possible, or no solution otherwise. The goal of the `BetaFinder` module, illustrated in fig. 7.11, is to determine the maximum value of β for which the model remains viable. Physically, this corresponds to the attempt to maximize the fraction of PBHs in the Universe.

The growth of β is limited by the requirements of the non-negativity of the $\{\alpha\}$ coefficients.

1. The code starts with a guess value $\beta_{\rm guess}$ and computes the corresponding cosmic history using the `Model` module.

2. The code then checks the positivity of the $\{\alpha\}$ coefficients. If all the coefficients are positive, the code increases $\beta_{\rm guess}$ by multiplying it (*exponential search*) and repeats the previous step.

3. When the code reaches a value of β such that at least one of the $\{\alpha\}$ coefficients is negative, the code starts a *binary search* to find the maximum value of β such that all the $\{\alpha\}$ coefficients are positive.

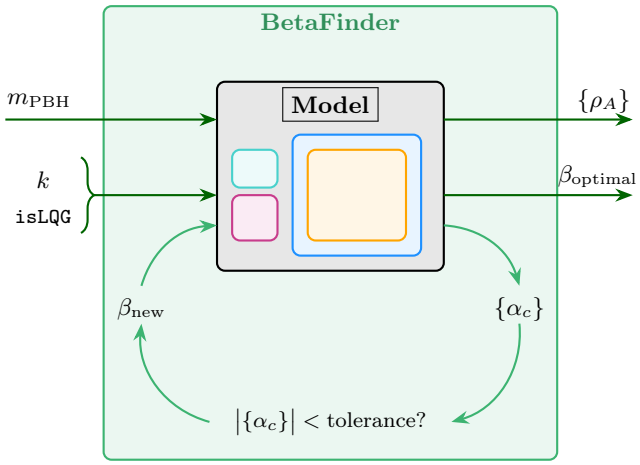

Figure 7.11: Pictorial representation of the `BetaFinder` module.

The outputs of the `BetaFinder` module are the results of this search; it produces the maximum value of β_{max} for which a species is fully formed by PBHs, their remnants, or their Hawking decay products. Maximizing $\beta \to \beta_{\mathrm{max}}$ is equivalent to minimizing one of the $\{\alpha_A\}$ coefficients, since the latter parametrizes the initial density of the corresponding species A. For light PBHs, 3 cases are possible:

1. The remnants fully account for the observed DM density, so $\alpha_c(\beta^{(c)}_{\mathrm{max}}) = 0$.
2. The baryons from HR fully account for the observed baryon density, setting $\alpha_b(\beta^{(b)}_{\mathrm{max}}) = 0$.
3. The photons from HR fully account for the observed photon density, so $\alpha_\gamma(\beta^{(c)}_{\mathrm{max}}) = 0$.

The initial density of neutrinos is constrained by α_γ by equations (7.2a) and (7.2b), so that $\tilde{\rho}_\nu$ vanishes when $\tilde{\rho}_\gamma$ does.

The expected value (and behavior) of $\beta^{(A)}_{\mathrm{max}}(m^i_{\mathrm{PBH}})$ can be derived from the conditions above:

$$\alpha_A(\beta^{(A)}_{\mathrm{max}}, m^i_{\mathrm{PBH}}) = 0 \implies \beta^{(A)}_{\mathrm{max}}(m^i_{\mathrm{PBH}}) \tag{7.26}$$

If $\beta > \beta^{(A)}_{\mathrm{max}}$, it would mean that the model should start with a negative initial density of species A in order to recover the observed density today which is unphysical. We will compare these expressions with the numerical results in sections 8.3 and 8.4.

In the phase `P1`, there is no HR and the only species that can be saturated is the initial CDM. A vanishing $\alpha^{\mathtt{P1}}_c$ (eq. (B.8)) gives:

$$\beta^{\mathtt{P1}(c)}_{\mathrm{max}} = \frac{\rho^{\mathrm{obs}}_{\mathrm{DM}}}{(\rho^{\mathrm{obs}}_b + \rho^{\mathrm{obs}}_{\mathrm{DM}}) + e^{-N_i}\,(1 + C_{\nu\gamma})\,\rho^{\mathrm{obs}}_\gamma} \tag{7.27}$$

The denominator of eq. (7.27) comprises two terms: $\rho^{\mathrm{obs}}_b + \rho^{\mathrm{obs}}_{\mathrm{DM}}$ which account for the collapsed baryons and initial CDM, and $e^{-N_i}\,(1 + C_{\nu\gamma})\,\rho^{\mathrm{obs}}_\gamma$ which accounts for the initial collapsed radiation (photons and neutrinos), blueshifted by their non-relativistic behavior inside PBHs.

In the phase `P2`, the vanishing of the α_A parameters (given in eq. (B.14)) leads to:

$$\beta^{\mathsf{P2}(c)}_{\max} = \frac{\rho^{\rm obs}_{\rm DM}}{-(1+C_{\nu\gamma})\, e^{N_b-N_i}\,(1-\epsilon)\,\epsilon_\gamma\,\rho^{\rm obs}_{\rm DM} + \Big([1-\epsilon_e-\epsilon_p]\,\rho^{\rm obs}_{\rm DM} + \epsilon\big[\rho^{\rm obs}_b + \{\epsilon_e+\epsilon_p\}\,\rho^{\rm obs}_{\rm DM}\big]\Big) + e^{-N_i}(1+C_{\nu\gamma})\,\epsilon\,\rho^{\rm obs}_\gamma} \tag{7.28}$$

$$\beta^{\mathsf{P2}(\gamma)}_{\max} = \frac{\rho^{\rm obs}_\gamma}{(1-\epsilon)\Big(e^{N_b}\,\epsilon_\gamma\,[\rho^{\rm obs}_b + \rho^{\rm obs}_{\rm DM}] + [1-\epsilon_e-\epsilon_p]\,\rho^{\rm obs}_\gamma\Big)} \tag{7.29}$$

$$\beta^{\mathsf{P2}(b)}_{\max} = \frac{e^{N_i}\,\rho^{\rm obs}_b}{(1-\epsilon)\Big(-[1+C_{\nu\gamma}]\,e^{N_b}\,\epsilon_\gamma\,\rho^{\rm obs}_b + e^{N_i}\big[\rho^{\rm obs}_b + \{\epsilon_e+\epsilon_p\}\,\rho^{\rm obs}_{\rm DM}\big] + [1+C_{\nu\gamma}][\epsilon_e+\epsilon_p]\,\rho^{\rm obs}_\gamma\Big)} \tag{7.30}$$

In eq. (7.28), the first (negative) term in the denominator $-(1+C_{\nu\gamma})\,e^{N_b-N_i}\,(1-\epsilon)\,\epsilon_\gamma\,\rho^{\rm obs}_{\rm DM}$ is the part of the initial CDM density that collapses into PBHs and is later converted into photons and neutrinos. The first part of the second term $(1-\epsilon_e-\epsilon_p)\,\rho^{\rm obs}_{\rm DM}$ subtracts the fraction of CDM converted into baryons, while the second part $\epsilon\big(\rho^{\rm obs}_b + (\epsilon_e+\epsilon_p)\,\rho^{\rm obs}_{\rm DM}\big)$ accounts for the fraction of baryons and CDM that are trapped in the remnants, effectively contributing to the total DM density. The last term $e^{-N_i}(1+C_{\nu\gamma})\,\epsilon\,\rho^{\rm obs}_\gamma$ accounts for the trapped photons and neutrinos in the remnants, which also contribute to the total DM density.

Eq. (7.29) has a similar structure, but with a common redshift factor that is factor out of $\alpha^{\mathsf{P2}}_\gamma$ and thus does not appear in $\beta^{\mathsf{P2}(\gamma)}_{\max}$. The first term in the denominator $(1-\epsilon)e^{N_b}\,\epsilon_\gamma\,(\rho^{\rm obs}_b + \rho^{\rm obs}_{\rm DM})$ is the contribution of the collapsed baryons and CDM into PBHs, which are later converted into photons. The second term $(1-\epsilon) - (-1+\epsilon_e+\epsilon_p)\,\rho^{\rm obs}_\gamma$ subtracts the fraction of initial photons that are radiated away as another species.

Similarly, the denominator eq. (7.30) can be decomposed into three parts. The first one $-(1-\epsilon)(1+C_{\nu\gamma})\,e^{N_b}\,\epsilon_\gamma\,\rho^{\rm obs}_b$ subtracts the fraction of initial baryons that are converted into photons through HR. The second term $(1-\epsilon)e^{N_i}\big(\rho^{\rm obs}_b + (\epsilon_e+\epsilon_p)\,\rho^{\rm obs}_{\rm DM}\big)$ and the third term $(1-\epsilon)(1+C_{\nu\gamma})(\epsilon_e+\epsilon_p)\,\rho^{\rm obs}_\gamma$ account for the fraction of the baryons produced by HR, related to the collapsed CDM, initial photons and neutrinos.

CHAPTER

8

RESULTS

This chapter presents the results of the analysis described in the previous chapter 7. We present our findings in two parts:

1. Individual cosmological histories for a given initial mass of the PBHs, in a given theory. This provides an in-depth understanding of each case.
2. General results, in which we compare the different cases and analyze the dynamics of the parameters of the model.

We start by presenting the limitations and assumptions of the model in sec. 8.1. In sec. 8.2, we summarize the lifetimes of the remnants and the PBHs, and how they are parameterized in the model. In sec. 8.3, we present the evolution of the density of species for different initial masses of the PBHs, first in the case of LQG in subsec. 8.3.1, then in the case of the MB effect in subsec. 8.3.2. Finally, in sec. 8.4, we present and provide an analysis of the global results of the model.

8.1 Limitations and assumptions

The model presented in chapter 7 computes the density of the species and their evolution, but ignores the temperature. A major assumption is that we use standard cosmology to estimate the temperature and subsequent events. The cosmic time, however, is computed in the model, and used to determine when the neutrinos decouple, or when the e^+-e^- annihilation epoch occurs. Some key events in the history of the early universe are presented in table 9 [Baumann, 2022; Planck, 2020; Fixsen, 2009].

Event	t (s)	T (eV)	z	N
Neutrino decoupling	1	10^6	6×10^9	-22.5
BBN	100	10^5	4×10^8	-19.8
Matter-radiation equality	10^{12}	0.8	3400	-8
Photon decoupling	10^{13}	0.25	1100	-7
Today	$4 \cdot 10^{17}$	$2.35 \cdot 10^{-4}$	0	0

Table 9: Key events in the history of the early Universe and their (approximate) cosmic time, temperature, redshift and number of e-folds. The redshift z and the number of e-folds N are related by $N = -\ln(1+z)$.

The model also assumes that massive particles are always non-relativistic, and that the neutrinos are massless.
Interactions between the species are generally neglected unless specified otherwise, and sudden changes (like the PBHs losing their mass or remnant diffusion) are assumed to happen instantaneously.

8.2 Lifetimes

In order to saturate the DM with either PBHs or remnants, one needs to be in the phase `P1` or `P2`. To do so, the lifetime of the PBHs or remnants must be larger than the age of the universe.
The lower bound on the lifetime of the rovellinos is given by eq. (5.67), and the total lifetime of the MBPBHs is given by eq. (6.17). In both cases, we fix the coefficient to be the same as in eq. (3.55). Let us make explicit how the lifetime is parameterized in the model:

$$\tau_{\text{tot}}^{\text{LQG}k} \equiv 78\ \left(m_0^3 + m_0^{3+k}\right) \tag{8.1}$$

$$\tau_{\text{tot}}^{\text{MB}k} \equiv 78\, m_0^{3+2k} \tag{8.2}$$

Both in equations (8.1) and (8.2), the usual semiclassical lifetime eq. (3.55) is recovered when $k \to 0$: $\tau_{\text{tot}}^{\text{LQG}0} = \tau_{\text{tot}}^{\text{MB}0} = \tau_{\text{BH}}$.

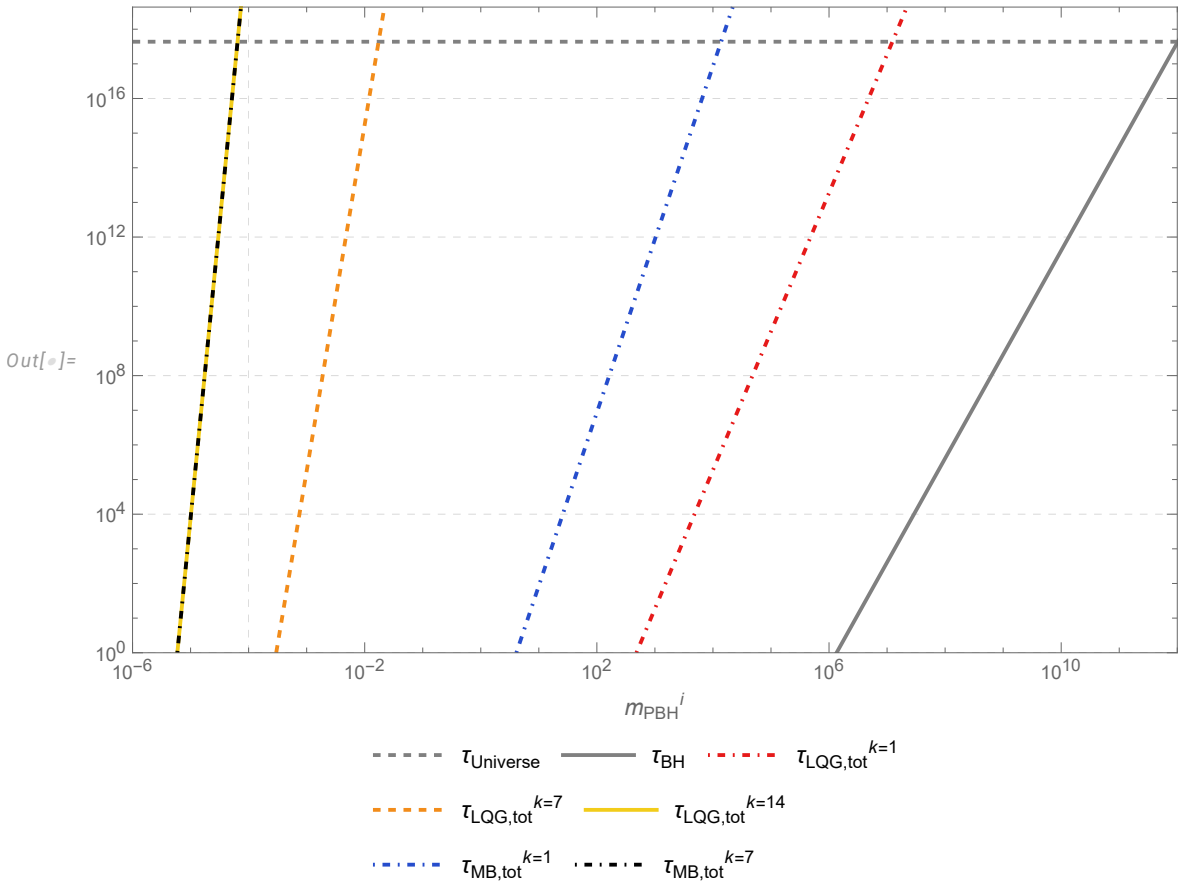

Figure 8.1: Lifetimes of PBHs τ_{PBH} and total lifetime of PBHs + remnants $\tau_{\text{tot}}^k \equiv \tau_{\text{PBH}} + \tau_{\text{REM}}^k$ as a function of the initial mass m_{PBH}^i of the PBHs. For k large enough, the total lifetime is larger than the age of the universe.

In order to reach the phase `P2` with the remnants for all masses in eq. (4.9), we need to have, in the lightest mass range of the PBHs ($m_{\text{PBH}}^i \sim 10^{-4}$kg),

$$k \geq 14 \text{ in LQG and } k \geq 7 \text{ with the MB effect} \tag{8.3}$$

In the following sections, we will focus on such values of k in order to always be in the phase `P1` or `P2`. For numerical stability reasons, we will raise the lower bound on the initial mass of the PBHs to $m^i_{\text{PBH, lower}} = 10^{-3}$ kg. As we will see in sec. 8.4, no qualitative change is expected between the results with $m^i_{\text{PBH}} = 10^{-3}$ kg and $m^i_{\text{PBH}} = 10^{-4}$ kg.

8.3 Case study

In this section, we present the results of the model for different values of the initial mass of the PBHs. Different cosmological scenarios are possible, and we show a representative example of each different case. The general results are shown in the next sec. 8.4.

8.3.1 Loop Quantum Gravity

Let us consider the case of LQG, in which the remnants have a fixed *planckian* mass given in eq. (5.72) and the HR budget is summarized in table 10. Five cases are presented, each with a qualitatively different cosmological scenario.

8.3.1.A 500 kg: the ideal case

When the PBHs start with an initial mass of $m^i_{\text{PBH}} = 500$ kg, they are small enough to evaporate before the decoupling of the neutrinos (and the e^+e^- annihilation era), and to produce a negligible amount of HR. The entire DM can then be composed of rovellinos ($f \equiv \rho_{\text{REM}}/\rho_{\text{DM}} = 1$) when $\beta \sim 10^{-12}$, as illustrated in fig. 8.2. Such a value of β is compatible with the expected $\beta^{\mathtt{P2}(c)}_{\max}$ given in eq. (7.28):

$$\beta^{\mathtt{P2}(c)}_{\max} \sim \frac{1}{e^{-N_i}\epsilon(1+C_{\nu\gamma})\frac{\rho^{\text{obs}}_\gamma}{\rho^{\text{obs}}_{\text{DM}}}} \sim \frac{1}{e^{60}10^{-11}\cdot 1.6\frac{10^{-31}}{10^{-27}}} \sim 10^{-12}$$

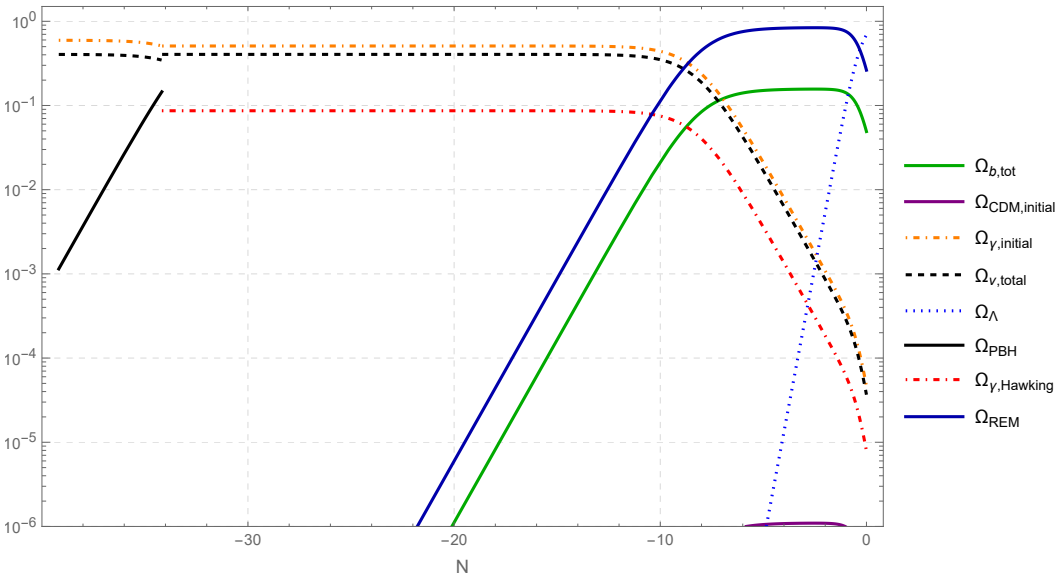

Figure 8.2: Evolution of the density of species in the case of LQG with an initial mass of the PBHs $m^i_{\text{PBH}} = 500$ kg. At early times, the universe is in RD due to the initial density of photons and neutrinos. The PBHs evaporate before dominating the universe, and the rovellinos create a MD era in the same order as in standard cosmology. The parameters of the model are $\beta = 8\cdot 10^{-13}$, $\alpha_b = 1$, $\alpha_c = 1\cdot 10^{-6}$, $\alpha_\gamma = 0.8$ and $f = 1$.

The proportion of photon density coming from the HR is $\sim 15\%$, and is growing with the mass of the PBHs. As the initial mass of the PBH increases, the fraction of photons coming from the HR will start saturating the universe's photon density, and f will not be able to stay at order 1.

8.3.1.B 3000 kg: Fiat lux

For PBHs formed with an initial mass of $m^i_{\rm PBH} = 3000$ kg, HR constrains the fraction of DM that can be explained by the PBHs to $f \sim 10^{-4}$. However, the mass fraction of PBHs β can be as high as $\sim 5\cdot 10^{-2}$ as all the relativistic species now appear later in the cosmic history: since all radiation comes from the HR, the universe starts with a non-standard Early Matter-Dominated (EMD) era. This high β value is not compatible with the (naive) expected $\beta^{\mathsf{P2}(\gamma)}_{\rm max}$ given in eq. (7.29):

$$\beta^{\mathsf{P2}(\gamma)}_{\rm max} \sim \frac{1}{e^{N_b}\left(\frac{\rho^{\rm obs}_b+\rho^{\rm obs}_{\rm DM}}{\rho^{\rm obs}_\gamma}\right)+1} \sim \frac{1}{e^{-32}\left(\frac{10^{-28}+10^{-27}}{10^{-31}}\right)+1} \sim 1$$

However, a more careful analysis (performed in appendix C) of eq. (B.14) shows that the two quantities are indeed consistent. The evolution of the density of species is shown in fig. 8.3. The number of e-folds at which the PBHs evaporate is $N_b = -31.6$, and $f = 9\%$.

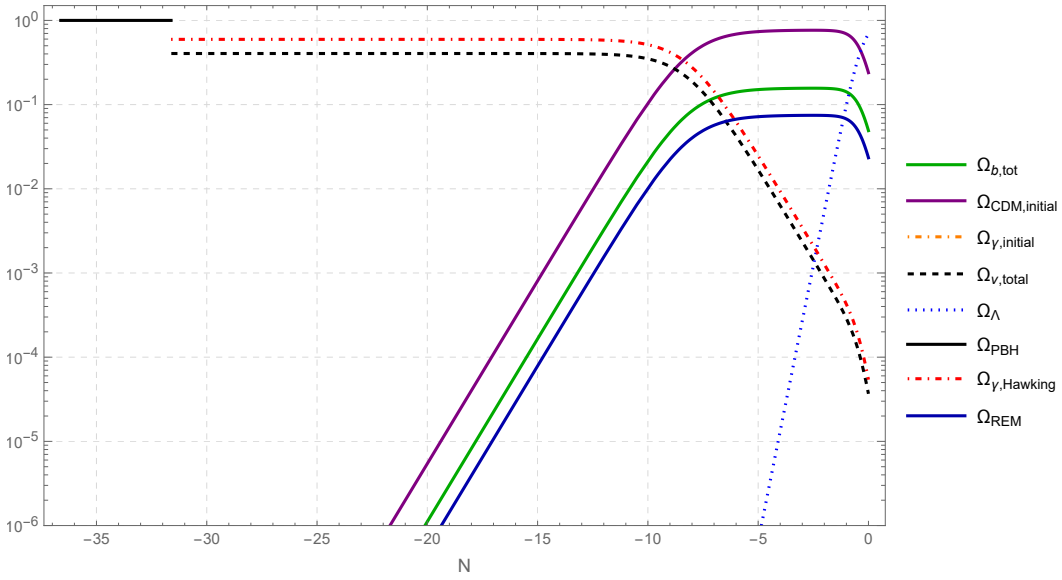

Figure 8.3: Evolution of the density of species in the case of LQG with an initial mass of the PBHs $m^i_{\rm PBH} = 3000$ kg. The universe starts with a (non-standard) EMD era due to PBHs. When they decay, a RD era starts. The parameters of the model are $\beta = 4\cdot 10^{-2}$, $\alpha_b = 1$, $\alpha_c = 0.9$, $\alpha_\gamma = 6\cdot 10^{-15}$ and $f = 8.9\%$.

8.3.1.C 10^5 kg: drop in the remnants

PBHs formed with an initial mass of $m^i_{\rm PBH} = 10^5$ kg generate a cosmic history similar to the previous case, but with a much smaller mass fraction $\beta \sim 10^{-9}$. As before, all the radiation today comes from HR of the PBHs, generating an EMD era. Understanding the drop in the mass fraction β requires the analysis in chapter C, since the naive estimation fails to recover the right order of magnitude:

$$\beta^{\mathsf{P2}(\gamma)}_{\rm max} \sim \frac{1}{e^{N_b}\left(\frac{\rho^{\rm obs}_b+\rho^{\rm obs}_{\rm DM}}{\rho^{\rm obs}_\gamma}\right)+1} \sim \frac{1}{e^{-26}\left(\frac{10^{-28}+10^{-27}}{10^{-31}}\right)+1} \sim 1$$

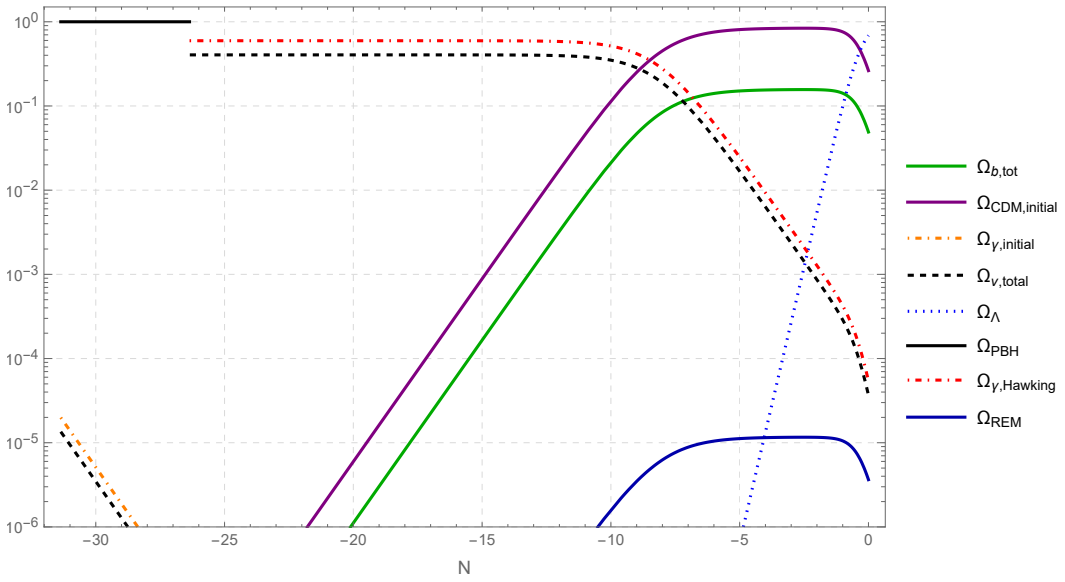

Figure 8.4: Evolution of the density of species in the case of LQG with an initial mass of the PBHs $m^i_{\text{PBH}} = 10^5$ kg. The universe starts with an EMD era due to PBHs followed by a RD era when the PBHs decay. The parameters of the model are $\beta = 2.7 \cdot 10^{-9}$, $\alpha_b = 1$, $\alpha_c = 1$, $\alpha_\gamma = 2.2 \cdot 10^{-7}$ and $f = 10^{-5}$.

8.3.1.D 10^8 kg: the baryons take over

$m^i_{\text{PBH}} = 10^8$ kg is large enough for the PBHs to not evaporate before the decoupling of the neutrinos, and therefore for HR not to thermalize. The constraint on the abundance of PBHs is then coming from the baryons: the fraction of the total baryon density made up of HR reaches 100% while $f \sim 10^{-15}$, as illustrated in fig. 8.5. However, this scenario is not likely to be realized in nature, as HR does not produce a net baryon number. In this work, we ignore this caveat, and simply present this case as an illustration of the model.

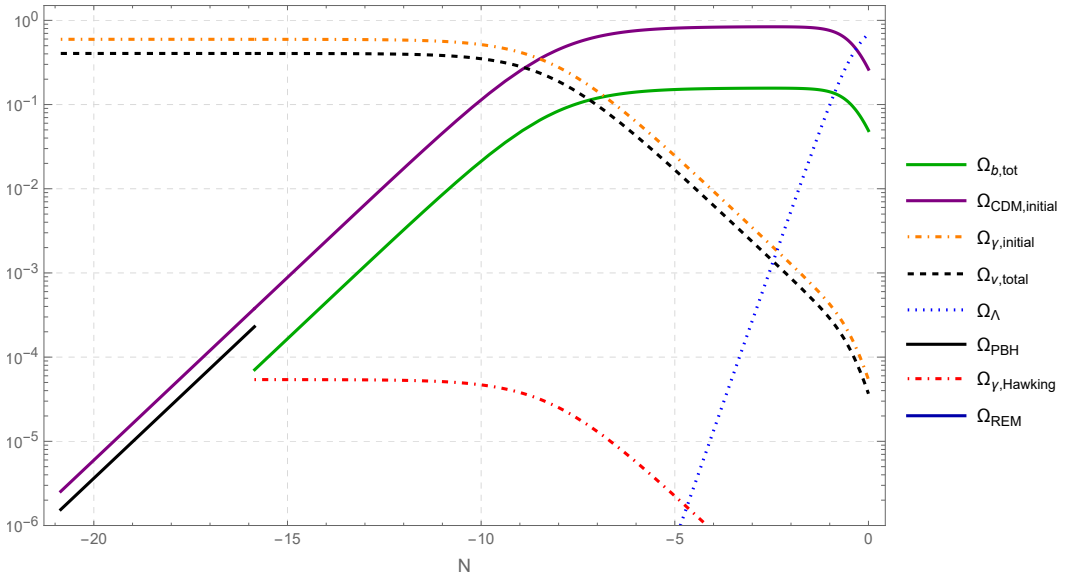

Figure 8.5: Evolution of the density of species in the case of LQG with an initial mass of the PBHs $m^i_{\text{PBH}} = 10^8$ kg. At early times, the universe is in an RD era due to the initial photon and neutrino densities. The PBHs evaporate before dominating the universe, and the density of rovellinos is negligible. The parameters of the model are $\beta = 5.7 \cdot 10^{-21}$, $\alpha_b = 9 \cdot 10^{-6}$, $\alpha_c = 1$, $\alpha_\gamma = 1$ and $f = 8 \cdot 10^{-17}$.

The mass fraction is $\beta \sim 10^{-21}$, which is compatible with the expected $\beta^{\mathrm{P2}(b)}_{\max}$ given in eq. (7.30):

$$\beta^{\mathrm{P2}(b)}_{\max} \sim \frac{1}{e^{-N_i \frac{\rho^{\mathrm{obs}}_{\gamma}}{\rho^{\mathrm{obs}}_{b}}}} \sim \frac{1}{e^{54 \frac{10^{-31}}{10^{-28}}}} \sim 10^{-21}$$

8.3.1.E 10^{11} kg: Redita Lux

For the largest mass of the PBHs before they stop evaporating, $m^i_{\mathrm{PBH}} = 10^{11}$ kg, the constraint on baryons gives way to a constraint on photons: the whole photon density is made up of HR photons. This scenario contains an important modification from subsections 8.3.1.B and 8.3.1.C, an EMD era is generated by the initial CDM and not the PBHs. As a result, the MD era is not followed by a RD era (when the PBHs evaporate), but directly by a ΛD era. The evolution of the density of species is shown in fig. 8.6. The mass fraction is $\beta \sim 10^{-3}$, within one order of magnitude from the analytic prediction from eq. (7.29):

$$\beta^{\mathrm{P2}(\gamma)}_{\max} \sim \frac{1}{e^{N_b \frac{\rho^{\mathrm{obs}}_{b}+\rho^{\mathrm{obs}}_{\mathrm{DM}}}{\rho^{\mathrm{obs}}_{\gamma}}}} \sim \frac{1}{e^{-5\left(\frac{10^{-28}+10^{-27}}{10^{-31}}\right)}} \sim 10^{-2}$$

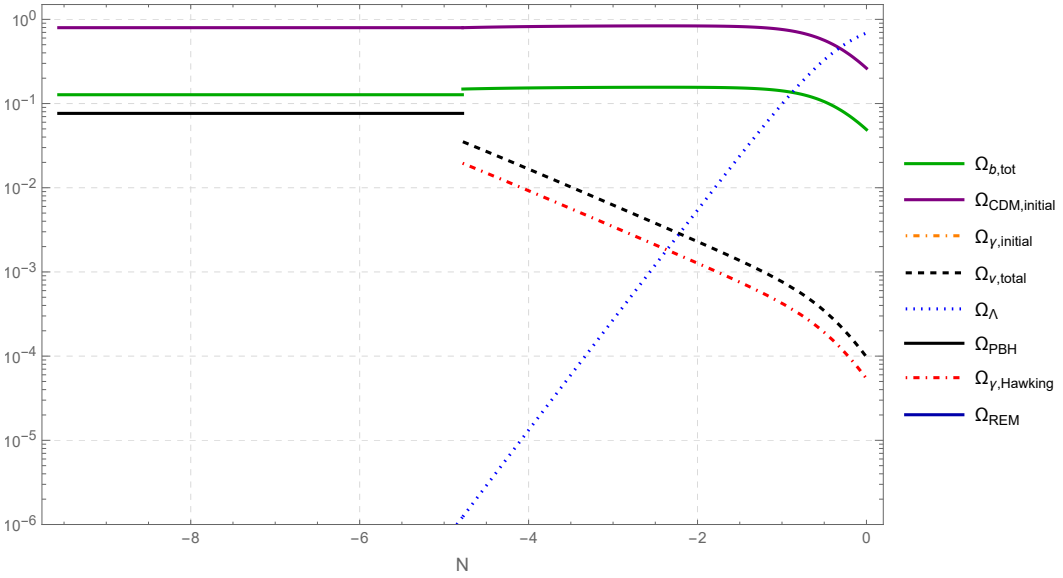

Figure 8.6: Evolution of the density of species in the case of LQG with an initial mass of the PBHs $m^i_{\mathrm{PBH}} = 10^{11}$ kg. The universe starts with an EMD era due to the initial CDM, and the density of PBHs is too low to generate a RD era when they decay. The parameters of the model are $\beta = 2.3 \cdot 10^{-3}$, $\alpha_b = 0.8$, $\alpha_c = 1$, $\alpha_\gamma = 2 \cdot 10^{-23}$ and $f = 10^{-20}$.

8.3.2 Memory burden

Let us now consider the case of PBHs being affected by the MBe, in which the remnants have a mass proportional to the initial mass of the PBHs, as given in eq. (6.14). The corresponding energy budget of the HR is shown in table 11. As in the case of LQG, we present here three examples, each with a qualitatively different cosmological scenario. The general results are then presented in subsec. 8.4.2.

8.3.2.A 10^5 kg: the ideal case

For PBHs formed with a small enough initial mass, they evaporate before the decoupling of the neutrinos and have little energy to inject in the thermal bath. The whole DM can then be made up of remnants with a mass fraction of $\beta \sim 10^{-22}$. The evolution of the density of species is shown in fig. 8.7. The analytical prediction for β is derived from eq. (7.28):

$$\beta^{\text{P2}(c)}_{\text{max}} \sim \frac{1}{(1+C_{\nu\gamma})\epsilon e^{-N_i}\frac{\rho^{\text{obs}}_{\gamma}}{\rho^{\text{obs}}_{\text{DM}}}} \sim \frac{1}{1.6\cdot 0.5\cdot e^{57}\frac{10^{-31}}{10^{-27}}} \sim 10^{-21}$$

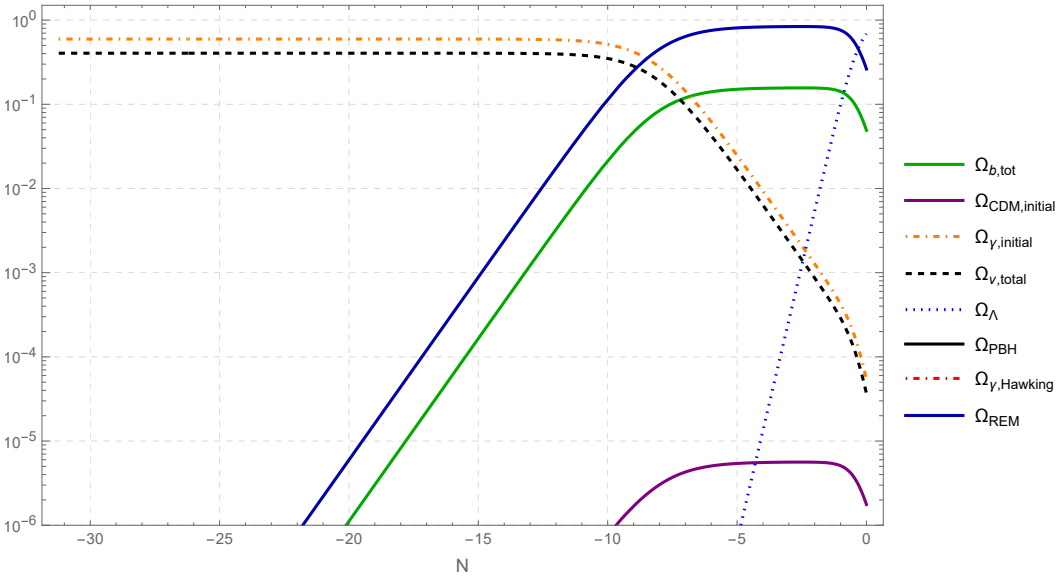

Figure 8.7: Evolution of the density of species in the case of MB with an initial mass of the PBHs $m^i_{\text{PBH}} = 10^5$ kg. At early times, the universe is in RD by the initial density of photons and neutrinos. The PBHs evaporate before dominating the universe, and the density of remnants accounts for the whole DM. The parameters of the model are $\beta = 5.9\cdot 10^{-22}$, $\alpha_b = 1$, $\alpha_c = 7\cdot 10^{-6}$, $\alpha_\gamma = 1$ and $f = 1$.

8.3.2.B 10^8 kg: the baryons take over

PBHs with $m^i_{\text{PBH}} = 10^8$ kg evaporate after the e^+-e^- annihilation era, and therefore generate a huge amount of baryons from HR. As shown in fig. 8.8, all the baryons today come from the HR, and the fraction of DM that can be explained by the MBPBHs is $f \sim 0.6$. The mass fraction of the PBHs is $\beta \sim 10^{-20}$, which can be predicted from eq. (7.30):

$$\beta^{\text{P2}(b)}_{\text{max}} \sim \frac{1}{(1-\epsilon)e^{-N_i}\frac{\rho^{\text{obs}}_{\gamma}}{\rho^{\text{obs}}_{b}}} \sim \frac{1}{0.5\cdot e^{54}\frac{10^{-31}}{10^{-28}}} \sim 10^{-20}$$

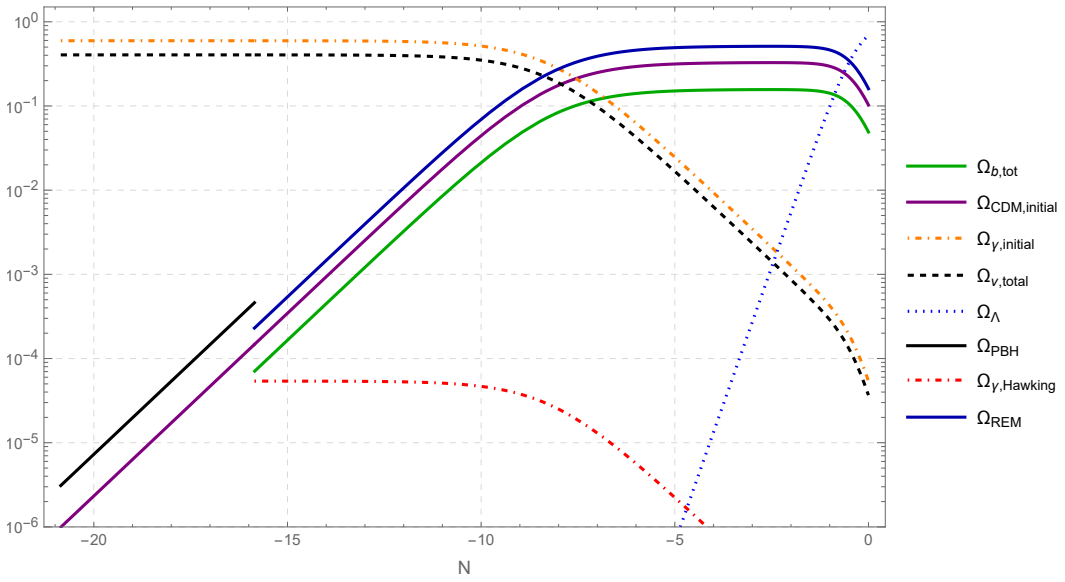

Figure 8.8: Evolution of the density of species in the case of MB with an initial mass of the PBHs $m^i_{\text{PBH}} = 10^8$ kg. At early times, the universe is in RD by the initial density of photons and neutrinos. The PBHs evaporate before dominating the universe, and their HR saturates the baryon density. The parameters of the model are $\beta = 1.1 \cdot 10^{-20}$, $\alpha_b = 5 \cdot 10^{-6}$, $\alpha_c = 0.4$, $\alpha_\gamma = 1$ and $f = 61\%$.

8.3.2.C 10^{11} kg: Redita Lux

For the largest mass of evaporating PBHs, $m^i_{\text{PBH}} = 10^{11}$ kg, the HR saturates the photon density and slightly less than a sixth of the baryon density, and $f \sim 0.1$. Similarly to the LQG case in subsec. 8.3.1.E, the universe is in an EMD era generated by the initial CMD, and not by the PBHs (as shown in fig. 8.9). The evaporation of the PBHs does not trigger a RD era, and the EMD era is directly followed by a ΛD one.

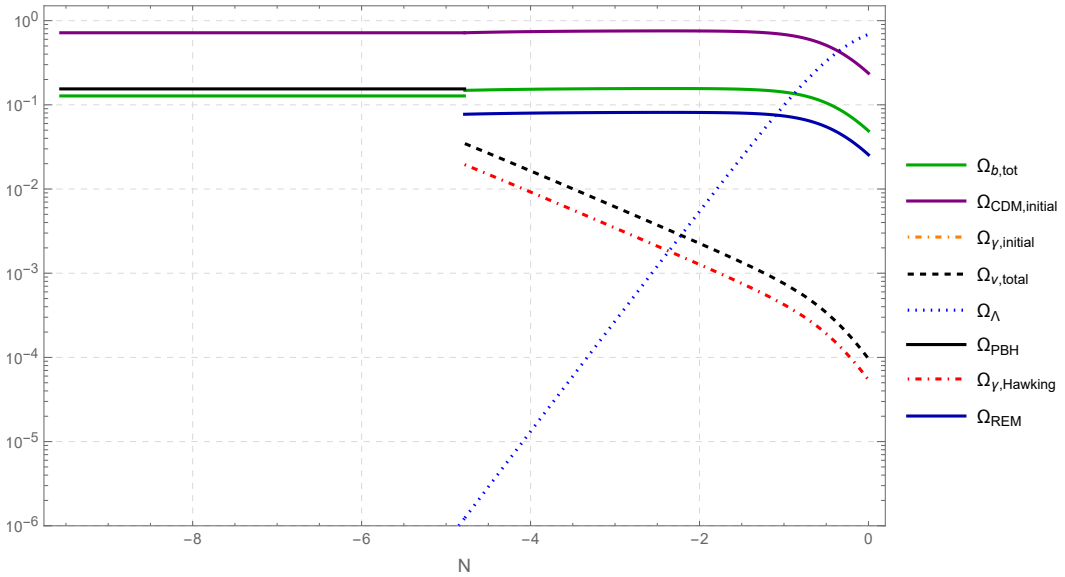

Figure 8.9: Evolution of the density of species in the case of MB with an initial mass of the PBHs $m^i_{\text{PBH}} = 10^{11}$ kg. At early times, the universe is in EMD era by the initial CDM, and the density of PBHs is too low to generate a RD era when they decay. The parameters of the model are $\beta = 4.7 \cdot 10^{-3}$, $\alpha_b = 0.9$, $\alpha_c = 0.9$, $\alpha_\gamma = 2 \cdot 10^{-23}$ and $f = 10\%$.

The mass fraction of the PBHs is $\beta \sim 5 \cdot 10^{-3}$, while the expected value from eq. (7.29) is:

$$\beta_{\max}^{\text{P2}(\gamma)} \sim \frac{1}{e^{N_b \frac{\rho_b^{\text{obs}}+\rho_{\text{DM}}^{\text{obs}}}{\rho_\gamma^{\text{obs}}}}} \sim \frac{1}{e^{-5\frac{10^{-28}+10^{-27}}{10^{-31}}}} \sim 10^{-2}$$

However, a more precise estimate is presented in chapter C, which enables an exact recovery of the order of magnitude of β.

8.3.3 Primordial Black Holes

When the initial mass is sufficiently large, say $m_{\text{PBH}}^i = 10^{13}$ kg, the PBHs are still present today, and the cosmology is independent of the theory. Ignoring the constraints external to this model mentioned in sec. 4.2, the PBHs can account for the entirety of DM, with a mass fraction $\beta \sim 10^{-18}$. The evolution of the density of species is shown in fig. 8.10.

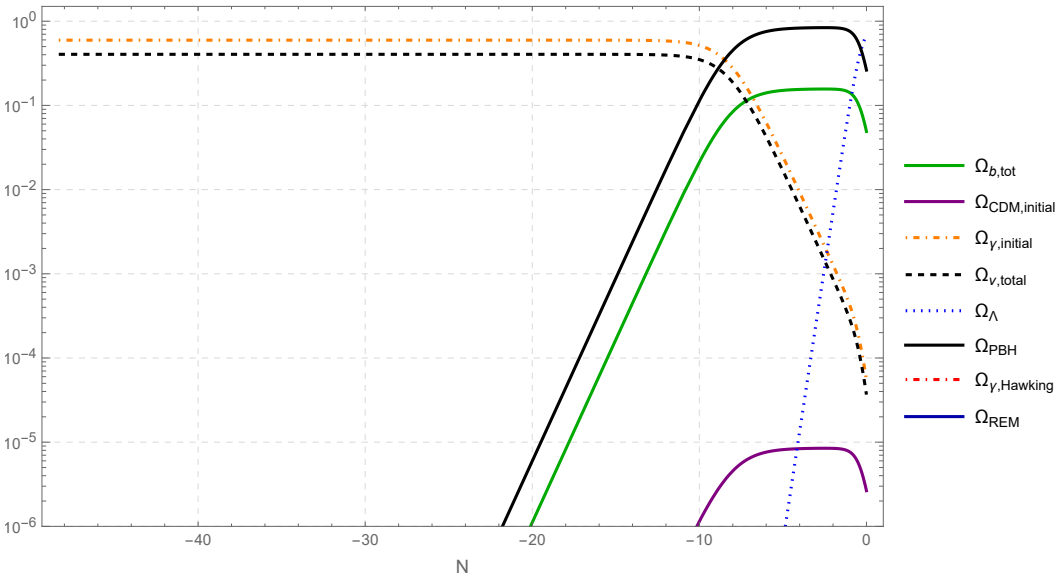

Figure 8.10: Evolution of the density of species in the case of PBHs with an initial mass of the PBHs $m_{\text{PBH}}^i = 10^{13}$ kg. At early times, the universe is in RD due to the initial density of photons and neutrinos. A MD era is generated by the PBHs, before the universe enters a ΛD era. The parameters of the model are $\beta = 2.9 \cdot 10^{-18}$, $\alpha_b = 1$, $\alpha_c = 10^{-5}$, $\alpha_\gamma = 1$ and $f = 1$.

From $\beta_{\max}^{\text{P1}(c)}$ given in eq. (7.27), we can predict the value of β:

$$\beta_{\max}^{\text{P1}(c)} \sim \frac{1}{(1+C_{\nu\gamma})e^{-N_i \frac{\rho_\gamma^{\text{obs}}}{\rho_{\text{DM}}^{\text{obs}}}}} \sim \frac{1}{1.6 \cdot e^{48\frac{10^{-31}}{10^{-27}}}} \sim 10^{-18}$$

8.4 General results

In this section, we present the general results of the model for the two cases of LQG and MB. In particular, we show the evolution of the mass fraction β as a function of the initial mass m_{PBH}^i of the PBHs, and several other quantities of interest, such as the fraction f of DM that can be explained by the PBHs or their remnants, the parameters α_A, etc.
In order to understand the evolution of the mass fraction β as a function of the initial mass m_{PBH}^i, it is useful to treat the different mass ranges separately: as discussed in sec. 8.3, the `BetaFinder` module computes the maximum mass fraction $\beta = \beta_{\max}$ for each mass, which comes from the condition $\alpha_A = 0$. Different masses will saturate different species, as illustrated in subsections 8.3.1 and 8.3.2.

8.4.1 Loop Quantum Gravity

The general results for the case of LQG are presented in fig. 8.11. The fraction of DM that can be explained by the rovellinos reaches $f = 1$ for light PBHs with an initial mass in the range 10^{-3} kg $\lesssim m^i_{\text{PBH}} \lesssim 10^3$ kg.
Let us now consider the evolution of the mass fraction β, and its dependence on the initial mass m^i_{PBH}. It is useful to recall that in the case of LQG, the mass of the rovellinos is fixed so that $\epsilon \propto 1/m^i_{\text{PBH}}$. Another important relation is the evolution of the scale factor $a = e^N$ with the mass of the PBHs during the RD and MD eras, both for the formation time N_i (using eq. (4.7)) and the decay time N_b (using eq. (3.54)):

$$e^{N_i} = a_i \sim \begin{cases} t_i^{1/2} \sim m^{1/2} & \text{in RD era} \\ t_i^{3/2} \sim m^{3/2} & \text{in MD era} \end{cases}$$

$$e^{N_b} = a_b \sim \begin{cases} t_b^{1/2} \sim m^{3/2} & \text{in RD era} \\ t_b^{3/2} \sim m^{9/2} & \text{in MD era} \end{cases}$$

- For PBHs with a mass below 10^3 kg, the illustrative case is shown in subsec. 8.3.1.A. The PBHs are formed in a RD era, and evaporate before the decoupling of the neutrinos. Maximizing the mass fraction β allows us to reach $\alpha_c \ll 1$ (or equivalently, $f = 1$); we expect the evolution of the mass fraction to be dictated by $\beta^{\text{P2}(c)}_{\text{max}}$ given in eq. (7.28):

$$\beta \sim \beta^{\text{P2}(c)}_{\text{max}} \sim \frac{e^{N_i}}{\epsilon} \sim {m^i_{\text{PBH}}}^{1/2} \cdot m^i_{\text{PBH}} \sim {m^i_{\text{PBH}}}^{3/2} \tag{8.4}$$

  The α_c parameter is stationary around $\alpha_c \sim 10^{-5}$, as expected from the `BetaFinder` module. The neutrino density is close to the one observed today since the HR product thermalizes.

- In the case of PBHs with an initial mass in $m^i_{\text{PBH}} \in [10^3, 10^4]$ kg, the photon and neutrino densities today are saturated by the HR product, creating an EMD era. The illustrative case is shown in subsec. 8.3.1.B. The PBHs evaporate before the decoupling of the neutrinos, and the evolution of the mass fraction is given by:

$$\beta \sim \beta^{\text{P2}(\gamma)}_{\text{max}} \sim \frac{1}{1 - \epsilon_e - \epsilon_p} \sim \text{const.} \tag{8.5}$$

  The α_c parameter goes to 1 as the total DM density is not accounted for by the remnants, but by an initial CDM. Despite the high β, the neutrino density does not overcome the one observed today, since the HR product still thermalizes.

  However, the prediction using $\beta^{\text{P2}(\gamma)}_{\text{max}}$ has to be confirmed using $\beta^{\text{P2}(\gamma;\varepsilon)}_{\text{max}}$ as done in sec. C.2.

  Let us note the presence of a "sweet spot" at the lower end of this mass range. When $m^i_{\text{PBH}} \sim 10^3$ kg, an interesting scenario arises: DM is still entirely composed of remnants, while HR already saturates the radiation density. As mentioned in the conclusion of this work, this region of parameter space could be probed by future observations with the Einstein Telescope.

- The illustrative case of PBHs with an initial mass in $[10^4, 10^6]$ kg is shown in subsec. 8.3.1.C. The expression eq. (8.5) is valid until the PBHs last long enough to sufficiently blueshift the collapsed matter. The dynamics of the mass fraction is then dominated by the second term of eq. (7.29)'s denominator:

$$\beta \sim \beta^{\text{P2}(\gamma)}_{\text{max}} \sim \frac{1}{e^{N_b}} \sim {m^i_{\text{PBH}}}^{-9/2} \tag{8.6}$$

  Now, this rough estimate should be treated with caution as the same reasoning failed to predict the right order of magnitude of the mass fraction in subsec. 8.3.1.C. Actually, the dynamics of β

in this region fails to be predicted by $\beta_{\max}^{\mathsf{P2}(\gamma)} = \beta_{\max}^{\mathsf{P2}(\gamma;\varepsilon=0)}$ as shown in fig. C.1.

The α_c parameter is still at 1, while the neutrino density is close to the one observed today, except at the end of this mass range, where PBHs have evaporated after the decoupling of the neutrinos, but before the e^+-e^- annihilation epoch, so a peak in the neutrino density is observed.

- For PBHs with an initial mass $m_{\text{PBH}}^i \in [10^6, 5 \cdot 10^8]$ kg, the illustrative case is shown in subsec. 8.3.1.D. The PBHs evaporate after the decoupling of the neutrinos, and the HR saturates the baryon density. The expected dynamics of the mass fraction is:

$$\beta \sim \beta_{\max}^{\mathsf{P2}(b)} \sim e^{N_i} \sim {m_{\text{PBH}}^i}^{1/2} \tag{8.7}$$

The α_b parameter goes to 0, while the α_γ parameter goes back to unity. The HR product does not thermalize anymore, and a discrepancy between the model and the observed neutrino density is growing with β.

- In the case of PBHs with an initial mass $m_{\text{PBH}}^i \in [5 \cdot 10^8, 10^{12}]$ kg, the illustrative case is shown in subsec. 8.3.1.E. The initial CDM generates an EMD era, and the HR from the PBHs saturates the photon density. The dynamics of the mass fraction is influenced by both terms in the denominator of eq. (7.29), and the slope $\mathrm{d}\beta/\mathrm{d}m_{\text{PBH}}^i$ is to be determined by the competition between the two terms. As in the previous "photon-saturated" case, effects from the denominator of $\alpha_\gamma^{\mathsf{P2}}$ should be taken into account to predict the full dynamics of the mass fraction, as done in sec. C.3.

The neutrino density is almost three times the one observed today, with a plateau correlated to the behavior of β.

- For PBHs with a mass above 10^{12} kg, they are still present today, so the dynamics of the mass fraction is independent of the theory. From subsec. 8.3.3, we see that the PBHs are formed in a RD era, so:

$$\beta \sim \beta_{\max}^{\mathsf{P1}(c)} \sim e^{N_i} \sim {m_{\text{PBH}}^i}^{1/2} \tag{8.8}$$

HR being neglected for non evaporating PBHs, the neutrino density is by construction equal to the one observed today.

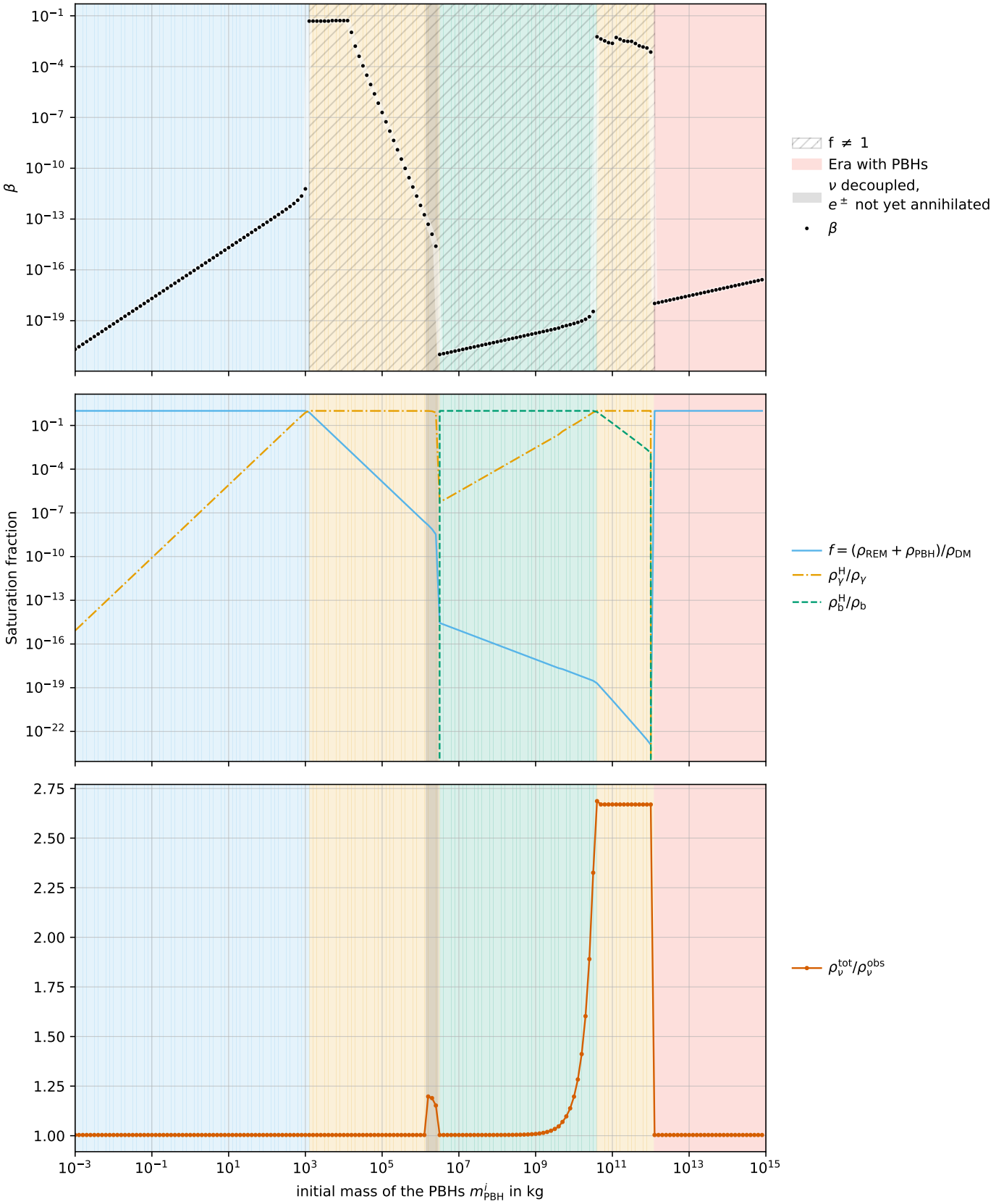

Figure 8.11: $\beta_{\max}$ as a function of the initial mass $m^i_{\rm PBH}$ in the case of LQG. The background color indicates the species saturated by the PBHs or their remnants (blue), photons from HR (orange) and baryons from HR (green). The grey area indicates the regions where the PBHs evaporate after the decoupling of the neutrinos but before the e^+-e^- annihilation epoch. The dashed region on the first panel indicates the region where $f \neq 1$ (when the total DM density cannot be accounted for by the PBHs or their remnants).

8.4.2 Memory burden

The general results for the case of MB are presented in fig. 8.12. The fraction of DM that can be explained by the PBHs or the remnants reaches $f = 1$ for PBHs with an initial mass up to 10^6 kg. The remarks made at the beginning of subsec. 8.4.1 about the evolution of the scale factors apply here as well. A crucial difference is that the mass of the remnants is proportional to the initial mass of the PBHs, so $\epsilon = q \sim$ const.

- For PBHs with a mass below 10^6 kg, the illustrative case is shown in subsec. 8.3.2.A. PBHs are formed in a RD era, and evaporate before the decoupling of the neutrinos. Since $f = 1$, the parameter α_c vanishes, and the mass fraction dynamics can be predicted from eq. (7.28):

$$\beta \sim \beta_{\max}^{\mathsf{P2}(c)} \sim \frac{e^{N_i}}{\epsilon} \sim {m_{\text{PBH}}^i}^{1/2} \tag{8.9}$$

  The α_c parameter is stationary around $\alpha_c \sim 10^{-5}$, as expected from the `BetaFinder` module. The neutrino density is close to the one observed today since the HR product thermalizes, except at the end of this mass range. However, the mass fraction being 6 orders of magnitude smaller than in the LQG case, the neutrino density is not significantly affected by the HR.

- In the case of PBHs with an initial mass $m_{\text{PBH}}^i \in [10^6, 5 \cdot 10^{10}]$ kg, the illustrative case is shown in subsec. 8.3.2.B. The PBHs evaporate after the e^+-e^- annihilation era, and the HR saturates the baryon density. The expected dynamics of the mass fraction is:

$$\beta \sim \beta_{\max}^{\mathsf{P2}(b)} \sim e^{N_i} \sim {m_{\text{PBH}}^i}^{1/2} \tag{8.10}$$

  The dynamics of $\beta_{\max}^{\mathsf{P2}(b)}$ and $\beta_{\max}^{\mathsf{P2}(c)}$ having the same scaling with the initial PBH mass, the ratio $\beta_{\max}^{\mathsf{P2}(b)}/\beta_{\max}^{\mathsf{P2}(c)}$ is constant as long as the HR product saturates the baryon density. The neutrinos emitted by the HR product do not thermalize, and the neutrino density grows with β.

- The illustrative case of PBHs with an initial mass in $[5 \cdot 10^{10}, 10^{12}]$ kg is shown in subsec. 8.3.2.C. The HR saturating the photon density, the universe has an EMD era generated by the initial CDM. As in the LQG case, the dynamics of the mass fraction is influenced by both terms in the denominator of eq. (7.29) (and by the denominator of $\alpha_\gamma^{\mathsf{P2}}$), and the slope $\mathrm{d}\beta/\mathrm{d}m_{\text{PBH}}^i$ is to be determined by the competition between the two terms, even though numerical instabilities start to appear.

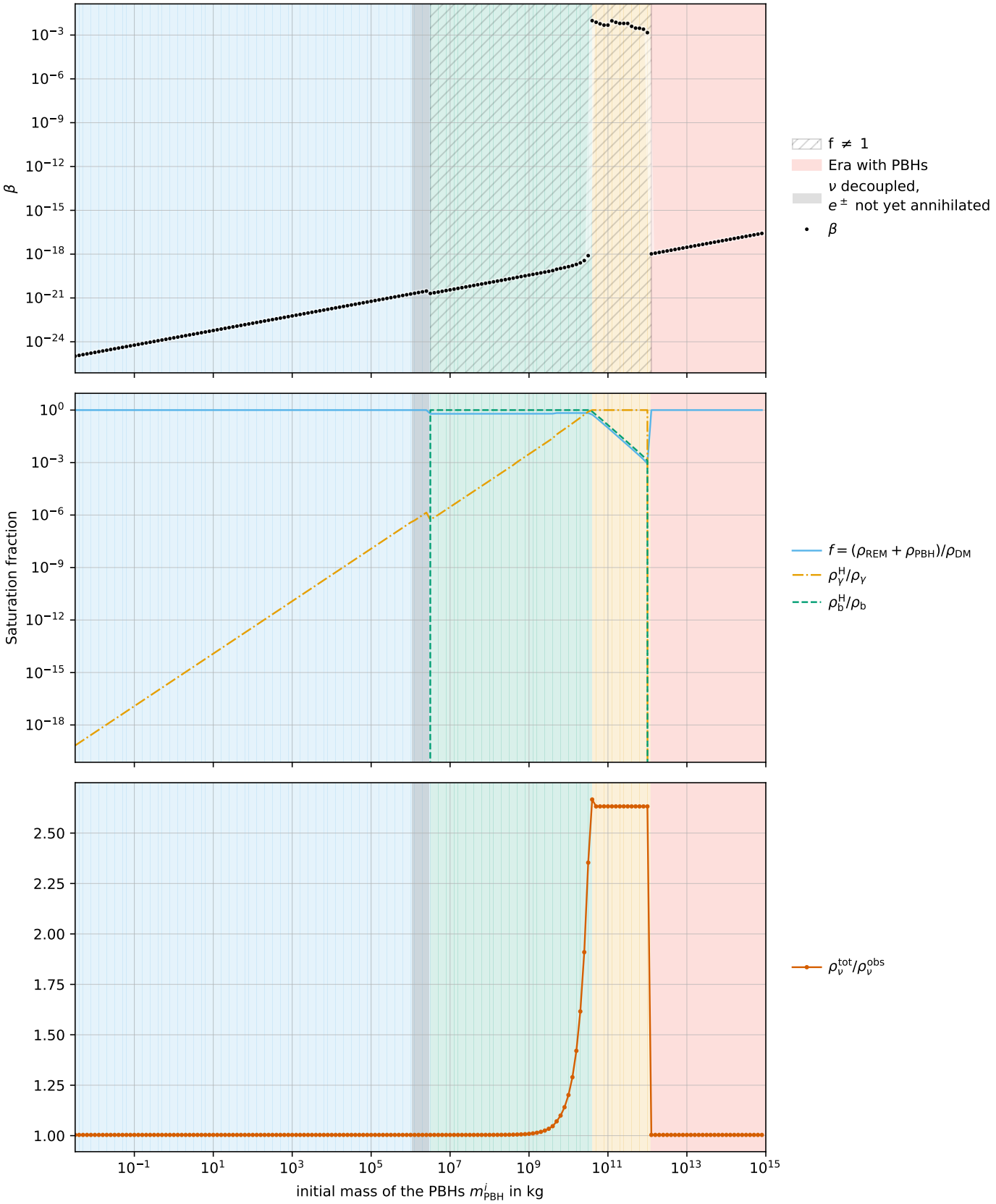

Figure 8.12: $\beta_{\max}$ as a function of the initial mass m^i_{PBH} in the case of MB. The background color indicates the species saturated by the PBHs or their remnants (blue), photons from HR (orange) and baryons from HR (green). The grey area indicates the regions where the PBHs evaporate after the decoupling of the neutrinos but before the e^+-e^- annihilation epoch. The dashed region on the first panel indicates the region where $f \neq 1$ (when the total DM density cannot be accounted for by the PBHs or their remnants).

CHAPTER

9

CONCLUSION

9.1 Our work and its implications

In this work, we have studied the possibility of explaining the observed DM density with PBHs or their remnants, phenomenologically using recent developments of LQG and effective QG theory predicting a MBe. Our analysis shows that in both cases (LQG and MBe), there exist remnant viability windows, in which remnants can contribute to the observed DM density for at least $f > 10^{-5}$.

- In the case of LQG, the remnant viability window is $m^i_{\rm PBH} \in [10^{-3}, 10^5]$ kg, before the injection of photons and baryons from the HR saturates the observed densities of these species.

  In the lowest mass range $m^i_{\rm PBH} \in [10^{-3}, 10^3]$ kg, the remnant can account for the totality of the DM density, while in the higher mass range $m^i_{\rm PBH} \in [10^3, 10^5]$ kg, f decreases down to 10^{-5}.

  These remnant viability windows assume a longer lifetime than the age of the universe. This translates to a limit on the model parameter $k_{\rm LQG}$ going up to 14 for the smallest PBH mass. In the most conservative case $k_{\rm LQG} = 1$, PBHs heavier than 10^7 kg lead to remnants still present in the universe.

- In the case of MBe, the remnant viability window is $m^i_{\rm PBH} \in [10^{-3}, 10^{12}]$ kg: the injection of photons and baryons from the HR never constrains f below 10^{-5}.

  The remnant can account for the totality of the DM density in the lowest mass range $m^i_{\rm PBH} \in [10^{-3}, 10^6]$ kg, and can still account for more than half of the DM density in the higher mass range $m^i_{\rm PBH} \in [10^6, 10^{10}]$ kg. Only when the initial PBH mass is above 10^{10} kg, the fraction of the DM density that can be accounted for by the remnants can be as low as $f \sim 10^{-3}$.

  These remnant viability windows assume the model parameter $k_{\rm MB}$ large enough for the remnants to be still present today, which translates to a limit on $k_{\rm MB}$ going up to 7. The most conservative case where $k_{\rm MB} = 1$ puts a limit on the initial PBH mass at $m^i_{\rm PBH} \gtrsim 10^4$ kg. Throughout our results, we have fixed $q_{\rm MB} = 0.5$. The outcomes remain qualitatively generic for other $q_{\rm MB}$ values, and our code can be directly used to study such cases quantitatively. In the limit $q_{\rm MB} \to 1$, the constraints from the Hawking evaporation are relaxed, allowing PBHs to constitute up to the totality of the DM in the whole considered mass range.

In addition, constraints on the initial density fraction of PBHs maximizing the abundance of remnants have been obtained for each mass range.

The case where DM is entirely made of remnants includes PBH masses of the order of grams, that could have been formed directly after the end of inflation. This would motivate the study of PBH formation during reheating (from tachyonic preheating, oscillons, long reheating, ...), in the specific context of LQG and MBe. For sufficiently low-scale inflation, the results show that it is impossible to have DM in the form of LQG or MB remnants. Therefore, it could be possible to exclude these DM models with more stringent limits on the energy scale of inflation from CMD B-mode experiments, like LiteBIRD [Allys et al., 2023].

In both scenarios, neutrino overproduction occurs only in mass ranges where $f = 1$ is already excluded by the overproduction of other species, and therefore does not set the leading bound on the $f \simeq 1$ regions. Let us mention that the effective number of relativistic degrees of freedom $N_{\rm eff}$ in our model can change because of the extra neutrinos (and subdominantly because of the gravitons) produced by the HR. From eq. (2.22), we can extract the change in the number of effective degrees of freedom:

$$\Delta N_{\rm eff} = \frac{\rho_\nu + \rho_g}{\rho_\gamma} \frac{8}{7} \left(\frac{11}{4}\right)^{4/3} - 3.046 \tag{9.1}$$

The difference between the effective number of relativistic degrees of freedom in our model and the one observed today is shown in fig. 9.1. The allowed band by Planck observation [Planck, 2020] $N_{\rm eff}^{\rm obs} = 2.99^{+0.17}_{-0.17}$ is shown for comparison. The extra radiation from neutrinos contributes to $\Delta N_{\rm eff}$ and is only relevant after the neutrino decoupling and before the CMB emission. In the future, Euclid and LiteBIRD should improve the Planck bound, possibly by one order of magnitude [Archidiacono et al., 2025].

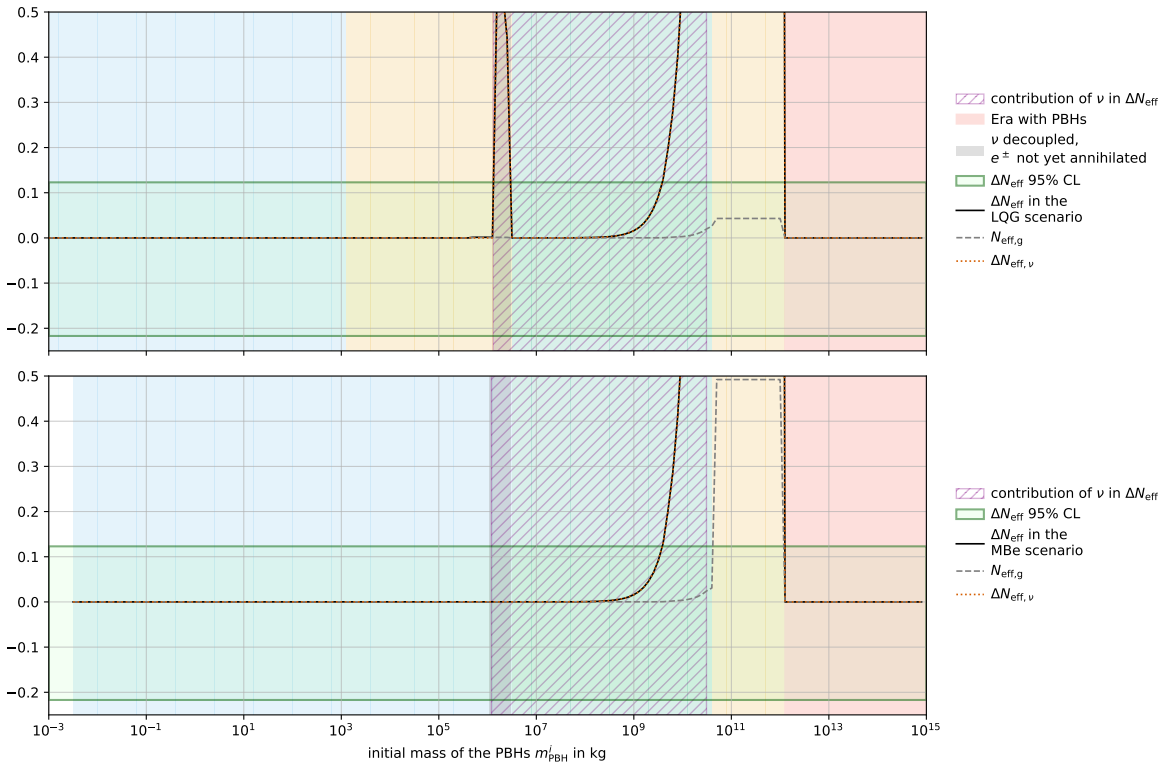

Figure 9.1: Effective number of relativistic degrees of freedom $N_{\rm eff}$ as a function of the initial PBH mass $m^i_{\rm PBH}$ in the LQG and MBe scenarios.

However, the excluded values of $N_{\rm eff}$ do not end the story, as a lower mass fraction of the PBHs

would allow recovering the observed $N_{\rm eff}$, while still being able to account for part of the DM density (in the case of MBe). The relevant mass range is $m^i_{\rm PBH} \in [10^{10}, 10^{12}]$ kg, which is the scenario where initial CDM generates an EMD era. It is worth noting that in this case, the threshold needed to form PBHs almost vanishes, which would enhance the formation rate of heavier PBHs. In such an EMD, a primordial density fluctuation grows linearly with the scale factor $\delta \sim (aH)^{-2} \sim a$ [Bagui et al., 2023] such that one needs $N \sim \ln\left(\sqrt{10^{-9}}\right) \sim 10$ e-folds of expansion to form a BH. We have observed many such cases, which motivates a study of *runaway* PBH formation scenarios.

Before closing, we stress that the aim of this work is not to propose specific observational signatures; our results are presented as a consistent cosmological viability analysis for remnant scenarios. Protocols to detect remnants have been proposed both for planckian remnants, using a grid of superconducting circuits that convert gravitational phase shift of the quantum wave into an electrical signal [Perez et al., 2024], and for light BHs ($m_{\rm PBH} \gtrsim 10^8$ kg), using the future space-based GW interferometers [Thoss and Loeb, 2025]. These protocols provide examples of how remnants might in principle be probed, but such considerations lie beyond the scope of our treatment here.

Finally, let us mention the possibility of indirectly detecting the presence of light PBHs in the early universe, which would have evaporated by today, through the generation of scalar-induced GWs, either from primordial [Romero-Rodríguez and Kuroyanagi, 2024] or Poisson fluctuations [Bagui et al., 2023; Papanikolaou et al., 2021]. The future Einstein Telescope (**ET**) could detect scalar-induced GWs from primordial inhomogeneities associated with PBHs of initial masses $m^i_{\rm PBH} \sim 10^5 - 10^{10}$ kg, corresponding to baryon saturation from Hawking evaporation in the MB scenario. ET could also probe the "sweet spot" region in the LQG scenario, namely $m^i_{\rm PBH} \sim 10^3$ and $\beta \sim 10^{-2}$, through scalar-induced GWs from Poisson-distributed PBHs. Moreover, the detection of an excess population of PBHs with masses below 10^3 kg could rule out the scenario in which DM consists entirely of rovellinos, at least under the assumptions adopted in this work.

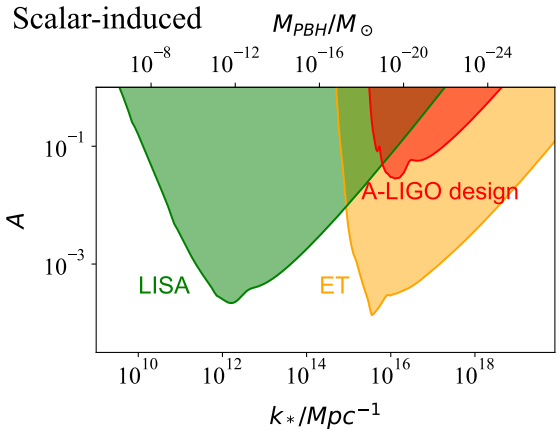

(a) Projected constraints on the primordial amplitude of the curvature power spectrum A as a function of the PBH mass $m_{\rm PBH}$ for scalar-induced GWs from primordial inhomogeneities. A corresponds to $\Delta_{\mathcal{R}}$ in our work (and that can be related to β once a collapsed threshold is defined). Taken from [Romero-Rodríguez and Kuroyanagi, 2024].

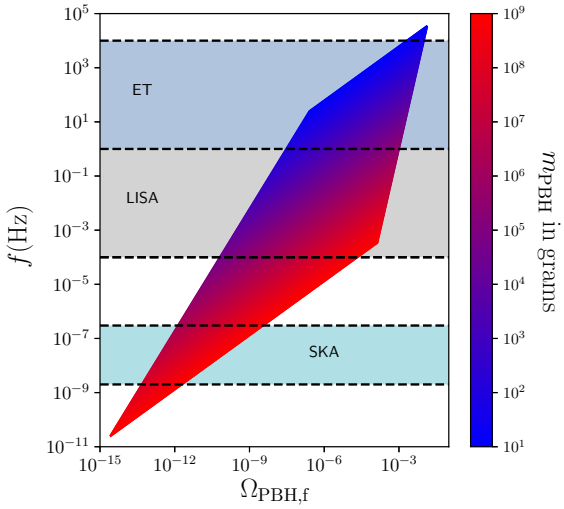

(b) Frequency at which the GWs induced by a (poissonian) dominating gas of PBHs peak, as a function of the initial abundance $\beta \equiv \Omega_{{\rm PBH},f}$ and their initial mass $m^i_{\rm PBH}$. Taken from [Papanikolaou et al., 2021].

Figure 9.2: Gravitational-wave signatures associated with PBH scenarios.

9.2 Future Work

An intrinsic limitation of our model is that it does not include the temperature: the decoupling of the neutrinos, the e^+-e^- annihilation, and the relativistic behavior of massive particles all require a proper treatment of the temperature.
Our model only considers the energy density of the species, which is sufficient to derive a coarse-grained picture of the cosmology, but most of the processes interesting for actual predictions depend on temperature. Future work should include the temperature in the model, which would allow us to derive, for example, the rate of gamma-ray emission from the PBHs and their remnants in the galactic halo, and compare it with observations. Omitting temperature effects prevented us from properly classifying the relativistic nature of the species, both in the early universe and in HR. Such changes in the code might justify changing the language from a high-level symbolic code such as `Mathematica` to one allowing an easier interfacing with other codes, such as `Python` or `C`.

Another continuation of this work would be to include extended mass distributions of the PBHs, allowing us to study specific scenarios with mass distributions predicted by different PBHs formation mechanisms. The various mass distributions would give different behaviors of the mass fraction β as a function of the initial PBH mass $m^i_{\rm PBH}$, and if coupled with the temperature, would allow the generation of signatures that could be compared with the observations. Nevertheless, this could heavily complicate the possible PBH cosmologies with multiple matter eras, runaway PBH formation, the need to consider additional effects such as PBH mergers in the early universe and the production of GWs, etc.

One avenue that was partially implemented — but not fully explored — in this work is the study of the diffuse radiation produced by the remnants. We show in fig. 9.3 the mass fraction $\beta_{\rm max}$ as a function of the initial PBH mass $m^i_{\rm PBH}$ in the LQG and MBe scenarios, with the minimal lifetime for the remnants ($k = 1$). Many questions remain unanswered, such as the mass dependence of the typical wavelength of the diffuse radiation, and the possibility that rovellinos (the remnants of the LQG scenario) are fully stable.

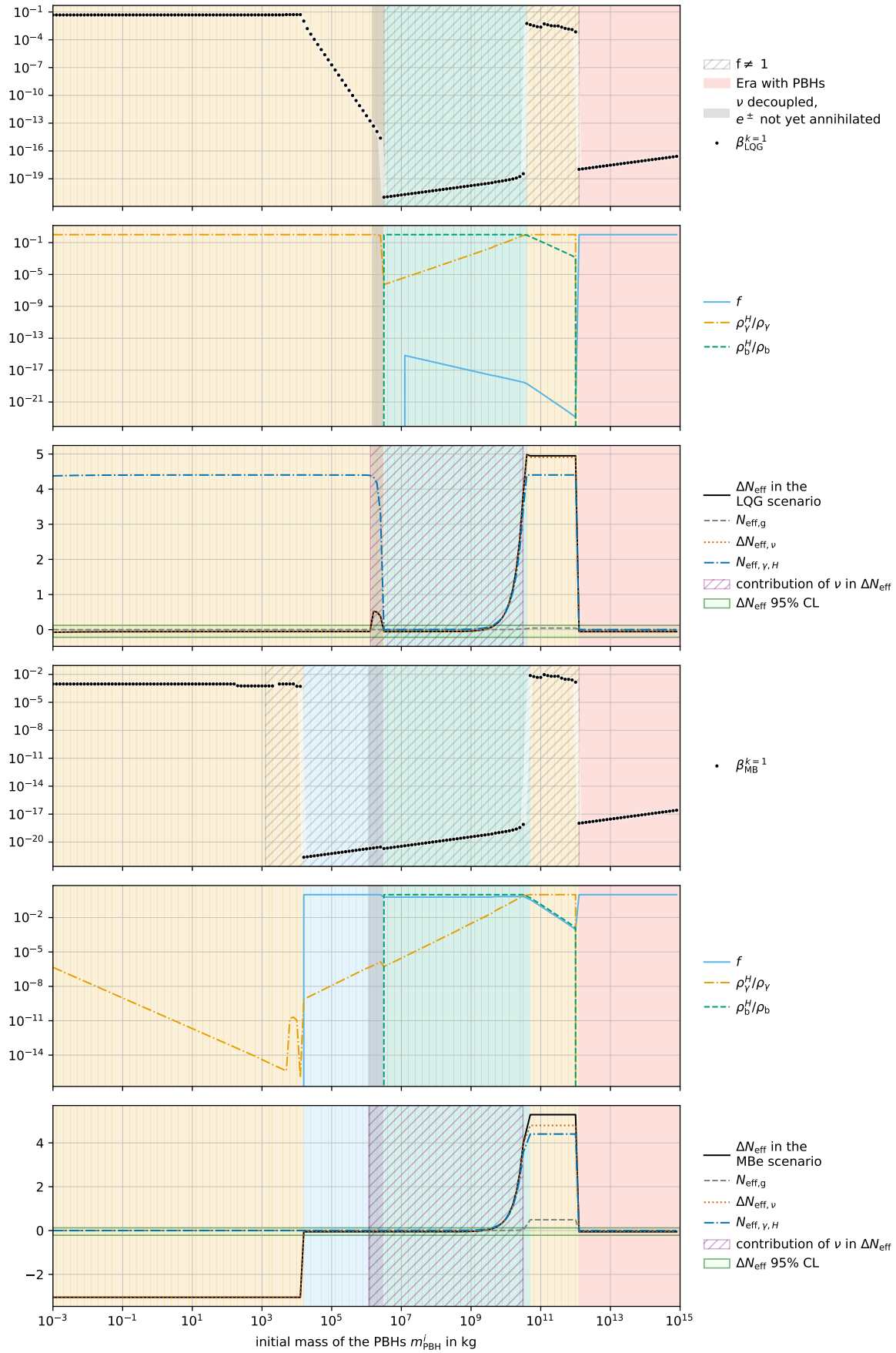

Figure 9.3: $\beta_{\max}$ as a function of the initial PBH mass m^i_{PBH} in the LQG and MBe scenarios, with $k = 1$ (minimal lifetime).

Many other interesting questions are worth studying, such as the prediction that two MBPBHs merging would start a new Hawking radiation phase, or the fate of old remnants in the LQG scenario with the possibility of a "diffuse radiation" from remnant decays that could contribute to a *dark radiation* component of the universe. Bouncing cosmologies and DM production from HR could easily be explored with the current framework.

In summary, our work has explored multiple PBHs cosmologies with LQG and MB effects, some leading to a significant or even the totality of DM in the form of remnants, others leading to standard model particles coming from the HR of these PBHs. The different regimes in the plausible parameter space have been identified and physically interpreted. More generally, this work emphasizes that PBHs open new avenues to probe and constrain QG effects, which additionally motivates searches for light PBHs or their remnants with various probes.

Finally, it is worth mentioning that the results of our work are the subject of a scientific article currently under preparation, with Sébastien Clesse, Emmanuel Frion, and Francesca Vidotto as co-authors.

APPENDIX

A

BLACKHAWK

We reproduce here the fractional energy densities of the different particle species emitted by a monochromatic distribution of Schwarzschild BHs, as computed by the `BlackHawk` code [Auffinger, 2023].
For our purpose, we set the following parameters:

- `metric` = 0: Kerr BH, along with `amin`=`amax`=0, so that we recover the Schwarzschild metric.
- `Mmin` = $m^i_{\rm PBH}$
- `BlackHawk_tot`: we compute the time-dependent Hawking spectra
- `spectrum_choice` = 0: the BH distribution is monochromatic, with a mass $m^i_{\rm PBH}$.
- `BH_remnant` = 1: the BH evaporation stops when the mass reaches a certain value $m_{\rm REM}$
- `M_remnant` = $m_{\rm REM}$: the mass of the remnant, in grams.
- `grav` = 1: we consider the emission of gravitons.
- `add_DM` = 0: we do not consider the emission of dark matter particles.
- `primary_only` = 0: we compute the secondary emission spectra.
- `hadronization_choice` = 2: `Pythia` table, at present epoch [Sjöstrand et al., 2015].

`BlackHawk` produces tables with the differential rate for each species, which we can integrate over time and the energy to obtain the total energy density emitted for each species. Results presented in table 10 for a PBH with initial mass $m \sim 10^{11}$ kg deviate from [MacGibbon, 1991] by less than one percent.

Mass	ν (%)	γ (%)	$e^{\pm}$ (%)	$p^{\pm}$ (%)	g (%)	ν_e (%)	ν_μ (%)	ν_τ (%)
$m = 10^{-3}\,\mathrm{kg}$	32.12	51.12	11.58	5.17	0.00	10.48	18.37	3.27
$m = 10^{-2}\,\mathrm{kg}$	32.12	51.12	11.58	5.17	0.00	10.48	18.37	3.27
$m = 10^{-1}\,\mathrm{kg}$	32.12	51.12	11.58	5.17	0.00	10.48	18.37	3.27
$m = 1\,\mathrm{kg}$	32.13	51.12	11.58	5.17	0.00	10.49	18.37	3.27
$m = 10\,\mathrm{kg}$	32.14	51.12	11.58	5.17	0.00	10.49	18.37	3.28
$m = 10^{2}\,\mathrm{kg}$	32.15	51.08	11.60	5.17	0.00	10.49	18.38	3.28
$m = 10^{3}\,\mathrm{kg}$	32.34	50.68	11.76	5.22	0.00	10.55	18.50	3.29
$m = 10^{4}\,\mathrm{kg}$	33.98	47.27	13.18	5.57	0.00	11.08	19.49	3.41
$m = 10^{5}\,\mathrm{kg}$	40.39	33.93	18.69	6.98	0.00	13.15	23.39	3.86
$m = 10^{6}\,\mathrm{kg}$	44.80	24.78	22.28	8.12	0.02	14.56	26.18	4.06
$m = 10^{7}\,\mathrm{kg}$	45.39	23.92	22.45	8.15	0.09	14.76	26.53	4.11
$m = 10^{8}\,\mathrm{kg}$	45.71	23.55	22.68	7.97	0.09	14.86	26.67	4.17
$m = 10^{9}\,\mathrm{kg}$	45.64	23.81	22.56	7.89	0.10	14.84	26.85	3.94
$m = 10^{10}\,\mathrm{kg}$	46.29	25.47	20.51	7.58	0.15	15.11	27.91	3.27
$m = 10^{11}\,\mathrm{kg}$	46.18	25.57	20.51	7.48	0.25	15.07	27.81	3.29

Table 10: Fractional energy output by particle species from Hawking evaporation of BH of various masses in the LQG scenario, including neutrino-flavor subfractions.

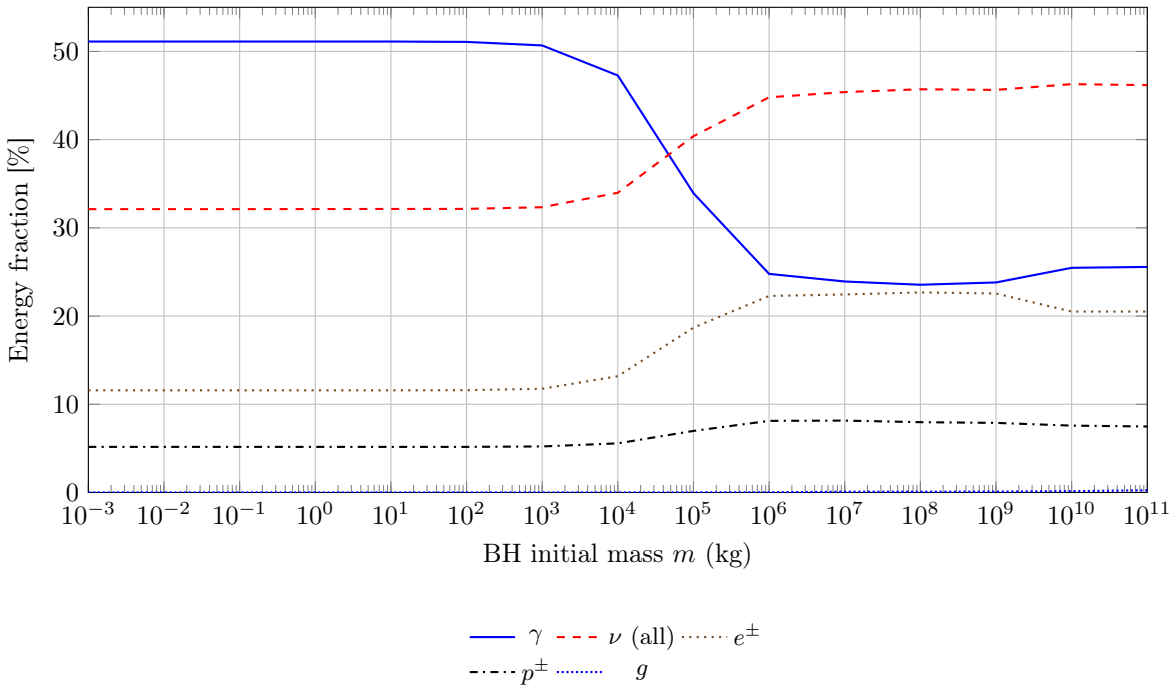

Figure A.1: Fractional energy carried by different particle species radiated by Hawking evaporation in the LQG scenario as a function of the initial BH mass.

Mass	ν (%)	γ (%)	$e^{\pm}$ (%)	$p^{\pm}$ (%)	g (%)	ν_e (%)	ν_μ (%)	ν_τ (%)
$m = 10^{-3}$ kg	32.13	51.12	11.58	5.17	0.00	10.48	18.37	3.27
$m = 10^{-2}$ kg	32.13	51.12	11.58	5.17	0.00	10.48	18.37	3.27
$m = 10^{-1}$ kg	32.13	51.12	11.58	5.17	0.00	10.48	18.37	3.27
$m = 1$ kg	32.13	51.12	11.58	5.17	0.00	10.49	18.37	3.27
$m = 10$ kg	32.13	51.12	11.58	5.17	0.00	10.49	18.37	3.28
$m = 10^{2}$ kg	32.15	51.08	11.60	5.17	0.00	10.49	18.38	3.28
$m = 10^{3}$ kg	32.35	50.67	11.77	5.22	0.00	10.56	18.50	3.29
$m = 10^{4}$ kg	34.05	47.12	13.24	5.59	0.00	11.11	19.54	3.41
$m = 10^{5}$ kg	40.53	33.66	18.81	7.01	0.00	13.19	23.47	3.87
$m = 10^{6}$ kg	44.86	24.66	22.31	8.15	0.02	14.58	26.23	4.05
$m = 10^{7}$ kg	45.54	23.72	22.52	8.13	0.09	14.80	26.60	4.13
$m = 10^{8}$ kg	45.80	23.46	22.75	7.89	0.09	14.90	26.71	4.20
$m = 10^{9}$ kg	45.55	24.32	22.01	8.02	0.12	14.82	27.07	3.65
$m = 10^{10}$ kg	46.53	25.79	20.24	7.25	0.18	15.21	28.12	3.20
$m = 10^{11}$ kg	44.93	25.23	20.72	6.30	2.82	14.63	25.85	4.45

Table 11: Fractional energy output by particle species from Hawking evaporation of BH of various masses in the MB scenario, including neutrino-flavor subfractions.

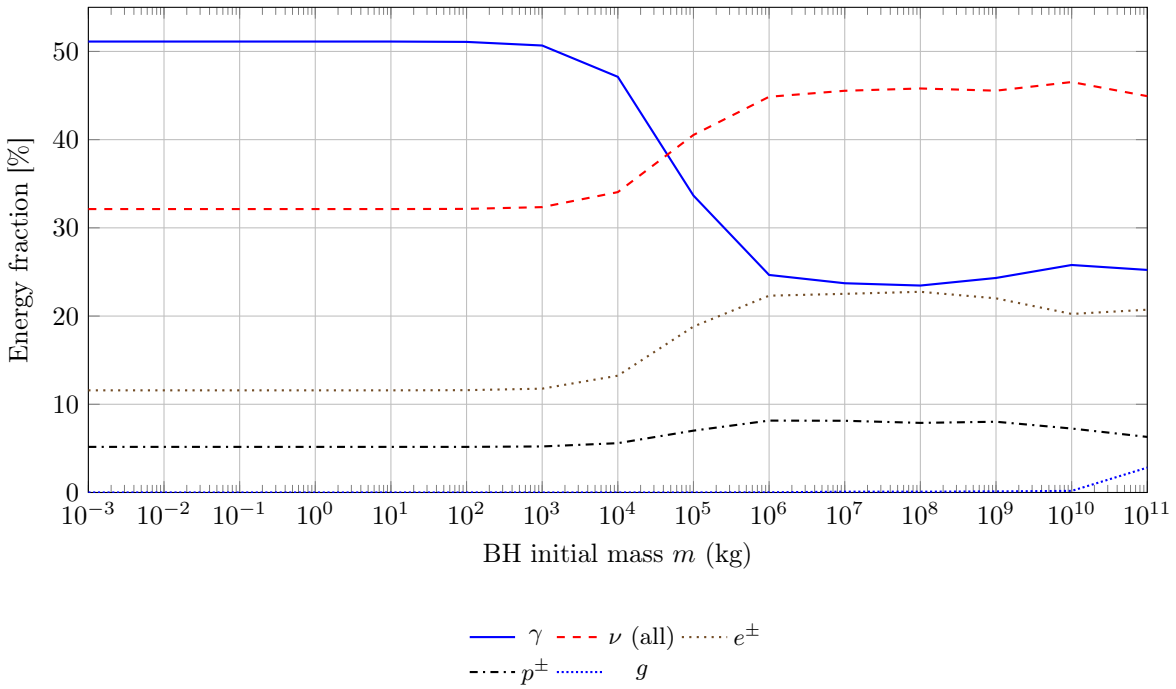

Figure A.2: Fractional energy carried by different particle species radiated by Hawking evaporation in the MB scenario as a function of the initial BH mass.

APPENDIX

B

DERIVATION OF THE $\{\alpha\}$ PARAMETERS IN EACH PHASE

B.1 Phase P0

The phase P0 corresponds to the epoch just before the formation of the PBH. We consider that the reheating process has already occurred, and that the following species are present: the photons γ, the neutrinos ν, some baryonic matter b and some primordial dark matter c. Their respective energy densities at $N = N_i^-$ are given by

$$\rho(N_i^-) = \tilde{\rho}_\gamma + \tilde{\rho}_\nu + \tilde{\rho}_b + \tilde{\rho}_c + \rho_\Lambda \tag{B.1}$$

We choose to parametrize these densities in terms of the current observed ones, blueshifted by scale factors e^{-3N_i} for non-relativistic species and e^{-4N_i} for relativistic species.

$$\begin{cases} \tilde{\rho}_b \equiv \alpha_b e^{-3N_i} \rho_b^{\text{obs}} & \text{(B.2a)} \\ \tilde{\rho}_c \equiv \alpha_c e^{-3N_i} \rho_{\text{DM}}^{\text{obs}} & \text{(B.2b)} \\ \tilde{\rho}_\gamma \equiv \alpha_\gamma e^{-4N_i} \rho_\gamma^{\text{obs}} & \text{(B.2c)} \\ \tilde{\rho}_\nu \equiv C_{\nu\gamma}\, \tilde{\rho}_\gamma & \text{(B.2d)} \end{cases}$$

where $C_{\nu\gamma}$ is the ratio of the neutrino energy density to the photon energy density defined in eq. (2.22). In some sense, we constrain α_ν with α_γ, and leave the energy density of the neutrinos predicted by the system today free. At $N = N_i$, a fraction β of the species collapses into a PBH:

$$\tilde{\rho}_b + \tilde{\rho}_c + \tilde{\rho}_\gamma + \tilde{\rho}_\nu \mapsto \rho_b^i + \rho_c^i + \rho_\gamma^i + \rho_\nu^i + \rho_{\text{PBH}}^i \tag{B.3}$$

where

$$\begin{cases} \rho_b^i \equiv (1-\beta)\tilde{\rho}_b & \text{(B.4a)} \\ \rho_c^i \equiv (1-\beta)\tilde{\rho}_c & \text{(B.4b)} \\ \rho_\gamma^i \equiv (1-\beta)\tilde{\rho}_\gamma & \text{(B.4c)} \\ \rho_\nu^i \equiv (1-\beta)\tilde{\rho}_\nu & \text{(B.4d)} \\ \rho_{\text{PBH}}^i \equiv \beta(\tilde{\rho}_\gamma + \tilde{\rho}_\nu + \tilde{\rho}_b + \tilde{\rho}_c) & \text{(B.4e)} \end{cases}$$

At $N = N_i^+$, the energy density is then given by

$$\rho(N_i^+) = \rho_b^i + \rho_c^i + \rho_\gamma^i + \rho_\nu^i + \rho_{\text{PBH}}^i + \rho_\Lambda \tag{B.5}$$

B.2 Phase P1

The phase P1 corresponds to the epoch from the formation of the PBH until their behavior is dominated by Hawking radiation and / or the memory burden effect. For large enough PBH mass, the P1 phase is still occurring today. In this case, the energy density today would be given by:

$$\rho\left(N_0^{(P1)}\right) = \left(\rho_\gamma^i + \rho_\nu^i\right) e^{4N_i} + \left(\rho_b^i + \rho_c^i + \rho_{\text{PBH}}^i\right) e^{3N_i} + \rho_\Lambda \tag{B.6}$$

Now, we require that the model be consistent with the observed energy density today, namely:

$$\begin{cases} \rho_\gamma^{\text{model}}(N=0) = \rho_\gamma^{\text{obs}} & \text{(B.7a)} \\ \rho_b^{\text{model}}(N=0) = \rho_b^{\text{obs}} & \text{(B.7b)} \\ \rho_c^{\text{model}}(N=0) + \rho_{\text{PBH}}^{\text{model}}(N=0) = \rho_{\text{DM}}^{\text{obs}} & \text{(B.7c)} \end{cases}$$

These requirements can be translated into the following constraints on the $\{\alpha\}$ parameters:

$$\begin{cases} \alpha_b = \dfrac{1}{1-\beta} & \text{(B.8a)} \\ \alpha_c = 1 - \dfrac{\beta}{1-\beta}\dfrac{\rho_b^{\text{obs}} + \rho_\gamma^{\text{obs}}(1+C_{\nu\gamma})e^{-N_i}}{\rho_{\text{DM}}^{\text{obs}}} & \text{(B.8b)} \\ \alpha_\gamma = \dfrac{1}{1-\beta} & \text{(B.8c)} \end{cases}$$

We refer to the $\{\alpha\}$ parameters in the P1 phase as $\{\alpha\}^{\text{P1}}$.

B.3 Phase P2

The phase P2 corresponds to the epoch where the PBHs are not well described by the semiclassical regime anymore. HR suddenly becomes enormous, and just after the PBHs undergo a phase transition. We make the approximation here that these two events happen simultaneously at $N = N_b$. Both in the LQG motivated scenario and in the one of the memory burden effect, the PBHs leave a remnant with a certain lifetime behind. The number of e-folds corresponding to the end of the lifetime of the remnant (and hence of the $P2$ phase) is denoted by N_r.
At $N = N_b^-$, the energy density is given by:

$$\rho(N_b^-) = \left(\rho_\gamma^i + \rho_\nu^i\right) e^{-4\delta N} + \left(\rho_b^i + \rho_c^i + \rho_{\text{PBH}}^i\right) e^{-3\delta N} + \rho_\Lambda \tag{B.9}$$

where $\delta N = N_b - N_i$. At $N = N_b$, the PBHs decay into a remnant and radiation (photons, neutrinos, protons, electrons and gravitons):

$$\rho_{\text{PBH}}(N_b) \equiv \rho_{\text{PBH}}^b \mapsto \rho_{\text{REM}}^b + \rho_{H\text{g}}^b + \rho_{H\gamma}^b + \rho_{H\nu}^b + \rho_{H\text{p}}^b + \rho_{H\text{e}}^b \tag{B.10}$$

where ρ_{REM}^b is the energy density of the remnant, and $\rho_{H\text{g}}^b$,$\rho_{H\gamma}^b$, $\rho_{H\nu}^b$, $\rho_{H\text{p}}^b$ and $\rho_{H\text{e}}^b$ are respectively the energy densities of the gravitons, photons, neutrinos, protons and electrons produced HR:

$$\frac{\rho_{\text{REM}}^b}{\rho_{\text{PBH}}^b} \equiv \epsilon \quad \text{(B.11a)} \qquad \frac{\rho_{H\text{g}}^b}{\rho_{\text{PBH}}^b} \equiv (1-\epsilon)\epsilon_g \quad \text{(B.11b)} \qquad \frac{\rho_{H\gamma}^b}{\rho_{\text{PBH}}^b} \equiv (1-\epsilon)\epsilon_\gamma \quad \text{(B.11c)} \qquad \frac{\rho_{H\nu}^b}{\rho_{\text{PBH}}^b} \equiv (1-\epsilon)\epsilon_\nu \quad \text{(B.11d)} \qquad \frac{\rho_{H\text{p}}^b}{\rho_{\text{PBH}}^b} \equiv (1-\epsilon)\epsilon_{\text{p}} \quad \text{(B.11e)} \qquad \frac{\rho_{H\text{e}}^b}{\rho_{\text{PBH}}^b} \equiv (1-\epsilon)\epsilon_{\text{e}} \quad \text{(B.11f)}$$

ϵ is the fraction of the PBH not evaporating, and is typically very small in the case of a rovellino, and is $\mathcal{O} \sim 1$ in the case of the memory burden effect. $(1-\epsilon)\epsilon_A$ is the fraction going into the species A, $A \in \{\text{g}, \gamma, \nu, \text{p}, \text{e}\}$.

$$\rho\left(N_0^{(P2)}\right) = \left(\rho_\gamma^i + \rho_\nu^i\right) e^{4N_i} + \left(\rho_b^i + \rho_c^i\right) e^{3N_i} + \left(\rho_{Hg}^b + \rho_{H\gamma}^b + \rho_{H\nu}^b\right) e^{4N_b} + \rho_{\text{REM}}^b e^{3N_b} + \rho_\Lambda \tag{B.12}$$

Now, we require that the model be consistent with the observed energy density today, namely:

$$\begin{cases} \rho_\gamma^i e^{4N_i} + \rho_{H\gamma}^b e^{4N_b} = \rho_\gamma^{\rm obs} & \text{(B.13a)} \\ \rho_b^i e^{3N_i} + \left(\rho_{H\rm e}^b + \rho_{H\rm p}^b\right) e^{3N_b} = \rho_b^{\rm obs} & \text{(B.13b)} \\ \rho_c^i e^{3N_i} + \rho_{\rm REM}^b e^{3N_b} = \rho_{\rm DM}^{\rm obs} & \text{(B.13c)} \end{cases}$$

These requirements can be translated into the following constraints on the $\{\alpha\}$ parameters:

$$\begin{cases} \alpha_b^{\texttt{P2}} = \dfrac{1}{1-\beta} - \dfrac{\beta(1-\epsilon)(\epsilon_e+\epsilon_p)}{(1-\beta)\rho_b^{\rm obs}} \dfrac{e^{N_i}(\rho_b^{\rm obs}+\rho_{\rm DM}^{\rm obs}) + (1+C_{\nu\gamma})\rho_\gamma^{\rm obs}}{e^{N_i}(1-\beta[1-\epsilon][1-\epsilon_e-\epsilon_p]) + (1+C_{\nu\gamma})e^{N_b}\beta(1-\epsilon)\epsilon_\gamma} & \text{(B.14a)} \\ \alpha_c^{\texttt{P2}} = \dfrac{1}{1-\beta} + \dfrac{\beta\epsilon}{(1-\beta)\rho_{\rm DM}^{\rm obs}} \dfrac{e^{N_i}(\rho_b^{\rm obs}+\rho_{\rm DM}^{\rm obs}) + (1+C_{\nu\gamma})\rho_\gamma^{\rm obs}}{e^{N_i}(1-\beta[1-\epsilon][1-\epsilon_e-\epsilon_p]) + (1+C_{\nu\gamma})e^{N_b}\beta(1-\epsilon)\epsilon_\gamma} & \text{(B.14b)} \\ \alpha_\gamma^{\texttt{P2}} = \dfrac{e^{N_i}(1-\beta[1-\epsilon][1-\epsilon_e-\epsilon_p])}{(1+C_{\nu\gamma})(1-\beta)\rho_\gamma^{\rm obs}} \dfrac{e^{N_i}(\rho_b^{\rm obs}+\rho_{\rm DM}^{\rm obs}) + (1+C_{\nu\gamma})\rho_\gamma^{\rm obs}}{e^{N_i}(1-\beta[1-\epsilon][1-\epsilon_e-\epsilon_p]) + (1+C_{\nu\gamma})e^{N_b}\beta(1-\epsilon)\epsilon_\gamma} - \dfrac{e^{N_i}(\rho_b^{\rm obs}+\rho_{\rm DM}^{\rm obs})}{(1+C_{\nu\gamma})(1-\beta)\rho_\gamma^{\rm obs}} & \text{(B.14c)} \end{cases}$$

We refer to the $\{\alpha\}$ parameters in the P2 phase as $\{\alpha\}^{\rm P2}$.

B.4 Phase P3

The phase P3 corresponds to the epoch where the remnants of the PBHs decay into radiation. At $N = N_r^-$, the energy density is given by

$$\rho(N_r^-) = \left(\rho_\gamma^i + \rho_\nu^i\right) e^{-4(\delta N+\Delta N)} + \left(\rho_b^i + \rho_c^i\right) e^{-3(\delta N+\Delta N)} + \left(\rho_{H\rm g}^b + \rho_{H\gamma}^b + \rho_{H\nu}^b\right) e^{-4\Delta N} + \left(\rho_{\rm REM}^b + \rho_{H\rm e}^b + \rho_{H\rm p}^b\right) e^{-3\Delta N} + \rho_\Lambda \tag{B.15}$$

where $\Delta N = N_r - N_b$. At $N = N_r$, the remnants decay into (diffuse) radiation:

$$\rho_{\rm REM}(N_r) \equiv \rho_{\rm REM}^r \mapsto \rho_d^r \tag{B.16}$$

where ρ_d^r is the energy density of the diffuse radiation:

$$\frac{\rho_d^r}{\rho_{\rm REM}^r} \equiv 1 \tag{B.17}$$

For small enough PBHs, the P3 phase is already occurring today. In this case, the energy density today would be given by:

$$\rho\left(N_0^{(P3)}\right) = \left(\rho_\gamma^i + \rho_\nu^i\right) e^{4N_i} + \left(\rho_b^i + \rho_c^i\right) e^{3N_i} + \left(\left[\rho_{H\rm g}^b + \rho_{H\gamma}^b + \rho_{H\nu}^b\right] e^{-4\Delta N} + \rho_d^r e^{-3\Delta N}\right) e^{4N_r} + \left(\rho_{H\rm e}^b + \rho_{H\rm p}^b\right) e^{3N_b} + \rho_\Lambda \tag{B.18}$$

Now, we require that the model be consistent with the observed energy density today, namely:

$$\begin{cases} \rho_b^i e^{3N_i} + \left(\rho_{H\rm e}^b + \rho_{H\rm p}^b\right) e^{3N_b} = \rho_b^{\rm obs} & \text{(B.19a)} \\ \rho_c^i e^{3N_i} = \rho_{\rm DM}^{\rm obs} & \text{(B.19b)} \\ \rho_\gamma^i e^{4N_i} + \rho_{H\gamma}^b e^{4N_b} + \rho_d^r e^{4N_r} = \rho_\gamma^{\rm obs} & \text{(B.19c)} \end{cases}$$

These requirements can be translated into the following constraints on the $\{\alpha\}$ parameters:

$$
\begin{cases}
\alpha_b^{\mathsf{P3}} = \dfrac{1}{1-\beta} - \dfrac{\beta(1-\epsilon)(\epsilon_e+\epsilon_p)}{(1-\beta)\rho_b^{\rm obs}} \dfrac{e^{N_i}(\rho_b^{\rm obs}+\rho_{\rm DM}^{\rm obs})+(1+C_{\nu\gamma})\rho_\gamma^{\rm obs}}{(1+C_{\nu\gamma})e^{N_r}\beta\epsilon + e^{N_i}(1-\beta[1-\{1-\epsilon\}\{\epsilon_e+\epsilon_p\}])+(1+C_{\nu\gamma})e^{N_b}\beta(1-\epsilon)\epsilon_\gamma} & \text{(B.20a)} \\
\alpha_c^{\mathsf{P3}} = \dfrac{1}{1-\beta} & \text{(B.20b)} \\
\qquad + \dfrac{e^{N_i}(1-\beta[1-\{1-\epsilon\}\{\epsilon_e+\epsilon_p\}])}{(1+C_{\nu\gamma})(1-\beta)\rho_\gamma^{\rm obs}} & \\
\alpha_\gamma^{\mathsf{P3}} = \times \dfrac{e^{N_i}(\rho_b^{\rm obs}+\rho_{\rm DM}^{\rm obs})+(1+C_{\nu\gamma})\rho_\gamma^{\rm obs}}{(1+C_{\nu\gamma})e^{N_r}\beta\epsilon + e^{N_i}(1-\beta[1-\{1-\epsilon\}\{\epsilon_e+\epsilon_p\}])+(1+C_{\nu\gamma})e^{N_b}\beta(1-\epsilon)\epsilon_\gamma} & \text{(B.20c)} \\
\qquad - \dfrac{e^{N_i}(\rho_b^{\rm obs}+\rho_{\rm DM}^{\rm obs})}{(1+C_{\nu\gamma})(1-\beta)\rho_\gamma^{\rm obs}} &
\end{cases}
$$

APPENDIX

C

DISCUSSION ON $\beta_{\max}$

C.1 The butterfly effect

Since the radiation redshifts faster than the PBHs, radiation collapsing into PBHs and being re-emitted by HR sees its density "boosted" (blueshifted) by a factor of order $\sim e^{N_b - N_i}$. Numerically, this translates to a high sensitivity to the initial density of photon, and explain why the "naive" estimation of deducing $\beta_{\max}^{\mathsf{P2}(\gamma)}$ from setting $\alpha_\gamma^{\mathsf{P2}} = 0$ does not yield the right order of magnitude or dynamic behavior of β. Instead, one should solve the equation:

$$\alpha_\gamma^{\mathsf{P2}}(\beta_{\max}^{\mathsf{P2}(\gamma;\varepsilon)}) = \varepsilon \implies \beta_{\max}^{\mathsf{P2}(\gamma;\varepsilon)} = \beta_{\max}^{\mathsf{P2}(\gamma;\varepsilon)}(\alpha_\gamma^{\mathsf{P2}}, \varepsilon) \tag{C.1}$$

where ε is a small number[1] (typically $\varepsilon \sim 10^{-10} - 10^{-30}$). Even with $\varepsilon \ll 1$, we can have

$$\text{denominator of } \alpha_\gamma^{\mathsf{P2}(\gamma)} \gtrsim \frac{1}{\varepsilon} \tag{C.2}$$

In other words, it is not sufficient to set the numerator of $\alpha_\gamma^{\mathsf{P2}(\gamma)}$ to zero, but we need to care about the denominator as well. Starting from eq. (B.14), solving the system eq. (C.1) gives:

$$\beta_{\max}^{\mathsf{P2}(\gamma;\varepsilon)} = \frac{\begin{array}{l} -(1+C_{\nu\gamma})e^{N_b}\varepsilon(1-\epsilon)\epsilon_\gamma\rho_\gamma^{\text{obs}} \\ -e^{N_i}\big(e^{N_b}[1-\epsilon]\epsilon_\gamma[\rho_b^{\text{obs}}+\rho_{\text{DM}}^{\text{obs}}] + [1-2\varepsilon]\rho_\gamma^{\text{obs}} - [1-\varepsilon][\epsilon_e+\epsilon_p+\epsilon\{1-\epsilon_e-\epsilon_p\}]\rho_\gamma^{\text{obs}}\big) \\ + \sqrt{\begin{array}{l} 4e^{N_i}(1-\varepsilon)\varepsilon(1-\epsilon)(e^{N_i}[1-\epsilon_e-\epsilon_p]-[1+C_{\nu\gamma}]e^{N_b}\epsilon_\gamma)\rho_\gamma^{\text{obs}\,2} \\ \quad + \Big(e^{N_i}\big[-\{(1-\epsilon)(1-\epsilon_e-\epsilon_p)\}+\varepsilon\{2-\epsilon_e-\epsilon_p-\epsilon(1-\epsilon_e-\epsilon_p)\}\big]\rho_\gamma^{\text{obs}} \\ \qquad - e^{N_b+N_i}[1-\epsilon]\epsilon_\gamma[\rho_b^{\text{obs}}+\rho_{\text{DM}}^{\text{obs}}] - [1+C_{\nu\gamma}]e^{N_b}\varepsilon[1-\epsilon]\epsilon_\gamma\rho_\gamma^{\text{obs}}\Big)^2 \end{array}} \end{array}}{2\varepsilon(1-\epsilon)(e^{N_i}[1-\epsilon_e-\epsilon_p]-[1+C_{\nu\gamma}]e^{N_b}\epsilon_\gamma)\rho_\gamma^{\text{obs}}} \tag{C.3}$$

Eq. (C.3) $\beta_{\max}^{\mathsf{P2}(\gamma;\varepsilon)}$ is the generalization of eq. (7.29) $\beta_{\max}^{\mathsf{P2}(\gamma)}$ to the case where $\alpha_\gamma^{\mathsf{P2}} = \varepsilon$ instead of $\alpha_\gamma^{\mathsf{P2}} = 0$. Instead of this long and complicated equation, let us see how $\beta_{\max}^{\mathsf{P2}(\gamma;\varepsilon)}$ behaves in the interesting mass ranges mentioned in subsections 8.3.1.B, 8.3.1.C and 8.3.2.C.

[1] Be careful not to confuse ε, which is what is left of $\alpha_\gamma^{\mathsf{P2}}$ after `BetaFinder` has converged, with ϵ, the ratio between the mass of the remnant and the initial mass of the PBH.

C.2 Loop Quantum Gravity

The first panel of fig. C.1 shows the α_A parameters as a function of the initial PBH mass $m^i_{\rm PBH}$ in the LQG scenario.

As expected from the `BetaFinder` module, the α_c parameter is steady at 10^{-5} when $f = 1$. Among the regions where $f \neq 1$, the one where $\rho^H_b/\rho^{\rm tot}_b \sim 1$ (with the green background) was already well understood in subsec. 8.4.1. We are left with the regions where $f \neq 1$ and $\rho^H_\gamma/\rho^{\rm tot}_\gamma \sim 1$ (with the orange background), which seemed more complex.

Now that we derived $\beta^{\mathsf{P2}(\gamma;\varepsilon)}_{\rm max}$, we can plot it for different values of ε in the second panel of fig. C.1. We see that $\beta^{\mathsf{P2}(\gamma;\varepsilon)}_{\rm max}$ is highly sensitive to the value of ε, but we do recover the expected behavior when $\varepsilon = \alpha^{\mathsf{P2}}_\gamma$. In particular, $\beta^{\mathsf{P2}(\gamma;\varepsilon=\alpha^{\mathsf{P2}}_\gamma)}_{\rm max}$ has a completely different behavior than $\beta^{\mathsf{P2}(\gamma;\varepsilon=0)}_{\rm max}$, which was the estimate used in subsections 8.3.1.B and 8.3.1.C: $\beta^{\mathsf{P2}(\gamma;\varepsilon=0)}_{\rm max}$ is almost theory-independent, while $\beta^{\mathsf{P2}(\gamma;\varepsilon=\alpha^{\mathsf{P2}}_\gamma)}_{\rm max}$ is closely related to which species is saturated by the PBHs or their remnants. In particular, the generalized $\beta^{\mathsf{P2}(\gamma;\varepsilon)}_{\rm max}$ keep a dependency on the scale factor at formation e^{N_i}, which is sensitive to whether the PBHs are formed in a RD or EMD era.

The third panel of fig. C.1 shows the ratio between the theoretical $\beta^{\mathsf{P2}(\gamma;\varepsilon)}_{\rm max}$ and the one obtained numerically. We see an agreement between the two quantities with fluctuations of less than one order of magnitude along the whole mass range. We used the expressions given in equations (7.27), (7.28) and (7.30) for the α_A with $A \in \{b, c\}$, and the one given in eq. (C.3) for α_γ.

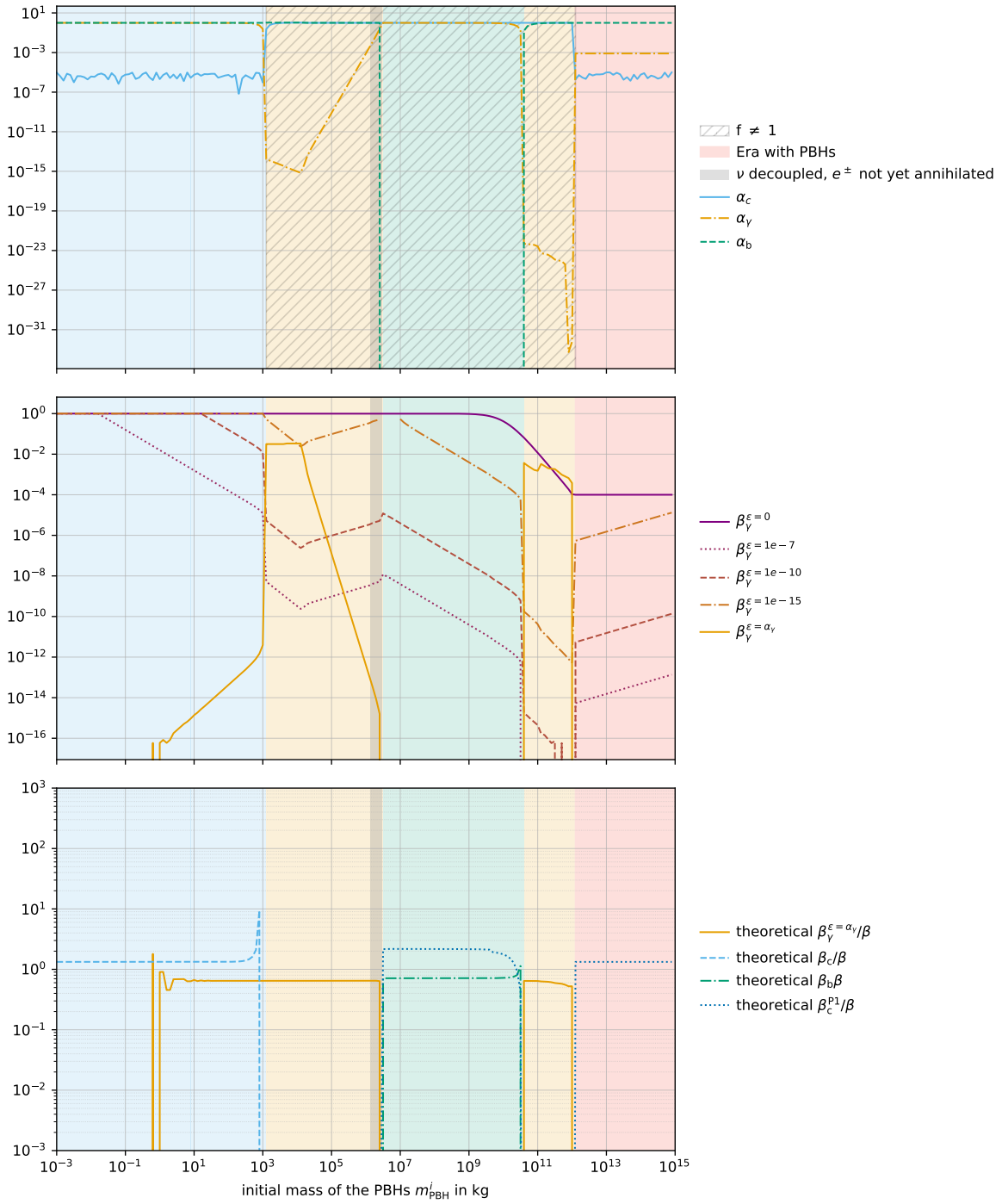

Figure C.1: α_A parameters as a function of the initial PBH mass $m^i_{\rm PBH}$ in the LQG scenario (first panel). The second panel shows the mass fraction $\beta_\gamma^{\rm P2(\gamma;\varepsilon)}$ for different values of ε. The third panel shows the ratio between theoretical and observed β.
The background color indicates the species saturated by the PBHs or their remnants (blue), photons from HR (orange) and baryons from HR (green). The grey area indicates the regions where the PBHs evaporate after the decoupling of the neutrinos but before the e^+-e^- annihilation era. The dashed region on the first panel indicates the region where $f \neq 1$ (when the total DM density cannot be accounted for by the PBHs or their remnants).

C.3 Memory Burden Effect

The first panel of fig. C.2 shows the α_A parameters as a function of the initial PBH mass $m^i_{\rm PBH}$ in the MBE scenario.

Similarly to the LQG case, the only region where the behavior of β seemed to require a more careful analysis is the one where $f \neq 1$ and $\rho^H_\gamma/\rho^{\rm tot}_\gamma \sim 1$ (with the orange background in fig. C.2). In the region where $f = 1$, the α_c parameter is steady at 10^{-5} and $\beta^{\mathsf{P2}(c)}_{\rm max}$ recovers satisfactorily the behavior of β, and in the region where the baryon density is saturated by the HR product (where $f \neq 1$ and $\rho^H_b/\rho^{\rm tot}_b \sim 1$, with the green background), $\beta^{\mathsf{P2}(b)}_{\rm max}$ is also in good agreement with the observed β.

In the second panel of fig. C.2, we plot $\beta^{\mathsf{P2}(\gamma;\varepsilon)}_{\rm max}$ for different values of ε. As in the LQG case, we see that $\beta^{\mathsf{P2}(\gamma;\varepsilon)}_{\rm max}$ is highly sensitive to the value of ε, but we do recover the expected behavior when $\varepsilon = \alpha^{\mathsf{P2}}_\gamma$. In particular, $\beta^{\mathsf{P2}(\gamma;\varepsilon=\alpha^{\mathsf{P2}}_\gamma)}_{\rm max}$ has a completely different behavior than $\beta^{\mathsf{P2}(\gamma;\varepsilon=0)}_{\rm max}$, which was the estimate used in subsec. 8.3.2.C.The reasons for the sensitivity to ε being the same as in the LQG case, we do not repeat them here.

In the third and final panel of fig. C.2, we plot the ratio between the theoretical $\beta^{\mathsf{P2}(\gamma;\varepsilon)}_{\rm max}$ and the one given by the `BetaFinder` module. We see an agreement between the two quantities with fluctuations of less than one order of magnitude along the whole mass range. As previously, we used the expressions given in equations (7.27), (7.28) and (7.30) for the α_A with $A \in \{b, c\}$, and the one given in eq. (C.3) for α_γ.

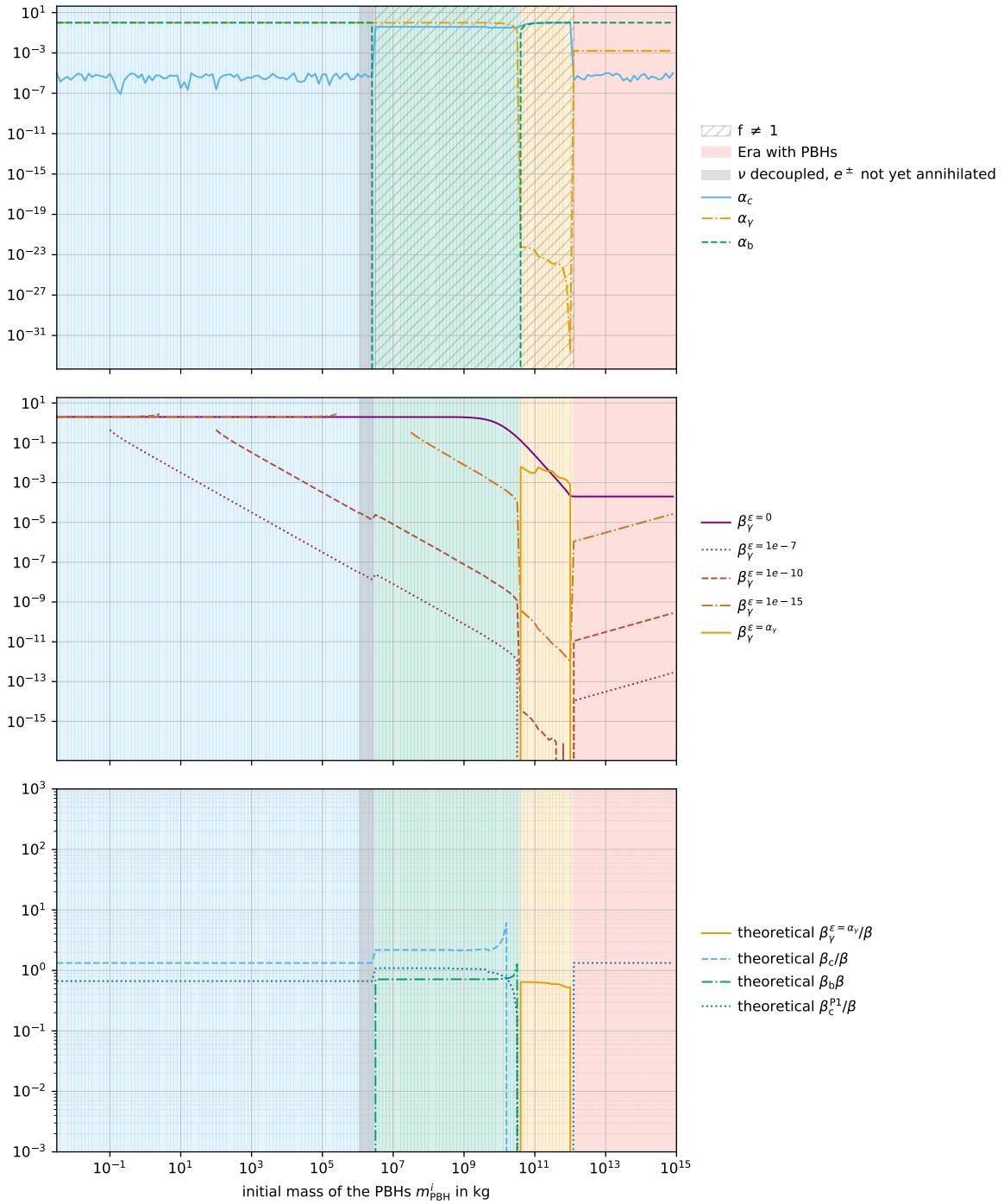

Figure C.2: α_A parameters as a function of the initial PBH mass $m^i_{\rm PBH}$ in the MB scenario (first panel). The second panel shows the mass fraction $\beta_\gamma^{\rm P2(\gamma;\varepsilon)}$ for different values of ε. The third panel shows the ratio between theoretical and observed β.
The background color indicates the species saturated by the PBHs or their remnants (blue), photons from HR (orange) and baryons from HR (green). The grey area indicates the regions where the PBHs evaporate after the decoupling of the neutrinos but before the e^+-e^- annihilation era. The dashed region on the first panel indicates the region where $f \neq 1$ (when the total DM density cannot be accounted for by the PBHs or their remnants).

BIBLIOGRAPHY

S. Aiello et al. Observation of an ultra-high-energy cosmic neutrino with KM3NeT. *Nature*, 638(8050): 376–382, 2025. doi: 10.1038/s41586-024-08543-1. [Erratum: Nature 640, E3 (2025)].

Y. Akrami et al. Planck 2018 results. X. Constraints on inflation. *Astron. Astrophys.*, 641:A10, 2020. doi: 10.1051/0004-6361/201833887.

Ana Alexandre, Gia Dvali, and Emmanouil Koutsangelas. New mass window for primordial black holes as dark matter from memory burden effect, 2024. URL https://arxiv.org/abs/2402.14069.

E. Allys et al. Probing Cosmic Inflation with the LiteBIRD Cosmic Microwave Background Polarization Survey. *PTEP*, 2023(4):042F01, 2023. doi: 10.1093/ptep/ptac150.

A. Arbey and F. Mahmoudi. Dark matter and the early universe: A review. *Progress in Particle and Nuclear Physics*, 119:103865, July 2021. ISSN 0146-6410. doi: 10.1016/j.ppnp.2021.103865. URL http://dx.doi.org/10.1016/j.ppnp.2021.103865.

Alexandre Arbey and Jérémy Auffinger. Blackhawk: a public code for calculating the hawking evaporation spectra of any black hole distribution. *The European Physical Journal C*, 79(8), August 2019. ISSN 1434-6052. doi: 10.1140/epjc/s10052-019-7161-1. URL http://dx.doi.org/10.1140/epjc/s10052-019-7161-1.

Alexandre Arbey and Jérémy Auffinger. Physics beyond the standard model with blackhawk v2.0. *The European Physical Journal C*, 81(10), October 2021. ISSN 1434-6052. doi: 10.1140/epjc/s10052-021-09702-8. URL http://dx.doi.org/10.1140/epjc/s10052-021-09702-8.

M. Archidiacono et al. Euclid preparation - LIV. Sensitivity to neutrino parameters. *Astron. Astrophys.*, 693:A58, 2025. doi: 10.1051/0004-6361/202450859.

Abhay Ashtekar and Parampreet Singh. Loop quantum cosmology: a status report. *Classical and Quantum Gravity*, 28(21):213001, September 2011. ISSN 1361-6382. doi: 10.1088/0264-9381/28/21/213001. URL http://dx.doi.org/10.1088/0264-9381/28/21/213001.

Jérémy Auffinger. Primordial black hole constraints with hawking radiation—a review. *Progress in Particle and Nuclear Physics*, 131:104040, July 2023. ISSN 0146-6410. doi: 10.1016/j.ppnp.2023.104040. URL http://dx.doi.org/10.1016/j.ppnp.2023.104040.

Eleni Bagui, Sebastien Clesse, Valerio De Luca, Jose María Ezquiaga, Gabriele Franciolini, Juan García-Bellido, Cristian Joana, Rajeev Kumar Jain, Sachiko Kuroyanagi, Ilia Musco, Theodoros Papanikolaou, Alvise Raccanelli, Sébastien Renaux-Petel, Antonio Riotto, Ester Ruiz Morales, Marco Scalisi, Olga Sergijenko, Caner Unal, Vincent Vennin, and David Wands. Primordial black holes and their gravitational-wave signatures, 2023. URL https://arxiv.org/abs/2310.19857.

Aurélien Barrau and Carlo Rovelli. Planck star phenomenology. *Physics Letters B*, 739:405–409, December 2014. ISSN 0370-2693. doi: 10.1016/j.physletb.2014.11.020. URL http://dx.doi.org/10.1016/j.physletb.2014.11.020.

Laura Baudis. A 100 y challenge : the nature of Dark Matter , June 2024. URL https://indico.cern.ch/event/1267450/contributions/5886937.

Daniel Baumann. Inflation. In *Theoretical Advanced Study Institute in Elementary Particle Physics: Physics of the Large and the Small*, pages 523–686, 2011. doi: 10.1142/9789814327183_0010.

Daniel Baumann. *Cosmology*. Cambridge University Press, 7 2022. ISBN 978-1-108-93709-2, 978-1-108-83807-8. doi: 10.1017/9781108937092.

Idrus Husin Belfaqih, Martin Bojowald, Suddhasattwa Brahma, and Erick I. Duque. Hawking evaporation and the fate of black holes in loop quantum gravity, 2025. URL https://arxiv.org/abs/2504.11998.

Gianfranco Bertone and Dan Hooper. History of dark matter. *Reviews of Modern Physics*, 90(4), October 2018. ISSN 1539-0756. doi: 10.1103/revmodphys.90.045002. URL http://dx.doi.org/10.1103/RevModPhys.90.045002.

Simeon Bird, Ilias Cholis, Julian B. Muñoz, Yacine Ali-Haïmoud, Marc Kamionkowski, Ely D. Kovetz, Alvise Raccanelli, and Adam G. Riess. Did ligo detect dark matter? *Physical Review Letters*, 116 (20), May 2016. ISSN 1079-7114. doi: 10.1103/physrevlett.116.201301. URL http://dx.doi.org/10.1103/PhysRevLett.116.201301.

Matthias Blau. Lecture notes on general relativity, March 2025. URL http://blau.itp.unibe.ch/GRLecturenotes.html.

Andrea Boccia and Fabio Iocco. A strike of luck: could the km3-230213a event be caused by an evaporating primordial black hole?, 2025. URL https://arxiv.org/abs/2502.19245.

Christian Byrnes, Gabriele Franciolini, Tomohiro Harada, Paolo Pani, and Misao Sasaki, editors. *Primordial Black Holes*. Springer Series in Astrophysics and Cosmology. Springer, 2025. ISBN 978-981–978886-6, 978-981–978889-7, 978-981–978887-3. doi: 10.1007/978-981-97-8887-3.

Christian T. Byrnes and Philippa S. Cole. Lecture notes on inflation and primordial black holes, 2021. URL https://arxiv.org/abs/2112.05716.

C. Patrignani et al. (Particle Data Group). Review of Particle Physics. *Chin. Phys. C*, 40(10):100001, 2016. doi: 10.1088/1674-1137/40/10/100001.

B. J. Carr, Kazunori Kohri, Yuuiti Sendouda, and Jun'ichi Yokoyama. New cosmological constraints on primordial black holes. *Physical Review D*, 81(10), May 2010. ISSN 1550-2368. doi: 10.1103/physrevd.81.104019. URL http://dx.doi.org/10.1103/PhysRevD.81.104019.

Bernard Carr and Florian Kühnel. Primordial black holes as dark matter candidates. *SciPost Physics Lecture Notes*, May 2022. ISSN 2590-1990. doi: 10.21468/scipostphyslectnotes.48. URL http://dx.doi.org/10.21468/SciPostPhysLectNotes.48.

Bernard Carr, Kazunori Kohri, Yuuiti Sendouda, and Jun'ichi Yokoyama. Constraints on primordial black holes. *Reports on Progress in Physics*, 84(11):116902, November 2021. ISSN 1361-6633. doi: 10.1088/1361-6633/ac1e31. URL http://dx.doi.org/10.1088/1361-6633/ac1e31.

Bernard Carr, Sebastien Clesse, Juan Garcia-Bellido, Michael Hawkins, and Florian Kuhnel. Observational evidence for primordial black holes: A positivist perspective. *Phys. Rept.*, 1054:1–68, 2024. doi: 10.1016/j.physrep.2023.11.005.

Bernard J. Carr. The Primordial black hole mass spectrum. *Astrophys. J.*, 201:1–19, 1975. doi: 10.1086/153853.

Arnab Chaudhuri, Kazunori Kohri, and Valentin Thoss. New bounds on memory burdened primordial black holes from big bang nucleosynthesis, 2025.

Marios Christodoulou and Fabio D'Ambrosio. Characteristic time scales for the geometry transition of a black hole to a white hole from spinfoams, 2024. URL https://arxiv.org/abs/1801.03027.

Marios Christodoulou and Carlo Rovelli. How big is a black hole? *Phys. Rev. D*, 91:064046, Mar 2015. doi: 10.1103/PhysRevD.91.064046. URL https://link.aps.org/doi/10.1103/PhysRevD.91.064046.

Piotr Chrusciel. *Geometry of Black Holes*. International Series of Monographs on Physics. Oxford University Press, 4 2023. ISBN 978-0-19-887320-4, 978-0-19-885541-5.

Sébastien Clesse and Juan García-Bellido. The clustering of massive primordial black holes as dark matter: Measuring their mass distribution with advanced ligo. *Physics of the Dark Universe*, 15: 142–147, March 2017. ISSN 2212-6864. doi: 10.1016/j.dark.2016.10.002. URL http://dx.doi.org/10.1016/j.dark.2016.10.002.

Antoine Dierckx. Pbh-rem: Primordial black hole remnant evolution model, 2025. URL https://github.com/adierckx/pbh-rem. Semi-analytical PBH population evolution with remnant prescriptions.

Alessandro Dondarini, Giulio Marino, Paolo Panci, and Michael Zantedeschi. The fast, the slow and the merging: probes of evaporating memory burdened pbhs, 2025. URL https://arxiv.org/abs/2506.13861.

Pietro Doná and Simone Speziale. Introductory lectures to loop quantum gravity, 2010. URL https://arxiv.org/abs/1007.0402.

Gia Dvali. Area law microstate entropy from criticality and spherical symmetry. *Physical Review D*, 97(10), May 2018. ISSN 2470-0029. doi: 10.1103/physrevd.97.105005. URL http://dx.doi.org/10.1103/PhysRevD.97.105005.

Gia Dvali. Entropy bound and unitarity of scattering amplitudes. *Journal of High Energy Physics*, 2021(3), March 2021. ISSN 1029-8479. doi: 10.1007/jhep03(2021)126. URL http://dx.doi.org/10.1007/JHEP03(2021)126.

Gia Dvali and Cesar Gomez. Black hole's quantum n-portrait, 2011. URL https://arxiv.org/abs/1112.3359.

Gia Dvali, Lukas Eisemann, Marco Michel, and Sebastian Zell. Black hole metamorphosis and stabilization by memory burden. *Physical Review D*, 102(10), November 2020. ISSN 2470-0029. doi: 10.1103/physrevd.102.103523. URL http://dx.doi.org/10.1103/PhysRevD.102.103523.

Gia Dvali, Juan Sebastián Valbuena-Bermúdez, and Michael Zantedeschi. Memory burden effect in black holes and solitons: Implications for pbh, 2024. URL https://arxiv.org/abs/2405.13117.

Gia Dvali, Michael Zantedeschi, and Sebastian Zell. Transitioning to memory burden: Detectable small primordial black holes as dark matter, 2025. URL https://arxiv.org/abs/2503.21740.

Fabio D'Ambrosio, Marios Christodoulou, Pierre Martin-Dussaud, Carlo Rovelli, and Farshid Soltani. End of a black hole's evaporation. *Physical Review D*, 103(10), May 2021. ISSN 2470-0029. doi: 10.1103/physrevd.103.106014. URL http://dx.doi.org/10.1103/PhysRevD.103.106014.

J.R. Espinosa, D. Racco, and A. Riotto. Cosmological signature of the standard model higgs vacuum instability: Primordial black holes as dark matter. *Physical Review Letters*, 120(12), March 2018. ISSN 1079-7114. doi: 10.1103/physrevlett.120.121301. URL http://dx.doi.org/10.1103/PhysRevLett.120.121301.

D. J. Fixsen. The temperature of the cosmic microwave background. *The Astrophysical Journal*, 707 (2):916–920, November 2009. ISSN 1538-4357. doi: 10.1088/0004-637x/707/2/916. URL http://dx.doi.org/10.1088/0004-637X/707/2/916.

Hal M. Haggard and Carlo Rovelli. Quantum-gravity effects outside the horizon spark black to white hole tunneling. *Physical Review D*, 92(10), November 2015. ISSN 1550-2368. doi: 10.1103/physrevd.92.104020. URL http://dx.doi.org/10.1103/PhysRevD.92.104020.

Muxin Han, Carlo Rovelli, and Farshid Soltani. Geometry of the black-to-white hole transition within a single asymptotic region. *Physical Review D*, 107(6), March 2023. ISSN 2470-0029. doi: 10.1103/physrevd.107.064011. URL http://dx.doi.org/10.1103/PhysRevD.107.064011.

Tomohiro Harada, Chul-Moon Yoo, and Kazunori Kohri. Threshold of primordial black hole formation. *Physical Review D*, 88(8), October 2013. ISSN 1550-2368. doi: 10.1103/physrevd.88.084051. URL http://dx.doi.org/10.1103/PhysRevD.88.084051.

S. W. Hawking. Particle Creation by Black Holes. *Commun. Math. Phys.*, 43:199–220, 1975. doi: 10.1007/BF02345020. [Erratum: Commun.Math.Phys. 46, 206 (1976)].

Sean A. Hayward. Formation and evaporation of nonsingular black holes. *Physical Review Letters*, 96(3), January 2006. ISSN 1079-7114. doi: 10.1103/physrevlett.96.031103. URL http://dx.doi.org/10.1103/PhysRevLett.96.031103.

Sina Kazemian, Mateo Pascual, Carlo Rovelli, and Francesca Vidotto. Diffuse emission from black hole remnants. *Classical and Quantum Gravity*, 40(8):087001, March 2023. ISSN 1361-6382. doi: 10.1088/1361-6382/acc232. URL http://dx.doi.org/10.1088/1361-6382/acc232.

Jinsu Kim. Cosmic Inflation: Mini Lecture. Lecture at Technische Universität Dresden, June 2017. June 22, 2017.

Jane H. MacGibbon. Can Planck-mass relics of evaporating black holes close the universe? *Nature*, 329:308–309, 1987. doi: 10.1038/329308a0.

Jane H. MacGibbon. Quark- and gluon-jet emission from primordial black holes. ii. the emission over the black-hole lifetime. *Phys. Rev. D*, 44:376–392, Jul 1991. doi: 10.1103/PhysRevD.44.376. URL https://link.aps.org/doi/10.1103/PhysRevD.44.376.

Pierre Martin-Dussaud. The lifetime of white hole remnants is m^5, 2025. URL https://arxiv.org/abs/2504.05492.

Fabio M. Mele. Quantum metric and entanglement on spin networks, 2017. URL https://arxiv.org/abs/1703.06415.

Charles W. Misner. Feynman quantization of general relativity. *Rev. Mod. Phys.*, 29:497–509, Jul 1957. doi: 10.1103/RevModPhys.29.497. URL https://link.aps.org/doi/10.1103/RevModPhys.29.497.

Charles W. Misner, K. S. Thorne, and J. A. Wheeler. *Gravitation*. W. H. Freeman, San Francisco, 1973. ISBN 978-0-7167-0344-0, 978-0-691-17779-3.

Gabriele Montefalcone, Dan Hooper, Katherine Freese, Chris Kelso, Florian Kuhnel, and Pearl Sandick. Does memory burden open a new mass window for primordial black holes as dark matter?, 2025. URL https://arxiv.org/abs/2503.21005.

Viatcheslav Mukhanov and Sergei Winitzki. *Introduction to quantum effects in gravity*. Cambridge University Press, 6 2007. ISBN 978-0-521-86834-1, 978-1-139-78594-5.

S. Navas et al. Review of particle physics. *Phys. Rev. D*, 110(3):030001, 2024. doi: 10.1103/PhysRevD.110.030001.

Izaak Neutelings. Kruskal diagrams of Schwarzschild black holes – TikZ.net, October 2021. URL https://tikz.net/relativity_kruskal_diagram.

Don N. Page. Particle Emission Rates from a Black Hole: Massless Particles from an Uncharged, Nonrotating Hole. *Phys. Rev. D*, 13:198–206, 1976. doi: 10.1103/PhysRevD.13.198.

Theodoros Papanikolaou. Primordial black holes in loop quantum cosmology: the effect on the threshold. *Classical and Quantum Gravity*, 40(13):134001, June 2023. ISSN 1361-6382. doi: 10.1088/1361-6382/acd97d. URL http://dx.doi.org/10.1088/1361-6382/acd97d.

Theodoros Papanikolaou, Vincent Vennin, and David Langlois. Gravitational waves from a universe filled with primordial black holes. *Journal of Cosmology and Astroparticle Physics*, 2021(03):053, March 2021. ISSN 1475-7516. doi: 10.1088/1475-7516/2021/03/053. URL http://dx.doi.org/10.1088/1475-7516/2021/03/053.

Alejandro Perez, Carlo Rovelli, and Marios Christodoulou. Detecting gravitationally interacting dark matter with quantum interference, 2024. URL https://arxiv.org/abs/2309.08238.

Patrick Peter and Jean-Philippe Uzan. *Primordial Cosmology*. Oxford Graduate Texts. Oxford University Press, 2 2013. ISBN 978-0-19-966515-0, 978-0-19-920991-0.

Planck. Planck2018 results: Vi. cosmological parameters. *Astronomy & Astrophysics*, 641:A6, September 2020. ISSN 1432-0746. doi: 10.1051/0004-6361/201833910. URL http://dx.doi.org/10.1051/0004-6361/201833910.

Alba Romero-Rodríguez and Sachiko Kuroyanagi. Lvk constraints on pbhs from stochastic gravitational wave background searches, 2024. URL https://arxiv.org/abs/2407.00205.

Carlo Rovelli. *Quantum gravity*. Cambridge Monographs on Mathematical Physics. Univ. Pr., Cambridge, UK, 2004. doi: 10.1017/CBO9780511755804.

Carlo Rovelli and Francesca Vidotto. Planck stars. *International Journal of Modern Physics D*, 23(12):1442026, October 2014a. ISSN 1793-6594. doi: 10.1142/s0218271814420267. URL http://dx.doi.org/10.1142/S0218271814420267.

Carlo Rovelli and Francesca Vidotto. *Covariant Loop Quantum Gravity: An Elementary Introduction to Quantum Gravity and Spinfoam Theory*. Cambridge Monographs on Mathematical Physics. Cambridge University Press, 11 2014b. ISBN 978-1-107-06962-6, 978-1-316-14729-0.

Carlo Rovelli and Francesca Vidotto. Planck stars, White Holes, Remnants and Planck-mass quasiparticles. The quantum gravity phase in black holes' evolution and its manifestations. 7 2024.

Misao Sasaki, Teruaki Suyama, Takahiro Tanaka, and Shuichiro Yokoyama. Primordial black hole scenario for the gravitational-wave event gw150914. *Physical Review Letters*, 117(6), August 2016. ISSN 1079-7114. doi: 10.1103/physrevlett.117.061101. URL http://dx.doi.org/10.1103/PhysRevLett.117.061101.

Joseph C. Schindler, Anthony Aguirre, and Amita Kuttner. Understanding black hole evaporation using explicitly computed penrose diagrams. *Physical Review D*, 101(2), January 2020. ISSN 2470-0029. doi: 10.1103/physrevd.101.024010. URL http://dx.doi.org/10.1103/PhysRevD.101.024010.

Roman Scoccimarro. Cosmology lecture notes, October 2024. URL https://cosmo.nyu.edu/roman/courses/cosmology_2021. [Online; accessed 29. Oct. 2024].

Claude Semay. Penrose-carter diagram for a uniformly accelerated observer. *European Journal of Physics*, 28(5):877–887, July 2007. ISSN 1361-6404. doi: 10.1088/0143-0807/28/5/011. URL http://dx.doi.org/10.1088/0143-0807/28/5/011.

Torbjörn Sjöstrand, Stefan Ask, Jesper R. Christiansen, Richard Corke, Nishita Desai, Philip Ilten, Stephen Mrenna, Stefan Prestel, Christine O. Rasmussen, and Peter Z. Skands. An introduction to pythia 8.2. *Computer Physics Communications*, 191:159–177, June 2015. ISSN 0010-4655. doi: 10.1016/j.cpc.2015.01.024. URL http://dx.doi.org/10.1016/j.cpc.2015.01.024.

Valentin Thoss and Abraham Loeb. Detecting dark objects in the solar system with gravitational wave observatories, 2025. URL https://arxiv.org/abs/2507.19577.

Valentin Thoss, Andreas Burkert, and Kazunori Kohri. Breakdown of hawking evaporation opens new mass window for primordial black holes as dark matter candidate. *Monthly Notices of the Royal Astronomical Society*, 532(1):451–459, April 2024. ISSN 1365-2966. doi: 10.1093/mnras/stae1098. URL http://dx.doi.org/10.1093/mnras/stae1098.

Oem Trivedi and Abraham Loeb. Could planck star remnants be dark matter?, 2025. URL https://arxiv.org/abs/2506.03334.

Michael Zantedeschi and Luca Visinelli. Ultralight black holes as sources of high-energy particles, 2025. URL https://arxiv.org/abs/2410.07037.

P. A. Zyla et al. Review of Particle Physics. *PTEP*, 2020(8):083C01, 2020. doi: 10.1093/ptep/ptaa104.

Ogan Özsoy and Gianmassimo Tasinato. Inflation and primordial black holes. *Universe*, 9(5):203, April 2023. ISSN 2218-1997. doi: 10.3390/universe9050203. URL http://dx.doi.org/10.3390/universe9050203.